Fakultät für Medizin
Institut für Virologie

Immunotherapeutic Approaches for the Treatment of Chronic HBV Infection and Hepatocellular Carcinoma

Julia Festag

Vollständiger Abdruck der von der Fakultät für Medizin der Technischen Universität München zur Erlangung des akademischen Grades eines

Doktors der Naturwissenschaften (Dr. rer. nat.)

genehmigten Dissertation.

Vorsitzender: Prof. Dr. Dr. Stefan Engelhardt

Prüfende der Dissertation:

1. Prof. Dr. Ulrike Protzer
2. Prof. Dr. Percy A. Knolle

Die Dissertation wurde am 20.08.2018 bei der Technischen Universität München eingereicht und durch die Fakultät für Medizin am 17.07.2019 angenommen.

Meiner Familie

und Marvin

Table of contents

ABSTRACT

Despite the availability of an effective vaccine, hepatitis B virus (HBV) infection represents a major health concern with 257 million humans chronically infected worldwide. Chronic HBV infection is associated with a high risk of developing liver cirrhosis and hepatocellular carcinoma (HCC) and more than 800,000 people die from HBV-associated diseases every year. Current treatment options are rarely able to cure the disease, as the viral covalently closed circular DNA (cccDNA) template is not targeted. HBV-specific immune responses, especially T cells, seem to be essential to achieve HBV cure and are functionally impaired in chronic HBV infections. New immunotherapeutic approaches therefore aim to restore the patient's adaptive immune response to recognize and eliminate virus-infected or malignant cells. In this dissertation, the potential of different immunotherapeutic strategies towards chronic HBV infection and HCC was explored. Previous studies on those therapeutic interventions have either not been transferred to the *in vivo* setting yet or had been only performed in HBV-transgenic mice, a model in which clearance of the virus cannot be demonstrated.

To overcome this obstacle and mimic chronic HBV infection, viral vectors delivering the HBV genome into mouse hepatocytes were generated and compared in the first part of the thesis. Adeno (Ad)-, high capacity adeno (HCA) - as well as adeno-associated viral (AAV) vector based HBV genome transduction models led to persistence of HBV in immunocompetent mice. The data revealed, that AAV-mediated HBV genome transfer was most convenient as it induced persistent viral replication even at high titers without inducing an immune response. Moreover, AAV-HBV-transduced hepatocytes exhibited formation of cccDNA.

In the second part of the thesis, immunotherapeutic approaches against chronic HBV infection and HBV-related HCC were investigated *in vivo* using the newly established AAV-HBV model of chronic HBV infection. First, a therapeutic vaccination approach using a modified vaccinia virus Ankara (MVA) expressing HBV proteins to boost a previous protein prime vaccination was explored. Therapeutic vaccination induced HBV-specific B- and T-cell responses and was able to break HBV-specific immune tolerance. However, high HBV antigen levels as well as prolonged exposure to HBV antigens negatively influenced vaccination induced immunity. Beside therapeutic vaccination, adoptive transfer of HBV-specific T cells represents another approach to restore the patient's immune response. Therefore, the therapeutic potential of genetically redirected T cells was explored. A chimeric antigen receptor recognizing the HBV envelope proteins (S-CAR) was previously generated. S-CAR-engrafted T cells demonstrated a profound antiviral activity in AAV-HBV-infected immunodeficient animals. Yet, they failed to completely eradicate HBV after adoptive T-cell transfer although S-CAR$^+$ T cells persisted in high numbers. Additionally, the therapeutic effect of T cells redirected with HBV-specific human

leukocyte antigen (HLA) A*02 restricted natural T-cell receptors (TCRs) was explored using a mouse strain with HLA-A*02 and an H-2 class I knockout. Hepatocytes of those mice were identified to poorly present endogenously processed peptides. However, AAV-mediated expression of HLA-A*02 in mouse hepatocytes led to the establishment of suitable target cells to study HBV-specific HLA-A*02 restricted TCR-redirected T cells. Finally, HBV-specific TCR-engrafted T cells were able to control HBV in AAV-HBV and AAV-HLA-A*02 co-infected immunodeficient animals.

Next, the adoptive T-cell therapy approach using natural TCRs was transferred to other preclinically relevant animal models, specifically rhesus macaque and pig. Human HBV-specific TCRs were expressed in macaque T cells and were specifically activated to induce a distinct antiviral effect in co-cultures with HBV-infected HLA-A*02 transduced primary macaque hepatocytes *in vitro*. Moreover, human TCR-engrafted T cells were specifically activated by HBV^+ HLA-$A*02^+$ primary pig hepatocytes *in vitro*. These results demonstrate first steps towards the examination of safety and efficacy of adoptive T-cell therapy for chronic HBV infection using natural TCRs in the rhesus macaque and pig model *in vivo.*

Finally, adoptive T-cell therapy towards HCC expressing the tumor-associated antigen glypican-3 (GPC3) was investigated. HLA-A*02 restricted GPC3-specific TCR P1-1-redirected T cells had previously been demonstrated to induce a profound cytotoxic effect towards hepatoma cells *in vitro*. Here, their potential to eradicate tumor cells in an HCC xenograft mouse model was explored. TCR P1-1-equipped T cells were able to slow down growth of HCC xenograft tumors, however, GPC3 expression was found to be downregulated in established tumors. Therefore, other cell lines were tested for their suitability as target cells for the recognition and elimination of TCR P1-1^+ T cells. During this process, TCR P1-1-redirected T cells did not reveal specificity for the predicted peptide $GPC3_{367}$ but demonstrated HLA-A*02 alloreactivity.

Taken together, the present thesis provides evidence, that immunotherapeutic strategies based on therapeutic vaccination and adoptive T-cell transfer have great potential towards cure of chronic HBV infection. New mouse models for chronic HBV infection as well as HCC were generated and evaluated and might represent powerful tools to study other therapeutic interventions. Moreover, the basis was laid to translate the TCR approach towards functionally relevant preclinical animal models.

ZUSAMMENFASSUNG

Obwohl ein effektiver Impfstoff verfügbar ist, stellt die Hepatitis B Virus (HBV) Infektion mit weltweit 257 Millionen chronisch infizierten Patienten ein großes Gesundheitsproblem dar. Chronische HBV Infektion ist mit einem hohen Risiko verbunden, an Leberzirrhose oder hepatozellulärem Karzinom (HCC) zu erkranken, und mehr als 800.000 Menschen sterben jährlich an den Folgeerkrankungen. Die verfügbaren Behandlungsmöglichkeiten sind selten im Stande die Infektion zu heilen, da die kovalent geschlossene zirkuläre DNA (cccDNA) als virales Template nicht beseitigt wird. HBV-spezifische Immunantworten, insbesondere T-Zellen, scheinen eine essentielle Rolle bei der Heilung der HBV Infektion zu haben und sind bei chronischen HBV Infektionen funktionell beeinträchtigt. Neue immuntherapeutische Ansätze versuchen daher, die adaptive Immunantwort des Patienten wiederherzustellen, um virusinfizierte oder entartete Zellen zu erkennen und zu eliminieren. In dieser Dissertation wurde das Potential verschiedener immuntherapeutischer Strategien gegen chronische HBV Infektion und HCC untersucht. Frühere Untersuchungen zu diesen therapeutischen Ansätzen wurden entweder noch nicht *in vivo* getestet oder nur in HBV-transgenen Mäusen durchgeführt, in denen die Viruselimination nicht erreicht werden kann.

Um eine chronische HBV Infektion nachzuahmen, wurden im ersten Teil dieser Arbeit virale Vektoren, die das HBV Genom in Maus Hepatozyten einbringen, erzeugt und verglichen. Das HBV-Genom wurde mittels adeno-, high capacity adeno – sowie adeno-assoziierten viralen (AAV) Vektoren vermittelt und führte zur Persistenz von HBV in immunkompetenten Mäusen. Die Daten zeigten, dass der AAV-vermittelte HBV-Genomtransfer am effizientesten war, da dieser selbst bei hohen Titern eine persistente virale Replikation induzierte, ohne eine Immunantwort hervorzurufen. Darüber hinaus zeigten AAV-HBV-transduzierte Hepatozyten die Bildung von cccDNA.

Im zweiten Teil der Dissertation wurden immuntherapeutische Ansätze gegen chronische HBV Infektion und HBV-assoziiertes HCC *in vivo* evaluiert. Hier wurde das neu etablierte AAV-HBV-Modell angewandt. Zuerst wurde ein bereits zuvor beschriebener therapeutischer Vakzinierungsansatz untersucht. Die Vakzinierung induzierte HBV-spezifische B- und T-Zellantworten und war in der Lage, die HBV-spezifische Immuntoleranz zu brechen. Jedoch beeinflussten hohe HBV-Antigen Level sowie eine verlängerte Exposition gegenüber HBV-Antigenen den therapeutischen Effekt negativ. Neben der therapeutischen Vakzinierung stellt der adoptive Transfer von HBV-spezifischen T-Zellen einen weiteren Ansatz zur Wiederherstellung der Immunantwort dar. Daher wurde das therapeutische Potential von genetisch modifizierten T-Zellen untersucht. T-Zellen, die einen bereits zuvor beschriebenen chimären Antigenrezeptor, spezifisch für die HBV-Hüllproteine (S-CAR), exprimieren, zeigten eine starke antivirale Aktivität in AAV-HBV-infizierten immundefizienten Mäusen. Obwohl diese

in hohen Zellzahlen persistierten, waren sie aber nicht in der Lage, HBV vollständig zu eliminieren. Des Weiteren wurde die therapeutische Wirkung von T-Zellen, die mit HBV-spezifischen humanem Leukozyten Antigen (HLA) A*02 restringierten natürlichen T-Zell Rezeptoren (TCR) ausgestattet wurden, analysiert. Hierzu wurde ein Mausstamm, der HLA-A*02 exprimiert, verwendet. Es konnte gezeigt werden, dass die Hepatozyten dieser Mäuse endogen prozessierte Peptide nur sehr schlecht präsentieren. Eine AAV-vermittelte Expression von HLA-A*02 in murinen Hepatozyten konnte dieses Problem lösen und HBV-spezifische TCR-exprimierende T-Zellen waren in der Lage, HBV in AAV-HBV und AAV-HLA-A*02 ko-infizierten Tieren zu bekämpfen.

Als nächstes wurde der adoptive T-Zell-Therapieansatz unter Verwendung natürlicher TCRs auf andere präklinisch relevante Tiermodelle, den Rhesus-Makaken und das Schwein, übertragen. Humane HBV-spezifische TCRs wurden in T-Zellen von Rhesus Makaken exprimiert und hatten *in vitro* eine deutliche antivirale Wirkung in Ko-Kulturen mit HBV-infizierten HLA-A*02 tranduzierten primären Makaken Hepatozyten. Darüber hinaus wurden humane TCR-exprimierende T-Zellen *in vitro* spezifisch durch HBV^+ $HLA\text{-}A*02^+$ primäre Schweine Hepatozyten aktiviert. Diese Ergebnisse stellen erste Schritte zur Untersuchung der Sicherheit und Wirksamkeit der adoptiven T-Zell-Therapie unter Verwendung natürlicher TCRs bei chronischer HBV Infektion im Rhesus-Makaken- und Schweine-Modell *in vivo* dar.

Schließlich wurde ein adoptiver T-Zell-Therapieansatz gegen HCC, welches das Tumor-assoziierte Antigen Glypican-3 (GPC3) exprimiert, analysiert. Bereits zuvor wurde gezeigt, dass T-Zellen, die mit dem HLA-A*02 restringierten GPC3-spezifischen TCR P1-1 ausgestattet wurden, *in vitro* eine ausgeprägte zytotoxische Aktivität gegenüber Hepatomzellen haben. In dieser Arbeit wurde ihr Potential zur Eliminierung von Tumorzellen in einem HCC-Xenograft-Mausmodell untersucht. TCR P1-1 exprimierende T-Zellen waren in der Lage, das Wachstum von HCC-Tumoren zu verlangsamen. Allerdings wurde festgestellt, dass die GPC3-Expression in etablierten Tumoren herunterreguliert wurde. Daher wurden andere Zelllinien auf ihre Eignung als Zielzellen für die Erkennung und Eliminierung von TCR $P1\text{-}1^+$ T-Zellen getestet. Während dieses Prozesses zeigten TCR P1-1-exprimierende T-Zellen keine Spezifität für das Peptid $GPC3_{367}$, sondern wiesen HLA-A*02 Alloreaktivität auf.

Zusammengefasst zeigt die vorliegende Dissertation, dass immuntherapeutische Strategien, die auf therapeutischer Vakzinierung und adoptivem T-Zell-Transfer basieren, großes Potential zur Heilung chronischer HBV Infektionen besitzen. Neue Mausmodelle für chronische HBV Infektion sowie HCC wurden entwickelt und evaluiert und repräsentieren leistungsstarke Werkzeuge zur Untersuchung unterschiedlicher therapeutischer Ansätze. Darüber hinaus wurde die Basis gelegt, den TCR-Ansatz auf andere funktionell relevante präklinische Tiermodelle zu übertragen.

ABBREVIATIONS

μg	microgram
μl	microliter
μm	micrometer
AAV	adeno-associated virus
Ad	adenovirus
ADCC	antibody-dependent cellular cytotoxicity
AFP	α -fetoprotein
ALT	alanine amino transferase
APC	antigen-presenting cell
BFA	brefeldin-A
bp	base pair
BSA	bovine serum albumin
CAR	chimeric antigen receptor
Casp-3	caspase-3
cccDNA	covalently closed circular DNA
CD	cluster of differentiation
cDNA	complementary DNA
CHB	chronic hepatitis B
CMV	cytomegalovirus
CTLA-4	cytotoxic T-lymphocyte-associated protein 4
DMEM	Dulbecoo's Modified Eagle Medium
DMSO	dimethyl sulfoxide
DNA	deoxyribonucleic acid
E : T	effector to target ratio
EDTA	ethylenediaminetetraacetic acid
EGFRt	truncated epidermal growth factor receptor
ELISA	enzyme-linked immunosorbent assay
ELISPOT	enzyme-linked immuno spot assay
FACS	fluorescence-activated cell sorting
FasR	first apoptosis signal receptor
FCS	fetal calf serum
Fluc	*firefly* luciferase
GAPDH	glyceraldehyde-3-phosphate dehydrogenase gene
GFP	green fluorescent protein
Gluc	*Gaussian* luciferase

GPC3	glypican-3
gRNA	guide RNA
GrzB	granzyme B
h	human
HBc	HBV core protein
HBcAg	hepatitis B core antigen
HBeAg	hepatitis B e antigen
HBsAg	HBV surface antigen
HBV	hepatitis B virus
HCA	high capacity adenovirus
HCC	hepatocellular carcinoma
HLA	human leukocyte antigen
hβ_2m	human β_2-microglobulin
i.m.	intramuscularly
i.p.	intraperitoneal
i.v.	intravenously
ICS	intracellular cytokine staining
IFNγ	interferon γ
IgG	immunoglobulin G
IL-10	interleukin 10
IL-2	interleukin 2
Iono	ionomycin
ITAM	immunoreceptor tyrosine-based activation motifs
ITR	inverted terminal repeats
IU	international unit
IVIS	In Vivo Imaging System
LAL	liver-associated lymphocyte
m	murine
MACS	magnetic-activated cell sorting
mg	milligram
MHC	major histocompatibility complex
min	minutes
ml	milliliter
mM	millimolar
MOI	multiplicity of infection
mRNA	messenger RNA
mV	millivolt

MVA	modified vaccinia virus Ankara
nd	not detected
NEAA	non-essential amino acids
NFAT	nuclear factor of activated T cells
ng	nanogram
NK cell	natural killer cell
nm	nanometer
nM	nanomolar
ns	not significant
NTCP	sodium taurocholate cotransporting polypeptide
OBI	occult hepatitis B infection
ORF	open reading frame
PBMC	peripheral blood mononuclear cells
PBS	phosphate buffered saline
PCR	polymerase chain reaction
PD-1	programmed cell death protein 1
PEG	polyethylene glycol
PEI	polyethylenimine
PEIU	Paul-Ehrlich-Institute-unit
Pen/Strep	penicillin / streptomycin
pfu	plaque forming unit
pg	picogram
PMA	phorbol myristate actetate
PMaH	primary macaque hepatocyte
PMH	primary murine hepatocyte
PrP	prion protein gene
qPCR	quantitative PCR
rcDNA	relaxed circular DNA
RNA	ribonucleic acid
RNase	ribonuclease
rpm	rounds per minute
RPMI	Roswell Park Memorial Institute Medium
s.c.	subcutaneous
scFv	single chain variable fragment
SCID	severe combined immunodeficiency
SD	standard deviation
SEB	staphylococcal enterotoxin B

SEM	standard error of mean
T	temperature
t	time
TAA	tumor-associated antigen
TAP	transporters associated with antigen processing
TCM	T-cell medium
TCR	T cell receptor
TIL	tumor-infiltrating lymphocyte
Tim-3	T-cell immunoglobulin and mucin-domain containing-3
TKI	tyrosine kinase inhibitor
TMB	3,3',5,5"-tetramethylbenzidine
TNF α	tumor necrosis factor α
T_{reg}	regulatory T cell
TTR	transthyretin
uPA	urokinase-type plasminogen activator
vg	viral genomes
WT	wildtype
XTT	2,3-Bis-(2-Methoxy-4-Nitro-5-Sulfophenyl)-2H-Tetrazolium-5-Carboxanilide

1 INTRODUCTION

1.1 Chronic hepatitis B virus infection

Despite the availability of an effective vaccine, worldwide approximately 257 million humans are suffering from chronic hepatitis B virus (HBV) infection accompanied by a high risk of developing liver cirrhosis and hepatocellular carcinoma. In 2015, more than 850,000 people died from HBV-associated diseases (WHO, 2017).

1.1.1 Hepatitis B virus

The hepatitis B virus, a member of the *Hepadnaviridae* family, is a small, enveloped, partially double stranded DNA virus that was first described in 1970 (Dane et al., 1970). Although HBV is a DNA virus, replication is through an RNA-replicative intermediate, and HBV therefore belongs to the para-retroviruses (Hu and Liu, 2017). Based on sequence comparisons, HBV is classified into ten genotypes, A to J, with each genotype exhibiting a distinct geographic distribution (Kramvis, 2014).

The infectious HBV virion (Dane particle) exhibits a spherical, double-shelled structure of about 42 nm in diameter. It consists of an outer lipoprotein envelope composed of hepatitis B surface proteins which surrounds an inner nucleocapsid containing the viral DNA genome (Dane et al., 1970; Ganem, 1991). The nucleocapsid is composed of 180 – 240 subunits of the HBV core protein (HBc) and contains a partially double-stranded relaxed circular DNA (rcDNA) of about 3.2 kb, as well as the virally encoded polymerase (Figure 1.1 A). Beside the Dane particles, non-infectious subviral particles are released from infected cells that can be detected in patient blood as hepatitis B surface antigen (HBsAg). Subviral particles are either filaments of variable lengths with a width of 22 nm or smaller spherical structures with a diameter of 20 nm (Ganem, 1991).

With each nucleotide exhibiting coding function, the highly organized genome encodes four partially overlapping open reading frames (ORFs): presurface-surface (preS-S), pre-core-core (preC-C), P and X (Figure 1.1 B). The viral envelope proteins are encoded by the preS-S ORF, whereby differential initiation of transcription of three in frame start codons result in related but functionally distinct proteins: the large (L), middle (M) and small (S) envelope proteins. HBc and hepatitis B e protein are encoded by the preC-C ORF, depending on the alternative initiation of translation at two in-frame start codons. HBc subunits form the viral nucleocapsid whereas the proteolytically processed and secreted hepatitis B e antigen (HBeAg) seems to have immunoregulatory functions. In detail, presence of HBeAg seems to prevent anti-HBc

seroconversion by eliciting tolerance in HBc/HBeAg-specific T cells and therefore mediates humoral- as well as cell-mediated immune evasion (Chen et al., 2004; Milich and Liang, 2003). Moreover, serum HBeAg is used as characteristic diagnostic marker of HBV infection (Ganem and Prince, 2004). Curiosly, loss of HBeAg is correlated with both, clearance of acute infection as well as establishment of chronic infection (Venkatakrishnan and Zlotnick, 2016). The viral polymerase protein is encoded by the P ORF and can be divided in three functional domains: reverse transcriptase, RNaseH and terminal protein serving as primer during synthesis of rcDNA genome (Seeger and Mason, 2015). The X ORF encodes a nonstructural protein, the HBx protein which is essential to initiate and maintain virus replication after infection and may contribute to the oncogenic potential of HBV (Bouchard and Schneider, 2004; Lucifora et al., 2011). Moreover, HBx might have a essential role in the viral life cycle by influencing the epigenetic regulation of HBV transcription (Riviere et al., 2015).

One very important step within the viral life cycle is the formation of the covalently closed circular DNA (cccDNA) serving as transcription template. After HBV enters the cell, the capsid is transported to the nucleus where it releases the viral DNA genome, the rcDNA. Cellular enzymes subsequently convert this rcDNA to cccDNA, the persistence form of HBV serving as template for mRNA synthesis (Seeger and Mason, 2015).

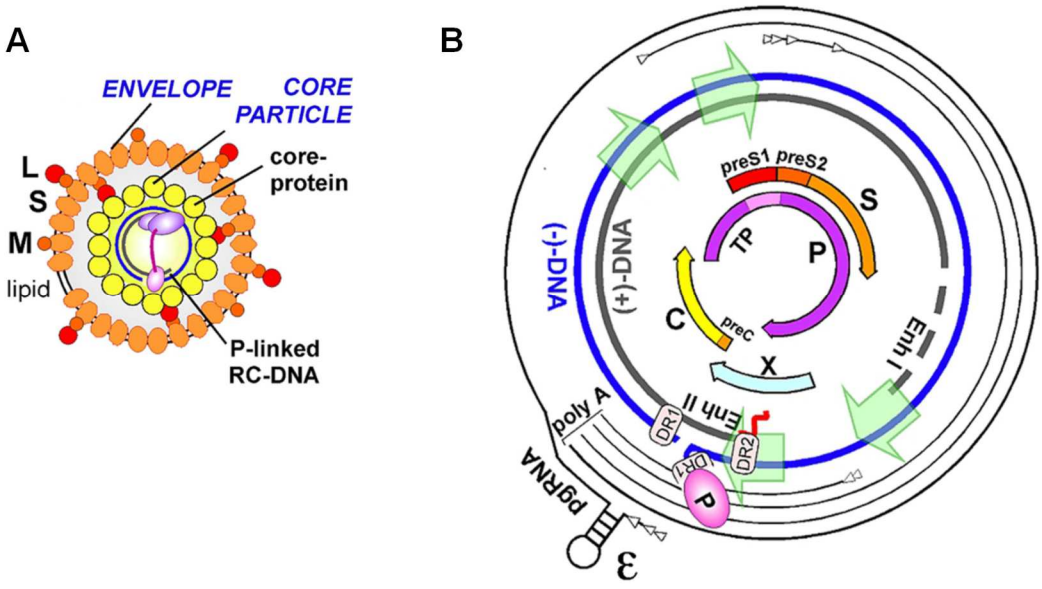

Figure 1.1 Virion structure and genome organization of HBV.
(A) HBV virions consist of an outer envelope which is composed of lipid-embedded small (S), middle (M) and large (L) surface proteins. The inner icosahedral nucleocapsid is assembled of HBV core proteins and harbors the viral genome as a relaxed-circular (rc) DNA that is covalently linked to the polymerase (P) protein. **(B)** Genome organization: Outer thin lines represent mRNA transcripts with transcription starts marked as arrowheads. ε: encapsidation signal on pregenomic (pg) RNA. Inner thicker circle shows the full-length minus (-) strand and the incomplete plus (+) strand. The innermost arrows indicate the translated HBV proteins: envelope proteins (preS1, preS2, S), polymerase (P) protein, X protein, core (C) and pre-core protein (preC). Green arrows: Enh I / Enh II transcriptional enhancers. DR1 / DR2: direct repeats. TP the terminal protein domain of P protein (Nassal, 2015).

1.1.2 Pathogenesis of HBV infection

Infection with HBV can be acute and self-limiting or become chronic. 95 % of adults are able to clear the infection, about half of them do not exhibit any symptoms, however, acute infections also cause a mortality rate of 0,5-1 % as a result of fulminant hepatitis and liver failure. HBV is transmitted via blood, blood products, unprotected sexual contact or by vertical transmission from mother to the neonate. The latter are very likely to develop chronic disease, as 90 % of infections of children up to six months of age result in chronicity. Next to the young age, immunosuppression is considered a risk factor to develop chronic hepatitis B (CHB) (Peeridogaheh et al., 2018). Presence of HBsAg in blood or serum for more than 6 months defines the chronic course of HBV infection (Cornberg et al., 2011). Most chronically infected patients die from sequelae of chronic HBV infection, like hepatocellular carcinoma. HBV itself has been demonstrated to be non-cytopathic, but the host immune response mediates inflammation and subsequent liver damage. For complete virus eradication, the cooperation of innate and adaptive immune response is required (Guidotti and Chisari, 2006).

The cell-mediated arm of adaptive immunity executed by $CD4^+$ helper and $CD8^+$ effector T cells has been observed to be strong and multispecific during an acute infection and bears a key role in virus clearance (Maini et al., 1999). In contrast, HBV-specific T cells are absent or seem to be dysfunctional in chronically infected carriers. Progressive functional exhaustion is characterized by increased expression of inhibitory receptors like PD-1 (programmed cell death protein 1), CTLA-4 (cytotoxic T-lymphocyte-associated protein 4), Tim-3 (T-cell immunoglobulin and mucin-domain containing-3) and 2B4 (CD244) with their corresponding ligands being upregulated in the liver (Boni et al., 2007; Raziorrouh et al., 2010; Schurich et al., 2011; Wang et al., 2014a).

In order to clear HBV infection, virus-specific $CD8^+$ cytotoxic T cells induce apoptosis of infected cells. Furthermore, pro-inflammatory cytokines like for instance IFNγ and TNFα exhibit a distinct antiviral effect (Guidotti et al., 1999; Thimme et al., 2003; Xia et al., 2016). Beside $CD8^+$ T cells, $CD4^+$ T helper cells play an important role in eliminating HBV. There is evidence that HBcAg-specific $CD4^+$ T cells are detected within four weeks after initial infection in case of an acute infection (Ferrari et al., 1990). They are essential to control HBV infection through induction and maintenance of $CD8^+$ T- and B-cell responses and might elicit direct antiviral effect by secretion of pro-inflammatory cytokines. Antibodies produced by B cells recognizing HBV envelope proteins are essential to eradicate the virus. They can be detected in patients who cleared the infection, but are missing in chronically infected patients (Chisari et al., 2010). Next to the B-cell response, a potent virus-specific T-cell response is absent, or T-cells are functionally impaired in chronic HBV carriers as mentioned above. Next to this exhausted virus specific T cells, other factors might be involved in virus persistence. For instance it has been

demonstrated that high viral loads lead to increased numbers of regulatory T cells (T_{regs}) which comes along with increased production of the inhibitory cytokine IL-10 (Peng et al., 2008). Furthermore, dysfunctionality in dendritic cells resulting in impaired activation of T cells has been associated with chronic HBV infection (Op den Brouw et al., 2009; Wang et al., 2001).

1.1.3 HBV-induced hepatocellular carcinoma

Worldwide, hepatocellular carcinoma (HCC) has become the third most frequent cancer (Ghouri et al., 2017) with average survival rates between six and 20 months (Byam et al., 2013). It represents the second most frequent cause of cancer related death and is estimated to be responsible for approximately 700,000 deaths per year (Sartorius et al., 2015).

Most cases of HCC are associated with chronic liver disease. This includes chronic hepatitis B or C virus infections which are predicted to account for over 90 % of all HCC cases (Jemal et al., 2011; Parkin, 2006). Also, other risk factors such as alcohol abuse, high-fat diet induced non-alcoholic steatohepatitis (NASH), a form of non-alcoholic fatty liver disease (NAFLD) or diabetes can lead to HCC formation (El-Serag et al., 2004; Forner et al., 2012). In Europe, North America and Japan chronic HCV infection together with alcohol abuse are major risk factors for developing HCC, whereas in eastern Asia and sub-Saharan Africa, the high prevalence of chronic infection with HBV explains the high incidence of HCC (El-Serag, 2011). Patients suffering from chronic HBV infection exhibit an up to 30-fold increased risk with approximately 25 % of them developing HCC (Yoo et al., 2018). Strikingly, even inactive carriers for HBV, characterized by HBV DNA <10.000 copies/ml, no serum HBeAg, normal liver enzymes and no signs of liver cirrhosis, still have a five-fold increased risk of developing HCC (Chen et al., 2010a).

Three major molecular mechanisms leading to HCC formation following chronic HBV infection have been proposed: i) integration of the viral genome into the host genome which results in altered expression of host genes (e.g. tumor-suppressor genes, proto-oncogenes), ii) viral protein expression (especially X protein) and iii) an increased incidence of genetic damage upon proliferation of hepatocytes to compensate cell loss during chronic inflammation (Peeridogaheh et al., 2018).

1.2 Treatment of chronic HBV infection and HCC

Treatment of chronic HBV infection aims at reducing viremia, improving hepatic function, preventing cirrhosis and HCC and most importantly inducing complete viral clearance. Successful therapy, also referred to as `functional cure´, is defined by the loss of HBsAg and/or seroconversion to anti-HBs and undetectable HBV DNA in serum. However, even if functional cure is achieved, without eradicating cccDNA, patients are still exposed to an increased risk

to develop HCC (Dargan et al., 2017), and may reactivate HBV for instance under immunosuppression.

1.2.1 Current therapies of chronic HBV infection

Currently, standard of care therapy is based on IFNα or pegylated IFNα and nucleos(t)ide analogues, but they hardly achieve virus elimination. Treatment with IFNα induces direct antiviral as well as immunomodulatory effects. However, due to induction of severe side effects including fever, myalgias, thrombocytopenia and depression, the dosing of IFNα is limited (Ganem and Prince, 2004). Nucleos(t)ide analogues selectively target the viral reverse transcriptase and result in strong viral suppression as long as drugs are taken (Wang et al., 2014b). FDA-approved nucleos(t)ide analogues are lamivudine, adefovir, entecavir, telbivudine, tenofovir disoproxil fumarate and tenofovir alafenamide and are well-tolerated (Yoo et al., 2018). As they do not target cccDNA, however, reactivation of HBV transcription and replication occurs upon treatment cessation (Revill et al., 2016).

Taken together, none of the approved therapies leads to viral clearance, explaining the need to identify more promising therapeutic strategies to treat patients suffering from chronic HBV infection.

1.2.2 Current therapies of HCC

Curative treatment options for HCC like tumor resection or liver transplantation are only available for early stage HCC patients (Bruix et al., 2016). Due to advanced tumor stage and preceding cirrhosis, less than 30 % of HCCs are suitable for hepatectomy at the time of diagnosis (Llovet and Bruix, 2008). For advanced-stage patients or unresectable HCC, systemic therapy with the multi-targeted tyrosine kinase inhibitor (TKI) sorafenib which inhibits tumor cell proliferation and angiogenesis has become standard of care in over 70 countries. Sorafenib, however, is only able to improve the median overall survival by approximately three months (Cheng et al., 2009; Llovet et al., 2008). As sorafenib treatment is characterized by limited efficacy and various adverse effects, significant effort was put into identifying novel and more effective TKIs. After several clinical trials failed to demonstrate improved efficacy of other TKIs, regorafenib was approved as second-line therapy (Bruix et al., 2017). Most recently, lenvatinib was approved as first-line therapy for unresectable HCC as its safety, tolerability and efficacy was verified. Unfortunately, overall survival is not improved compared to sorafenib treatment resulting in just three to four months prolonged survival (Kudo et al., 2018).

In summary, prognosis of HCC remains poor explaining the high need for new therapeutic approaches to treat HCC or eliminate HBV as one of its major causes.

1.3 Novel immunotherapeutic strategies for treatment of chronic HBV infection and HCC

As treatment options for chronic HBV infection and HCC are still limited, new therapies are urgently needed. Promising approaches are immunotherapies which aim to induce or boost the patient's adaptive immune response to recognize and eliminate virus infected or malignant cells.

A potent HBV-specific T-cell response is associated with clearance of HBV infection (Maini et al., 1999). For HCCs, lymphocyte and in particular $CD8^+$ T-cell infiltrations have been demonstrated to be associated with good prognosis (Hiroishi et al., 2010; Unitt et al., 2006) rendering chronic HBV infections as well as HCC as suitable targets for immunotherapies. Moreover, HCC is characterized by expression of tumor-associated antigens (TAA), for instance glypican-3 (GPC3) and alpha-fetoprotein (AFP). Those tumor-associated antigens are barely expressed in healthy human tissue, but expression is reactivated in up to 60 % and 80 % of all HCC, respectively (Butterfield et al., 2001; Komori et al., 2006). Furthermore, in HBV-associated HCCs, viral proteins may still be expressed on tumor cells, rendering these cells as a target for HBV-specific immune-based therapies. Therefore, the induction of effector cells that specifically recognize GPC3, AFP or HBV proteins can help to eliminate tumor cells as well as virus-infected cells or at least control HCC growth.

1.3.1 The concept of adaptive immunity

The adaptive immune system is responsible for the elimination of pathogen-infected or malignant cells. Lymphocytes are the 'effector cells' of adaptive immunity and are subdivided into B lymphocytes or B cells and T lymphocytes or T cells. Both originate from pluripotent hematopoietic stem cells in the bone marrow. B cells depict the humoral part of the adaptive immune system as they differentiate into plasma cells that produce antibodies to neutralize extracellular antigens. T lymphocytes represent the cellular arm of the adaptive immune response and specifically recognize intracellular antigens. Their maturation and differentiation are taking place in the thymus which is why they are called thymus-dependent (T) lymphocytes or T cells. After completion of their development, they enter the bloodstream, migrate into a peripheral lymphoid organ and recirculate between blood and peripheral lymphoid tissue. Mature recirculating T cells stay naive T cells until they encounter their specific antigen and subsequently proliferate and differentiate into effector T cells. These T cells are also called "armed effector cells" as they have the ability to act vary rapidly upon activation. Therefore, they bear a pivotal role in recognition and elimination of virus-infected and malignant cells, whereby their cytotoxicity is mediated by granule exocytosis, Fas-mediated programmed cell death and targeted cytokine production (Murphy and Weaver, 2016).

The receptor responsible for antigen-recognition of T cells, the T-cell receptor (TCR) does not recognize antigen directly, instead short peptide fragments of pathogen-derived protein antigens, which are bound to major histocompatibility complex (MHC) molecules on the surface of other cells are detected. A schematic illustration of the TCR-MHC complex is depicted in Figure 1.2. The TCR consists of a highly variable α– and β–chain heterodimer, linked by a disulfide bond. α and β subunits both consist of a constant (c) and a variable (v) domain, whose variety is generated by somatic recombination during T-cell maturation. The variable domain mediates the recognition of antigen and is responsible for TCR specificity. Beside the extracellular domains, the TCR further consists of a transmembrane region and a short intracellular domain. Furthermore, the complete TCR complex contains the invariant accessory chains CD3γ, CD3δ, and CD3ε, which together build the CD3 complex as well as the CD3ζ chains, which are present as a largely intracytoplasmic homodimer. The CD3 complex is required for signaling via the receptor. TCR signaling is mediated via immunoreceptor tyrosine-based activation motifs (ITAMs) within the CD3 complex. Phosphorylation of ITAMs leads to induction of the signaling cascade upon antigen recognition. Finally, the activation of several transcription factors, for instance NFκB and NFAT (nuclear factor of activated T cells) is induced and leads to expression of genes responsible for cell proliferation, differentiation and effector functions (Murphy and Weaver, 2016).

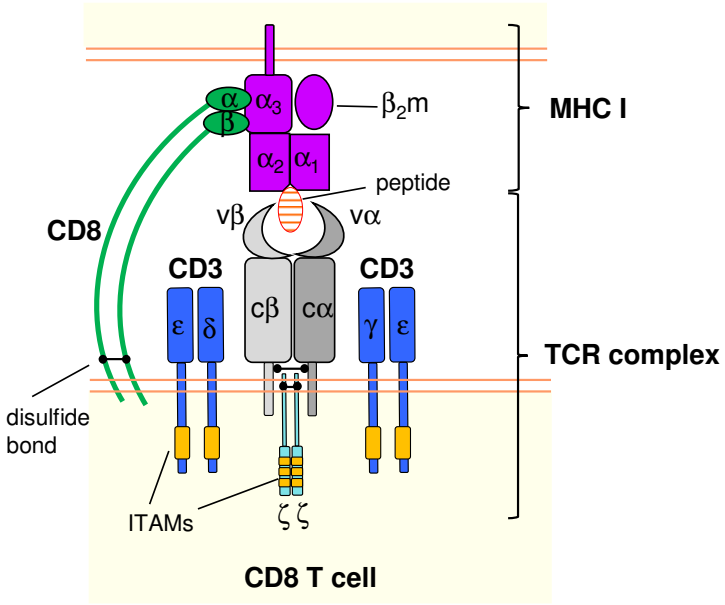

Figure 1.2 The T-cell receptor (TCR) complex binding to an MHC-peptide complex.
MHC I consists of a membrane anchored α-chain, consisting of three domains (α_1, α_2, α_3) and the not-covalently associated β_2-mircoglobin (β_2m). The TCR complex is made up by the TCR heterodimer (built by an α and a β chain), the associated CD3 complex (extracellular: ε, δ, γ and intracellular: ζ homodimer) and the CD8 co-receptor. Variable (v) domains of the TCR are responsible for antigen recognition presented in the peptide-binding groove (built by (α_1 and α_2) of the MHC I molecule. Signaling of the TCR-complex is achieved via phosphorylation of ITAMs (immunoreceptor tyrosine-based activation motifs).

T cells are classified into two subpopulations, $CD4^+$ T helper cells and $CD8^+$ cytotoxic T cells. $CD4^+$ T cells differentiate into several subsets bearing various effector functions. T_h1, T_h2 and T_h17 represent the main functional classes and are defined on the basis of secretion of different cytokine combinations (T_h1: IFNγ; T_h2: IL-4, IL5, IL-13; T_h17: IL-17). The main functions of T_h1 and T_h2 $CD4^+$ T cells include providing support for $CD8^+$ T cells and to help B cells for antibody production. In contrast, T_h17 $CD4^+$ T cells help to recruit cells from the innate immune system to sites of infection. Another important $CD4^+$ T cell subset is represented by T_{regs} which are responsible to suppress T-cell responses for instance by secreting inhibitory cytokines like IL-10 or TGFβ and consuming IL-2 (Murphy and Weaver, 2016).

Furthermore, the TCR is associated either with the CD4 or the CD8 co-receptor. The co-receptor is inseparably involved in signaling of the T cell. $CD4^+$ T cells recognize peptides presented by MHC class II which is predominantly expressed by antigen-presenting cells (APC) like dendritic cells, macrophages and B cells. In cytotoxic T cells, the CD8 co-receptor, which is composed of a disulfide-bond-linked αβ-heterodimer, is responsible for recognition of MHC I at its α_3 domain. The MHC I molecule is ubiquitously expressed by all nucleated cells and composed of four domains, three of them are contributed by the α-chain (α_1, α_2, α_3). The smaller β_2-microglobulin chain represents the fourth domain of the MHC I molecule and is non-covalently linked with the α-chain. The high polymorphism of MHC I molecules is determined by the peptide-binding groove of MHC I which is generated by α_1 and α_2 and is responsible for peptide specificity. Cytosolic proteins are processed by the proteasome and reach the endoplasmic reticulum via transporters associated with antigen processing (TAP). Here, short fragments of these polypeptides, usually with a length of eight to ten amino acids, are loaded onto MHC I. Subsequently, the MHC I-peptide complex is transported to the cell surface via the Golgi. Human MHC I and MHC II molecules are each divided into three human leukocyte antigen (HLA) genes: HLA-A, HLA-B, HLA-C and HLA-DR, HLA-DP und HLA-DQ respectively (Murphy and Weaver, 2016).

The described concepts of the adaptive immune response can be used for the design of novel therapeutic approaches.

1.3.2 Antibody-based therapies

1.3.2.1 Monoclonal antibodies

The administration of a monoclonal antibody directed against TAAs or viral proteins is one option to induce a cytotoxic immune response towards virus infected or tumor cells. Usually, the effect of antibody-dependent cellular cytotoxicity (ADCC) is exploited. This means that the target cell is coated with the antibody and thus gets opsonized. Thereafter effector cells like natural killer (NK) cells recognize those opsonized cells and initiate cell lysis.

In 1986, the first monoclonal CD3 specific antibody muromonab (also called OKT3) leading to apoptosis of T cells and subsequently to a reduced risk of transplant rejection was approved for solid organ transplant recipients who became steroid resistant (Hooks et al., 1991). Nowadays, a huge number of monoclonal antibodies are used for treatment of various diseases, including different types of cancer.

For therapy of $GPC3^+$ HCC, treatment with the monoclonal antibody codrituzumab (GC-33) revealed ADCC-dependent elimination of HCC cells in preclinical studies (Ishiguro et al., 2008; Nakano et al., 2009; Takai et al., 2009; Zaghloul et al., 2015). Phase I clinical studies demonstrated promising results (Ikeda et al., 2014; Zhu et al., 2013), however, in a randomized phase II placebo controlled study, codrituzumab did not exhibit an anti-cancer effect (Abou-Alfa et al., 2016). Additional attempts to reveal that codrituzumab provides an additive effect on standard of care therapy with sorafenib were performed. Again, combination of codrituzumab and sorafenib was not more effective than monotreatment with sorafenib in advanced HCCs (Abou-Alfa et al., 2017).

Hepatitis B immune globulin (HBIG) derived from plasma of vaccinated patients with high anti-HBsAg titers is used as passive vaccination for instance during pregnancy to prevent mother-to-child transmission (Eke et al., 2017). Recently, the therapeutic potential of a monoclonal antibody against chronic HBV infection was found to substantially suppress HBV in mouse models (Zhang et al., 2016).

1.3.2.2 Checkpoint inhibitors

Antibodies that inhibit the so-called immune checkpoints represent an approach to trigger anti-tumor immunity. Thereby immune-inhibitory pathways that are activated by cancer cells are blocked. These immune checkpoints include PD-1 and its ligand (PD-ligand-1), CTLA-4 or Tim-3.

Once a T-cell is activated via the TCR (signal 1) and typically CD28 (signal 2), the inhibitory receptor CTLA-4 is translocated to the cell surface. CTLA-4 binds CD80 or CD86, the ligands for CD28, with greater affinity than CD28 (Krummel and Allison, 1995; Walunas et al., 1994).

Shuttling CTLA-4 to the cell surface dampens T-cell activation in two ways: i) prevention of TCR downstream signaling and ii) outcompeting CD28 for its ligands. Therefore, CTLA-4 plays a major role in suppressing T-cell function and thus also T-cell mediated antitumor activity. Blockade of CTLA-4 has been demonstrated to have long lasting anti-tumor effects. Inhibition of CTLA-4 with the antibody ipilimumab led to prolongation of overall survival for patients with metastatic advanced-stage melanoma (Hodi et al., 2010). Nevertheless, ipilimumab treatment goes along with severe side effects, called immune-related adverse effects (Weber et al., 2012). Ipilimumab is approved for metastatic melanoma since 2011, furthermore antitumor effects were also demonstrated in renal cell cancer or metastatic pancreatic adenocarcinoma (Royal et al., 2010; Yang et al., 2007). Another CTLA-4 antibody tremelimumab is being clinically investigated for different applications (Joshua et al., 2015; Maio et al., 2017).

Beside inhibition of CTLA-4, blockade of the PD-1 axis seems to be a promising approach in clinical oncology. PD-1 is also an inhibitory receptor expressed on T cells that inhibits T-cell activation (Parry et al., 2005). Ligands for PD-1, PD-L1 and PD-L2, are expressed on antigen-presenting cells (APCs) and malignant cells. Expression of PD-1 ligands on tumor cells are able to mediate T-cell suppression. Thus, blockade of the PD-1/PD-ligand axis is an auspicious attempt to dampen T-cell inhibition. Two PD-1 antibodies have been approved in 2014 and 2015 for advanced-stage melanoma as their therapeutic effect was even better than treatment with the anti-CTLA-4 antibody ipilimumab with less severe side effects (Robert et al., 2015). The combination of inhibition of CTLA-4 and PD-1 showed even better response rates than mono-treatment with one antibody for advanced-stage melanoma (Larkin et al., 2015). Moreover, PD-1 antibodies are approved for metastatic squamous non-small cell lung carcinoma (Brahmer et al., 2015) and a lot of effort is put to expand the application to other malignancies. Next to PD-1, targeting PD-L1 and therefore preventing T-cell inhibition via the PD-1/PD-L1 axis has demonstrated great success. Antibodies against PD-L1 are approved for the treatment of urothelial carcinoma, metastatic non-small cell lung cancer and metastatic Merkel cell carcinoma (Balar et al., 2017; Gaiser et al., 2018; Peters et al., 2017).

Tim-3 is another exhaustion-associated inhibitory receptor expressed on T cells that dampens the T-cell response and induces apoptosis (Jin et al., 2010). In preclinical models inhibition of Tim-3 in combination with PD-1 resulted in improved anti-tumor activity (Ngiow et al., 2011; Sakuishi et al., 2010). A challenge for the development of antibodies targeting Tim-3 is that several ligands for Tim-3 have been identified: galectin-9, phosphatidylserine, HMGB1, and most recently, CEACAM1 (Chiba et al., 2012; Huang et al., 2015; Nakayama et al., 2009; Zhu et al., 2005). Recent data showed that functional blockade of Tim-3 is targeting the binding to phosphatidylserine and CEACAM1 (Sabatos-Peyton et al., 2018).

For treatment of HCC as well as chronic HBV infection checkpoint inhibitors may be a feasible treatment option. In fact, treatment with the anti-CTLA-4 antibody tremelimumab together with ablation has resulted in accumulation of intratumoral $CD8^+$ T cells in patients with advanced HCC (Duffy et al., 2017). A clinical trial using a PD-1 antibody (nivolumab) for treatment of advanced HCC demonstrated durable objective response rates of 20 % in a non-comparative trial (El-Khoueiry et al., 2017). Additional evidence for the suitability of treating HCC with checkpoint inhibitors comes from analysis of HCC tumor-infiltrating lymphocytes (TILs), in which expression of PD-1, CTLA-4 and Tim-3 were significantly higher than in control tissue or blood. Furthermore, antibodies against PDL-1 or Tim-3 led to increased T-cell proliferation and restored T-cell responses (Zhou et al., 2017). Along the same line, enhanced Tim-3 expression on TILs in combination with T-cell dysfunction negatively correlated with patient survival in HBV-associated HCCs (Li et al., 2012). Moreover, T cells of chronically HBV-infected patients revealed enhanced Tim-3 and CTLA-4 expression along with functional exhaustion, which could be recovered by blocking the Tim-3 or CTLA-4 pathway (Schurich et al., 2011; Wu et al., 2012). Other reports indicate, that T cells from CHB patients demonstrated expression of inhibitory receptors like PD-1, CTLA-4 and Tim-3, however, expression and response to blockade was dominated by PD-1 (Bengsch et al., 2014). In the woodchuck model of HBV infection safety and efficacy of PD-L1 blockade was investigated, but although therapy was found to be safe, efficacy was only observed in a minority of animals, suggesting a monotherapy targeting PD-L1 will only have minor therapeutic benefit (Balsitis et al., 2018). As approved for advanced-stage melanoma, the greatest antitumor or antiviral effect might be in combining checkpoint inhibitors.

1.3.2.3 Next-generation antibodies

Next-generation antibodies have been engineered to enhance potency and safety of first-generation monoclonal antibodies. Moreover, the ability to include non-natural properties became available. A huge variety of antibody formats and architectures are investigated (Kontermann and Brinkmann, 2015). One novel class of those therapeutic antibodies are bispecific antibodies, also called BiTE (bi-specific T-cell engager), which had huge success in preclinical and clinical studies. Bispecific antibodies are able to simultaneously bind a target antigen on the tumor cell surface and the CD3 complex on T cells, resulting in cytotoxicity that is independent of TCR specificity, peptide antigen presentation and co-stimulation (Baeuerle and Reinhardt, 2009). To date, two bispecific antibodies are approved. Catumaxomab was the first bispecific antibody that has been approved in Europe in 2009 for the treatment of malignant ascites with binding moieties for CD3 and epithelial cell adhesion molecule (EpCAM) (Heiss et al., 2010). In 2014 blinatumomab was approved in the US and subsequently in Europe in 2015. Blinatumomab that is targeting CD3 and CD19 is now used as second-line treatment of Philadelphia chromosome-negative relapsed or refractory acute lymphoblastic

leukemia (ALL) (Topp et al., 2015; Topp et al., 2012; Topp et al., 2014; Topp et al., 2011). Additional ongoing studies revealed the potential of blinatumomab for other applications like refractory/relapsed non-Hodgkin lymphoma (Goebeler et al., 2016). More than 30 engineered antibodies are investigated in clinical trials, from which two thirds are focusing on cancer treatment (Thakur and Lum, 2016).

For treatment of $GPC3^+$ HCC, bispecific antibodies targeting CD3 on T cells and GPC3 on tumor cells have been investigated *in vitro* and *in vivo*. Those anti-GPC3/CD3 bispecific antibodies demonstrated effective redirection of T cells towards GPC3 expressing tumor cells and initiated a robust anti-tumor effect (Bi et al., 2017; Ishiguro et al., 2017).

The redirection of T cells towards HBV-infected and thus HBsAg-expressing hepatocytes has also been extensively evaluated *in vitro*. Here, T cells are engaged with bispecific antibodies with binding moieties for CD3 or CD28 on T cells as well as for HBsAg (Hasreiter, 2014; Quitt, 2013). Further studies using an anti-HBsAg/CD3 bispecific antibody revealed promising results in a preclinical model of HBV infection (Kruse et al., 2017).

Bispecific antibodies often aim to directly engage T cells, but other formats are also investigated. For instance, analysis of bispecific antibodies exhibiting specificities against two different epitopes on HBsAg demonstrated profound capacity in neutralizing HBV (Tan et al., 2013). The bispecific antibody was superior to both parental antibodies and approaches like that could help to combat mutations of HBV.

1.3.3 Therapeutic vaccination

In contrast to a prophylactic vaccine that is administered to prevent a certain disease, therapeutic vaccination represents a treatment option after disease occurrence. Therapeutic vaccination aims to induce or boost the patient's defective immune response towards malignant or virus infected cells. A big variety of vaccine formulations is being investigated for the treatment of various malignancies. Thereby, the goal is to overcome the target-specific central tolerance and activate the patient's immune system to ultimately eliminate the pathogen or the tumor.

In order to treat HCC, therapeutic vaccination strategies are clinically investigated, amongst others, a GPC3 peptide vaccine demonstrated safety and induction of cytotoxic T-cell responses in HCC patients in phase I trials (Sawada et al., 2012; Tsuchiya et al., 2017; Yoshikawa et al., 2011) and an improvement of one year recurrence rate in a phase II study (Sawada et al., 2016). Other approaches aim at targeting the tumor-associated antigen AFP and revealed promising result in a phase I trial (Nakagawa et al., 2017). Targeting a combination of tumor antigens, namely AFP, GPC3 and MAGE-A1 by vaccination with tumor

antigen pulsed dendritic cells provided encouraging results for the treatment of HCC, as the median time to progression was enhanced by 25 months in a small study (Lee et al., 2015).

Vaccine therapies have been shown to partially restore HBV-specific immunity *in vitro* (Kosinska et al., 2017). However, results from few clinical trials demonstrated only suboptimal antiviral effects. Existing prophylactic vaccines (Pol et al., 2001) as well as DNA-based vaccines (Fontaine et al., 2015; Mancini-Bourgine et al., 2004) failed to induce an antiviral effect in chronic HBV carriers. Moreover, combination therapies with antivirals (Godon et al., 2014; Vandepapeliere et al., 2007) or new vaccine formulations (Lok et al., 2016; Xu et al., 2013) displayed disappointing results. A DNA vaccine boosted by a poxvirus vector encoding for the HBV envelope protein demonstrated great success in chimpanzees (Pancholi et al., 2001), but failed to induce an antiviral effect in patients suffering from chronic HBV infection (Cavenaugh et al., 2011).

It is of utmost importance to induce both, humoral and cellular immune responses in order to break immune tolerance and induce or boost functional HBV-specific immune responses. One approach towards this goal is to include a recombinant viral vector to the vaccination scheme, for instance modified vaccinia virus Ankara (MVA), to a protein-prime vaccination strategy.

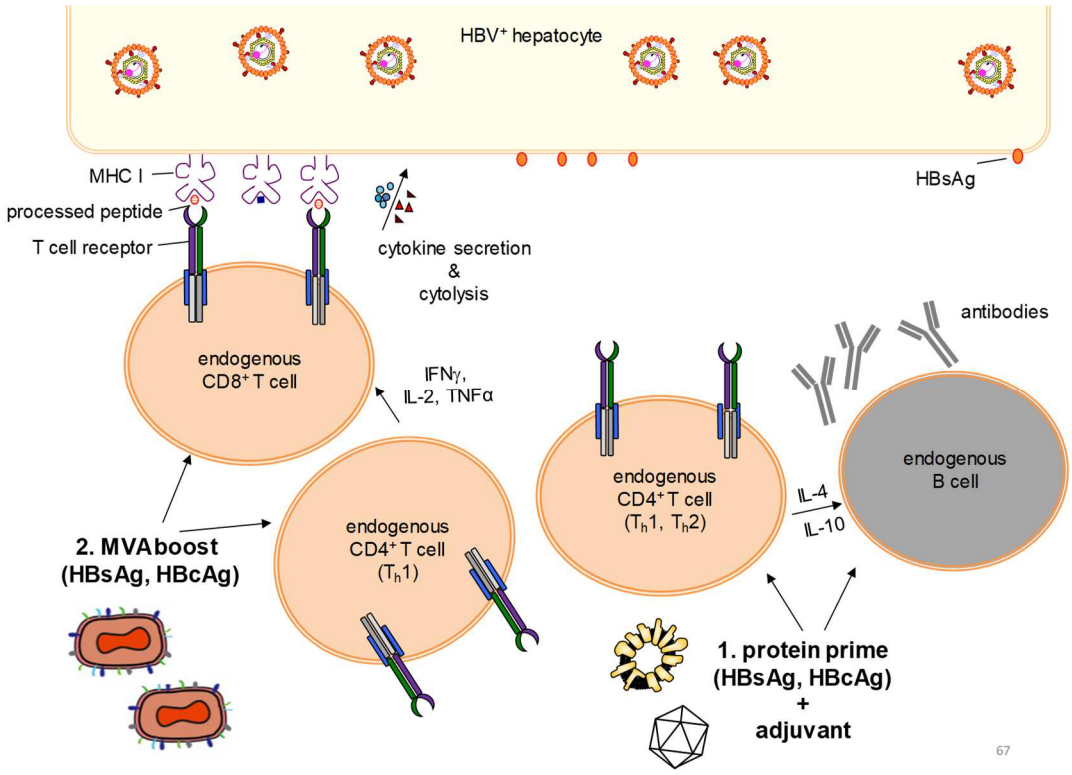

Figure 1.3 Induction of humoral and cellular HBV-specific immune response by heterologous prime/boost vaccination.
Therapeutic vaccination to treat chronic HBV infection includes: i) protein priming using HBsAg, HBcAg and an adjuvant to induce a B-cell-mediated antibody response and to prime T-cell responses, ii) boost with a recombinant MVA (modified vaccinia virus Ankara) expressing HBsAg and HBcAg to trigger cytotoxic T-cell responses towards HBV-infected hepatocytes.

Preclinical data from HBV-transgenic mice primed with HBV proteins, followed by an MVA boost vaccination demonstrated promising results (Backes et al., 2016). Here, priming with HBV proteins, in particular HBsAg and HBcAg induced production of neutralizing antibodies by B cells and primed T cells which resulted in seroconversion and complexation of circulating HBV serum antigens (Figure 1.3). A subsequently performed vaccination step using a recombinant MVA encoding for HBsAg and HBcAg aimed at boosting virus-specific effector T cells which than eliminated HBV-infected hepatocytes (Figure 1.3). This vaccination strategy was able to overcome immune tolerance in high viremic HBV-transgenic animals, as it induced potent humoral as well as cell-mediated HBV-specific immune responses (Backes et al., 2016).

1.3.4 Adoptive T-cell therapy

The aim of adoptive T-cell therapy is to redirect the patient's own immune cells towards a certain target. Here, the patients T cells are expanded and/or manipulated *ex vivo* and subsequently re-infused into the patient. This can be managed through selection and expansion of tumor-infiltrating lymphocytes (TILs) or through genetic modification of donor T cells that leads to the expression of a natural T-cell receptor (TCR) or a chimeric antigen receptor (CAR).

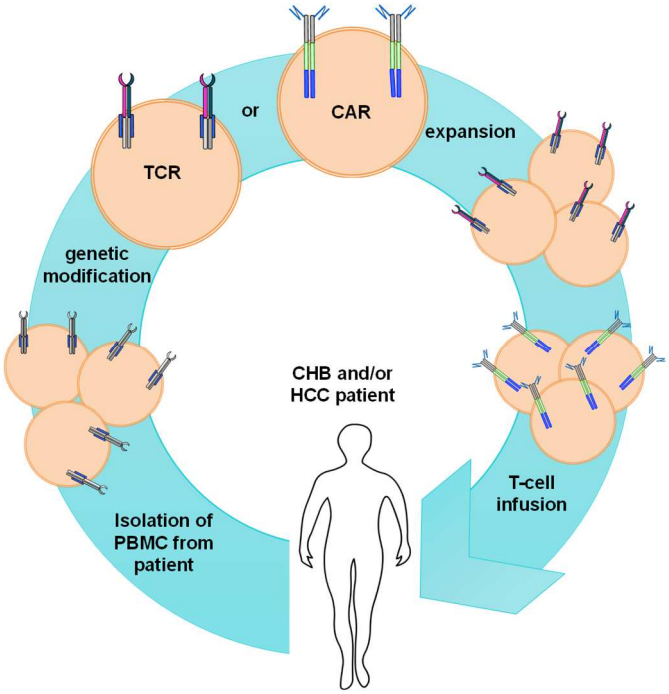

Figure 1.4 Adoptive T-cell transfer for treatment of chronic hepatitis B (CHB) or hepatocellular carcinoma (HCC).
For adoptive T-cell transfer peripheral blood mononuclear cells (PBMC) from the patient suffering from CHB or HCC are isolated. Subsequently T cells are genetically modified, resulting in expression of an additional natural T-cell receptor (TCR) or chimeric antigen receptor (CAR) and thus redirecting the T cells towards malignant or virus infected cells. After *ex vivo* expansion of modified T cells, they are re-infused into the patient.

Adoptive T-cell therapy is a promising approach to treat patients suffering from chronic HBV infection or HCC and is schematically illustrated in Figure 1.4. Clinical evidence highlights the potential of adoptive T-cell therapy as patients with leukemia and chronic HBV infection were able to clear the infection after bone marrow transplant from donors that had a HBV-specific T-cell response (Ilan et al., 1993; Lau et al., 1997).

1.3.4.1 Chimeric antigen receptor

Chimeric antigen receptors (CAR) are engineered receptors that enable redirection of T cells towards any target antigen that is expressed on the cell surface. The receptor gains its specificity from an scFv (single-chain variable fragment) that is typically obtained from an antibody. Here, the variable domains of the heavy (V_H) and the light chain (V_L) of the antibody are connected via a linker. Using a scFv for antigen-specificity enables the recognition of an extracellular antigen independent of the peptide-MHC-complex (Gross et al., 1989). Beside the scFv, a CAR consists of a spacer, a transmembrane domain and intracellular signaling domain(s). First generation CARs only had CD3ζ as an intracellular signaling domain, second generation CARs combined CD3ζ and as costimulatory signal domain CD28 (Davila et al., 2014) or 41BB (Maude et al., 2014). Third generation CARs even combine CD3ζ and two costimulatory domains (Guedan et al., 2018).

CAR T-cell therapy is a break-through technology as it provided substantial benefits in clinical trials targeting relapsed or refractory B-cell malignancies. Two CARs targeting CD19 were approved in the US in 2017: tisagenlecleucel for relapsed/refractory B-cell precursor acute lymphoblastic leukemia (ALL) (Maude et al., 2018) and axicabtagene ciloleucel for relapsed/refractory diffuse large B-cell lymphoma (DLBCL) (Neelapu et al., 2017). As of August 2017 more than 200 clinical trials were ongoing worldwide with most of them using a CD19-CAR to treat lymphoma or leukemia patients (Hartmann et al., 2017).

Even if not yet as successful as for blood-borne malignancies, CAR T-cell therapy is also studied for the treatment of solid tumors or viral infections. Preclinical results indicate great potential of GPC3-specific CARs targeting $GPC3^+$ HCC. Third generation GPC3-CARs had profound antitumor activity in HCC xenograft models (Gao et al., 2014; Li et al., 2016b). Antitumor activity was also observed in patient-derived xenografts and was highly depending on GPC3 expression (Jiang et al., 2016). A GPC3-CAR was also successfully investigated in preclinical studies for the treatment of lung squamous cell carcinoma (Li et al., 2016a). Moreover, a second generation GPC3-CAR introduced into NK cells demonstrated promising antitumor effects in HCC xenograft models (Yu et al., 2018).

Functionality of a CAR directed against the HBV surface protein (S-CAR) for the treatment of chronic HBV infection and HBV-associated HCC has already been investigated *in vitro* and *in vivo* (Bohne et al., 2008; Krebs et al., 2013). The S-CAR studied here is a second-generation CAR with CD3ζ and CD28 signaling domains, an IgG1 spacer and the C8 scFv specifically recognizing HBV surface protein (Figure 1.5). Upon contact with HBsAg on the surface of an HBV-infected hepatocyte, the S-CAR-redirected T cell is activated, leading to cytokine secretion and elimination of the HBV-infected target cell (Bohne et al., 2008) (Figure 1.5). The antiviral effect of the S-CAR in HBV-transgenic mice has been demonstrated to be transient and HBV is expressed from the transgene again when T cells vanish (Krebs et al., 2013).

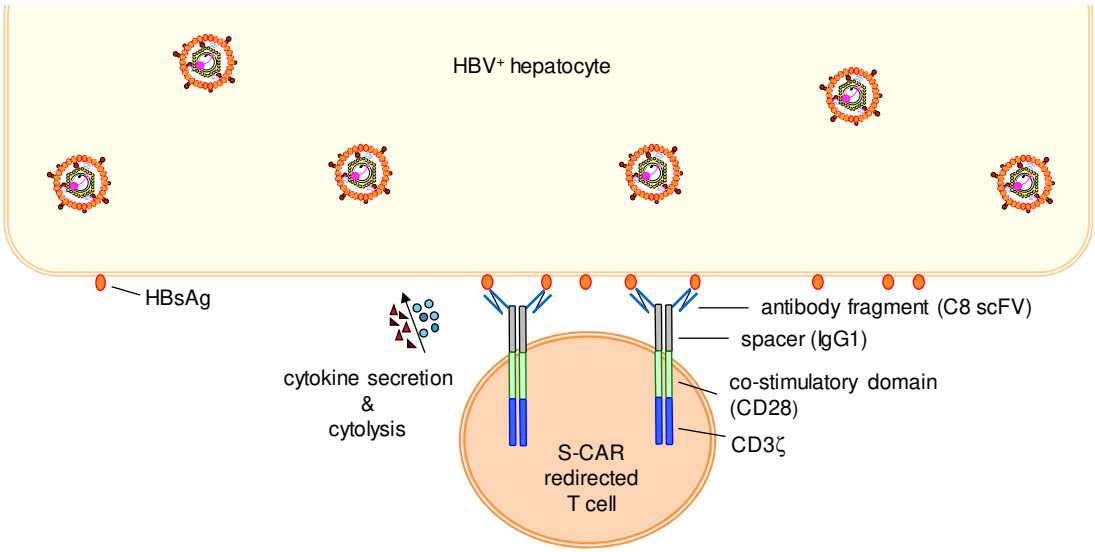

Figure 1.5 Activation of a T cell redirected by an HBV surface protein-specific chimeric antigen receptor (S-CAR).
The S-CAR is composed of an antibody fragment (C8 scFv) responsible for antigen specificity, an IgG1 spacer as well as CD28 and CD3ζ signaling domains. HBV surface antigen (HBsAg) on the surface of HBV-infected hepatocytes is recognized via the scFv, leading to T-cell activation. Subsequently S-CAR-redirected T cells eliminate their target cells by cytokine secretion and cytolysis.

1.3.4.2 Natural T-cell receptors

The adoptive transfer of T cells armed with a natural TCR can be achieved by expansion of autologous TILs or by genetically introducing a TCR with desired specificity into the patients' T cells. TIL therapy takes advantage of naturally occurring tumor-specific T cells already present within the tumor. Those TILs are isolated from a tumor resection of the patient, *ex vivo* activated, expanded and reinfused into the patient. Objective response rates of up to 50 % with up to 20 % complete tumor regression have been observed when re-infusing TILs in patients suffering from metastatic melanoma (Rosenberg et al., 2011). Promising results were also reported for TIL therapy in patients with metastatic uveal melanoma (Chandran et al., 2017). Despite those successes in TIL therapy, a major draw-back is that other malignancies only rarely contain identifiable tumor-reactive lymphocytes (Berger et al., 2009). An alternative

to isolation and expansion of TILs is to genetically modify T cells to express a reactive TCR. Importantly, TCRs recognize their target in context of MHC molecules, thus, redirection of T cells with a natural TCR is only possible for patients expressing the respective MHC molecule. First clinical trials using TCR-redirected T cells demonstrated success for different cancer types when treating patients with TCRs specific for tumor-associated antigens like for instance NY-ESO-1 (Robbins et al., 2015), MAGE-A3 (Lu et al., 2017), MAGE-A4 (Kageyama et al., 2015) or MART-1 (Johnson et al., 2009).

Hepatocellular carcinoma represents a suitable target for adoptive T-cell therapy with first promising results using autologous TIL therapy in patients with primary HCC with 12 of 15 patients demonstrating no evidence of disease after 14 months (Jiang et al., 2015). Furthermore, a GPC3-specific HLA-A*02 restricted TCR has been developed and its reactivity towards a GPC3$^+$ HLA-A*02$^+$ HCC target cell line was evaluated *in vitro* (Figure 1.6) (Dargel et al., 2015).

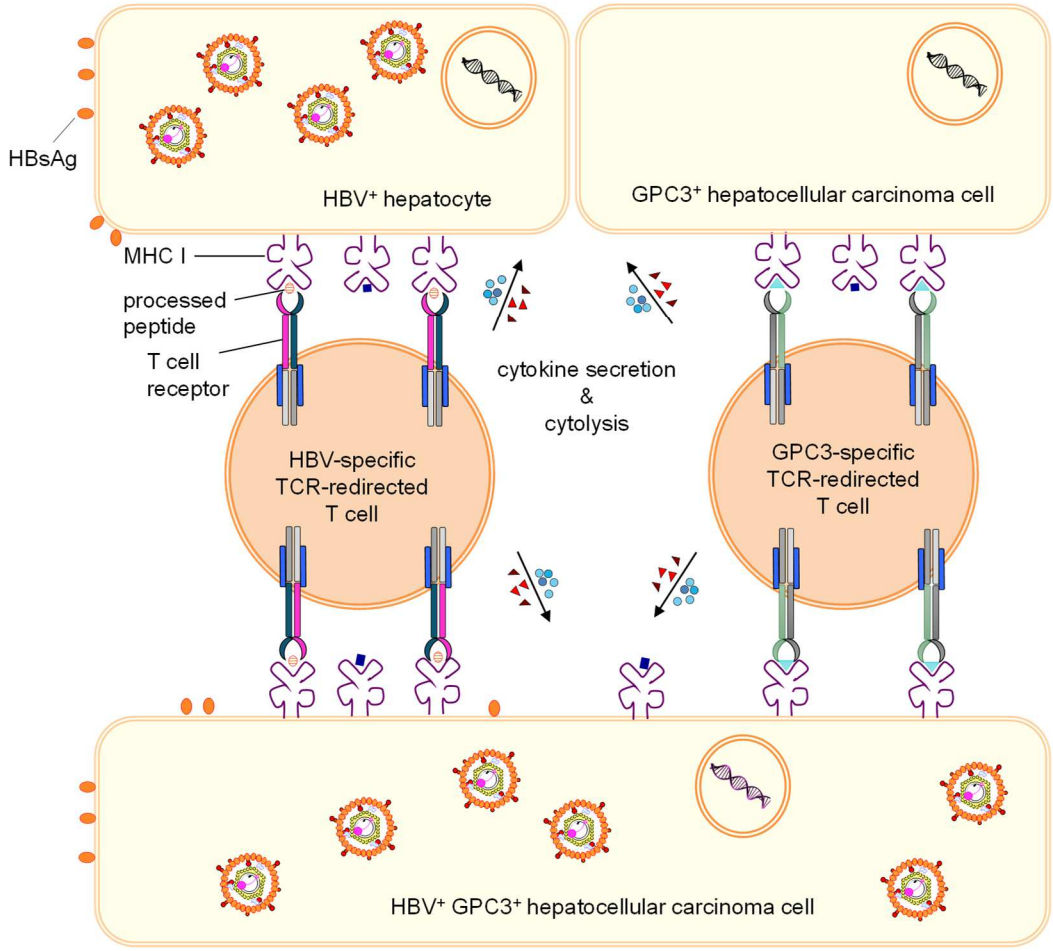

Figure 1.6 Activation of T cells redirected by expression of either an HBV-specific or GPC3-specific natural T-cell receptor (TCR).
HBV- or GPC3- redirected T cells recognize HBV-infected, GPC3$^+$ HCC or HBV-associated GPC3$^+$ HCC cells via the MHC I-peptide complex. Upon activation, TCR-redirected T cells eliminate their target cells by cytokine secretion and cytolysis.

Moreover, TCRs enabling redirection of T cells towards HBV-infected cells for the treatment of chronic HBV infection and HBV-associated HCC have already been identified and characterized (Gehring et al., 2011; Wisskirchen et al., 2017). Here, TCRs recognize peptides from HBV surface protein or core protein in context of HLA-A*02 (Figure 1.6) and exhibit high functional avidity. Moreover, preclinical studies in immunodeficient mice demonstrated a pronounced anti-tumor (Koh et al., 2013) or anti-viral effect (Kah et al., 2017; Koh et al., 2018) of T cells redirected with HBV-specific TCRs. Additional encouraging results were obtained in a first in man trial, in which a patient suffering from HBV-related HCC was adoptively transferred with HBsAg-specific TCR-redirected T cells followed by a substantial decrease in serum HBsAg levels (Qasim et al., 2015).

1.4 Model systems to study treatment of chronic HBV infection

The narrow host range of HBV, which naturally only infects humans and chimpanzees, prevents the infection of small animals by HBV virions. This represents a challenge since *in vivo* models are needed for understanding the pathogenesis of chronic HBV infection and HBV-related HCC and for investigation of new therapeutic strategies or drugs.

1.4.1.1 Mouse models

Immunocompetent transgenic mice expressing an 1.3 overlength copy of the HBV genome (Guidotti et al., 1995) have been used a lot in the past 20 years. Although HBV cannot be cleared, as the HBV genome is integrated into the mouse genome, this model has substantially contributed to understanding pathogenesis of HBV infection. For instance, those mice do not exhibit liver damage, indicating that HBV itself is non-cytopathic (Guidotti et al., 1995). Another broad application is the evaluation of therapeutics, for example antivirals like lamivudine and entecavir (Julander et al., 2003; Weber et al., 2002). However, this model is not suitable for assessment of viral entry, spread and clearance. Importantly, cccDNA is not established in HBV-transgenic mice and hence, investigation of cccDNA establishment as well as approaches to target the molecule are not possible.

In addition, hydrodynamic-based transfection of HBV DNA is an efficient method to transfer HBV DNA into the liver of immunocompetent mice. Importantly, not all animals survive, serum marker for HBV persistence decline fast after initial high-level expression and not 100 % of injected animals demonstrate persistent infection. Moreover, persistence of HBV transgenes was reported to be highly dependent on the plasmid backbone and the genetic background of the mouse (Huang et al., 2006). Beside using the full-length HBV DNA, *in vitro* circularized cccDNA was observed to induce persistent infection upon hydrodynamic transfection (Wang et al., 2017). Hydrodynamic injection of HBV DNA solves the problem of central tolerance

existing in HBV-transgenic mice, and is mostly used to study acute, self-limiting infection and the evaluation of its clearance.

Transfer of the HBV genome by viral vectors, in detail adenoviral (Ad) or adeno-associated viral (AAV) vectors permits efficient transduction of hepatocytes of immunocompetent mice. High dose infection with Ad-HBV induces HBV-specific T- and B-cell responses and mimics an acute, self-resolving infection (von Freyend et al., 2011), whereas low dose infection with Ad-HBV results in persistent infection (Huang et al., 2012). Nevertheless, adenoviral infection induces a strong vector-specific immune response. Conversely, AAV infection does not lead to the induction of an obvious immune response but induces immune tolerance to the transgene (Mingozzi et al., 2003). Using AAV as a vehicle for HBV delivery leads to sustained viremia and immune tolerance, that mimics chronic infection in humans and even results in liver fibrosis as seen in clinical HBV carriers (Dion et al., 2013; Kan et al., 2017; Yang et al., 2014; Ye et al., 2015). This mouse model is particularly suited to study the potential of therapeutic approaches to eradicate HBV from transduced hepatocytes. Moreover, there is evidence that cccDNA, the main nuclear transcription template of HBV, is present in AAV-HBV transduced hepatocytes (Lucifora et al., 2017). Recently, another way to establish a mouse model with cccDNA persistence was reported: recombinant HBV cccDNA was successfully delivered into the mouse liver using a replication-defective recombinant adenoviral vector (Li et al., 2018). Yet, none of the above described mouse models supports natural infection or re-infection of mouse hepatocytes, depicting the major limitations.

These limitations are possible to overcome in using human-liver chimeric mice. Here, immunodeficient mice harbor for instance the urokinase-type plasminogen activator (uPA) transgene, specifically expressed in the liver, which leads to necrosis of hepatocytes. This liver failure permits repopulation of the liver with human hepatocytes which have been demonstrated to be fully supportive of HBV infection (Dandri et al., 2001; Tsuge et al., 2005). The same result can be obtained using fumaryl acetoacetate hydrolase (Fah) knockout mice. The advantage of those mice is, that liver injury can be induced by administration and withdrawal of a certain compound (NTBC) (Azuma et al., 2007; Bissig et al., 2010). A third model is based on TK-NOG mice, in which hepatocyte depletion can be achieved by administration of ganciclovir (Hasegawa et al., 2011). A disadvantage of those human chimeric mice is that they are immunodeficient and therefore not suitable to study adaptive immunity towards HBV infection. Consequently, chimeric mice reconstituted with both, immune cells and hepatocytes of human origin are needed. Those double-humanized mice have been developed and demonstrated to support persistent HBV infection, human immune responses as well as chronic liver inflammation and fibrosis, representing a mouse model to study chronic hepatitis B and associated diseases (Bility et al., 2014; Washburn et al., 2011).

1.4.1.2 Other animal models

The chimpanzee represents the only immunocompetent animal model fully susceptible to HBV infection. Chimpanzees can develop acute and chronic HBV infection and therefore closely mimic the pathogenesis of HBV infection in humans. Currently, ethical limitations as well as high costs restrict the use of chimpanzees for HBV research (Wieland, 2015).

The Tupaia, better known as tree shrew, which displays a close phylogenic relationship with primates, has been found to be susceptible to HBV infection. Therefore, they bear an important role as source of primary hepatocytes. Sodium taurocholate cotransporting polypeptide (NTCP) was found to be the cellular receptor for HBV using the Tupaia model (Yan et al., 2012). Establishment of chronic HBV infection has been shown in neonatal shrews, but *in vivo* infection efficiency needs to be further improved (Wang et al., 2012; Yang et al., 2015).

Duck and woodchuck are useful animal models, as they are susceptible to viruses similar to HBV, namely duck hepatitis B virus (DHBV) and woodchuck hepatitis virus (WHV). They are used to study infection, immune response against viral infection but also for instance vaccination strategies (Kosinska et al., 2010; Mason, 2015). However, those mentioned animals are not inbred and detection reagents are not readily available which highly impedes their use.

With the identification of NTCP being the receptor for cellular entry of HBV, the narrow host specificity and liver tropism of HBV could be explained. NTCP is a multiple transmembrane transporter for bile salts predominantly expressed in the liver, whose protein sequence varies among species (Yan et al., 2012). Knowing the entry receptor for HBV offers the possibility of natural HBV infection of non-susceptible species by introducing human NTCP into hepatocytes. This has been demonstrated to be the limiting factor for HBV replication for the cynomolgus and rhesus macaque, as non-human primate models, *in vitro* and *in vivo* (Burwitz et al., 2017; Lempp et al., 2017). Further experiments revealed pig hepatocytes to be fully susceptible to HBV infection after inducing human NTCP expression with pigs representing another preclinically relevant animal model (Lempp et al., 2017). Importantly, mice, rats and dogs were not supporting HBV infection upon NTCP expression, indicating that unknown factors are needed for nuclear entry and cccDNA formation that are available in macaque and pig hepatocytes, but not in the other animals investigated (Lempp et al., 2017).

1.5 Aim of the study

Despite of available treatment options, prognosis of chronic HBV infection as well as HCC remains poor. Both diseases are characterized by expression of viral antigens and TAA, respectively, rendering them as target cells for immunotherapeutic approaches which represent a promising attempt for the treatment of both diseases. Important questions regarding their functionality *in vivo* using appropriate animal models, however, still needed to be addressed.

Viral proteins expressed in virus-infected or malignant cells may render those cells as targets for immunotherapeutic approaches. The potential of T cells equipped with HBV-specific natural TCRs, or chimeric antigen receptor directed against HBsAg and a therapeutic vaccination strategy have been investigated *in vitro* or in HBV-transgenic mice, respectively. Yet, clearance of the virus could not be obtained, as the HBV genome is integrated into the mouse genome. To overcome this obstacle, we wanted to make use of viral-vector-mediated transfer of the HBV genome.

Therefore, the AAV-mediated transfer of the HBV genome was compared to an established adenoviral vector and a newly generated high-capacity adenoviral vector. Analysis of replication duration as well as induction of anti-vector and HBV-specific immunity gave insight which mouse model of chronic HBV infection was most suitable for our purposes.

Next, the best model was used to investigate the ability of the therapeutic vaccination strategy and the above mentioned adoptive T-cell therapy approaches to achieve functional cure in a mouse model of chronic HBV infection.

Subsequently, first steps towards the examination of safety and efficacy of adoptive T-cell therapy for chronic HBV infection using natural TCRs in other preclinically relevant animal models were taken. Therefore, *in vitro* studies analyzing functionality of HBV-specific T cells in co-culture with HBV-infected rhesus macaque or pig hepatocytes were performed.

Finally, adoptive T-cell therapy towards TAA-expressing HCC were investigated. TCR-redirected T cells recognizing the HCC-associated antigen GPC3 have been demonstrated to induce a profound cytotoxic effect towards hepatoma cells *in vitro*. In the following study, their potential to eradicate tumor cells in an HCC xenograft mouse model was investigated.

2 RESULTS

2.1 Generation and functional characterization of *in vivo* models to study chronic HBV infection/HBV-associated HCC

Chronic HBV infection as well as HBV-associated HCCs represent suitable targets for immunotherapeutic approaches. Viral proteins may still be expressed on tumor cells, rendering these cells as targets for HBV-specific immune-based therapies. To evaluate the potential of immunotherapeutic strategies against chronic HBV infection as well as HBV-associated HCC to achieve functional cure, an appropriate *in vivo* model is indispensable. In the following section, viral-vector-based HBV genome transduction models are investigated.

2.1.1 Generation and comparison of HBV genome transduction using adenoviral, high capacity adenoviral and adeno-associated viral vector

In contrast to HBV-transgenic mice, viral-vector based HBV genome delivery in mouse hepatocytes facilitates investigation of an HBV cure. We decided to use the AAV (adeno-associated virus)-HBV model of chronic HBV infection that has been reported by Dion et al. (2013). To this end, immunocompetent C57Bl/6J were intravenously (i.v.) infected with 2×10^{11} viral genomes (vg) of a serotype 2 AAV packed with an AAV serotype 8 capsid encoding for a 1.2-fold overlength of the HBV genome, called AAV-HBV hereafter. Persistence of HBV markers, like serum HBeAg and serum HBsAg were monitored over two months. Stable serum HBeAg and HBsAg levels were observed from one-week post infection onwards (Figure 2.1 A and B). Normal alanine aminotransferase (ALT) levels indicated immune tolerance to HBV as well as the AAV vector (Figure 2.1 C). HBcAg staining of liver sections 14 days post infection demonstrated that HBcAg was expressed in around 60-70 % of hepatocytes and was present in both cytoplasm and nuclei (Figure 2.1 D). To determine tissue specificity of AAV-mediated HBV genome transduction, I analyzed AAV- and HBV-DNA in numerous organs. For this purpose, two pairs of primers were used (Figure 2.1 E): 1. one pair to amplify the AAV vector DNA, as the forward primer binding site was located in the AAV2 ITR and the reverse primer in the HBV X region (blue). 2. one pair to amplify all HBV genomes (including the AAV vector, replicated HBV and HBV packaged virus) with their binding sites within the HBV S region (grey). We found HBV DNA exclusively in the liver, but not in other organs and tissues like spleen, brain, kidney, heart, muscle, testis, lung or intestine 14 days post infection. The overall HBV genome content was higher than that of the AAV vector, suggesting HBV replication in mouse livers (Figure 2.1 E). Taken together, AAV-HBV infection led to persistence as well as liver-specific HBV expression.

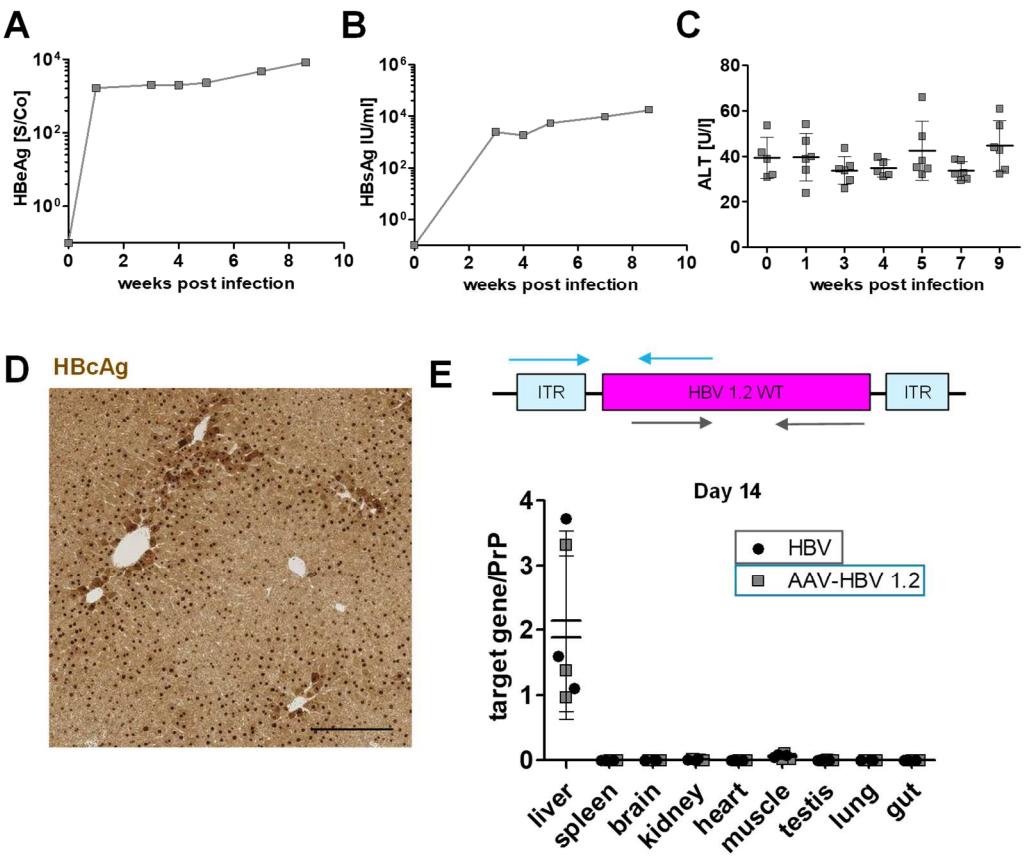

Figure 2.1 Characterization of HBV genome transduction using AAV-HBV.
Time course of **(A)** serum HBeAg, **(B)** serum HBsAg and **(C)** serum alanine amino transferase (ALT) levels after intravenous infection of 2 x 10^{11} vg AAV-HBV in C57Bl/6J mice. (n=6) **(D)** Representative immunohistochemical HBcAg staining of liver section at day 14 post infection. Scale bar indicates 100 µm. **(E)** Schematic representation of primer binding positions for AAV vector (AAV-HBV 1.2; blue) and whole HBV genomes (HBV, grey). Levels of AAV vector and whole HBV genomes relative to PrP in indicated organs day 14 post infection. Mean and SD are shown. (n=3)

Moreover, the presence of HBV-specific T cells was analyzed 60 days post infection. Lymphocytes isolated from liver or spleen were stimulated with overlapping HBV S- and core specific peptide pools *ex vivo*. We could not detect $CD8^+$ T cells that were activated to secrete IFNγ upon peptide stimulation (Figure 2.2 A and B) indicating HBV-specific immune tolerance. Hence, AAV-HBV infection resembled a chronic HBV infection in patients, as we did not detect an HBV-specific immune response.

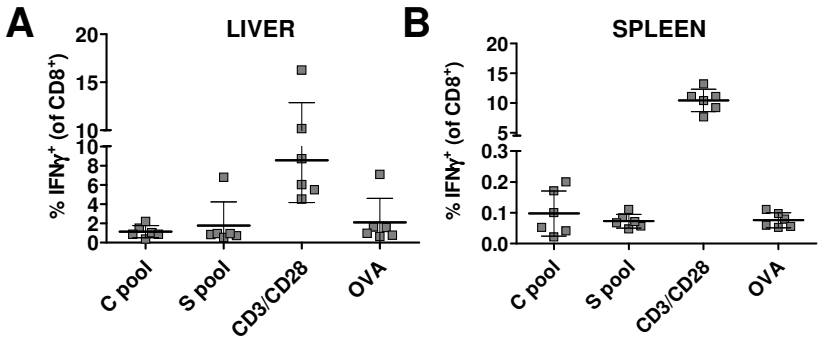

Figure 2.2 Analyses of HBV-specific $CD8^+$ T cells after AAV-HBV infection.
Intracellular cytokine staining of $CD8^+$ T cells isolated from **(A)** liver or **(B)** spleen after *ex vivo* stimulation with overlapping HBV S- and core peptide pools 60 days post infection. CD3/CD28 stimulation served as positive, stimulation with an ovalbumin (OVA) derived peptide as negative control. Mean and SD are shown. (n=6)

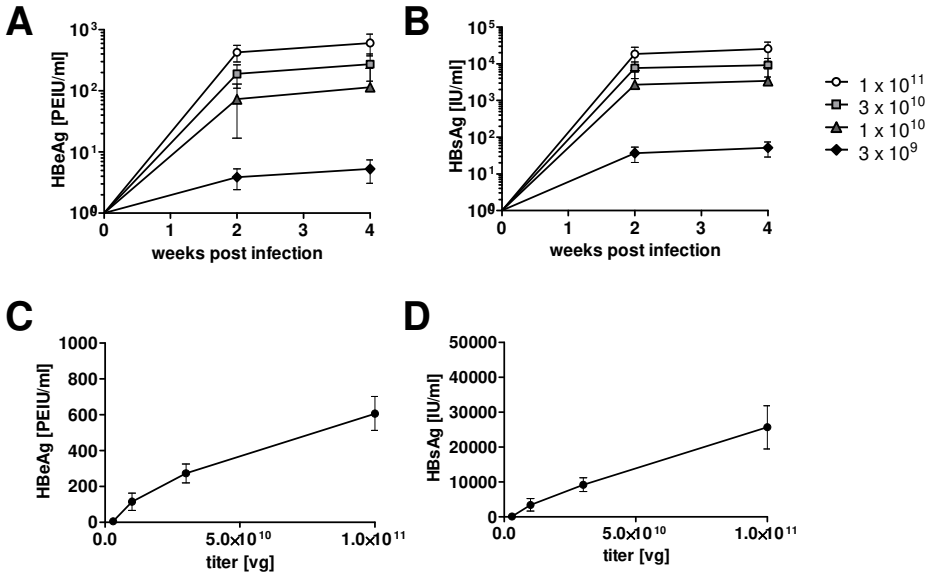

Figure 2.3 Dose-dependence of AAV-HBV infection in C57Bl/6J mice.
Time course of **(A)** serum HBeAg and **(B)** serum HBsAg. Correlation of **(C)** serum HBeAg levels and **(D)** serum HBsAg levels of week 4 post infection plotted against infection dose (vg). Mean and SD are shown. (n=6)

To determine the dose-dependence of AAV-HBV infection, different titers of AAV-HBV were used for i.v. infection of immunocompetent C57Bl/6J mice. Serum HBeAg and HBsAg titers

correlated to the dose of AAV-HBV used for infection (Figure 2.3 A, B, C and D). In addition, AAV vector and whole HBV genome content in liver DNA as well as the number of HBc^+ hepatocytes correlated with the inoculated dose of AAV-HBV (Figure 2.4 A and B).

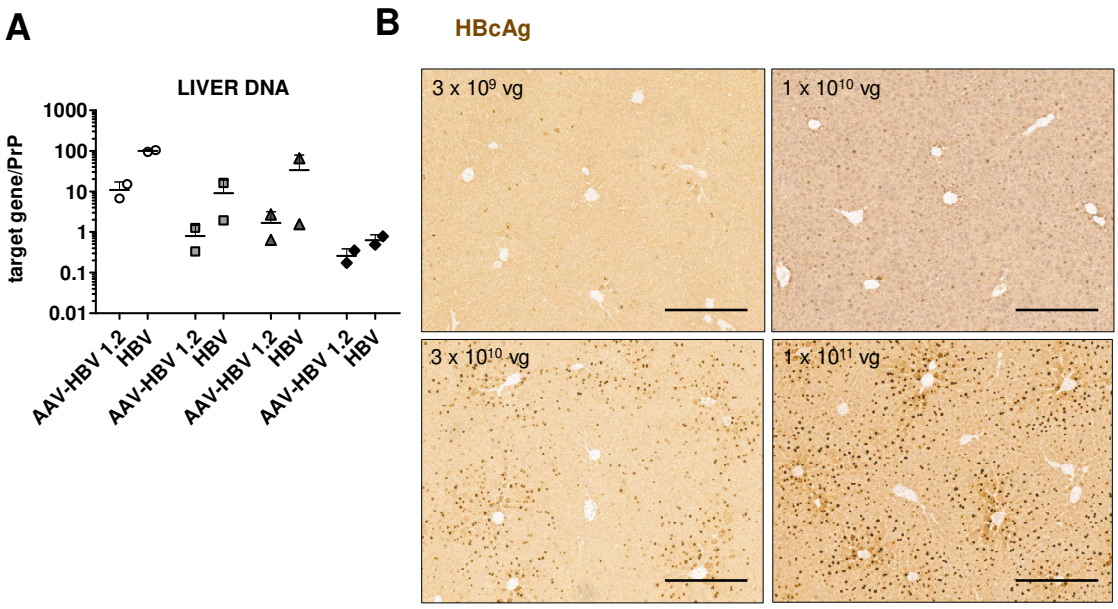

Figure 2.4 Analyses of liver tissue of AAV-HBV-infected C57Bl/6J mice.
(A) Levels of AAV vector (AAV-HBV 1.2) and whole HBV genomes (HBV) relative to PrP four weeks post infection. **(B)** Representative immunohistochemical HBcAg stainings of liver sections four weeks post infection. Scale bars indicate 300 µm. Mean and SD are shown. (n=2)

As a next step, we compared the AAV-mediated HBV genome transfer to the established adenoviral (Ad-HBV, first generation adenovirus) (Huang et al., 2012; von Freyend et al., 2011) and the newly generated high capacity adenoviral vector (HCA-HBV, gutless adenovirus). The HCA is lacking all protein-coding adenoviral sequences and is therefore thought to reduce vector-mediated immune responses. Here, the 1.3 overlength HBV genome was used for a better comparison to pre-existing data on Ad-HBV. Moreover, the X^- version was chosen, as it represents broader laboratory applicability due to safety reasons as X is characterized as an oncogene (Kim et al., 1991). Immunocompetent C57Bl/6 mice were injected i.v. with 1 x 10^8, 5 x 10^8 or 2 x 10^9 plaque forming units (pfu) HCA-HBV X^- or Ad-HBV X^- as well as with 1 x 10^{10} or 3 x 10^{10} vg AAV-HBV X^-. Indicators of HBV replication, like serum HBeAg and serum HBsAg were monitored over three months.

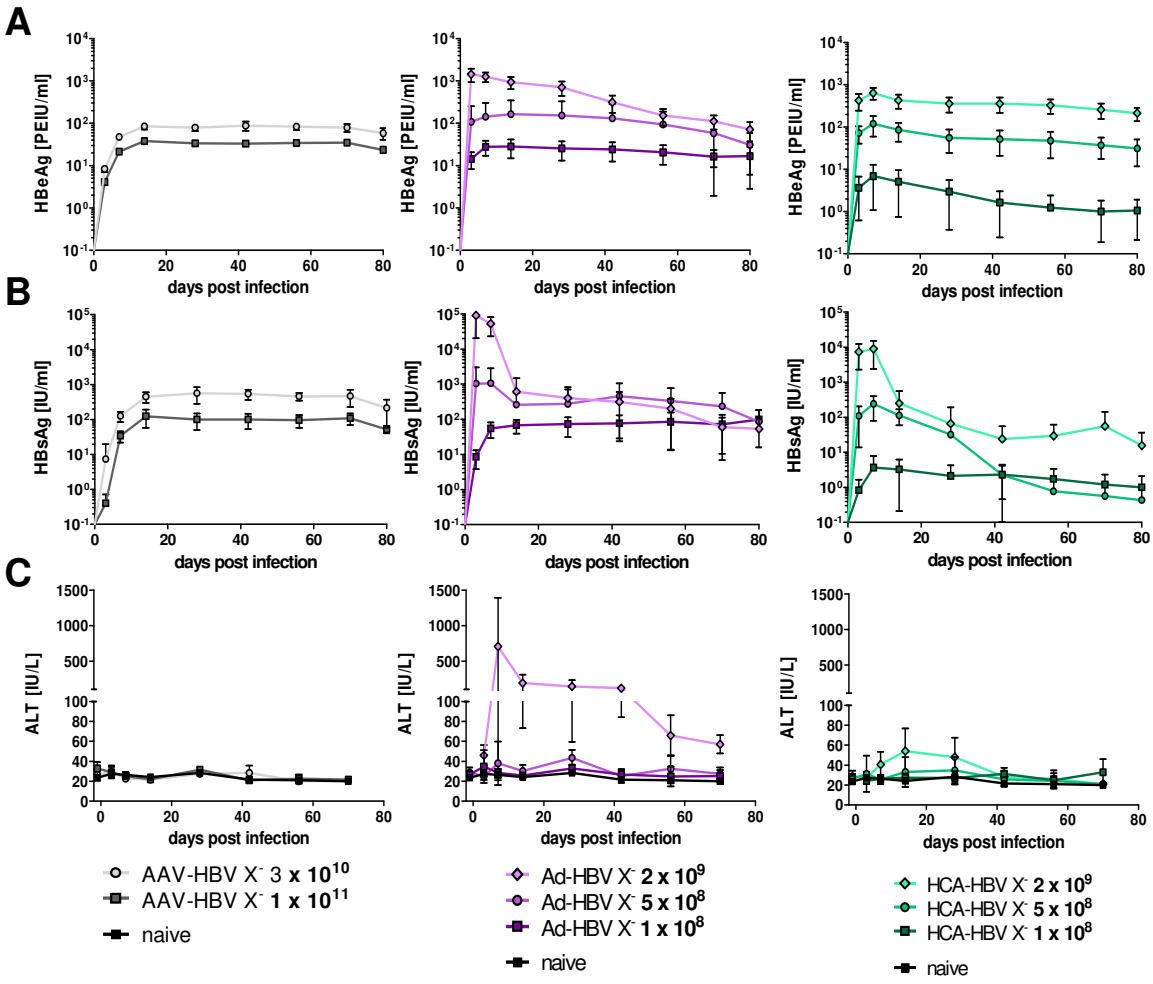

Figure 2.5 Serology after HBV genome (1.3 X-) transduction using adenoviral (Ad), high capacity adenoviral (HCA) or adeno-associated viral (AAV) vector.
Time course of **(A)** serum HBeAg, **(B)** serum HBsAg and **(C)** serum alanine amino transferase (ALT) levels. Mean and SD are shown. (n=4-6)

Overall, serum HBeAg and HBsAg levels were dose-dependent with all viral vectors used. (Figure 2.5 A and B). All groups showed sustained HBeAg levels over time, however, kinetics of expression differed between adenoviral vector- and AAV-mediated genome transduction. HBeAg levels raised extremely fast in adenoviral vector groups with a subsequent slow decline for the higher titer groups. In contrast, serum HBeAg levels increased more slowly in AAV groups and stayed stable afterwards (Figure 2.5 A). Serum HBsAg levels exhibited the same kinetics, even if the decline in high titer adenoviral vector groups was more pronounced (Figure 2.5 B). Furthermore, transduction with the highest titer of the Ad vector (2 x 10^9 pfu) was accompanied by a strong increase in serum ALT elevations, which was less pronounced using HCA or absent using AAV for genome transfer (Figure 2.5 C).

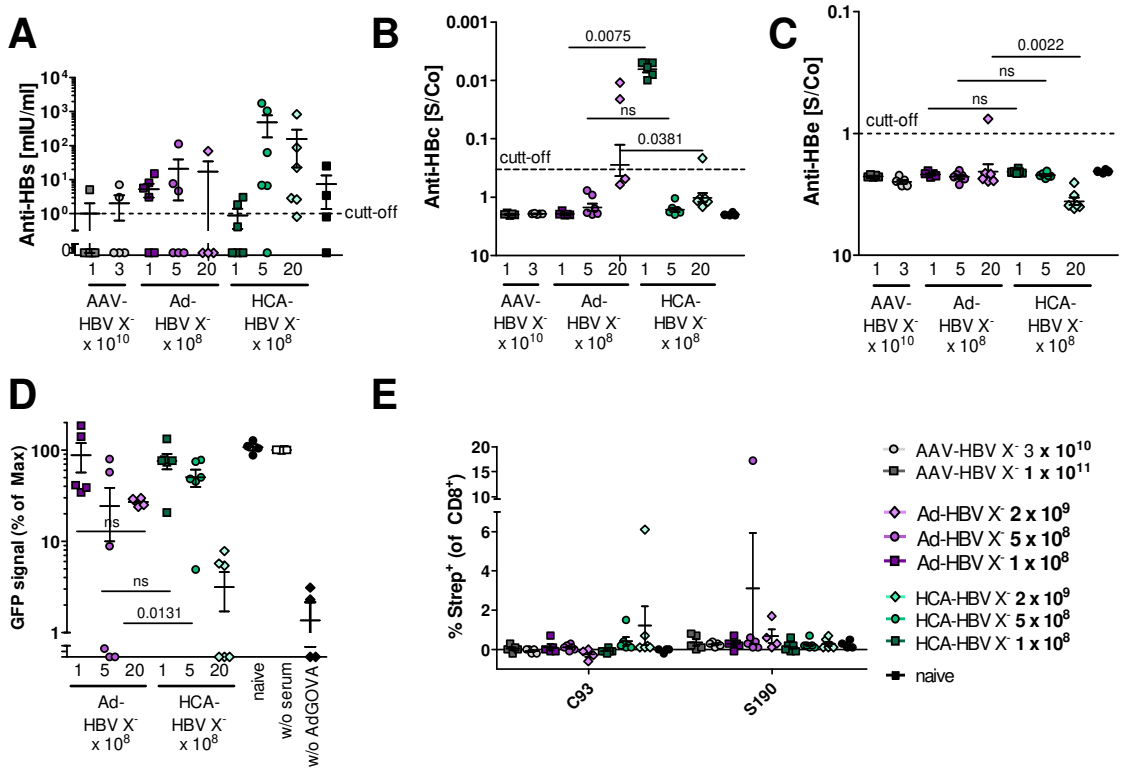

Figure 2.6 HBV- and vector specific immune responses after vector-mediated HBV genome transfer.
Serum of day 80 post infection was used for determination of **(A)** anti-HBs antibodies, **(B)** anti-HBc antibodies, **(C)** anti-HBe antibodies and **(D)** neutralization assay demonstrating anti-adenovirus antibodies. We co-incubated serum of all animals with an adenovirus encoding for GFP (Ad-GOVA) before transducing HEK 293 cells. 24 hours later, GFP expression was analyzed. **(E)** Staining of HBV-specific intrahepatic $CD8^+$ T cells directly *ex vivo* using S190 and C93 streptamers. Data is represented as relative values after background subtraction determined by OVA peptide. Mean and SEM are shown. (n=4-6, Mann-Whitney test, numbers in graphs indicate p values, ns = not significant)

We further examined whether HBV persistence was associated with a lack of HBV-specific immune responses, which would mimic the situation in a chronically HBV-infected patient. The above mentioned decline in HBsAg levels was accompanied by a seroconversion to antibodies to HBsAg (anti-HBs) in several animals infected with both adenoviral vectors (Figure 2.6 A). Next to anti-HBs antibodies, we determined the presence of antibodies against HBV core protein (anti-HBc) and HBeAg (anti-HBe). In serum of all animals that received 1 x 10^8 pfu HCA as well as two mice of the 2 x 10^9 pfu Ad and HCA groups anti-HBc antibodies were measured (Figure 2.6 B). In only one mouse of the high titer Ad group anti-HBe antibodies were detected (Figure 2.6 C). Furthermore, anti-adenovirus antibodies were found in a substantial number of animals by a neutralization assay. GFP expression was diminished in a titer dependent manner in mice that were injected with an adenovirus. There was no difference when comparing Ad with HCA concerning the induction of anti-adenovirus antibodies except for the high titer groups (Figure 2.6 D). Beside the humoral immune response against HBV, the existence of HBV-specific $CD8^+$ T cells was characterized three months post infection. Intrahepatic lymphocytes

were analyzed using S190 and C93 streptamers. In all but two animals, HBV-specific specific $CD8^+$ T cells were absent (Figure 2.6 E). However, we detected a population of C93-specific T cells amongst intrahepatic $CD8^+$ T cells from one animal (2 x 10^9 pfu HCA) as well as population of S190-specific T cells in another one (5 x 10^8 pfu Ad) (Figure 2.6 E).

To determine the transduction efficacy of the viral vectors, HBV gene expression and replication in the liver was compared. A considerably high number of hepatocytes was $HBcAg^+$ when mice were infected with 2 x 10^9 pfu HCA, whereas only few cells showed nuclear HBcAg when using 2 x 10^9 pfu Ad (Figure 2.7 A). We also noted, that HBcAg expression was very low in all other groups (Figure 2.7 A and B). Moreover, HBV DNA copies in sera of all animals was investigated as well as rcDNA copies in liver tissue. A dose-dependency of liver HBV DNA was observed. After injection of the high titer of the HCA, substantially more HBV DNA in serum and liver tissue was found compared to high titer Ad infection (Figure 2.7 C and D). After AAV-HBV transduction cccDNA was described to be found in liver tissue (Lucifora et al., 2017). Notably we also found cccDNA in livers of animals infected with AAV (Figure 2.7 E). To answer the question whether using Ad-HBV leads to a lower number of hepatocytes transduced or if immune response against the vector leads to lower numbers of $HBcAg^+$ cells and liver rcDNA when compared to the high-capacity adenoviral vector, we again infected mice and analyzed rcDNA in liver tissue as early as five days post infection. This early timepoint should allow for examination before the onset of anti-vector immune response. At day five post infection rcDNA levels in liver tissue were very comparable between HCA and Ad vector transduction when comparing the respective titers (Figure 2.7 F). This indicated equal transduction rates and control of HBV replication in Ad-HBV but not in HCA-HBV-infected mice.

Taken together, all viral-vector based HBV genome transduction models investigated led to persistence of HBV in immunocompetent C57Bl/6J mice. The most suitable vector depends on the requirements of specific experiments.

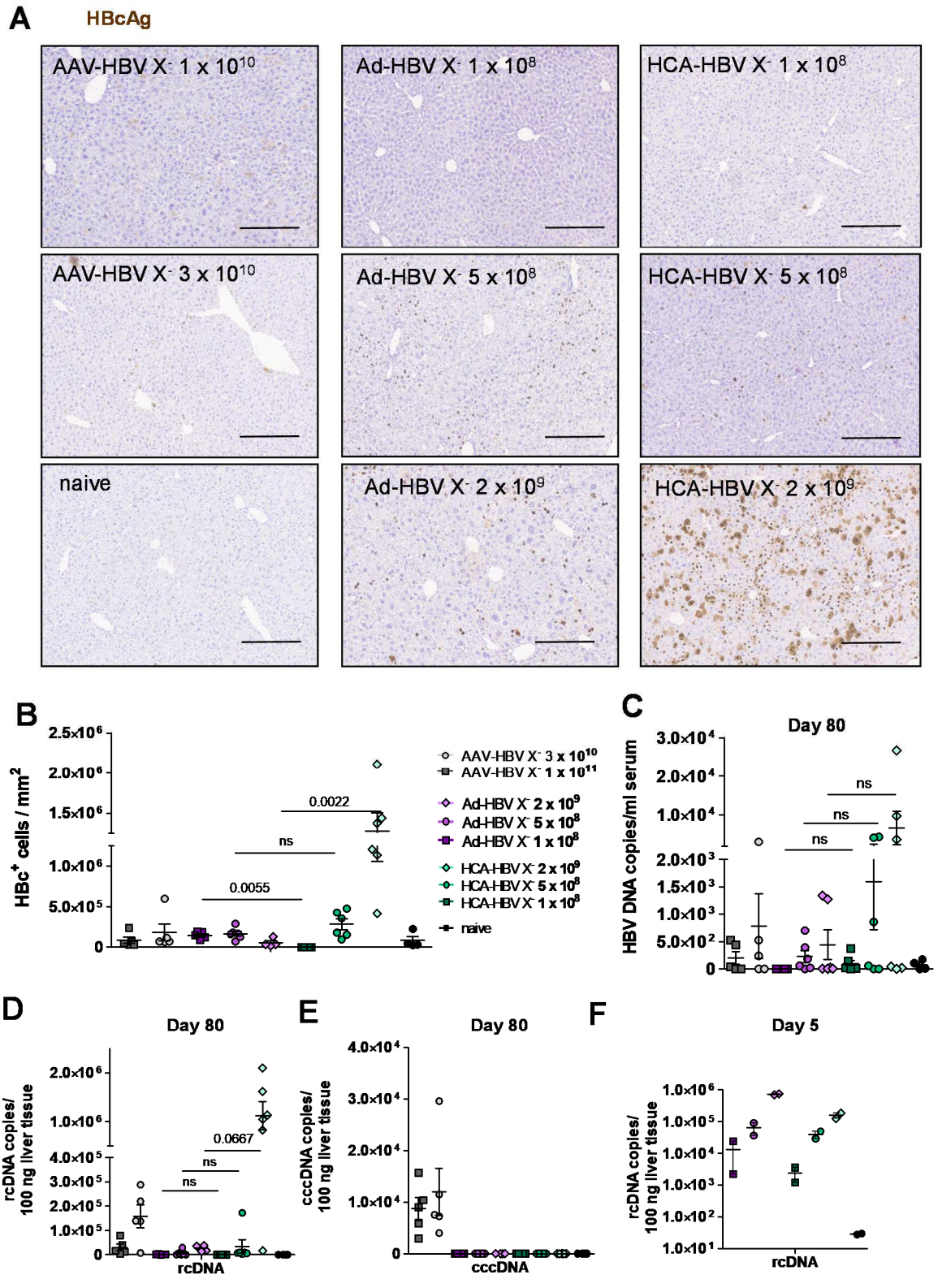

Figure 2.7 End-point analyses after vector-mediated HBV genome transfer.
(A) Representative immunohistochemical HBcAg stainings of liver sections 80 days post infection. Scale bars indicate 300 µm. **(B)** Automated quantification of HBc^+ cells per mm^2. **(C)** HBV DNA copies/ml serum at day 80 post infection. **(D)** rcDNA copies and **(E)** cccDNA copies per 100ng liver tissue at day 80 post infection. **(F)** rcDNA copies per 100ng liver tissue day 5 post infection. Mean and SEM are shown. (n=2-6, Mann-Whitney test, numbers in graphs indicate p values, ns = not significant)

2.1.2 Generation and investigation of HBV genome variants using the adeno-associated viral vector

We aimed at investigating AAVs with different HBV genome variants as there could be a broad applicability in exploring the efficacy of therapeutic approaches against HBV infections. From AAV-HBV 1.2 WT (Dion et al., 2013) (Figure 2.8 A). I generated X^- (X protein is not expressed) and E^- (HBeAg is not expressed) variants. X^- was generated by introducing a stop codon after the first seven amino acids (C to G mutation), for the E^- variant, the stem-loop mutation was introduced (G to A at position 1896) (Lok et al., 1994). The same mutants were generated from 1.3-fold overlength HBV genomes. The 1.3 overlength variants were chosen to be further investigated. To verify gene expression and HBV production of the constructs, pAAV-HBV 1.3WT, pAAV-HBV 1.3X^- as well as pAAV-HBV 1.3E^- were transfected into HepG2 cells. The amount of AAV vector DNA and production of HBeAg was analyzed. Function of the knock-out in pAAV-HBV 1.3E^- could be confirmed, as there was no measurable HBeAg secretion. Notably, HBeAg production was greatly reduced in the X^- variant when compared to the WT variant (Figure 2.8 B) while AAV vector DNA was comparable in all three variants, showing constant transfection efficiency (Figure 2.8 C). Following the *in vitro* plasmid vector verification, the respective AAVs were produced by triple transfection of HEK 293T cells.

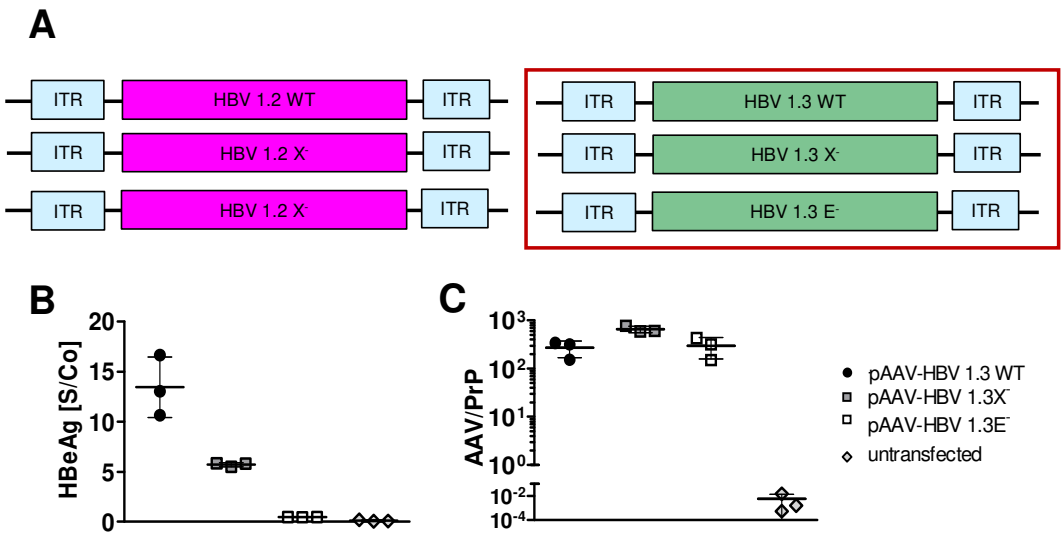

Figure 2.8 Schematic representation of pAAV-HBV constructs and *in vitro* verification of their replication ability.
(A) Schematic representation of 6 AAV-HBV constructs. HBV genome is flanked by AAV2 ITRs. **(B)** HBeAg in supernatant and **(C)** cellular AAV vector DNA relative to PrP after transfection into HepG2 cells. Mean and SD of triplicates are shown.

Next, immunocompetent C57Bl/6 mice were intravenously infected with either AAV-HBV 1.3WT, AAV-HBV 1.3X$^-$ or AAV-HBV 1.3E$^-$. Serum HBeAg, HBsAg and ALT levels were monitored over three months. Our *in vitro* data could be confirmed *in vivo*, as HBeAg was absent using the E$^-$ variant and considerably reduced (1 log) in the X$^-$ variant when compared to the WT genome (Figure 2.9 A). HBsAg levels were reduced 1 log in using AAV-HBV 1.3X$^-$ compared to WT and E$^-$ genome. Importantly HBsAg levels were found to be significant different between WT and E$^-$ genome (Figure 2.9 B). ALT levels remained normal throughout the three months, indicating no induction of an obvious immune response (Figure 2.9 C). We analyzed HBV DNA copies in the serum of the animals on day 80 post infection and found significant lower viremia in all HBV-X$^-$ and most HBV-E$^-$ compared to HBV-WT infected mice (Figure 2.9 D). To determine the induction of an HBV-specific immune response, the existence of HBV specific antibodies was evaluated on day 80 post infection.

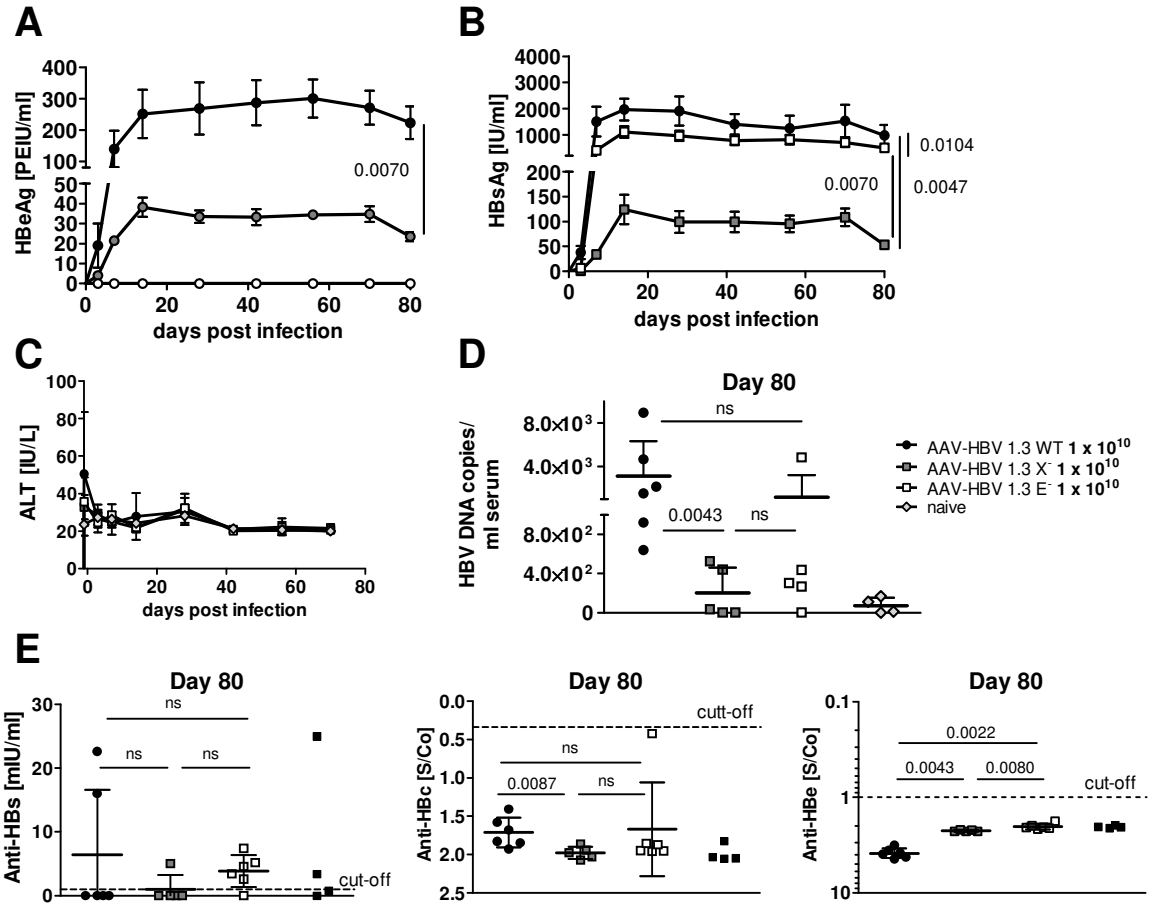

Figure 2.9 Serology of HBV genome transduction using AAV as a viral vector.
Time course of **(A)** serum HBeAg, **(B)** serum HBsAg and **(C)** serum alanine amino transferase (ALT) levels. **(D)** HBV DNA copies/ml serum at day 80 post infection. **(E)** Anti-HBs, anti-HBc and anti-HBe antibodies 80 days post infection. Mean and SD are shown. (n=4-6, Mann-Whitney test, numbers in graphs indicate p values, ns = not significant)

Except for very low amounts of anti-HBs antibodies in some mice, no HBV-specific antibodies were detected (Figure 2.9 E). To examine the HBV gene expression and replication in the liver, we analyzed HBc$^+$ hepatocytes in liver sections. A markedly high number of hepatocytes was HBcAg$^+$ when mice were infected with the WT genome, which was reduced in the E$^-$ and almost absent in the X$^-$ variant (Figure 2.10 A and B). We wanted to exclude the possibility that a mistake during the titration of the AAV stocks led to the substantially lower HBV replication in the X$^-$ variant. For this purpose, we determined the amount of AAV genome in liver tissue of all animals. A significant lower amount of AAV backbone was observed if mice were infected with the X$^-$ variant (Figure 2.10 C). In contrast we did not find a difference in rcDNA copies or cccDNA copies comparing WT genome with X$^-$ (Figure 2.10 D and E). However, when mice were killed already three days after infection, the amount of AAV genomes as well as HBV

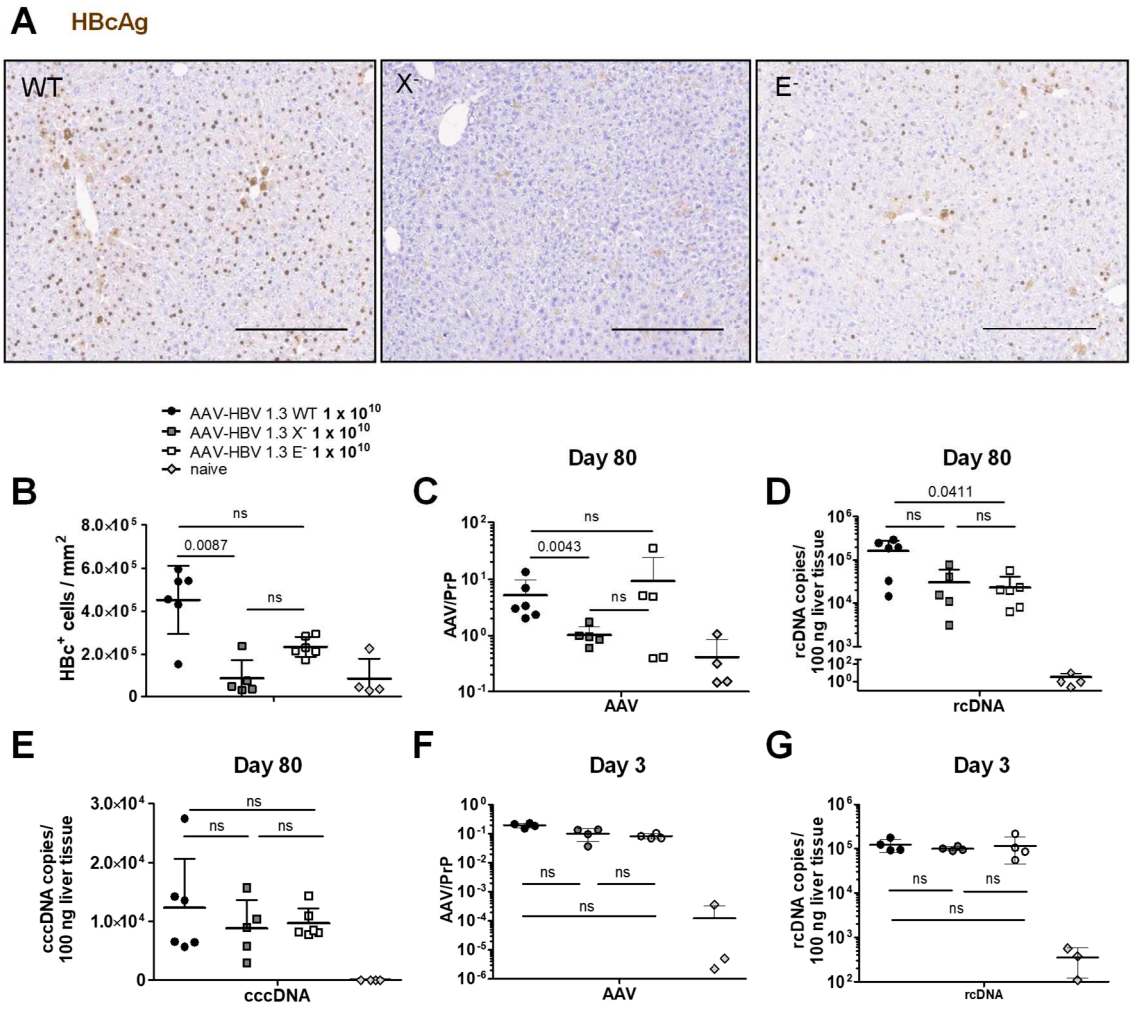

Figure 2.10 Analyses of liver tissue after AAV-mediated HBV genome transfer.
(A) Representative immunohistochemical HBcAg stainings of liver sections at day 80 post infection. Scale bars indicate 300 µm. **(B)** Automated quantification of HBc$^+$ cells per mm^2. **(C)** AAV vector DNA at day 80 post infection. **(D)** rcDNA copies and **(E)** cccDNA copies per 100ng liver tissue at day 80 post infection. **(F)** AAV vector DNA relative to PrP at day 3 post infection. **(G)** rcDNA copies per 100ng liver tissue at day 3 post infection. Mean and SD are shown. (n=3-6, Mann-Whitney test, numbers in graphs indicate p values, ns = not significant)

rcDNA in liver tissue was comparable in all genome variants (Figure 2.10 F and G) indicating equally efficient transduction. It is important to note, that we found a significant difference in HBV DNA copy levels comparing WT and E^- variant (Figure 2.10 D) suggesting that HBeAg influences viremia.

In summary, AAV-mediated transfer of all HBV genomes examined led to HBV persistence in immunocompetent C57Bl/6J mice. Importantly, viremia was substantially reduced after AAV-HBV infection if the X protein was missing. Lack of HBeAg did not reveal to have major effects on anti-HBV immunity but led to lower serum HBsAg levels as well as HBV DNA copies in serum and liver tissue.

2.2 *In vivo* evaluation of immunotherapeutic strategies against chronic HBV infection/HBV-associated HCC using AAV-HBV infection

New therapy options for chronic HBV infection and HCC are urgently needed as current treatment options are limited and do rarely cure the diseases. Immunotherapeutic approaches are promising candidates and aim to induce or boost the patient's adaptive immune response to recognize and eliminate virus infected or malignant cells. In the following sections, different approaches to regain functionality of the adaptive immune response towards HBV$^+$ cells will be explored.

2.2.1 Therapeutic vaccination

Therapeutic vaccination for chronically HBV-infected patients is meant to restore the patients defective or impaired adaptive immune response towards the virus. To evaluate the potential of therapeutic vaccination to achieve functional cure, the above characterized AAV-HBV model of chronic HBV infection was used. Therefore, we used the previously described vaccination scheme (Backes et al., 2016) with some modifications. Four or twelve weeks after AAV-HBV infection, when persistent HBV infection had been established, we started to vaccinate the animals. Two protein prime vaccinations using HBsAg and HBcAg with cyclic-di-AMP as an adjuvant were performed in a two-weeks interval to induce neutralizing antibodies and prime HBV-specific CD4$^+$ as well as CD8$^+$ T cells. Co-administration of an appropriate adjuvant is crucial. In the present study cyclic-di-AMP is used, which gives rise to balanced CD4$^+$ T-cell responses (Burdette et al., 2011; Parvatiyar et al., 2012). Moreover, we boosted with a viral vector, in detail modified Vaccinia virus Ankara (MVA) expressing HBsAg and HBcAg two weeks after the last protein prime, to boost HBV-specific T cells. This vaccination scheme will

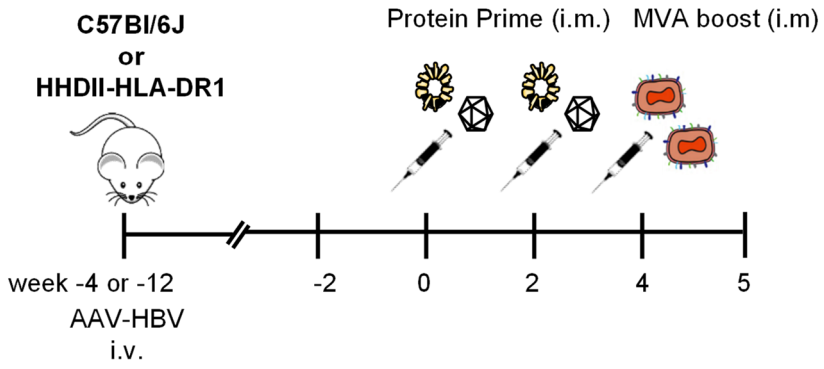

Figure 2.11 Schematic overview: Therapeutic vaccination scheme.
C57Bl/6J or HHDII-HLA-DR1 mice were intravenously injected with AAV-HBV four weeks or twelve weeks prior start of therapeutic vaccination. Vaccination consisted of two protein primes (week 0 and 2, 10 µg HBcAg + 10 µg HBsAg + 10 µg cyclic-di-AMP, intra muscularly (i.m.)) followed by an MVA boost (week 4, 1x10^7 PFU of MVA Core, 1x10^7 PFU of MVA HBsAg, i.m.). Except stated otherwise, mice were sacrificed six days after MVA boost.

be called TherVacB hereafter (Figure 2.11). All experiments in this section were performed together with Anna Kosinska.

2.2.1.1 Influence of HBV titer on antiviral effect of therapeutic vaccination

2.2.1.1.1 Antiviral effect of therapeutic vaccination in C57Bl/6J mice harboring different HBV titers

To assess if success of TherVacB is dependent on the level of viremia, immunocompetent wildtype mice were infected with different doses of AAV-HBV, in detail we used 3 x 10^9, 1 x 10^{10}, 3 x 10^{10} or 1 x 10^{11} vg for infection. The experiment was performed as described in Figure 2.11. Animals were bled regularly to check serum HBeAg, HBsAg and ALT levels. We observed clearance of HBsAg- and HBeAg levels in mice infected with 3 x 10^9 vg, a decrease in mice receiving 1 x 10^{10} vg, whereas there was no effect on serum antigens levels in the two groups injected with 3 x 10^{10} vg or 1 x 10^{11} vg (Figure 2.12 A and B). Moreover, ALT was slightly elevated in animals receiving 1 x 10^{10} vg (Figure 2.12 C). Seroconversion from HBeAg to anti-HBe antibodies was only detected in the group infected with the lowest AAV-HBV titer. Anti-HBs and anti-HBc antibodies could be detected in all mice and the antibody titer inversely correlated with HBV antigen levels (Figure 2.12 D).

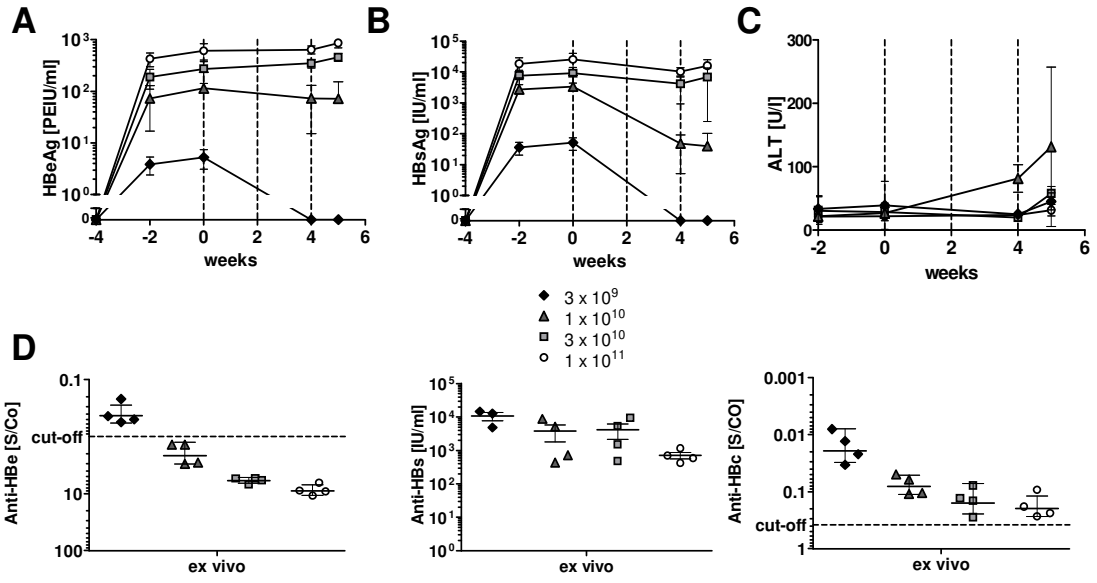

Figure 2.12 Serology of TherVacB treated C57Bl/6J mice harboring different HBV titers. Time course of **(A)** serum HBeAg, **(B)** serum HBsAg and **(C)** serum alanine amino transferase (ALT) levels. Dotted lines show timepoints of vaccination. **(D)** Anti-HBs, anti-HBc and anti-HBe antibodies day 6 after MVA boost. Mean and SD are shown. (n=4)

After vaccination, HBV-specific CD8+ T cells were detected in splenocytes and liver-associated lymphocytes (LALs) in low-titer but not in high-titer groups, measured by IFNγ expression upon stimulation with HBsAg- and HBcAg-derived peptides (Figure 2.13 A and B). Overall, the HBcAg response was superior to the HBsAg response and the amount of HBV-specific CD8+ T cells was higher in the 3 x 10^9 vg group than in animals injected with 1 x 10^{10} vg AAV-HBV. Notably, HBV-specific effector responses were found to be more pronounced in liver as compared to spleen (Figure 2.13 A and B). The MVA epitope B8R served as positive control after MVA vaccination in an IFNγ ELISpot assay with splenocytes of vaccinated mice, to ensure vaccination was performed equally amongst all groups. Unfortunately, too many cells

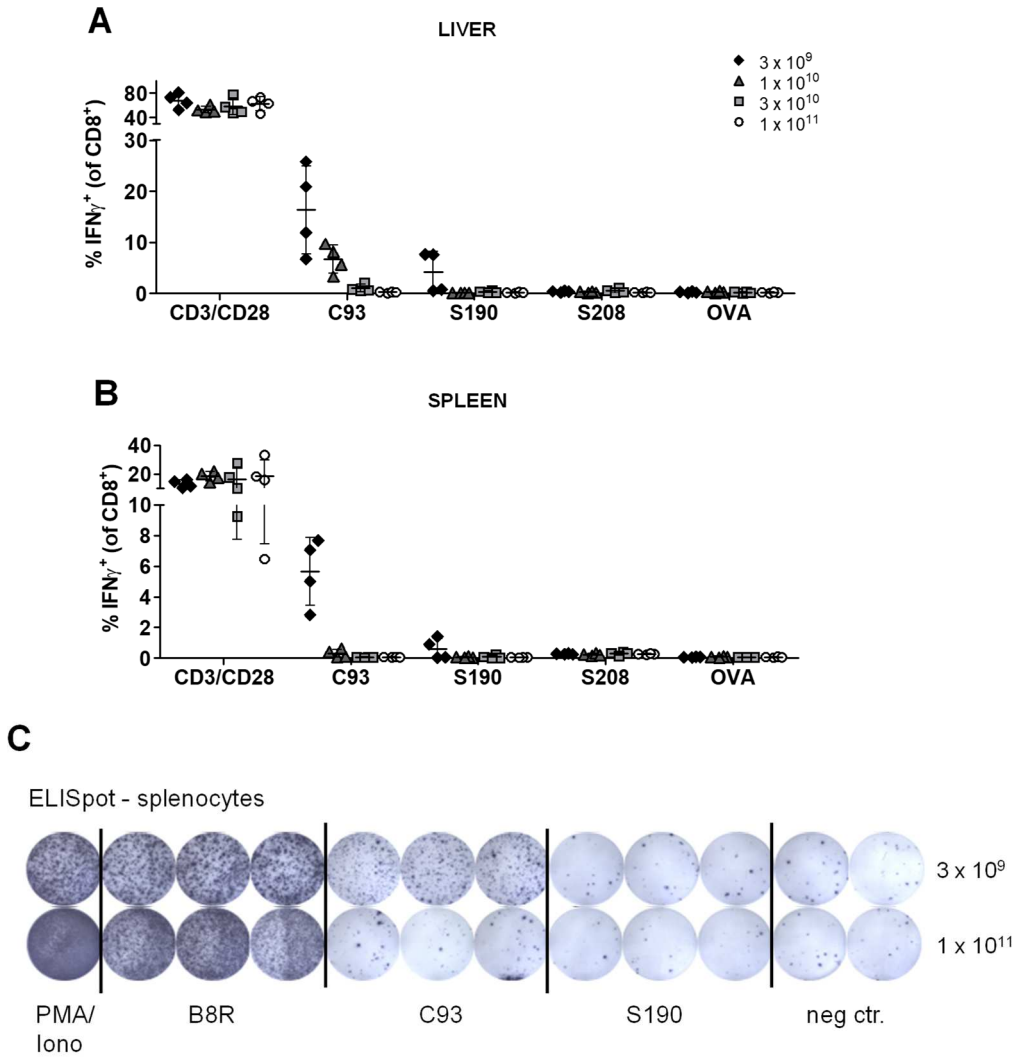

Figure 2.13 HBV-specific T-cell response induced by TherVacB in C57Bl/6J wildtype mice day 6 after MVA boost.
Intracellular cytokine staining of CD8+ T cells isolated from **(A)** liver or **(B)** spleen after *ex vivo* stimulation with HBV-specific (C93, S190 and S208) peptides. CD3/CD28 stimulation served as positive, stimulation with an OVA peptide as negative control. Mean and SD are shown. (n=4) **(C)** Representative IFNγ ELISpot plot of splenocytes after *ex vivo* stimulation with HBV-specific (C93 and S190) or MVA specific (B8R) peptides. Phorbol myristate actetate (PMA)/ ionomycin (Iono) served as positive control, stimulation with an OVA peptide as negative control.

responded in positive control wells as well as after stimulation with the MVA peptide, which is why the software was not able to count the spots. Nevertheless, this assay demonstrates equal response to B8R amongst the groups, whereas activation of HBV-specific T cells was titer dependent, confirming our ICS results (Figure 2.13 C).

To evaluate the antiviral effect of TherVacB-induced immunity, HBV protein expression in the liver was analyzed. The number of HBc^+ hepatocytes was not altered when compared to the start of vaccination (four weeks post infection, see Figure 2.3 D) in groups infected with 3×10^{10} vg or 1×10^{11} vg. On the contrary, vaccinated animals in the 3×10^9 vg, 1×10^{10} vg groups showed profound reduction of HBc^+ hepatocytes (Figure 2.14 A). Analyses of liver DNA revealed HBV replication in the liver of infected mice. HBV DNA was still detected six days after MVA boost, even in the 3×10^9 vg group (Figure 2.14 B).

In summary, the success of TherVacB-induced immunity was dependent on the level of viremia in immunocompetent C57Bl6/J mice infected with AAV-HBV. An antiviral effect was only observed in low-titer HBV-replicating animals.

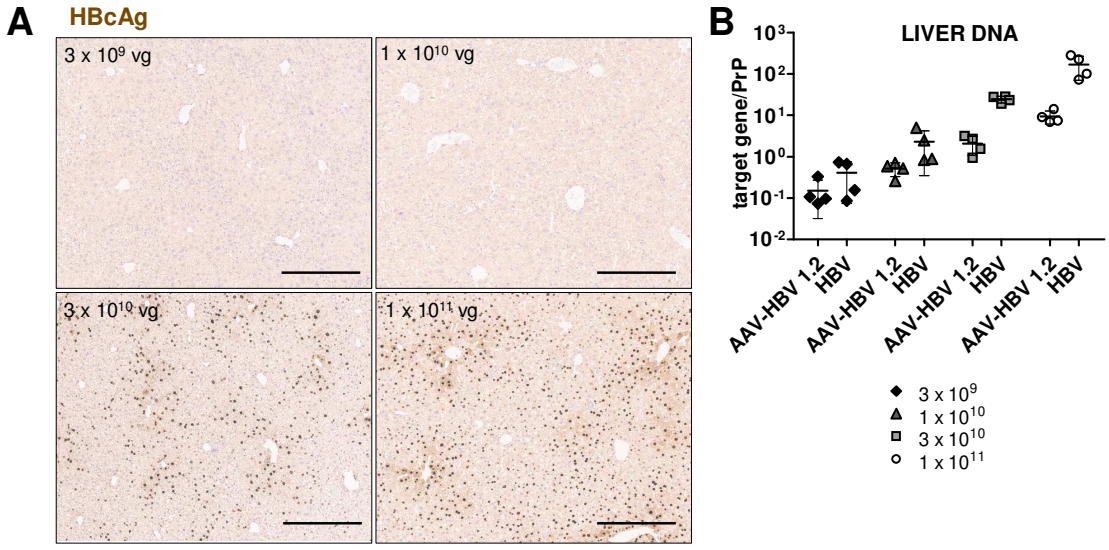

Figure 2.14 Analyses of liver tissue after TherVacB treatment in C57Bl6/J mice.
(A) Representative immunohistochemical HBcAg stainings of liver sections six days after MVA boost. Scale bars indicate 300 µm. **(B)** Levels of AAV vector (AAV-HBV 1.2) and whole HBV genomes (HBV) six days after MVA boost. Mean and SD are shown. (n=4)

2.2.1.1.2 Antiviral effect of therapeutic vaccination in HHDII-HLA-DR1 mice harboring different HBV titers

To determine the success of TherVacB in immunocompetent animals expressing the human HLA-A*02 and HLA-DR1 molecules, HHDII-HLA-DR1 mice (Pajot et al., 2004) were used. The experiment was performed as described in section 2.2.1.1. Interestingly, in these mice TherVacB could not induce HBs or HBe seroconversion, independent of viremia (Figure 2.15 A, B and D). ALT levels indicating liver damage stayed on physiological levels upon TherVacB treatment (Figure 2.15 C). We observed low levels of anti-HBs antibodies in all mice, anti-HBc antibodies in around 50 % of the animals, but this did not correlate inversely with HBV antigen levels as observed in C57Bl/6J wildtype mice before (Figure 2.15 D).

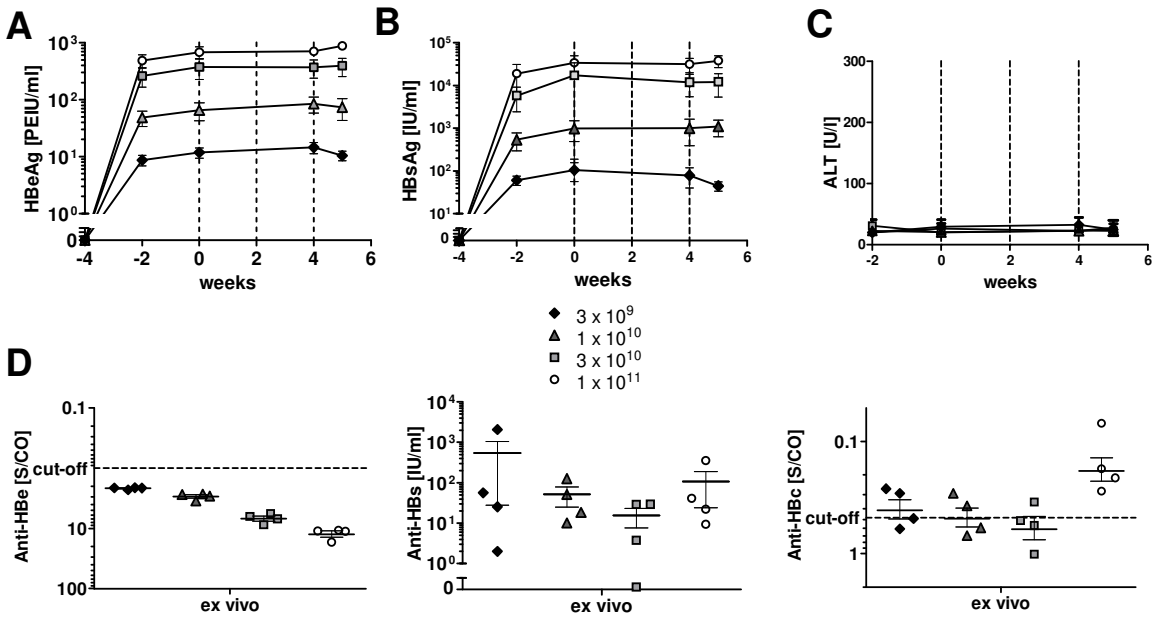

Figure 2.15 Serology of TherVacB treated HHDII-HLA-DR1 mice harboring different HBV titers. Time course of **(A)** serum HBeAg, **(B)** serum HBsAg and **(C)** serum alanine amino transferase (ALT) levels. Dotted lines show timepoints of vaccination. **(D)** Anti-HBs, anti-HBc and anti-HBe antibodies day 6 after MVA boost. Mean and SEM are shown. (n=4)

TherVacB-induced HBV-specific $CD8^+$ T cells in all animals, determined by ICS upon *ex vivo* peptide stimulation with HLA-A*02-restricted peptides derived from HBsAg and HBcAg. Again, the HBcAg response was superior to HBsAg response. Notably, HBV-specific effector cells were found in comparable frequencies in liver and spleen. Moreover, their presence was independent of viremia as seen in C57Bl/6J mice (Figure 2.16 A and B).

In conclusion, TherVacB treatment failed to induce an antiviral effect in HHDII-HLA-DR1 mice, independent of viremia although significant T-cell responses were observed.

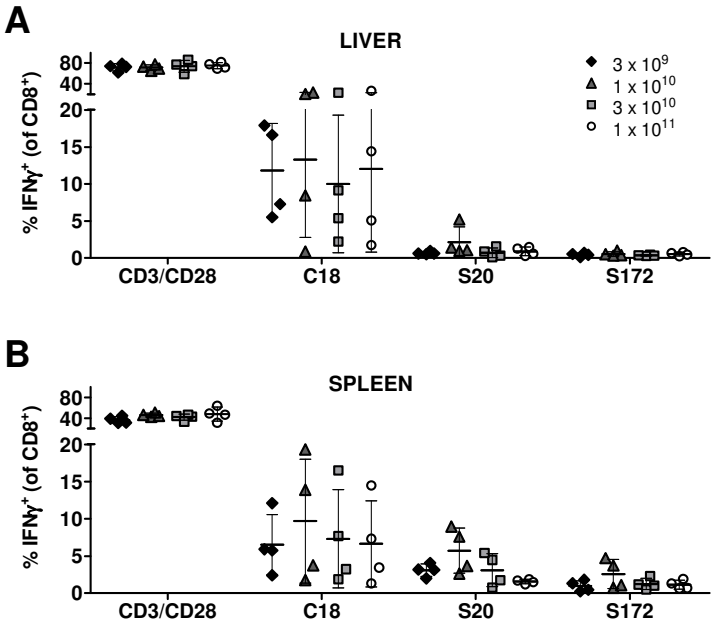

Figure 2.16 HBV-specific T-cell response induced by TherVacB in HHDII-HLA-DR1 mice harboring different HBV titers day 6 after MVA boost.
Intracellular cytokine staining of $CD8^+$ T cells isolated from **(A)** liver or **(B)** spleen after *ex vivo* stimulation with HBV-specific HLA-A*02-restricted peptides C18, S20 and S172. CD3/CD28 stimulation served as positive control. Mean and SD are shown. (n=4)

2.2.1.1.3 Determination of the reason for the absence of HBV-specific T cells upon therapeutic vaccination in high viremic C57Bl/6J mice

To examine if functional HBV-specific $CD8^+$ T cells were not detected six days after MVA boost in high viremic animals because of functional exhaustion or even activation-induced cell death, we infected immunocompetent wildtype mice with a low (3 x 10^9 vg) and a high (3 x 10^{10} vg) dose of AAV-HBV and shifted analyses to day 3 after MVA boost. We observed the same effects on serological level as reported in section 2.2.1.1.1. Upon TherVacB treatment, serum HBeAg and HBsAg levels decreased tremendously in low titer mice, whereas the effect in high titer mice was almost absent. Animals that got infected but not vaccinated (TherVacB only) did not reveal any changes in serum antigen levels (Figure 2.17 A and B). Moreover, slight ALT elevations were detected in vaccinated low titer mice. Animals that got only infected (3 x 10^9 vg), only vaccinated or got vaccinated upon high titer infection did not exhibit an elevation of serum ALT levels (Figure 2.17 C).

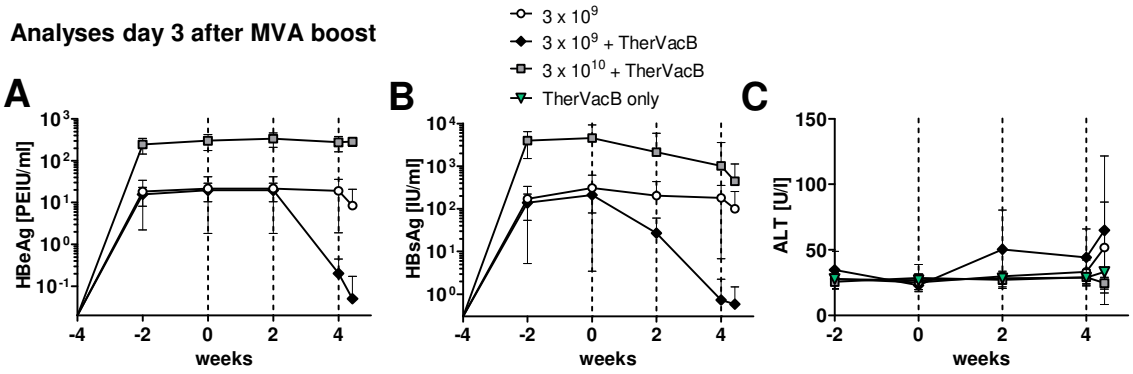

Figure 2.17 Serology of TherVacB treated high or low viremic C57Bl/6J mice.
Time course of **(A)** serum HBeAg, **(B)** serum HBsAg and **(C)** serum alanine amino transferase (ALT) levels. Dotted lines show timepoints of vaccination. Mean and SD are shown. (n=3-6)

To further characterize the TherVacB-induced HBV-specific T-cell response, the presence of HBV-specific intrahepatic CD8+ T cells was analyzed by a streptamer staining directly *ex vivo*. Three days after MVA boost we found a small population of MVA-specific CD8+ T cells by B8R streptamer staining in all mice that got vaccinated, but the abundance of HBV-specific CD8+ T cells (C93-streptamer) was significantly reduced in high compared to low viremic animals (Figure 2.18 A).

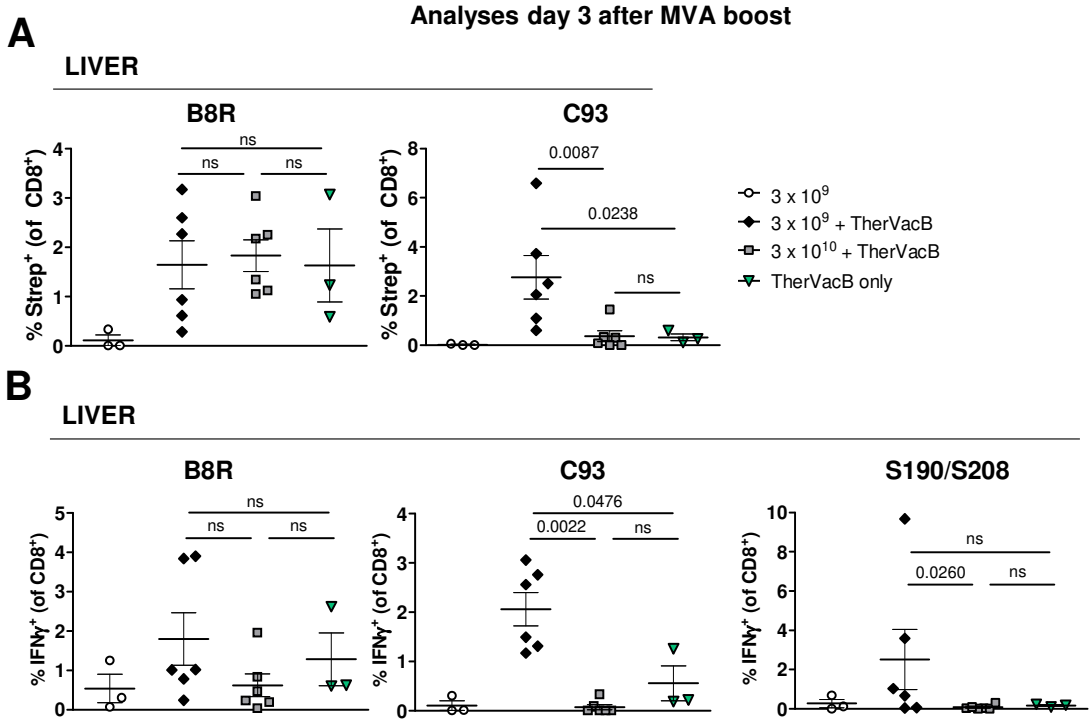

Figure 2.18 HBV-specific T-cell response induced by TherVacB in high or low viremic C57Bl/6J mice day 3 after MVA boost.
(A) Staining of HBV-specific intrahepatic CD8+ T cells *ex vivo* using B8R or C93 streptamers. **(B)** Intracellular cytokine staining of intrahepatic CD8+ T cells after *ex vivo* stimulation with HBV peptides (C93, S190/S208) and MVA peptide (B8R). Data is represented as relative values after background subtraction determined by OVA peptide. Mean and SD are shown. (n=3-6, Mann-Whitney test, numbers in graphs indicate p values, ns = not significant)

The presence of B8R- or C93-specific T cells determined by streptamer staining positively correlated with T-cell functionality. Upon *ex vivo* stimulation with the corresponding peptides, the frequency of intrahepatic IFNγ$^+$ CD8$^+$ T cells were not significant different within the vaccinated groups when stimulated with MVA-peptide B8R. However, HBV peptides C93 and S190/S208 could only activate CD8$^+$ T cells to secrete IFNγ if animals had been infected with the low dose of AAV-HBV (Figure 2.18 C). The data indicated that most T cells detected were functional.

As HBV-specific CD8$^+$ T cells were absent on day 3 after MVA boost in a high viremic environment, we were aiming to study the composition of subpopulations among the lymphocytes isolated from spleen and liver, as they are able to influence each other. When analyzing the frequency of CD3$^+$ T cells, CD19$^+$ B cells, CD3$^-$ NK1.1$^+$ CD49.b$^+$ NK cells and CD3$^+$ NK1.1$^+$ CD49.b$^+$ NKT cells, we found a higher percentage of NKT cells in high viremic vaccinated animals than in non-vaccinated animals amongst intrahepatic lymphocytes (Figure 2.19 A). B- and T-cell populations were equally represented throughout all groups, whereas the high viremic and vaccinated group demonstrated a significantly higher frequency of NK cells when compared to the low viremic and vaccinated animals within the LAL compartment (Figure 2.19 A).

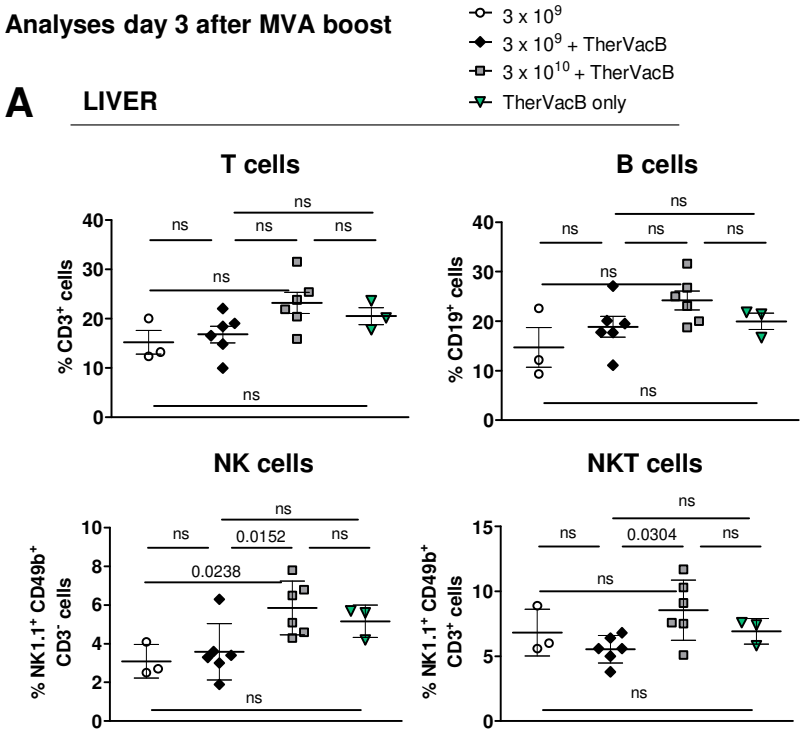

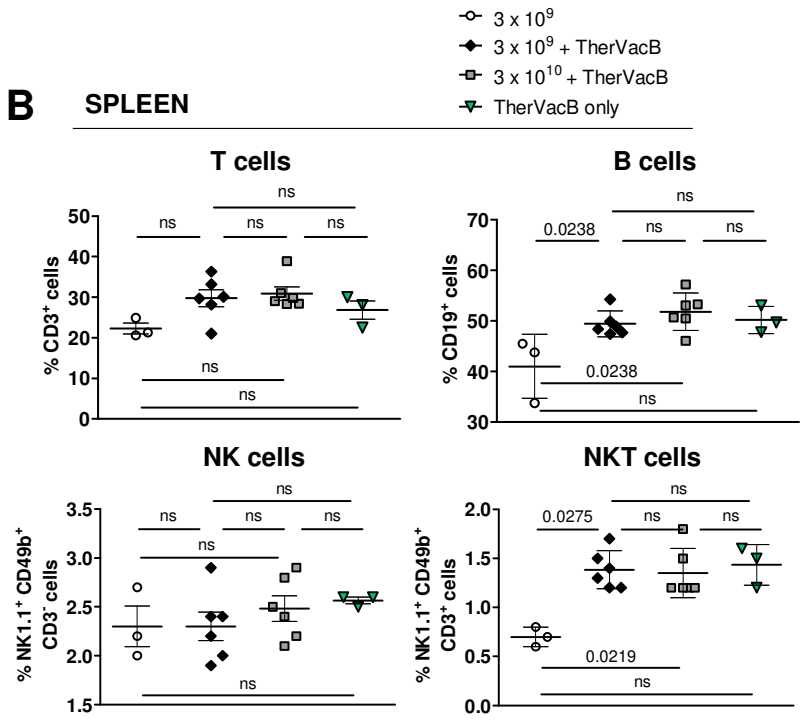

Figure 2.19 Analyses of subpopulations within lymphocytes after TherVacB treatment in high or low viremic C57Bl/6J mice day 3 after MVA boost.
Frequency of $CD3^+$ T-cells, $CD19^+$ B-cells. $CD3^-$ $NK1.1^+$ $CD49b^+$ NK^- cells and $CD3^+$ $NK1.1^+$ $CD49b^+$ NKT cells in lymphocytes isolated from **(A)** liver and **(B)** spleen. Mean and SD are shown. (n=3-6, Mann-Whitney test, numbers in graphs indicate p values, ns = not significant)

This difference in NK-cell frequency was liver-specific, as it was not seen in the spleen (Figure 2.19 B). T cells from spleen showed an equal frequency of around 25 % throughout all groups, whereas a significantly lower amount of B cells and NKT cells were present in not vaccinated animals (Figure 2.19 B).

In summary, HBV-specific $CD8^+$ T cells were neither detected three days nor six days after MVA boost in high viremic TherVacB treated animals while they were readily detected in low viremic TherVacB-vaccinated mice. A higher abundance of NK cells in the liver of high viremic animals was observed indicating that NK cell-mediated elimination of HBV-specific T cells could play a role (Peppa et al., 2013).

2.2.1.2 Long-term antiviral effect of therapeutic vaccination

TherVacB-induced immunity was not able to eradicate HBV and its transcription template from the liver of low titer mice when analyses were performed six days after MVA boost (see Figure 2.14). We therefore followed mice treated with TherVacB after low dose AAV-HBV infection and analyzed them ten weeks after MVA boost of HBV-specific immunity. All animals showed clearance of serum HBeAg and HBsAg levels upon vaccination, one mouse experienced a relapse in serum HBeAg beginning week 5 after MVA boost. Importantly, TherVacB-induced

immunity was not able to control this relapse again. In contrast, two serum HBsAg relapses detected week 3 and 5 of two different mice were controlled immediately afterwards (Figure 2.20 A and B). Vaccination was accompanied by moderate ALT elevations, but ALT levels returned to physiological levels quickly (Figure 2.20 C). Ten weeks after MVA boost, functional HBV-specific T cells were still detected in liver and spleen of vaccinated but not in non-vaccinated animals. As seen in previous experiments, HBcAg-specific response was superior to that to HBsAg. Moreover, the frequency of $CD8^+$ T cells that secreted IFNγ upon stimulation with HBV peptides was much higher in liver than in spleen (Figure 2.20 D and E). Determination of AAV and HBV DNA in liver tissue of vaccinated and control animals revealed no significant change when comparing analyses six days to ten weeks after MVA boost (Figure 2.20 F).

In fact, ten weeks after MVA boost, mice had not eradicated HBV and its transcription template although they still exhibited functional intrahepatic HBV-specific T cells and had controlled antigenemia.

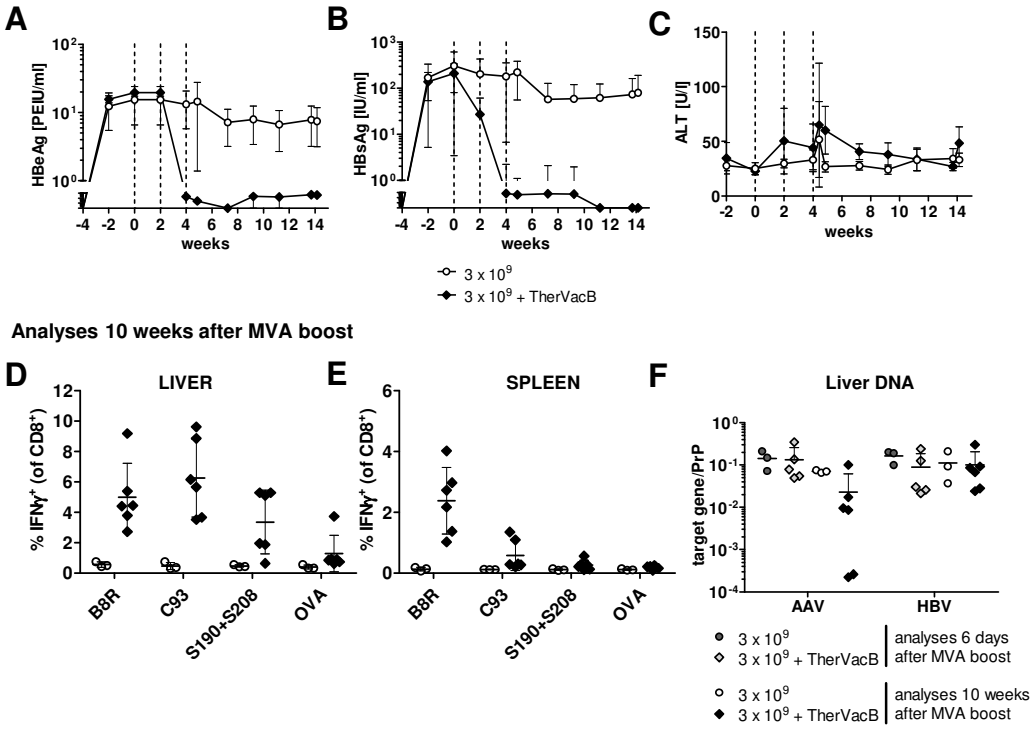

Figure 2.20 Long-term effect of TherVacB in low titer C57Bl/6J mice.
Time course of **(A)** serum HBeAg, **(B)** serum HBsAg and **(C)** serum alanine amino transferase (ALT) levels. Dotted lines show timepoints of vaccination. **(D)** Intracellular cytokine staining of $CD8^+$ T cells isolated from **(D)** liver or **(E)** spleen upon *ex vivo* stimulation with HBV (C93 and S190/S208) or MVA (B8R) peptides. Stimulation with an OVA peptide served as negative control. **(F)** Levels of AAV vector (AAV) and whole HBV genomes (HBV) relative to PrP at indicated time points. Mean and SD are shown. (n=3-6)

2.2.1.3 Influence of duration to HBV exposure on the antiviral effect of therapeutic vaccination

To determine, if TherVacB would provide the same achievement if study subjects were exposed to HBV for an extended time period, mice were either vaccinated three months after AAV-HBV infection or after only one month as addressed in sections above. Animals were of the same age at the start of vaccination. Moreover, we included a group of animals, that was only AAV-HBV-infected (AAV-HBV only) and a group of HBV-naïve mice that got vaccinated (TherVacB only). The effect of TherVacB treatment was notably higher in animals that were exposed to HBV for only one month compared to the group that was infected three months prior to vaccination as indicated by serological analyses (Figure 2.21 A and B). Serum analyses depicted a decrease in serum HBeAg levels along with seroconversion to anti-HBe antibodies when animals were exposed to HBV for only one month (Figure 2.21 A and D). In contrast, serum HBsAg levels decreased to the same extent in both groups (Figure 2.21 B). Furthermore, neither anti-HBs nor anti-HBc antibody levels were different amongst the TherVacB treated groups (Figure 2.21 D). Notably, we only found serum ALT elevation in the group that was infected with AAV-HBV one month prior to vaccination (Figure 2.21 C).

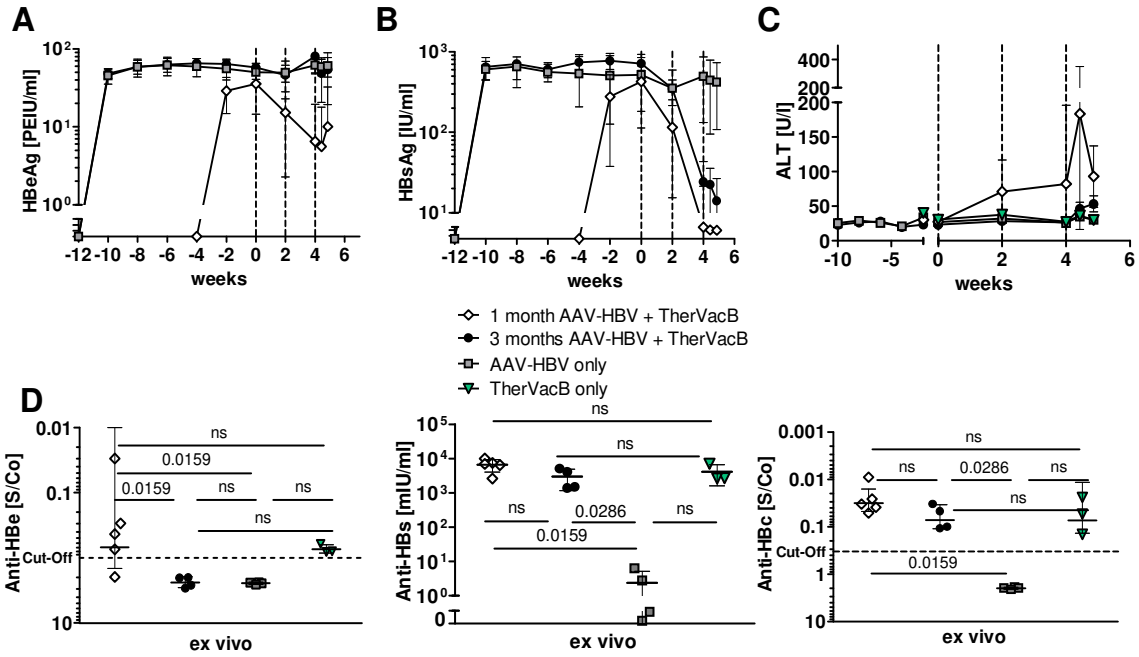

Figure 2.21 Serology upon TherVacB treatment after different durations of HBV exposure. Time course of **(A)** serum HBeAg, **(B)** serum HBsAg and **(C)** serum alanine amino transferase (ALT) levels of 1 x 10^{10} vg AAV-HBV-infected C57Bl/6J mice. Dotted lines show timepoints of vaccination. **(D)** Anti-HBs, anti-HBc and anti-HBe antibodies on day 6 after MVA boost. Mean and SD are shown. (n=3-5, Mann-Whitney test, numbers in graphs indicate p values, ns = not significant)

To evaluate TherVacB-induced T-cell responses, we analyzed intrahepatic HBV-specific T cells directly *ex vivo*. The frequency of MVA-specific (B8R streptamer) as well as HBV core-

specific (C93 streptamer) T cells did not differ amongst all vaccinated groups (Figure 2.22 A). In addition, we also analyzed the T-cell phenotype. High expression of activation/exhaustion marker PD-1 (programmed cell death protein 1) was observed on C93-, but not on B8R-specific T cells and was independent of duration of prior HBV infection. The exhaustion marker CTLA-4 (cytotoxic T-lymphocyte-associated Protein 4) was not significantly different in B8R- or C93-specific CD8⁺ T cells when comparing animals that were vaccinated one month or three months after start of HBV exposure (Figure 2.22 B and C). In contrast, C93-specific CD8⁺

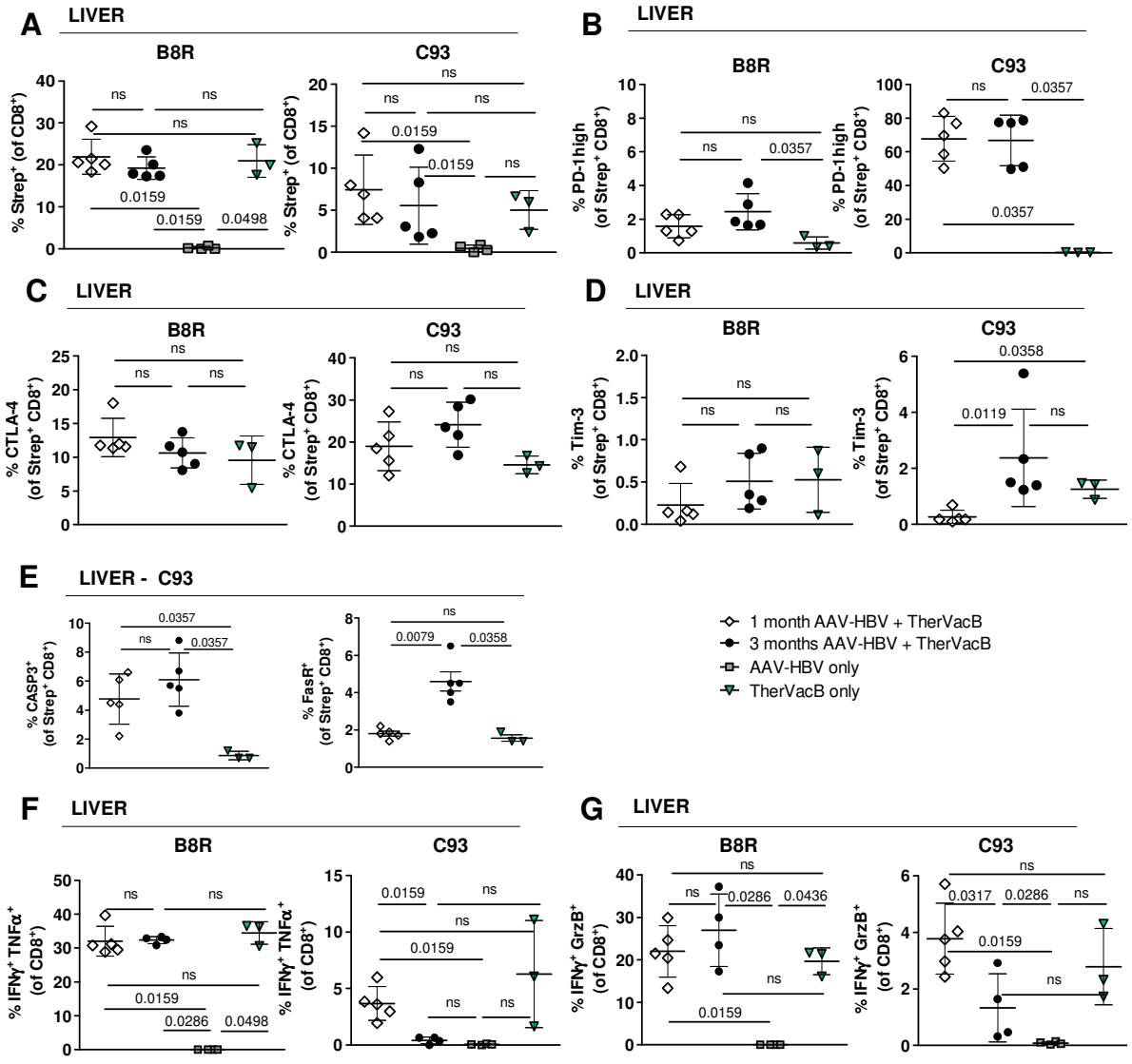

Figure 2.22 HBV-specific T-cell response induced by TherVacB after different durations of HBV exposure in C57Bl/6J mice day 6 after MVA boost.
(A) Staining of HBV-specific intrahepatic CD8⁺ T cells *ex vivo* using B8R or C93 streptamers. Frequency of CD8⁺ Strep⁺ **(B)** PD1 high⁺, **(C)** CTLA-4⁺ or **(D)** Tim3⁺ T cells. **(E)** Frequency of CD8⁺ C93⁺ Cas3⁺ or FasR⁺ T cells. Intracellular cytokine staining of intrahepatic CD8⁺ T cells after *ex vivo* stimulation with HBV peptide C93 and MVA peptide B8R. Frequency of CD8⁺ **(F)** IFNγ⁺TNFα⁺ or **(G)** IFNγ⁺ GrzB⁺ T cells. Data is represented as relative values after background subtraction determined by OVA peptide. Mean and SD are shown. (n=3-5, Mann-Whitney test, numbers in graphs indicate p values, ns = not significant)

T cells from the three months AAV-HBV + TherVacB treated group demonstrated substantially higher expression of the exhaustion marker Tim-3 (T-cell immunoglobulin and mucin-domain containing-3). This difference was not present in B8R-specific T cells (Figure 2.22 D). To determine, if these HBV-specific T cells were more prone to apoptosis, the expression of caspase-3 (Casp-3) and FasR (first apoptosis signal receptor) was analyzed within the intrahepatic C93^{+} CD8^{+} T cells. The expression of Casp-3 was not significantly different, but expression of FasR was considerably increased when animals were exposed to HBV three months compared to one month prior to vaccination (Figure 2.22 E). Importantly, we also provided evidence for lower functionality of HBV-specific T cells. Upon *ex vivo* stimulation with corresponding peptides, a significant lower amount of intrahepatic CD8^{+} T cells responded with IFNγ and TNFα as well as IFNγ and GrzB expression when mice were exposed to HBV for three months compared to one month before TherVacB treatment. This effect was HBV specific, as MVA responses were not changed amongst vaccinated groups (Figure 2.22 F and G). The difference in TherVacB success was also demonstrated when liver tissue was analyzed. Vaccination demonstrated to influence HBV levels in the liver of animals that were exposed to HBV for three months prior to vaccination compared to unvaccinated control animals. The reduction of HBc^{+} hepatocytes as well as HBV DNA in liver was further enhanced in the group of mice that were infected one month before TherVacB treatment started (Figure 2.23 A and B).

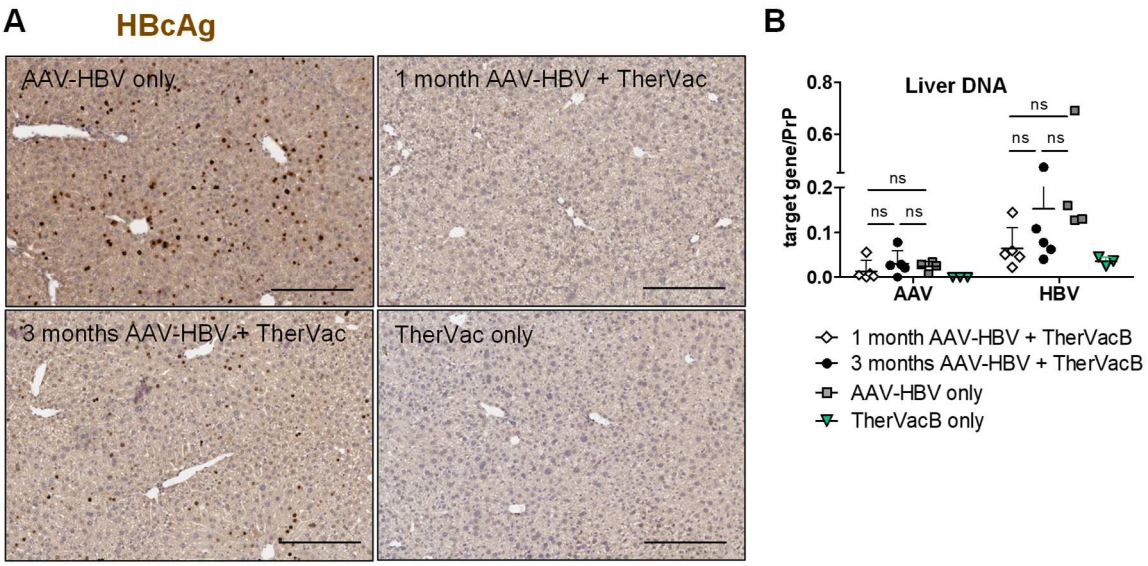

Figure 2.23 Analyses of liver tissue upon TherVacB treatment after different durations of HBV exposure day 6 after MVA boost.
(A) Representative immunohistochemical HBcAg stainings of liver sections. Scale bars indicate 300 µm. **(B)** Levels of AAV vector (AAV) and whole HBV genomes (HBV). (n=3-5, Mann-Whitney test, numbers in graphs indicate p values, ns = not significant)

In short, success of TherVacB was dependent on the duration of prior HBV exposure. HBV-specific T cells demonstrated less functionality accompanied with an increased expression of FasR when animals were infected three months instead of one month prior to vaccination.

2.2.1.4 Potential of therapeutic vaccination on HBV mutants

To explore the efficacy of TherVacB on HBV carriers that are serum HBeAg negative or developed the HBeAg stem-loop mutation, we vaccinated animals that got infected with AAVs encoding for either 1.3WT or 1.3E$^-$ HBV genome. Moreover, we included a group that was infected with AAV-HBV 1.3X$^-$, as using this genome variant is less restricted due to bio safety regulations (see section 2.1.2). TherVacB applied one month after infection demonstrated to be successful to achieve functional cure in all variants, as serum HBeAg and HBsAg levels declined and seroconversion to anti-HBe and anti-HBsAg was observed (Figure 2.24 A, B and D). Not all animals experienced anti-HBe production upon TherVacB treatment in the E$^-$ variant, but interestingly, some of them did. Moderate serum ALT elevations were observed in WT and E$^-$ genomes, but not in animals vaccinated after infection with X$^-$ genome (Figure 2.24 C).

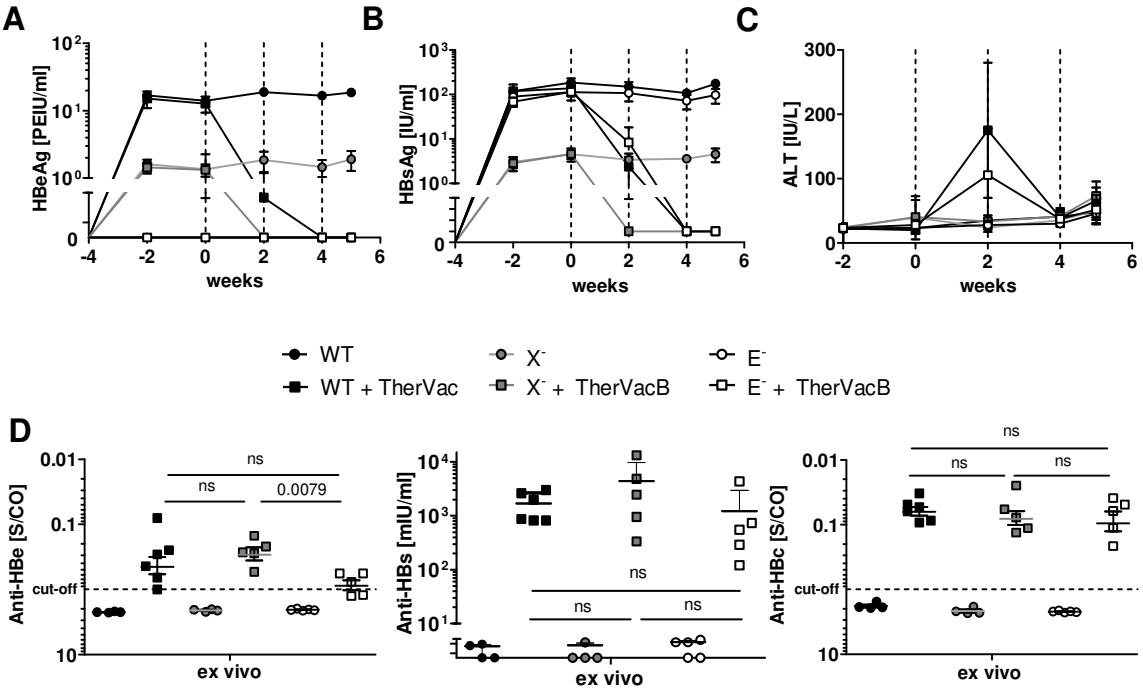

Figure 2.24 Serological analyses after TherVacB treatment of C57Bl/6J mice infected with AAV-HBV 1.3WT, AAV-HBV 1.3X$^-$ or AAV-HBV 1.3E$^-$.
Time course of **(A)** serum HBeAg, **(B)** serum HBsAg and **(C)** serum alanine amino transferase (ALT) levels of 1 x 10^{10} vg AAV-HBV-infected C57Bl/6J mice. Dotted lines show timepoints of vaccination. **(D)** Anti-HBe, anti-HBs and anti-HBc antibodies day 6 after MVA boost. Mean and SD are shown. (n=4-6, Mann-Whitney test, numbers in graphs indicate p values, ns = not significant)

To examine TherVacB-induced cytotoxic T-cell responses, we analyzed intrahepatic HBV-specific T cells directly *ex vivo* as well as their functionality upon *ex vivo* stimulation with the

respective peptides. Upon vaccination we found C93-specific T cells in all groups. Their frequency tended to be lower in HBV-E$^-$ infection, but surprisingly their functionality was significantly enhanced (Figure 2.25 A and B). Significantly more CD8$^+$ T cells were activated to secrete IFNγ upon stimulation with peptide S190 in HBV-E$^-$ and HBV-X$^-$ groups when compared to the WT variant (Figure 2.25 B). Overall, HBcAg response was again superior to HBsAg response (Figure 2.25 A and B).

Taken together, our data provides evidence that TherVacB induces HBV-specific immune responses in X protein as well as HBeAg negative study subjects and functionality of HBV-specific CD8$^+$ T cells was even increased in animals infected with HBV-E$^-$ genome variant.

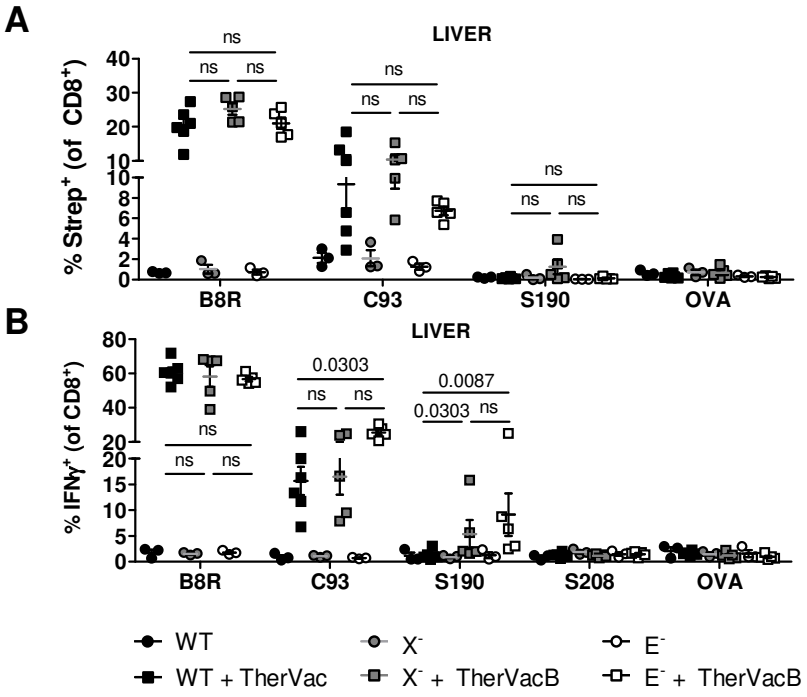

Figure 2.25 HBV-specific T-cell response induced by TherVacB in C57Bl/6J mice infected with AAV-HBV 1.3WT, AAV-HBV 1.3X$^-$ or AAV-HBV 1.3E$^-$ day 6 after MVA boost.
(A) Staining of HBV-specific intrahepatic CD8$^+$ T cells *ex vivo* using B8R, C93, S190 or OVA streptamers. **(B)** Intracellular cytokine staining of intrahepatic CD8$^+$ T cells upon *ex vivo* stimulation with HBV peptides (C93, S190/S208) and MVA peptide (B8R). Stimulation with an OVA peptide served as negative control. Mean and SD are shown. (n=3-6, Mann-Whitney test, numbers in graphs indicate p values, ns = not significant)

2.2.2 Chimeric antigen receptor redirected T cells

Beside therapeutic vaccination, adoptive transfer of HBV-specific T cells represents another approach to restore the patient's immune response towards HBV-infected hepatocytes or HBV-associated HCC. One possibility to redirect T cells is to genetically introduce a chimeric antigen receptor (CAR) that recognizes a target antigen that is expressed on the cell surface.

The potential of T cells redirected with a chimeric antigen receptor towards HBV surface proteins (S-CAR) have already been intensively investigated *in vitro* and in HBV-transgenic mice (Bohne et al., 2008; Krebs et al., 2013). To determine the potential of S-CAR grafted T cells to achieve clearance of chronic HBV infection, the AAV-HBV model was used. Importantly, immunocompetent mice develop an immune response against the S-CAR which greatly reduces the antiviral potential of S-CAR$^+$ T cells (Festag, 2018). Given this result, I performed an experiment in immunodeficient mice. Rag2$^{-/-}$ mice were injected with 1 x 10^{10} vg (low titer) or 1 x 10^{11} vg (high titer) of AAV-HBV. 24 days later, mice received redirected CD8$^+$ T cells expressing either S-CAR or SΔ-CAR (control S-CAR with no functional intracellular signal domain) (Figure 2.26 A). Mice were bled regularly to determine transferred cells in full blood as well as serum HBeAg and HBsAg and ALT levels. S-CAR T cells expanded

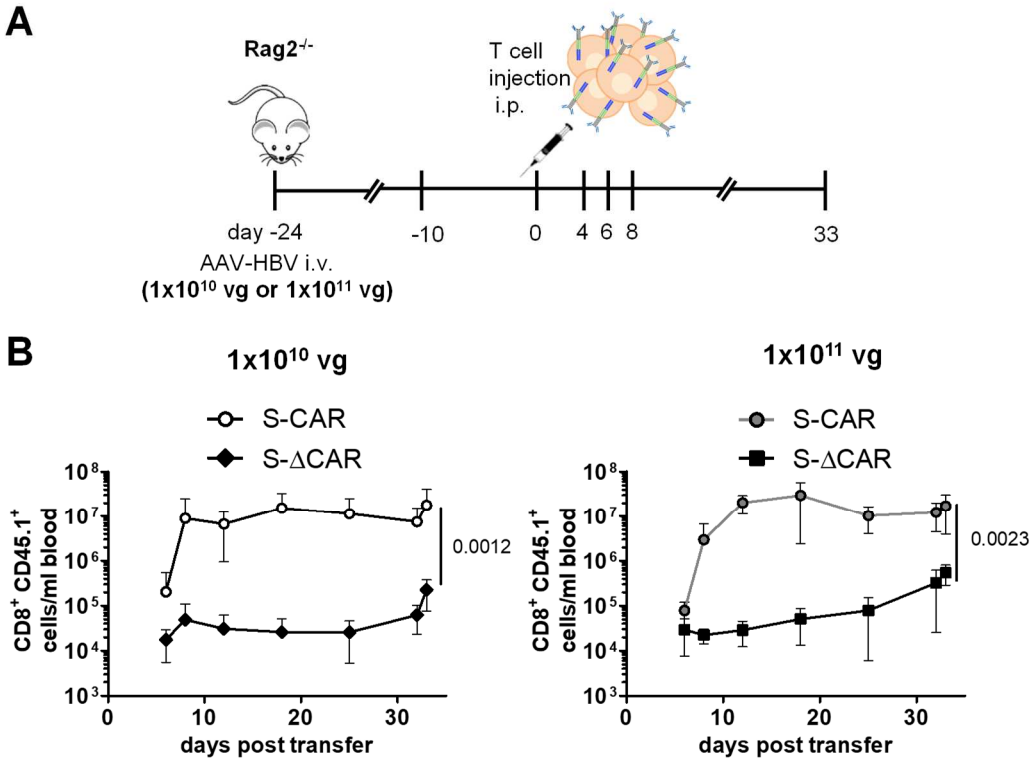

Figure 2.26 Engraftment of S-CAR T cells in AAV-HBV-infected immunodeficient Rag2$^{-/-}$ mice. **(A)** Schematic overview: Rag2$^{-/-}$ mice were intravenously injected with 1 x 10^{10} vg or 1 x 10^{11} vg AAV-HBV. 24 days later, when chronic infection was established, mice received either 1 x 10^6 S-CAR- or 1 x 10^6 SΔ-CAR-engrafted CD8$^+$ T cells intraperitoneally. **(B)** Time course of total count of transferred (CD45.1$^+$) CD8$^+$ T cells. Mean and SD are shown. (n=3-4, Mann-Whitney test numbers in graphs indicate p values)

extensively, reaching a plateau of numbers up to 10^7 S-CAR T cells per ml blood from day 8 after T-cell transfer onwards. This level was constant until the end of the experiment. SΔ-CAR T cells could also be detected over time with an average of around 10^5 cells per ml blood (Figure 2.26 B). We note that the engraftment of S-CAR T cells was independent of the AAV-HBV titer.

On day 8 after adoptive T-cell transfer, serum HBsAg and HBeAg levels of S-CAR treated mice started to decline which continued until day 33 after T-cell transfer. Finally, a reduction of 2-3 logs and 0.5-1 logs in serum HBsAg and HBeAg levels, respectively, was observed. Interestingly, serum marker for HBV persistence were reduced to the approximately same value, independent of where they started off (Figure 2.27 A and B). Antigen levels in SΔ-CAR treated mice remained unchanged until the end of the experiment (Figure 2.27 A and B). Serum

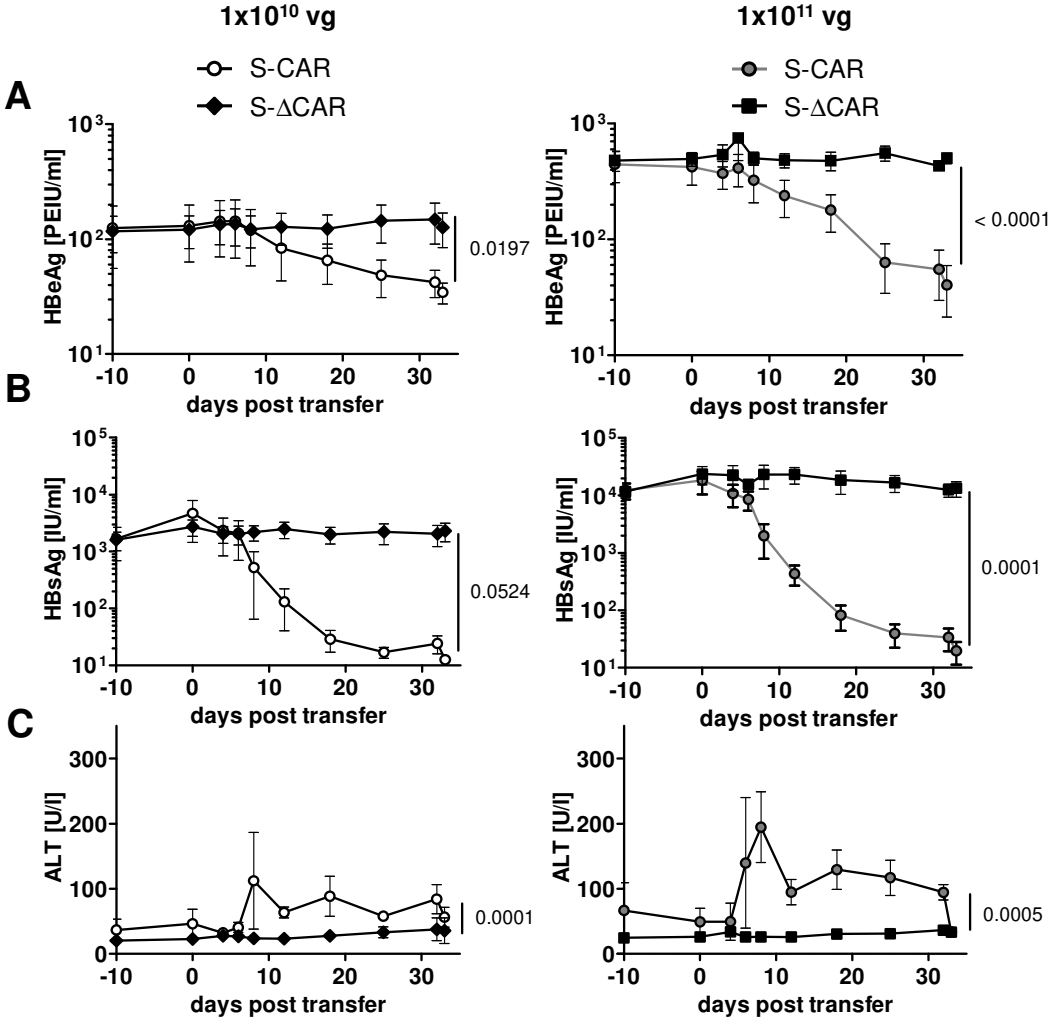

Figure 2.27 Serological analyses after S-CAR or SΔ-CAR T-cell treatment in AAV-HBV-infected immunodeficient Rag2$^{-/-}$ mice.
Time course of **(A)** serum HBeAg, **(B)** serum HBsAg and **(C)** serum alanine amino transferase (ALT) levels. Mean and SD are shown. (n=3-4, Mann-Whitney test for not normally distributed data: HBsAg 1 x 10^{10} vg, HBeAg 1 x 10^{11} vg, unpaired t test for normally distributed data: HBeAg and ALT 1 x 10^{10} vg, HBsAg and ALT 1 x 10^{11} vg, numbers in graphs indicate p values)

ALT levels, indicating liver damage, peaked at day 8 or 10 in S-CAR treated mice (up to 250 U/l and 150 U/l in high and low titer mice, respectively) and remained elevated (around 100 U/l) indicating ongoing hepatocyte killing. There was no ALT elevation detected in mice receiving SΔ-CAR T cells (Figure 2.26 C).

One month after T-cell transfer, high numbers of intrahepatic lymphocytes accumulated in S-CAR treated mice (up to 4 x 10^7 transduced S-CAR T cells) per liver. Within splenocytes we found the same numbers of transferred cells after treatment with S-CAR T cells, while SΔ-CAR T cells were only present in low numbers in liver and spleen (Figure 2.28 A). Splenocytes and LALs were used for *ex vivo* re-stimulation with HBsAg. About 30-45 % of S-CAR T cells were reactivated upon contact with HBsAg, as determined by IFNγ and TNFα secretion (Figure 2.28 B). Importantly, S-CAR T cells had a tendency to respond less well to unspecific activation using CD3/CD28 antibodies as compared to SΔ-CAR T cells *ex vivo* (Figure 2.28 B).

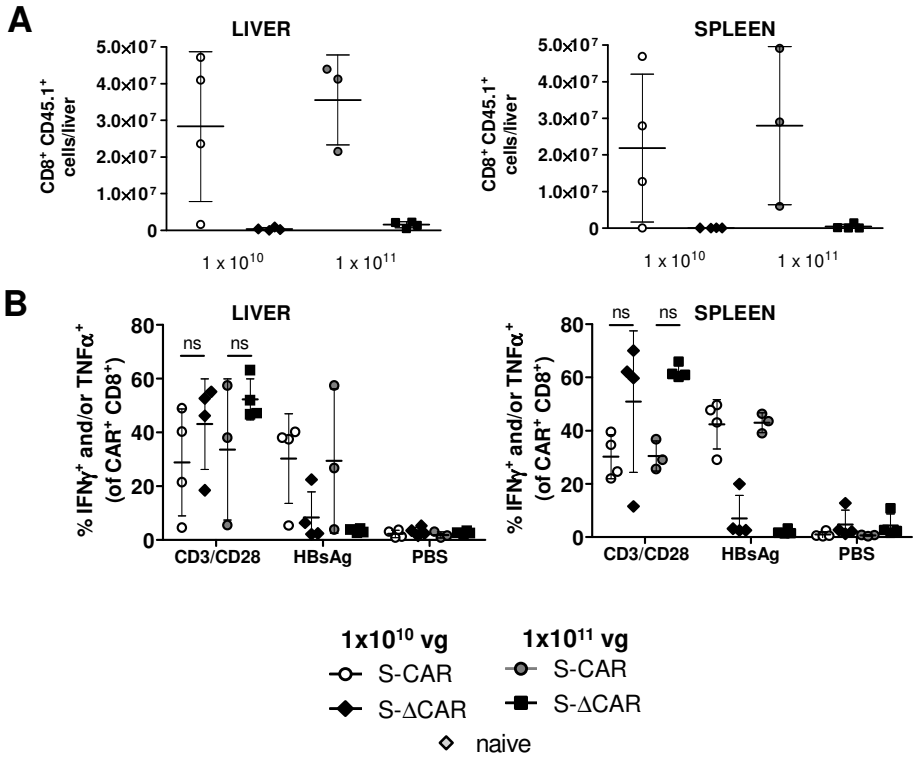

Figure 2.28 *Ex vivo* T cell analyses after S-CAR or SΔ-CAR T-cell treatment in AAV-HBV-infected immunodeficient Rag2$^{-/-}$ mice.
(A) Total count of transferred (CD45.1$^+$) CD8$^+$ T cells isolated from liver or spleen. **(B)** Intracellular cytokine staining of CAR$^+$ CD8$^+$ T cells isolated from liver or spleen after *ex vivo* stimulation with HBsAg. CD3/CD28 stimulation served as positive control, stimulation with PBS as negative control. Mean and SD are shown. (n=3-4, Mann-Whitney test, ns = not significant)

Furthermore, S-CAR T-cell treatment resulted in a profound reduction of HBcAg expressing hepatocytes as well as a strong decrease in AAV and HBV DNA in liver tissue (Figure 2.29 A and B). In general, the effect of S-CAR T cells was more pronounced in animals receiving the high titer of AAV-HBV, however, they retained the same amount of HBc$^+$ hepatocytes and HBV

DNA as the mice infected with the low dose of AAV-HBV at the end of the experiment (Figure 2.29 A and B).

In summary, S-CAR-redirected T cells had a profound antiviral activity in AAV-HBV-infected Rag2$^{-/-}$ animals but failed to completely eradicate HBV within one month after adoptive T-cell transfer.

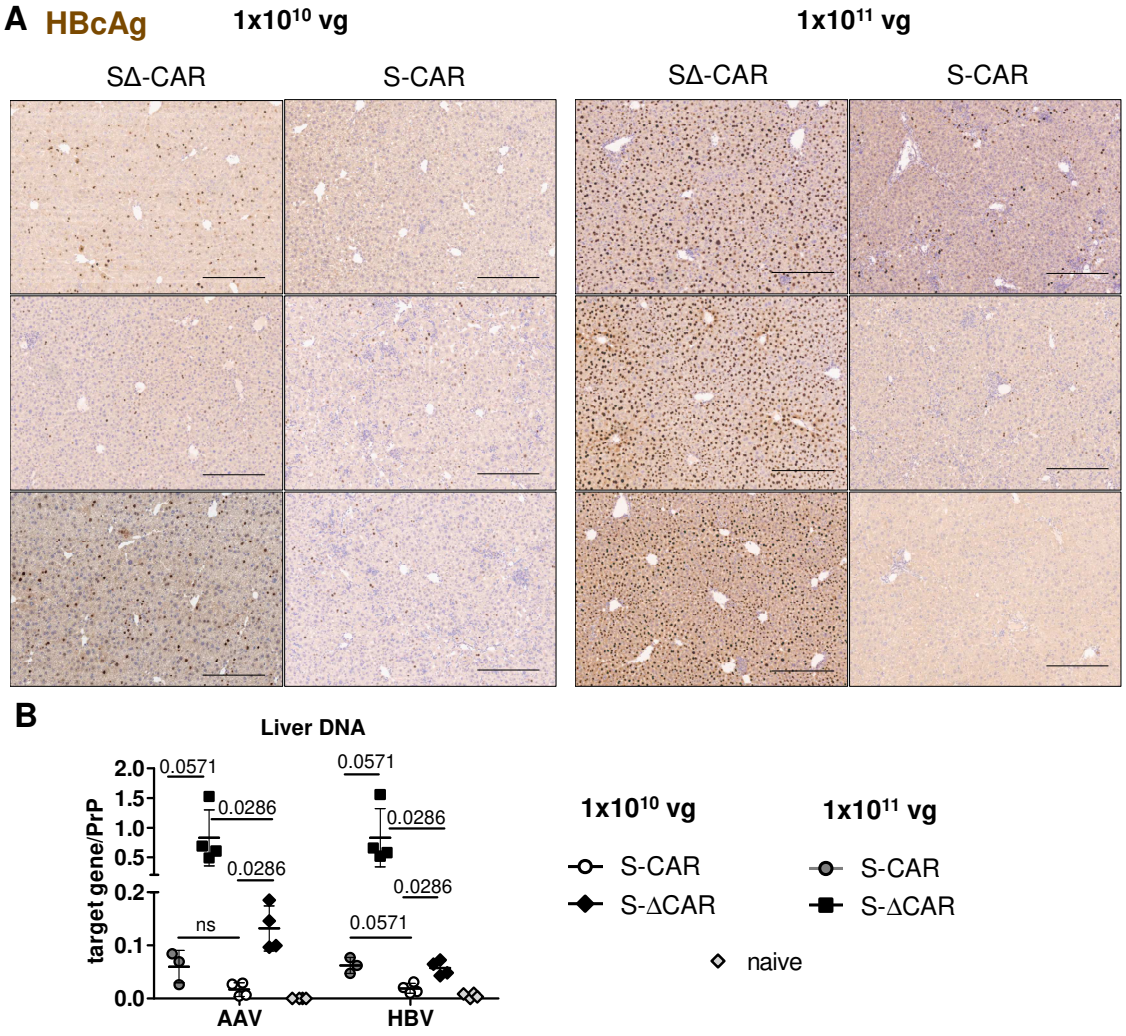

Figure 2.29 Liver analyses after S-CAR or SΔ-CAR T-cell treatment in AAV-HBV-infected immunodeficient Rag2$^{-/-}$ mice.
(A) Representative immunohistochemical HBcAg stainings of liver sections. Scale bars indicate 300 µm. **(B)** Levels of AAV vector (AAV) and whole HBV genomes (HBV) relative to PrP 33 days after adoptive T-cell transfer. (n=3-4, Mann-Whitney test)

2.2.3 Natural T cell receptor redirected T cells

Another possibility to genetically modify T cells is the redirection with a natural TCR. To study human TCRs *in vivo*, an appropriate mouse model is of utmost importance.

2.2.3.1 Antiviral effect of HBV-specific HLA-A*02 restricted TCR-redirected T cells in HHDII-HLA-DR1 mice

HHDII-HLA-DR1 mice express the human leukocyte antigens HLA-A*02 and DR1 of class I and class II instead of the murine molecules and therefore are a suitable model to investigate human HLA-A*02 and DR1 restricted TCRs *in vivo* (Pajot et al., 2004). The functionality of HBV-specific HLA-A*02 restricted TCRs has already been investigated *in vitro* (Wisskirchen et al., 2017). In this study, eleven TCRs specific for HBV surface (peptide S20 or S172) or core (C18) protein have been evaluated in comprehensive functional analyses. For each specificity described, one TCR with high functional avidity was chosen to be further evaluated *in vivo*: TCR 4G for peptide S20, TCR WL31 for peptide S172, TCR 6K for peptide C18. For this purpose, HHDII-HLA-DR1 mice were infected with AAV-HBV and then treated by adoptive transfer of T cells that were retrovirally transduced to express TCR 4G-, 6K-, WL31- or a control (HER2-specific) TCR one month later. To further enhance the possibility of an antiviral effect, mice that were adoptively transferred with TCR 4G redirected T cells, were injected with TCR 6K equipped T cells ten days later and vice versa (Figure 2.30 A). Serum HBeAg, HBsAg and serum ALT levels remained steady when monitoring animals over 30 days after transfer of HBV-specific T cells (Figure 2.30 B, C and D). The transferred cells could be distinguished from the endogenous cells because of a congenic marker, as recipient mice were CD45.2$^+$ and donor mice CD45.1/2$^+$. An extreme low number of transferred cells was detected in the blood of the animals (Figure 2.31 A), and engraftment of TCR$^+$ cells was only found for TCR 4G and 6K (Figure 2.31 B). Nevertheless, after *ex vivo* stimulation with the corresponding peptides, 6 % of transferred CD8$^+$ T cells isolated from liver were activated to secrete IFNγ when stimulated with peptide C18 and S20 (Figure 2.31 C). In contrast, we did not recover S172-specific T cells from liver or spleen (Figure 2.31 C and D). Interestingly, the frequency of activated C18-specific T cells was equal in liver and spleen, whereas a substantially higher amount of activated S20-cpecific T cells was detected in the spleen compared to the liver (Figure 2.31 C and D).

Taken together, adoptively transferred HBV-specific T cells did not have an antiviral effect in HHDII-HLA-DR1 mice even if functional TCR$^+$ T cells could be recovered from liver and spleen.

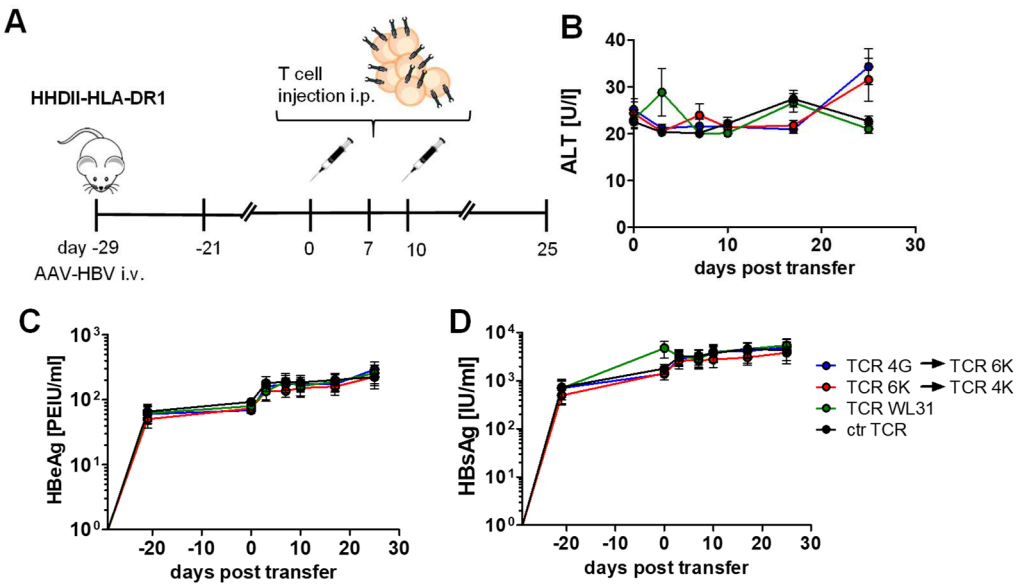

Figure 2.30 Antiviral effect of HLA-A*02 restricted HBV-specific TCR⁺ T cells after adoptive transfer into AAV-HBV-infected HHDII-HLA-DR1 mice.
(A) Schematic overview: HHDII-HLA-DR1 mice were i.v. injected with 1 x 10^{10} vg AAV-HBV. 29 days later, when chronic infection was established, mice received either 4 x 10^6 TCR 4G-, TCR 6K- or TCR WL31-engrafted CD8⁺ T cells or 3 x 10^6 control (HER2-specific) TCR-engrafted CD8⁺ T cells intraperitoneally. On day 10, mice that got TCR 4G⁺ T cells before, were adoptively transferred with 2 x 10^6 TCR 6K⁺ CD8⁺ T cells and vice versa. Time course of **(B)** serum alanine amino transferase (ALT), **(C)** serum HBeAg and **(D)** serum HBsAg levels. Mean and SD are shown. (n=5)

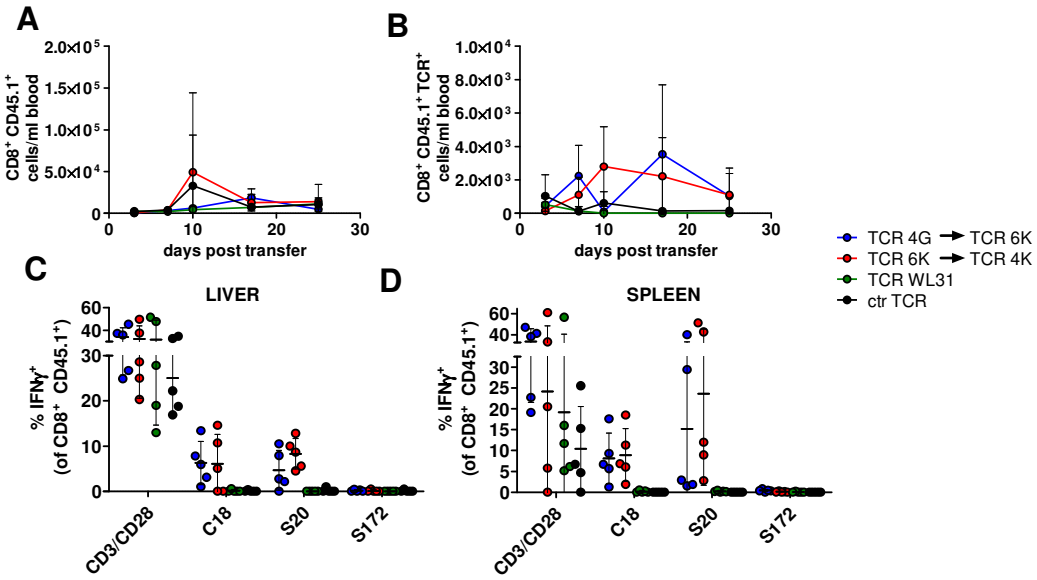

Figure 2.31 Engraftment of HLA-A*02 restricted HBV-specific TCR⁺ T cells after adoptive transfer in AAV-HBV-infected HHDII-HLA-DR1 mice.
Total count of **(A)** transferred (CD45.1⁺) and **(B)** transduced (CD45.1⁺ TCR⁺) CD8⁺ T cells. TCR⁺ T cells were visualized by Vβ-antibodies: TCR 4G: Vβ5.1, TCR 6K: Vβ14, TCR WL31: Vβ13.1. Intracellular cytokine staining of CD8⁺ T cells isolated from **(C)** liver or **(D)** spleen. T cells were *ex vivo* stimulated with HBV peptides C18, S20, S172. CD3/CD28 stimulation served as positive control. Mean and SD are shown. (n=5)

2.2.3.2 HHDII expression on hepatocytes of HHDII-HLA-DR1 mice

Adoptive transfer of HBV-specific, HLA-A*02 restricted TCR$^+$ T cells into AAV-HBV-infected HHDII-HLA-DR1 mice did not reveal an anti-viral effect. As the recovered transferred T cells were functional, we investigated the HHDII expression on hepatocytes of HHDII-HLA-DR1 mice. Therefore, we isolated primary mouse hepatocytes (PMH) and splenocytes of HHDII-HLA-DR1 mice and analyzed their HHDII surface expression by flow cytometry using an HLA-A*02 antibody. Splenocytes could be stained for HLA-A*02 surface expression but at a reduced level compared to PBMC from a human HLA-A*02$^+$ donor (Figure 2.32 A and B). Importantly, HLA-A*02 surface expression was not detected on PMHs (Figure 2.32 C).

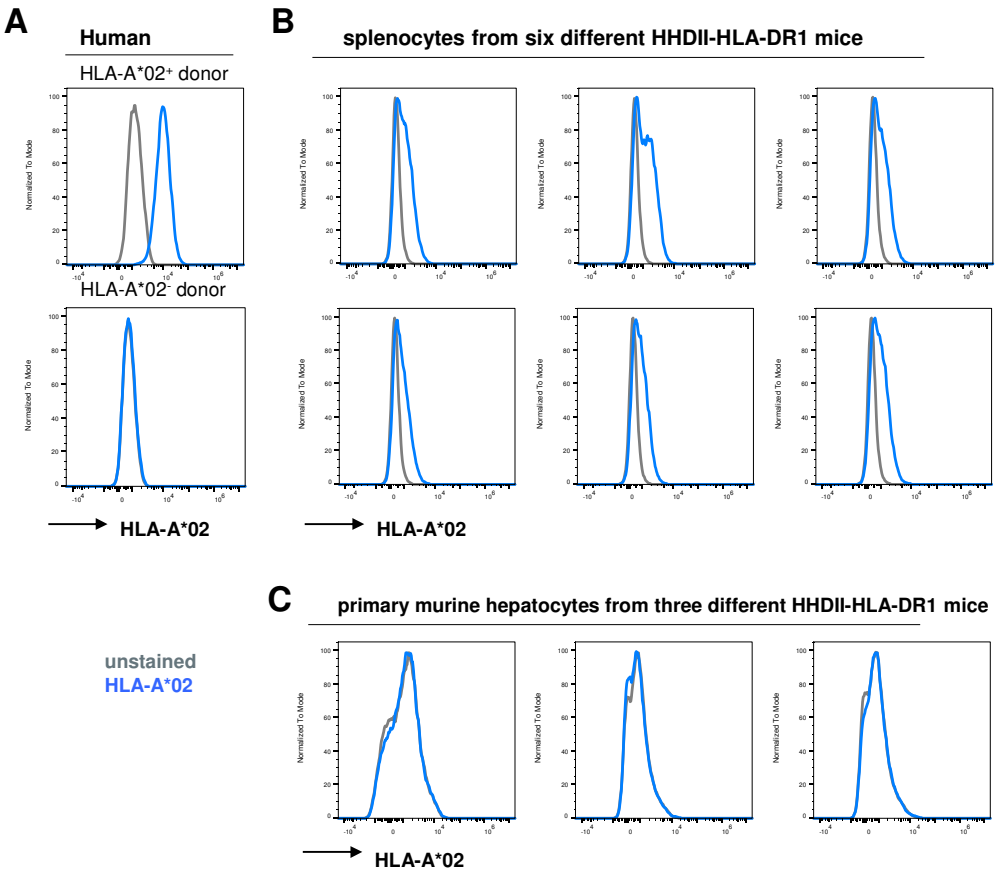

Figure 2.32 HLA-A*02 surface expression on splenocytes and primary hepatocytes from HHDII-HLA-DR1 mice.
Flow cytometry analyses of HLA-A*02 surface expression on **(A)** PBMC of human HLA-A*02$^+$ and HLA-A*02$^-$ donors, **(B)** splenocytes isolated from 6 different HHDII-HLA-DR1 mice and **(C)** hepatocytes isolated from 3 different HHDII-HLA-DR1 mice.

2.2.3.3 Antiviral effect of redirected T cells upon AAV-mediated hepatic expression of HLA-A*02/HHDII *in vitro*

As described in section 2.2.3.2, we could not obtain any evidence for HLA-A*02 surface expression on primary murine hepatocytes of HHDII-HLA-DR1 mice. The HHDII molecule consists of the human α_1 and α_2 as well as β_2m domains of the human HLA-A*02 and human β_2m molecule. Murine parts are the α_3 (H-2D^b), transmembrane and cytoplasmic domains as well as the CD8 co-receptor. The complete MHC molecule is expressed as a single protein. This variant was described to function better than a completely humanized molecule (Pascolo et al., 1997). In theory, HHDII molecule expression should allow perfect interaction with a murine T cell, engrafted with a human TCR, as α_3 and its binding partner CD8 are both of murine origin (Figure 2.33).

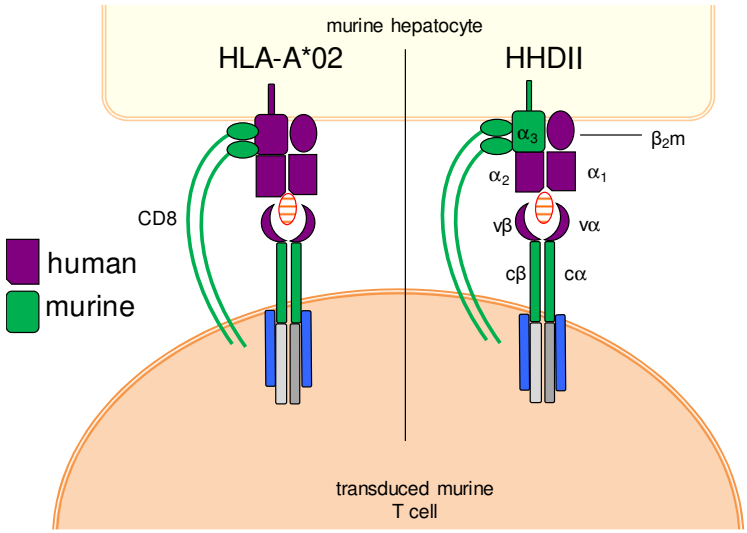

Figure 2.33 Schematic representation of interaction of HLA-A*02/HHDII with a TCR complex. HLA-A*02: all parts are of human origin. HHDII: α_1, α_2 as well as β_2m are of human origin (HLA-A*02), β_2m is covalently linked to α_1. Murine parts are the α_3 (H-2D^b), transmembrane and cytoplasmic domains (Pascolo et al., 1997) as well as the CD8 co-receptor, enabling perfect interaction with a murine T cell, engrafted with a human TCR. To reduce mispairing with the endogenous TCR, constant domains are murinized for our TCRs.

HHDII expression was demonstrated to be superior when administering it with an AAV vector than expressing it as a transgene (Huang et al., 2014). Therefore, I cloned three different AAVs encoding for different HLA-A*02/HHDII versions under control of the liver specific TTR promoter: i) HLA-A*02 and human β_2-microglobulin (pAAV-HLA-A*02), ii) HHDII (pAAV-HHDII) and iii) β-globin intron and HHDII (pAAV-βG-intron-HHDII) (Figure 2.34 A). For verification of gene expression and to ensure, that the antibody used for staining of HLA-A*02 detects the HHDII molecule, Huh7 cells were transfected with a plasmid encoding the HHDII molecule. Flow cytometry analysis demonstrated that the antibody binds HHDII very well (Figure 2.34 B). After AAV production, HHDII-HLA-DR1$^{WT/HHDII}$ mice were infected with the respective AAVs.

17 days later, primary murine hepatocytes were isolated (Figure 2.34 C) and their HLA-A*02 surface expression was analyzed by flow cytometry directly *ex vivo*. HLA-A*02 staining was not observed on PMHs obtained from a C57Bl/6J wildtype mouse. Only marginal expression was found on PMHs from HHDII-HLA-DR1$^{HHDII/HHDII}$ or HHDII-HLA-DR1$^{WT/HHDII}$ as well as HHDII-HLA-DR1$^{WT/HHDII}$ either transduced with AAV-βG-intron-HHDII or AAV-HHDII. Importantly, a small HLA-A*02^{+} population of 18 % and 27 %, respectively, was found in two out of four HHDII-HLA-DR1$^{HHDII/HHDII}$ mice. For all animals transduced with AAV-HLA-A*02, HLA-A*02 surface expression could be proven on up to 99% of cells (Figure 2.34 D).

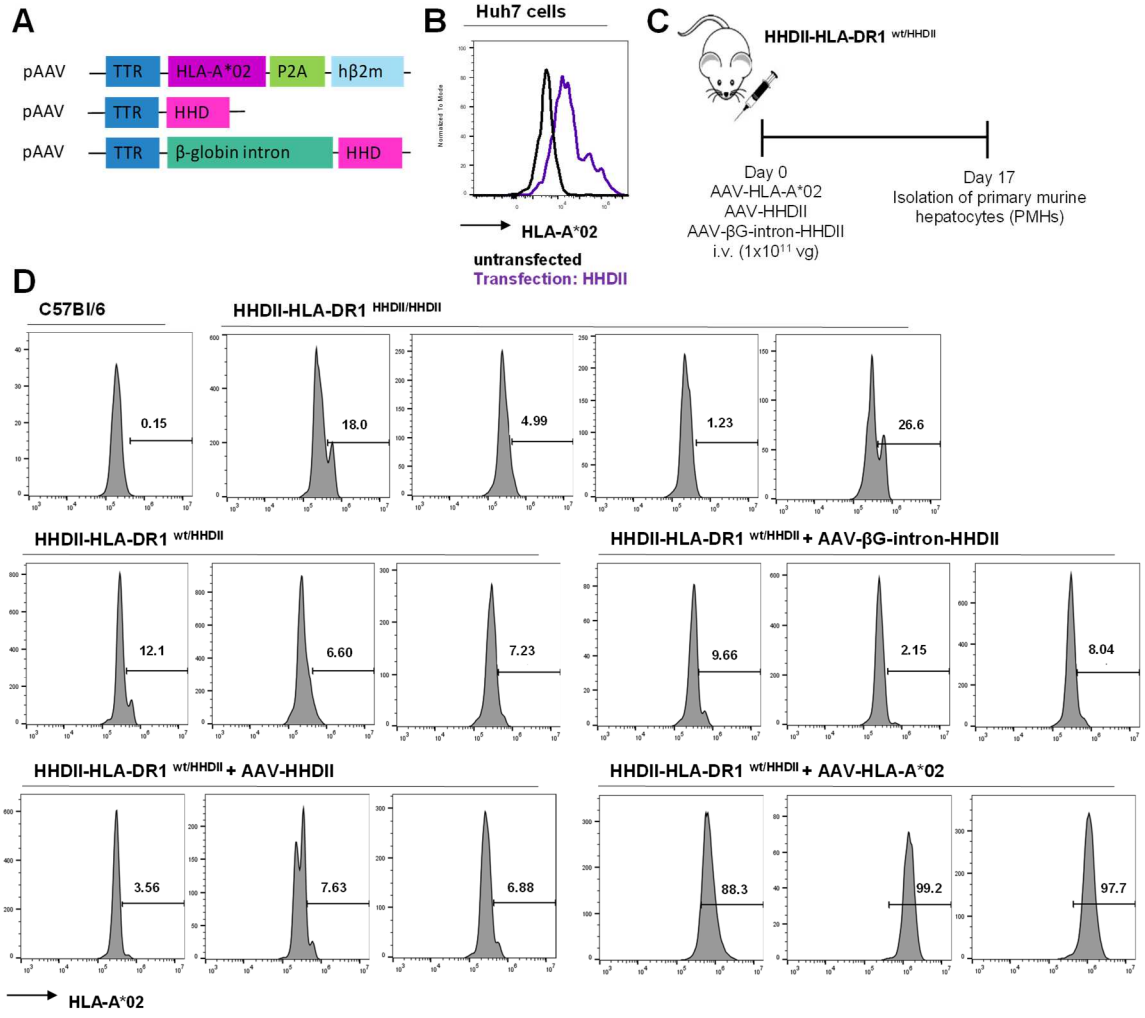

Figure 2.34 HLA-A*02 surface expression on primary hepatocytes after transduction with AAVs encoding for different HLA-A*02/HHDII variants.
(A) Schematic representation of three AAV constructs. HLA-A*02 or HHDII gene is flanked by AAV2 ITRs and expressed under control of the liver-specific TTR promoter. The P2A element allows equimolar expression of HLA-A*02 and hβ$_2$m. The insertion of the β-globin intron should enhance transgene expression (Palmiter et al., 1991) **(B)** Flow cytometry analyses of HLA-A*02 surface expression on Huh7 cells after transfection with pAAV-HHDII **(C)** Schematic overview: HHDII-HLA-DR1 mice backcrossed with C57Bl/6J wildtype (WT) mice were and intravenously injected with 1.5 x 10^{11} vg AAV-HLA-A*02, AAV-HHDII or AAV-βG-intron-HHDII. 17 days later primary hepatocytes were isolated and **(D)** used for flow cytometry analyses of HLA-A*02 surface expression.

Next, freshly isolated PMHs were plated for a co-culture experiment with HBV-specific or mock T cells. PMHs were transduced with Ad-HBV as natural HBV infection of murine cells is not possible (Figure 2.35 A). Uninfected cells served as negative and peptide-loaded PMHs as positive control. To evaluate activation of TCR^+ T cells, the supernatant from day 2 after start of co-incubation was analyzed for IFNγ content. IFNγ levels were extremely high with 35 ng/ml if TCR^+ T cells were co-incubated with PMHs loaded with their cognate peptide. This was observed in all PMHs except the ones derived from the wildtype C57Bl/6J mouse (Figure 2.35 B). When endogenous peptides were presented after Ad-HBV transduction, T cells were only activated to secrete sustained amounts of IFNγ of 0.4 and 2 ng/ml when PMHs were derived from AAV-HHDII or AAV-HLA-A*02 transduced animals, respectively, and the amount of produced IFNγ was around five times higher after co-culture with PMHs from AAV-HLA-A*02 transduced animals. Six days after start of co-incubation, viability of target cells was analyzed via an XTT viability assay. Viability of Ad-HBV transduced PMHs was only altered upon co-incubation with TCR-engrafted T cells when PMHs were derived from mice transduced with AAV-HHDII (Figure 2.35 C). Independent of AAV-mediated expression of HHDII and HLA-A*02, hepatocytes from all HHDII-HLA-DR1 mice, but not from the wildtype mouse, were eliminated up to 90 % upon peptide loading, especially in co-culture with TCR 6K-redirected T cells. HBV-independent viability loss was detected in PMHs from a HHDII-HLA-$DR1^{HHDII/HHDII}$ mouse (Figure 2.35 C). Overall core-specific TCR $6K^+$ T cells produced more IFNγ and eliminated more target cells than S-specific TCR 4G redirected T cells.

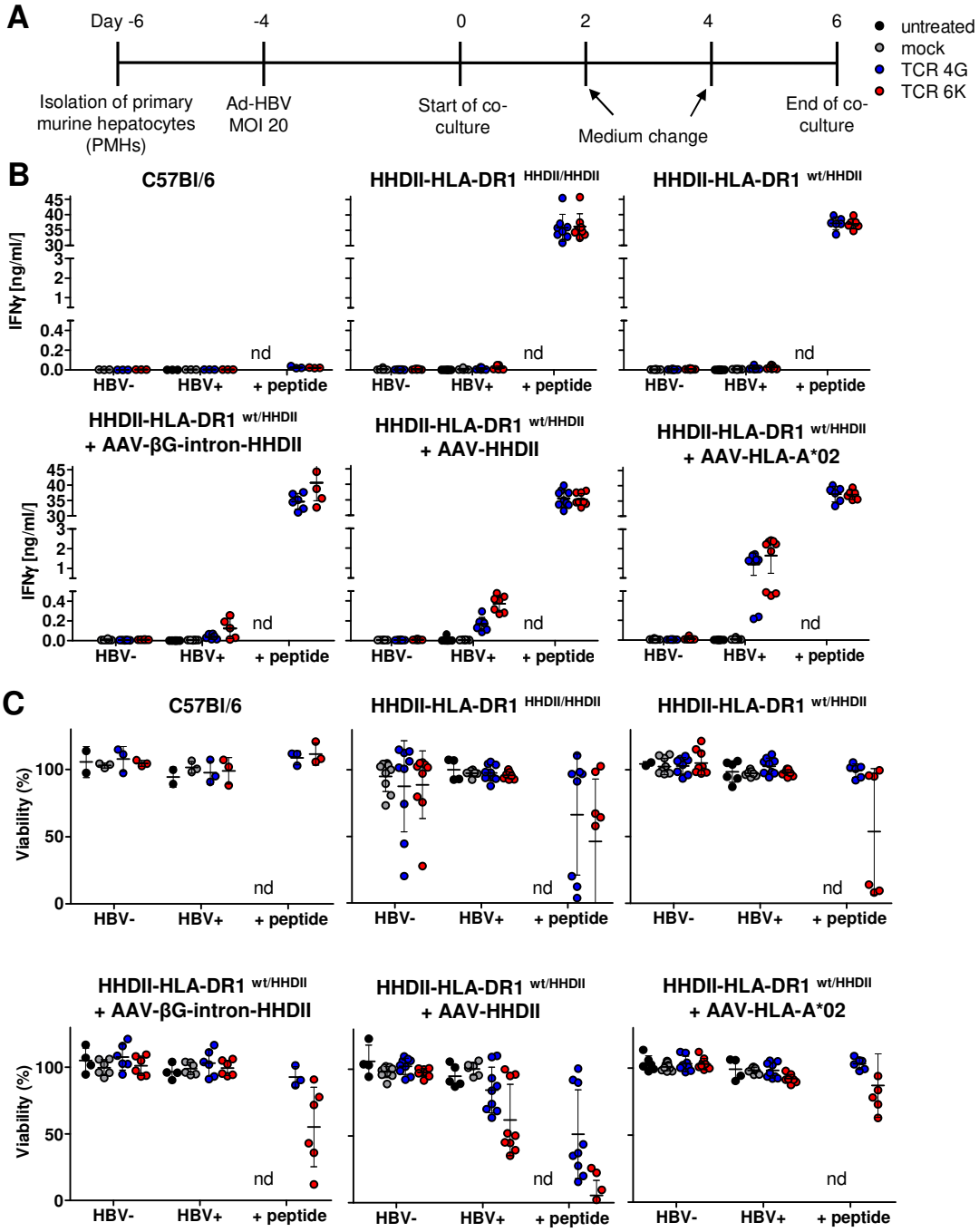

Figure 2.35 Co-culture of PMHs of HHDII-HLA-DR1 mice infected with AAVs encoding for different HLA-A*02/HHDII variants with HBV-specific TCR⁺ T cells.
(A) PMHs isolated from animals injected with 1.5 x 10^{11} vg AAV-HLA-A*02, AAV-HHDII or AAV-βg-intron-HHDII were plated for a co-culture with HBV-specific HLA-A*02 restricted TCR-redirected murine T cells (effector to target ratio E:T = 0.5 : 1). Experiment set-up is shown: 2 days after plating, PMHs were transduced with Ad-HBV. Four days later murine HBV-specific TCR⁺ T cells were added. PMHs and T cells were co-incubated for six days with medium changes every other day **(B)** Supernatant of day 2 after start of co-culture with HBV-specific HLA-A*02 restricted TCR-redirected murine T cells was used for analysis of IFNγ secretion via ELISA. **(C)** XTT viability assay of PMHs six days after start of co-culture. Individual values, mean and SD of duplicates/triplicates pooled from 1-3 mice are shown. Ad-HBV transduction: HBV⁺, no Ad-HBV: HBV⁻, +peptide: PMHs were loaded with either 1µM peptide S20 for TCR 4G or C18 for TCR 6K, nd= not determined.

To determine the antiviral effect of TCR 4G- and 6K-redirected T cells, HBeAg secreted into the supernatant of co-cultures was analyzed. TCR 4G- or 6K-redirected T cells reduced HBeAg levels at day 6 after start of co-culture up to 80 % compared to untreated target cells except for C57Bl/6J WT PMHs, from which HBeAg secretion was not altered (Figure 2.36 A). In co-cultures with PMHs derived from uninfected HHDII-HLA-DR1 mice or animals infected with AAV-βG-intron-HHDII reduction of HBeAg levels were about 20 % and 40 % for TCR 4G- and 6K-engrafted T cells, respectively. For PMHs from mice that additionally expressed HHDII or HLA-A*02 from the AAV vector, TCR-engrafted T cells led to a decline of HBeAg levels for TCR 4G$^+$ T cell treated cells of 50 % and 70 %, respectively. TCR 6K-redirected T cells led to a reduction of 70 % and 80 % in HBeAg levels, respectively (Figure 2.36 A).

Moreover, DNA of Ad-HBV transduced PMHs was isolated and the number of rcDNA copies after six days of co-incubation was evaluated. A reduction of rcDNA copies ranging from 20 % to 80 % was seen in all but C57Bl/6J derived PMHs after co-culture with HBV-specific T cells. As seen in HBeAg level reduction, T cells could preferably eliminate rcDNA after AAV-HHDII and AAV-HLA-A*02 transduction (Figure 2.36 B). In PMHs of animals transduced with AAV-HHDII also mock transduced T cells led to an explicit decrease in rcDNA copies compared to untreated controls (Figure 2.36 B).

In summary, infection of HHDII-HLA-DR1$^{WT/HHDII}$ animals with either AAV-HHDII or AAV-HLA-A*02 with subsequent Ad-HBV transduction generated hepatocyte target cells that were recognized by HBV-specific HLA-A*02 restricted T cells. Moreover, TCR$^+$ T cells exhibited an antiviral effect in co-culture assays. The antiviral effect towards HBV$^+$ HLA-A*02 transduced hepatocytes was predominantly cytokine-mediated, whereas HBV-specific T cells eliminated HBV$^+$ HHDII-transduced hepatocytes.

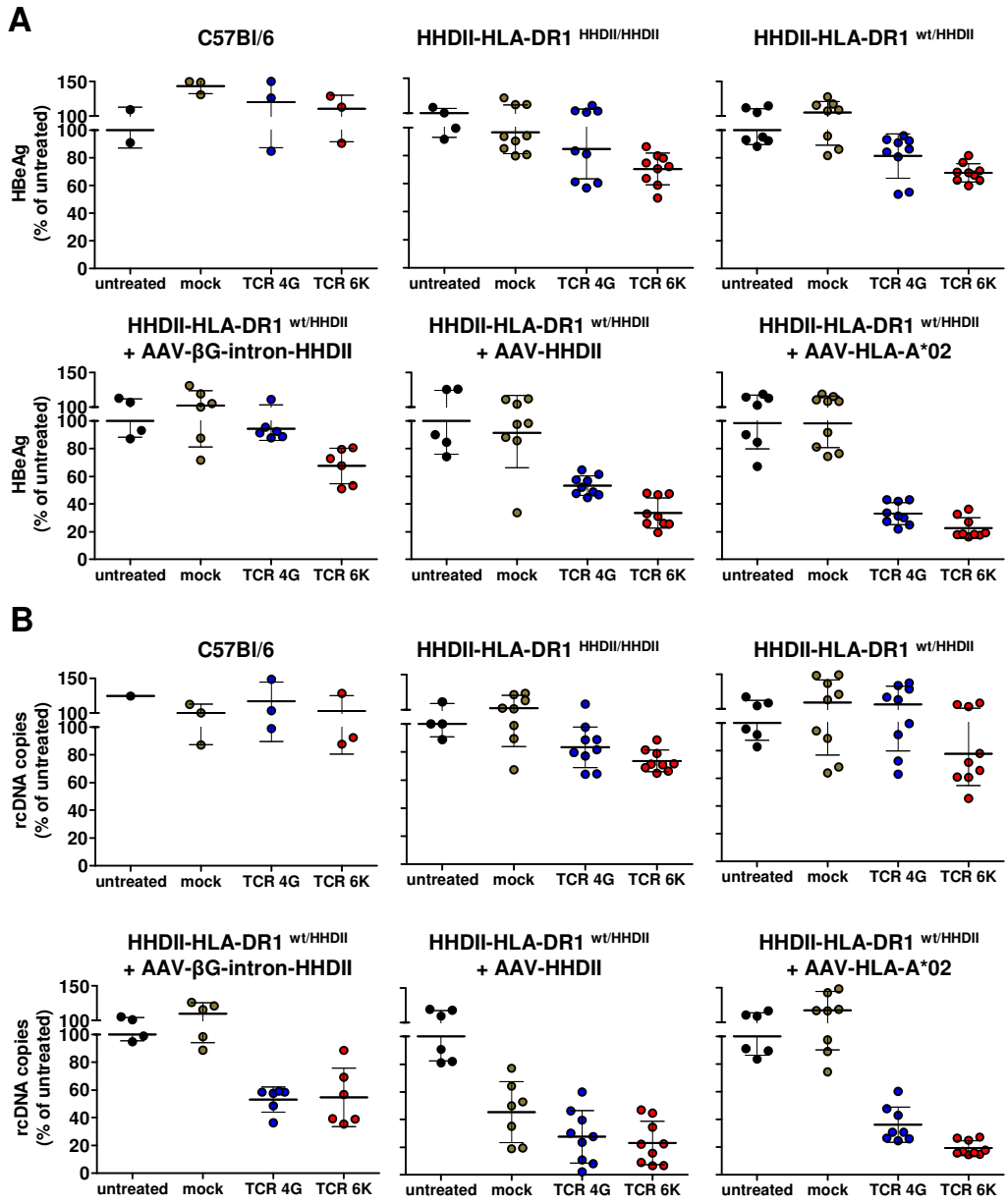

Figure 2.36 Antiviral effect of HBV-specific T cells towards Ad-HBV transduced PMHs of HHDII-HLA-DR1 mice transduced with AAVs encoding for different HLA-A*02/HHDII variants.
(A) Supernatant of day 6 after start of co-culture was used to determine HBeAg levels via ELISA and are plotted as % of HBeAg levels compared to untreated PMHs. **(B)** Ad-HBV transduced PMHs were lysed six days after start of co-culture and their intracellular rcDNA copies content was analyzed by qPCR. Values are plotted as % of rcDNA copies compared to untreated PMHs. Individual values, mean and SD duplicates/triplicates pooled from 1-3 mice are shown.

AAV-mediated hepatic expression of HHDII as well as HLA-A*02 rendered hepatocytes as suitable target cells for HLA-A*02-restricted T cells. As HLA-A*02 surface expression determined by flow cytometry as well as IFNγ levels upon co-culture with HBV-specific T cells were higher when AAV-HLA-A*02 was used, we chose it to be further investigated. For this purpose, HHDII-HLA-DR1 mice were i.v. infected with AAV-HLA-A*02 or AAV-empty together with AAV-HBV. 57 days later PMHs were isolated and their HLA-A*02 surface expression

evaluated by flow cytometry (Figure 2.37 A). Cells isolated from animals co-transduced with AAV-HLA- A*02 and AAV-HBV highly expressed HLA-A*02, whereas PMHs from AAV-empty and AAV-HBV-infected animals could not be stained for HLA-A*02 (Figure 2.37 B). HBcAg staining of liver sections 57 days post infection demonstrated that HBcAg was expressed in around 20 % of hepatocytes (Figure 2.37 C).

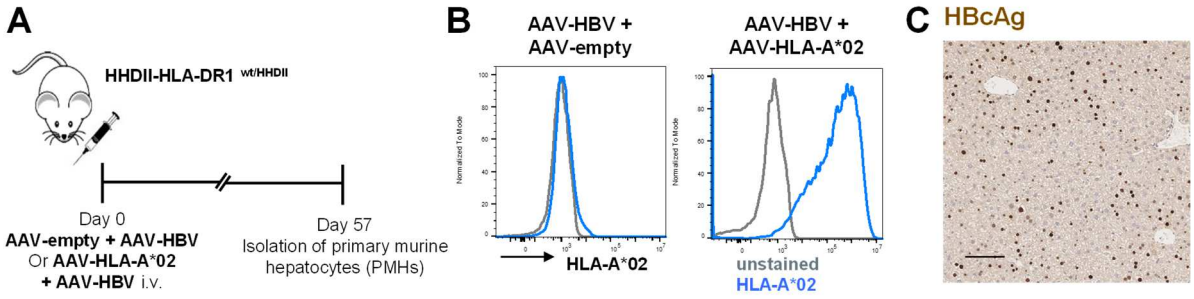

Figure 2.37 Characterization of primary hepatocytes after co-transduction of mice with AAV-HBV and AAV-HLA-A*02.
(A) Schematic overview: HHDII-HLA-DR1$^{WT/HHDII}$ mice were intravenously injected with 1.5 x 10^{11} vg AAV-HLA-A*02 or AAV-empty and 3 x 10^{10} vg AAV-HBV. 57 days later primary hepatocytes were isolated and **(B)** used for flow cytometry analyses of HLA-A*02 surface expression. Representative plots are shown. **(C)** Representative immunohistochemical HBcAg staining of liver sections day 57 after infection. Scale bars indicate 100 µm.

Again, PMHs were plated for a co-culture with HBV-specific T cells (Figure 2.38 A) to investigate, if those co-transduced hepatocytes would serve as suitable target cells for studying human HLA-A*02 restricted HBV-specific TCRs. TCR$^+$ T cells were secreting high amounts of IFNγ of when co-incubated with HLA-A*02$^+$ and HBV$^+$ PMHs indicating their activation (Figure 2.38 B). Core-specific TCR 6K$^+$ T cells could eliminate HBV$^+$ and HLA-A*02$^+$ target cells, TCR 4G and TCR WL31 engrafted T cells only decreased target cell viability in one out of three animals. PMHs were not killed, if they were HBV$^+$ but HLA-A*02$^-$ (Figure 2.38 C). Interestingly, HBeAg levels analyzed in supernatant six days after start of co-culture were not specifically diminished after PMHs were treated with TCR$^+$ T cells (Figure 2.38 D). In contrast to that, rcDNA levels were massively reduced by more than 90 % when TCR 4G$^+$, 6K$^+$ or WL31$^+$ T cells were co-incubated with PMHs isolated from AAV-HLA-A*02 and AAV-HBV-infected animals, which was not observed for PMHs from AAV-empty and AAV-HBV co-transduced animals (Figure 2.38 E).

In short, AAV-HLA-A*02 and AAV-HBV co-transduced hepatocytes served as suitable target cells for HBV-specific HLA-A*02 restricted TCR-redirected T cells.

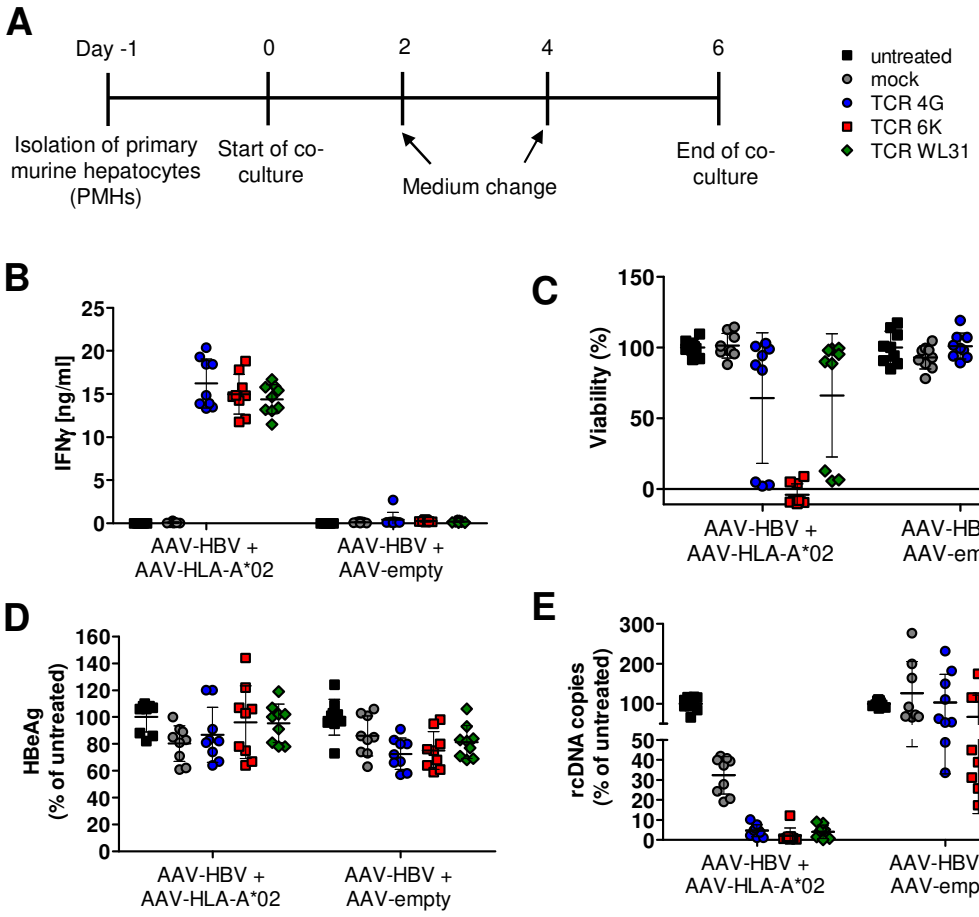

Figure 2.38 Co-culture of HBV-specific T cells with primary hepatocytes from mice co-infected with AAV-HBV and AAV-HLA-A*02.
(A) PMHs were plated for a co-culture with TCR 4G-, TCR 6K- or TCR WL31-redirected murine T cells (effector to target ratio E:T = 0.5 : 1). Experiment set-up is shown: one day after plating, murine HBV-specific TCR$^+$ T cells were added. PMHs and T cells were co-incubated for six days with medium changes every other day. **(B)** Supernatant of day 2 after start of co-culture was used for analysis of IFNγ secretion via ELISA. **(C)** XTT viability assay of PMHs six days after start of co-culture. **(D)** Supernatant of day 6 after start of co-culture was used to determine HBeAg levels in co-cultures via ELISA and are plotted as % compared to untreated PMHs. **(E)** PMHs were lysed six days after start of co-culture and their intracellular rcDNA content was analyzed by qPCR. Values are plotted as % of rcDNA copies compared to untreated PMHs. Individual values, mean and SD of triplicates pooled from 3 mice are shown.

2.2.3.4 Antiviral activity of HBV-specific HLA-A*02 restricted T cells in HHDII-HLA-DR1 mice co-infected with AAV-HLA-A*02 and AAV-HBV

HBV-specific T cells demonstrated recognition and elimination of HBV and HLA-A*02 co-transduced hepatocytes *in vitro* (see section 2.2.3.3). Therefore, we investigated their functionality *in vivo* by co-injection of AAV-HLA-A*02 or AAV-empty together with AAV-HBV.

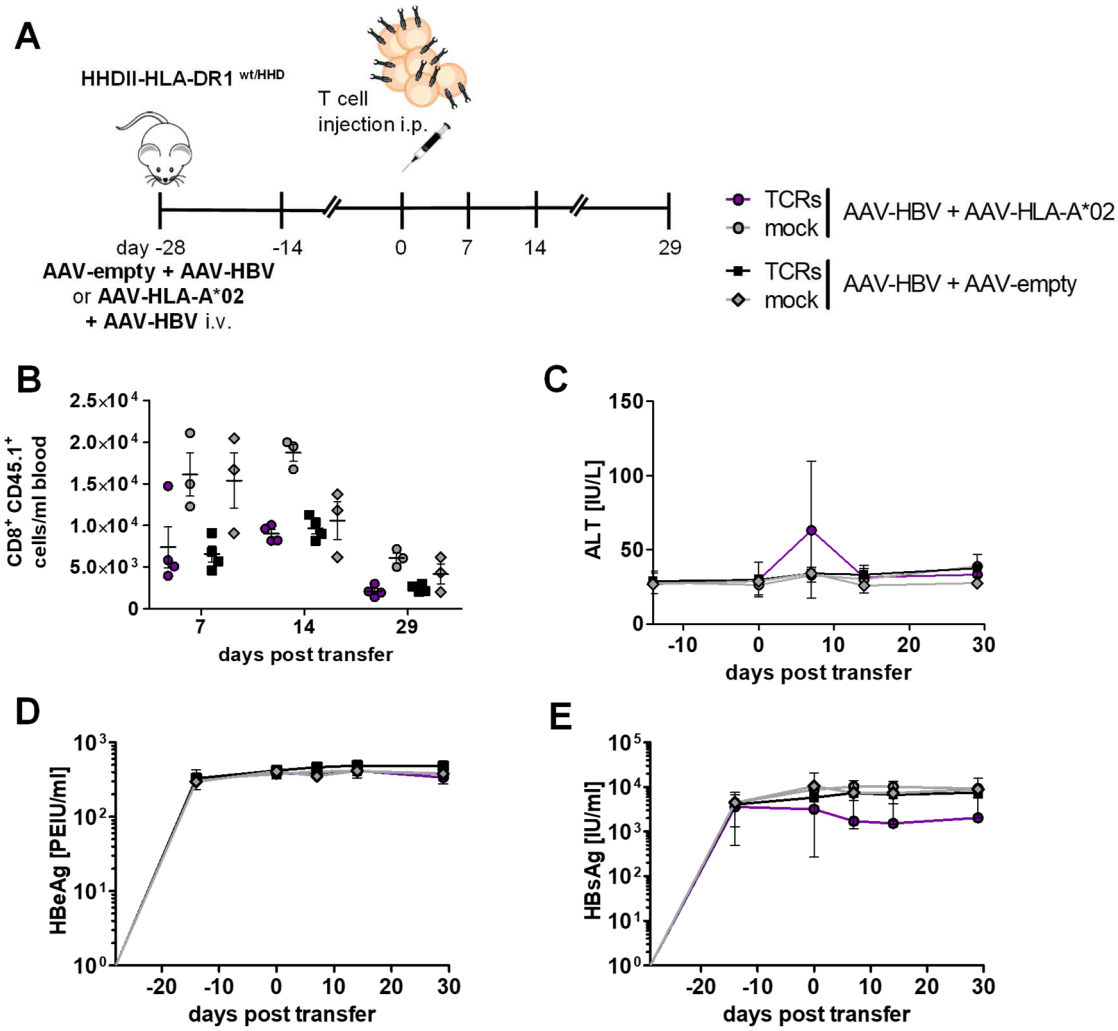

Figure 2.39 Antiviral effect of HLA-A*02 restricted HBV-specific TCR$^+$ T cells after adoptive transfer into AAV-HBV and AAV-HLA-A*02 infected HHDII-HLA-DR1$^{WT/HHDII}$ mice.
(A) Schematic overview: HHDII-HLA-DR1$^{WT/HHDII}$ mice were intravenously injected 1.5 x 10^{11} vg AAV-HLA-A*02 or AAV-empty and 3 x 10^{10} vg AAV-HBV. 28 days later, when chronic infection was established, mice received either 1 x 10^6 TCR 4G + 1 x 10^6 TCR 6K + 1 x 10^6 TCR WL31 engrafted CD8$^+$ T cells in 5 x 10^6 total cells (TCRs) or 5 x 10^6 mock T cells intraperitoneally. **(B)** Total count of transferred (CD45.1$^+$) CD8$^+$ T cells. Time course of **(C)** serum alanine amino transferase (ALT), **(D)** serum HBeAg and **(E)** serum HBsAg levels. Mean and SD are shown. (n=3-4)

Animals were adoptively transferred with either a mixture of T cells containing TCR 4G$^+$, TCR 6K$^+$ and TCR WL31$^+$ CD8$^+$ T cells (TCRs) or mock T cells (Figure 2.39 A). Engraftment of transferred cells was very poor in this experiment, as we only found very low amounts of transferred cells in the circulation of the mice, when animals were treated with TCR$^+$ T cells. Unexpectedly, we even found mock transduced T cells to survive better in the recipient animals

(Figure 2.39 B). ALT levels were slightly increased up to 60 U/l in two of four mice on day 7 after T-cell transfer when mice were co-infected with AAV-HLA-A*02 and AAV-HBV but went down to physiological levels thereafter (Figure 2.39 C). Strikingly, we could not observe an antiviral effect in all the experimental groups, as serum HBeAg and HBsAg levels stayed stable for one month after adoptive transfer (Figure 2.39 D and E).

Since we observed poor T-cell engraftment and HBV-specific HLA-A*02 restricted TCR$^+$ T cells did neither expand nor reveal an antiviral effect in AAV- HLA-A*02 and AAV-HBV co-infected HHDII-HLA-DR1$^{WT/HHDII}$ mice, we hypothesized that TCR$^+$ T cells were rejected.

2.2.3.5 Immune response against TCR-equipped T cells in HHDII-HLA-DR1 mice

Mock transduced T cells survived better in HHDII-HLA-DR1 mice compared to T cells expressing a human TCR (see section 2.2.3.4). Therefore, we assessed the possibility of a rejection of TCR$^+$ T cells by the endogenous adaptive immune system of the recipient mice. Thus, we first evaluated an antibody response against human TCR constituent (for detail see Figure 2.33). Serum of day 7 post transfer (see experiment section 2.2.3.4) was co-incubated with freshly transduced murine T cells. Those T cells were either mock transduced or expressing TCR 4G, 6K or WL31. Antibodies bound to the TCR-redirected T cells were then detected by a polyclonal PE-labelled anti-mouse IgG (mIgG) antibody (Figure 2.40 A) and visualized by flow cytometry.

Serum of animals that were treated with a mixture of HBV-specific TCR$^+$ T cells depicted a strong mIgG signal for TCR 6K. Antibody responses against TCR WL31 were weaker, and only one mouse had developed antibodies against TCR 4G. Serum of mock T cell treated animals did not reveal anti mIgG signal (Figure 2.40 B and C).

To evaluate the induction of human TCR-specific cell-mediated immunity, splenocytes of adoptively transferred mice were co-incubated with freshly transduced T cells *ex vivo* and analyzed for IFNγ secretion. Importantly, we provide evidence for TCR 6K- and TCR WL31-specific CD8$^+$ T cells within splenocytes of recipient mice, whereas CD8$^+$ T cells were not activated to secrete IFNγ when co-incubated with TCR 4G expressing T cells or mock T cells (Figure 2.40 D). Furthermore, we determined the amount of remaining TCR$^+$ target cells after 72h of co-incubation. The results of the ICS could be confirmed, as the number of TCR 6K$^+$ and WL31$^+$ T cells was substantially reduced when co-incubated with splenocytes from TCR treated mice compared to splenocytes from mock treated mice. The number of 4G$^+$ T cells was not altered (Figure 2.40 E).

In conclusion, murine T cells equipped with TCR 6K or TCR WL31 were immunogenic in HHDII-HLA-DR1$^{WT/HHDII}$ mice, as an antibody- as well as a cytotoxic CD8$^+$ T cell response was observed. There is no evidence, that TCR 4G was recognized as a foreign protein by recipient mice. The missing engraftment of TCR-redirected T cells as well as their antiviral effect shown in Figure 2.39 might be explained by the immune response developed in immunocompetent mice.

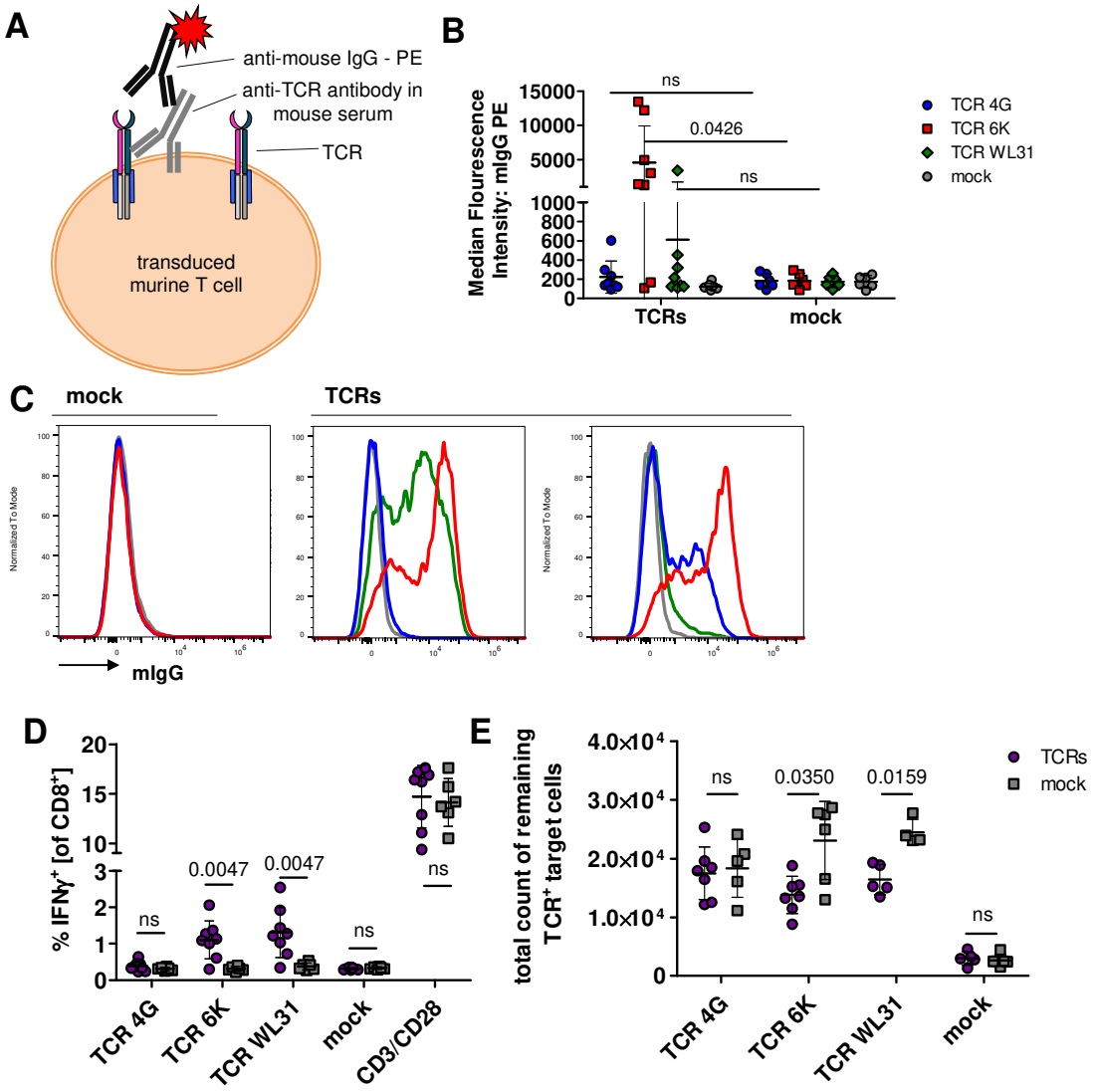

Figure 2.40 Immune response against TCR$^+$ T cells in HHDII-HLA-DR1 mice.
(A) Schematic representation of flow cytometry assay for analyzing anti-TCR antibodies within mouse serum: freshly transduced TCR$^+$ or mock T cells were incubated with serum (day 7 post T-cell transfer) of respective mice. Bound antibodies were visualized with a PE-labelled anti-mouse IgG (mIgG) antibody. Analysis of anti-TCR antibodies: **(B)** mean fluorescence intensity of bound mIgG-PE and **(C)** representative flow cytometry plots. *Ex vivo* co-culture of splenocytes isolated from mice treated with TCR$^+$ or mock transduced T cells with freshly transduced TCR$^+$ or mock T cells: **(D)** intracellular cytokine staining (16h after start of co-incubation). CD3/CD28 stimulation served as positive control. **(E)** Total count of remaining TCR$^+$ target cells 72h after start of co-incubation. (n=6-8, Mann-Whitney test, numbers in graphs indicate p values, ns = not significant)

2.2.3.6 Antiviral effect of HBV-specific HLA-A*02 restricted TCR-redirected T cells in immunodeficient animals

Given the fact that immunocompetent mice developed a humoral as well as a cell-mediated immune response against some of the investigated HBV-specific HLA-A*02 restricted human TCRs (see section 2.2.3.5), I implemented an adoptive transfer experiment in immunodeficient $Rag2^{-/-}\gamma c^{-/-}$ mice. Animals were transduced with AAV-HLA-A*02 or AAV-HBV or co-transduced with both. 18 days later, animals were treated with either a mixture of T cells containing TCR $4G^+$, TCR $6K^+$ and TCR $WL31^+$ $CD8^+$ T cells (TCRs) or mock T cells (Figure 2.41 A).

Overall, numbers of transferred T cells in the circulation were low again. Interestingly, TCR^+ cells were detected at lowest in the group that was co-transduced with AAV-HLA-A*02 and AAV-HBV (Figure 2.41 B). Sixty days after adoptive T-cell transfer, lymphocytes isolated from spleen and liver were stimulated with HBV-specific peptides directly *ex vivo*. $CD8^+$ T cells isolated from liver or spleen from AAV-HBV + AAV-HLA-A*02 transduced and TCR treated animals did respond less well to stimulation with HBV peptides compared to animals that were treated with TCRs but had only been transduced with one AAV. IFNγ response after unspecific activation via CD3/CD28 stimulation did not differ within all groups (Figure 2.41 C). In contrast, except for TCR 4G, $CD4^+$ T cells did not exhibit a difference in re-stimulation capacity between TCR treated groups (Figure 2.41 D).

Serum of animals co-infected with AAV-HLA-A*02 and AAV-HBV depicted a decrease in HBeAg and HBsAg levels starting on day 7 when adoptively transferred with TCR^+ T cells (Figure 2.42 A and B). This start of decline in serum HBV markers was accompanied by a profound but transient ALT elevation up to 1300 U/l on day 7 after transfer, indicating liver damage (Figure 2.42 C). Serum HBeAg and HBsAg levels further demonstrated a profound decline of 2 logs and 3 logs, respectively but were not cleared completely. Animals that were treated with mock T cells or had been infected with only HBV or HLA-A*02 and then got TCR^+ T cells depicted stable serum HBeAg and HBsAg levels (Figure 2.42 A and B). To determine the antiviral effect of those HBV-specific TCRs, liver DNA was analyzed for its AAV- as well as HBV-DNA content. TCR^+ T cells substantially reduced AAV and HBV DNA in HBV and HLA-A*02 infected animals about 1 log compared to the control groups but failed to completely eradicate it (Figure 2.42 D). To further evaluate the antiviral effect of redirected T cells, HBcAg expression in the liver was analyzed. Hepatocytes of AAV-HLA-A*02 infected animals stained negative for HBcAg, whereas livers of AAV-HBV and mock treated as well as HBV and HLA-A*02 co-infected animals demonstrated > 50 % HBc^+ hepatocytes. Importantly, as a result if T-cell activity, liver sections obtained from TCR-redirected T cells did not reveal HBc^+ hepatocytes anymore (Figure 2.42 E).

In fact, HBV-specific HLA-A*02 restricted TCR-redirected T cells exhibited a profound antiviral effect in AAV- HLA-A*02 and AAV-HBV co-infected Rag2$^{-/-}\gamma c^{-/-}$ mice but did not clear the infection.

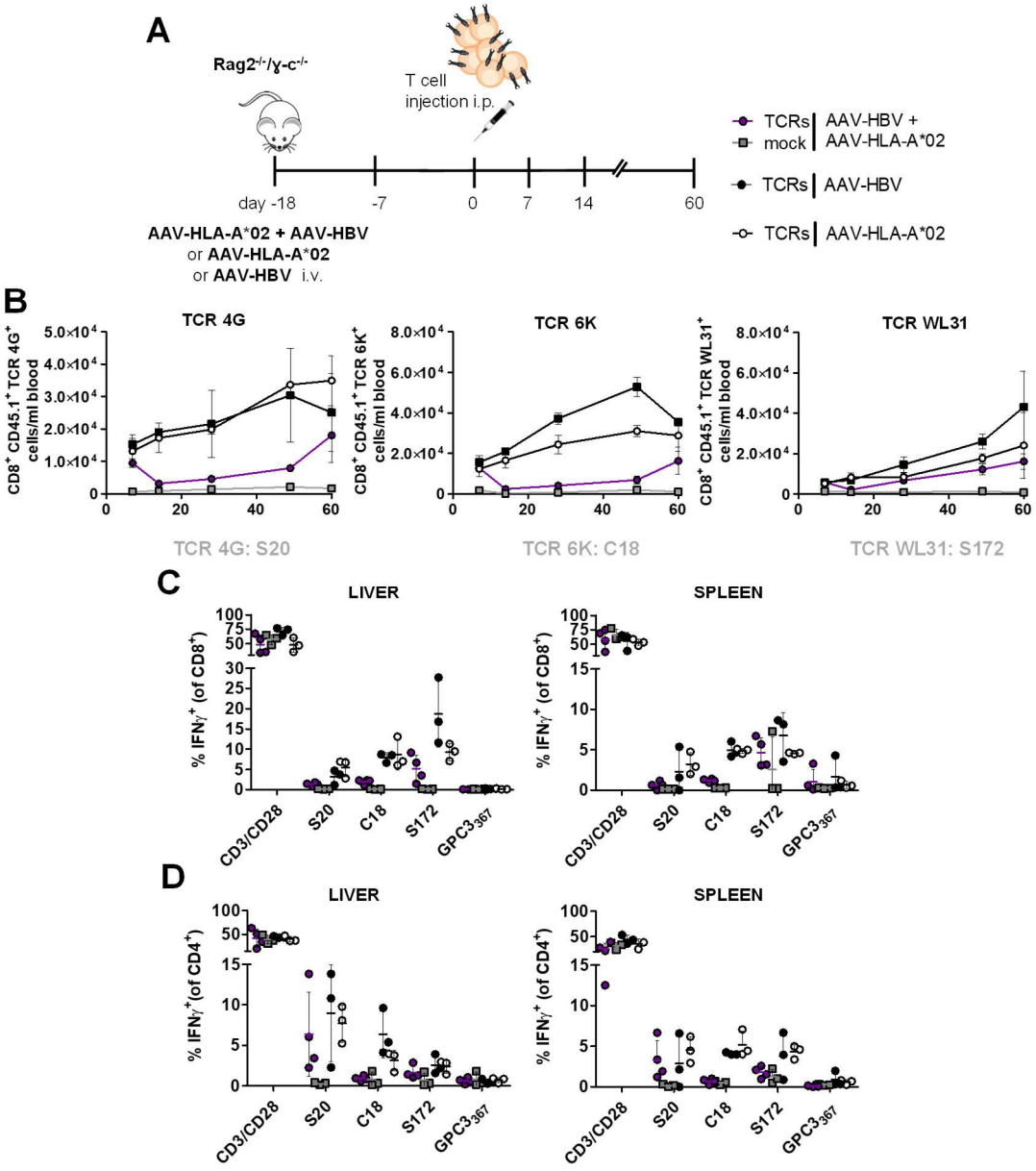

Figure 2.41 Antiviral effect of HLA-A*02 restricted HBV-specific TCR$^+$ T cells after adoptive transfer into AAV-HBV and AAV-HLA-A*02 infected Rag2$^{-/-}\gamma c^{-/-}$ mice.
(A) Schematic overview: Rag2$^{-/-}\gamma c^{-/-}$ mice were i.v. injected 1.5 x 10^{11} vg AAV-HLA-A*02 or 3 x 10^{10} vg AAV-HBV or with both. 18 days later, when chronic infection was established, mice received either 0.33 x 10^6 TCR 4G + 0.33 x 10^6 TCR 6K + 0.33 x 10^6 TCR WL31 engrafted CD8$^+$ T cells in 1 x 10^6 total cells (TCRs) or 1 x 10^6 mock T cells intraperitoneally. CD45.1 WT mice were used as T cell donors. **(B)** Total count of transduced CD45.1$^+$ CD8$^+$ TCR$^+$ T cells. TCR$^+$ T cells visualized by staining with Vβ-antibodies: TCR 4G: Vβ5.1, TCR 6K: Vβ14, TCR WL31: Vβ13.1. Intracellular cytokine staining after *ex vivo* stimulation of **(C)** CD8$^+$ T cells or **(D)** CD4$^+$ T cells isolated from liver or spleen with 1 µM peptides C18 (TCR 4G), S20 (TCR 6K) or S172 (TCR WL31) that were loaded on T2 cells. CD3/CD28 stimulation served as positive control, peptide GPC3$_{367}$ (irrelevant peptide, presented by T2 cells) as negative control. Mean and SD are shown. (n=3-5)

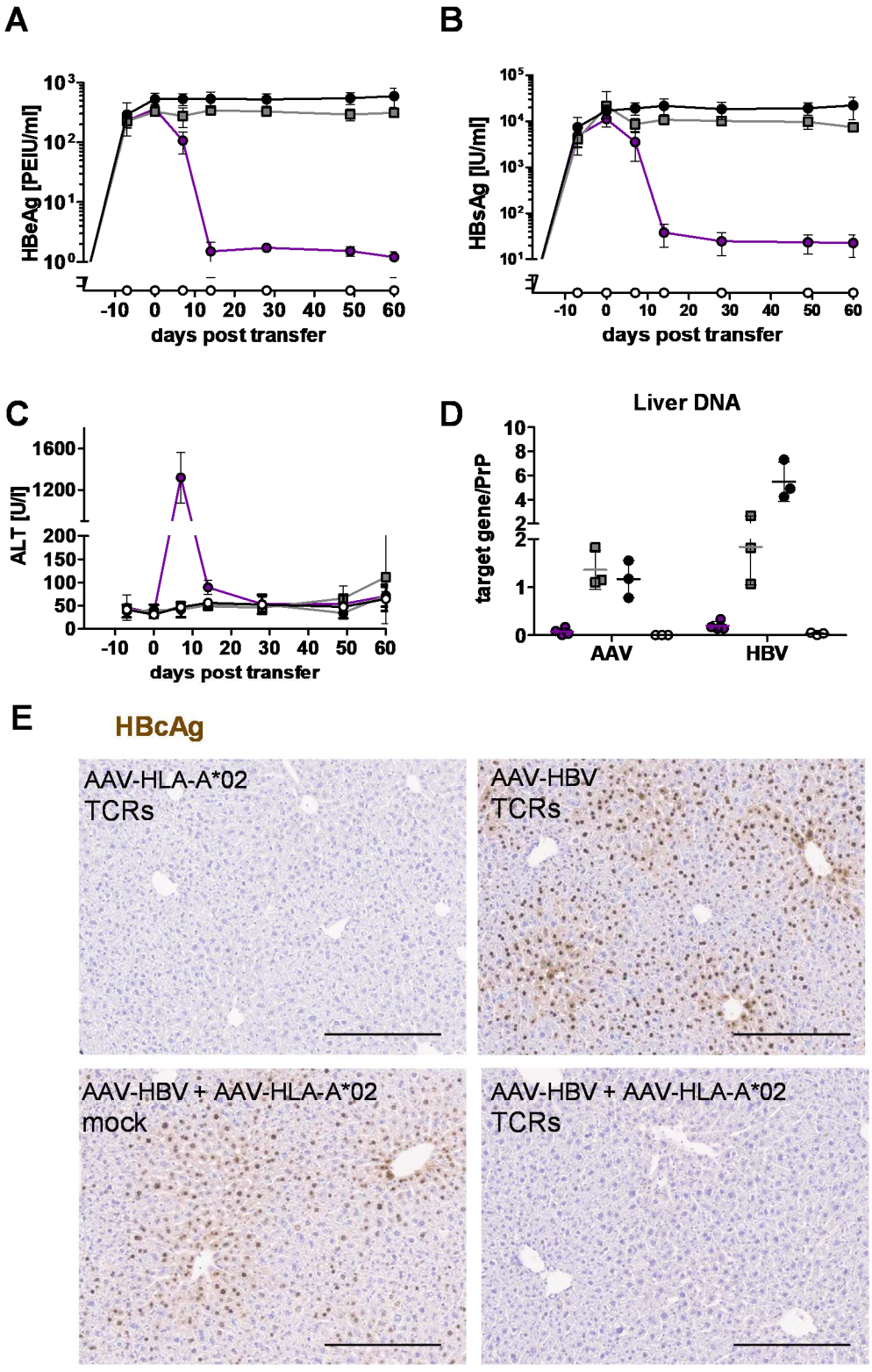

Figure 2.42 *Ex vivo* analyses after adoptive transfer of HLA-A*02 restricted HBV-specific TCR$^+$ T cells into AAV-HBV and AAV-HLA-A*02 infected Rag2$^{-/-}\gamma c^{-/-}$ mice.
Time course of **(A)** serum HBeAg, **(B)** serum HBsAg and **(C)** serum alanine amino transferase (ALT) levels. **(D)** Levels of AAV vector (AAV) and whole HBV genomes (HBV) in liver tissue 60 days after adoptive T-cell transfer. **(E)** Representative immunohistochemical HBcAg stainings of liver sections. Scale bars indicate 300 µm. Mean and SD are shown. (n=3-4)

Finally, we evaluated the capacity of pre-existing HBV-specific T cells to deal with a subsequent HBV infection. For this purpose, immunodeficient Rag2$^{-/-}$ γc$^{-/-}$ mice received either TCR 4G-, TCR 6K- and TCR WL31-engrafted (TCRs) or mock T cells intraperitoneally. I performed the co-transduction with AAV-HLA-A*02 and AAV-HBV 25 days later (Figure 2.43 A). ALT levels of mice adoptively transferred with TCR^{+} T cells reached a peak of around 600 U/l on day 14 post infection and rapidly declined to physiological levels thereafter (Figure 2.43 B). Serum HBeAg and HBsAg levels could be controlled by TCR treated mice after an initial rise, but still persistent infection was manifesting. Serum HBeAg levels of 100 PEIU/ml and serum HBsAg levels of 1000 IU/ml were detected in mock treated animals (Figure 2.43 C and D). Furthermore, the anti-viral effect of pre-existing HBV-specific T cells could be

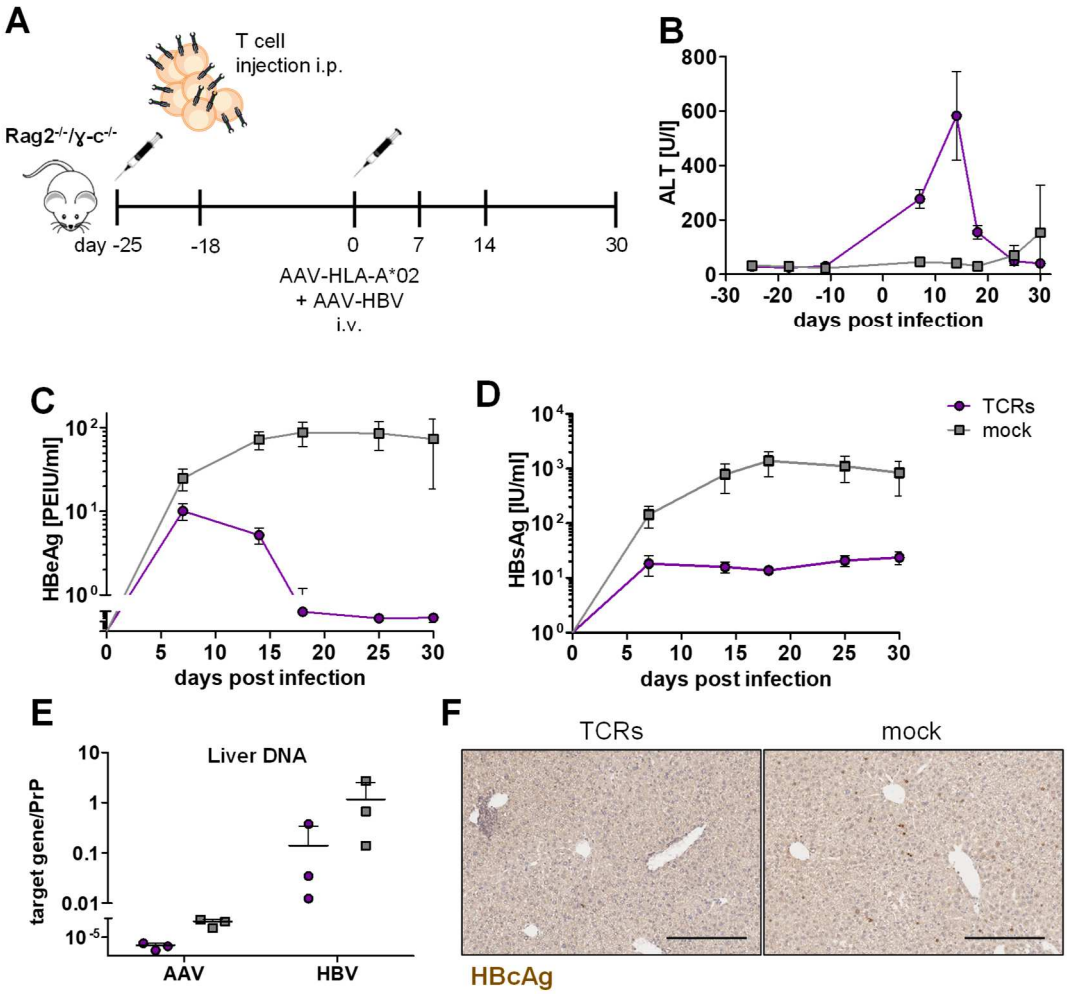

Figure 2.43 Antiviral effect of HLA-A*02 restricted HBV-specific TCR^{+} T cells after adoptive transfer with subsequent AAV-HBV and AAV-HLA-A*02 infection.
(A) Schematic overview: Rag2$^{-/-}$γc$^{-/-}$ mice were treated with either 1.2 x 10^6 TCR 4G + 1.2 x 10^6 TCR 6K + 0,6 x 10^6 TCR WL31 engrafted CD8^{+} T cells in 7 x 10^6 total cells (TCRs) or 7 x 10^6 mock T cells intraperitoneally. 25 days later, mice were co-infected with 1.5 x 10^{11} vg AAV-HLA-A*02 and 3 x 10^{10} vg AAV-HBV. Time course of **(B)** serum alanine amino transferase (ALT), **(C)** serum HBeAg and **(D)** serum HBsAg levels. **(E)** Levels of AAV vector (AAV) and whole HBV genomes (HBV) 30 days after AAV infection. **(F)** Representative immunohistochemical HBcAg stainings of liver sections. Scale bars indicate 300 µm. Mean and SD are shown. (n=3)

confirmed in a profound decline of about 1 log in AAV and HBV DNA levels as well as HBc^+ hepatocytes in the liver of TCR compared to mock treated animals (Figure 2.43 E and F).

In short, pre-existing TCR^+ T cells also demonstrated a distinct anti-viral effect if $Rag2^{-/-}\gamma c^{-/-}$ mice were experiencing the AAV-HLA-A*02 and AAV-HBV co-infection subsequently, but could not prevent establishment of a persistent AAV-HBV infection and HBV replication.

2.3 HBV-specific T cells - translation to the rhesus macaque and pig model

The AAV-HBV model mimicking chronic HBV infection proved to be very useful in determining functionality of immunotherapeutic approaches but would be outcompeted by a preclinical animal model of natural HBV infection. Successful infection with HBV virions after transducing hepatocytes with human NTCP has been reported for the cynomolgus and rhesus macaque *in vitro* (Lempp et al., 2017) as well as the rhesus macaque *in vitro* and *in vivo* (Burwitz et al., 2017). Moreover, pig hepatocytes allowed establishment of HBV infection when expressing human NTCP *in vitro* (Lempp et al., 2017). As the examination of immunotherapeutic strategies in a non-human primate model would be preferable for clinical development, we were aiming to investigate the potential of macaque T cells equipped with HBV-specific HLA-A*02 restricted TCRs towards HBV-infected macaque hepatocytes *in vitro*.

2.3.1 Transduction of macaque T cells with human TCRs

As a first step of translating adoptive T-cell therapy towards the macaque model, TCRs have to be expressed on macaque T cells. Therefore, the transduction protocol for human T cells had to be adapted for macaque T cells (Festag, 2018). I perfomed a tranduction of macaque

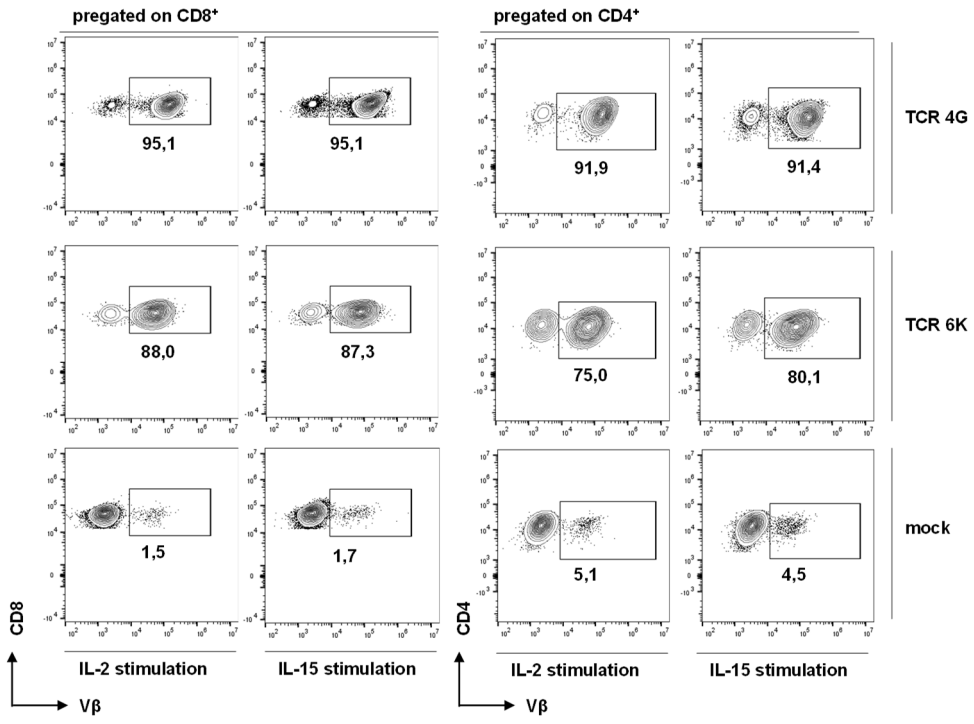

Figure 2.44 Expression of human HLA-A*02 restricted HBV-specific TCRs on rhesus macaque PBMC after retroviral transduction.
Rhesus macaque PBMC were transduced with TCR 4G, 6K or mock transduced while either stimulated with IL-2 or IL-15. Flow cytometry plots of either $CD8^+$ or $CD4^+$ T cells stained with respective Vβ antibodies are illustrated (day 7 after initial activation). Mock samples are stained with a mixture of Vβ antibodies.

T cells with retroviruses encoding for TCR 4G or 6K and compared if stimulation with IL-2 or IL-15 during the transduction process would be more efficient. Successful expression of TCR 4G and TCR 6K on CD8$^+$ as well as on CD4$^+$ T cells could be obtained with both, IL-2 and IL-15 stimulation (75-95 % of CD8$^+$/CD4$^+$ T cells) (Figure 2.44). Hence, transduction efficiency of macaque T cells was comparable to human T cells (data not shown).

2.3.2 Functionality of TCRs expressed on macaque T cells

To prove if TCRs are not only expressed on macaque T cells but also lead to specific activation, TCR$^+$ macaque T cells were co-cultured with HBV-infected HepG2-NTCP cells and compared to human TCR-redirected T cells.

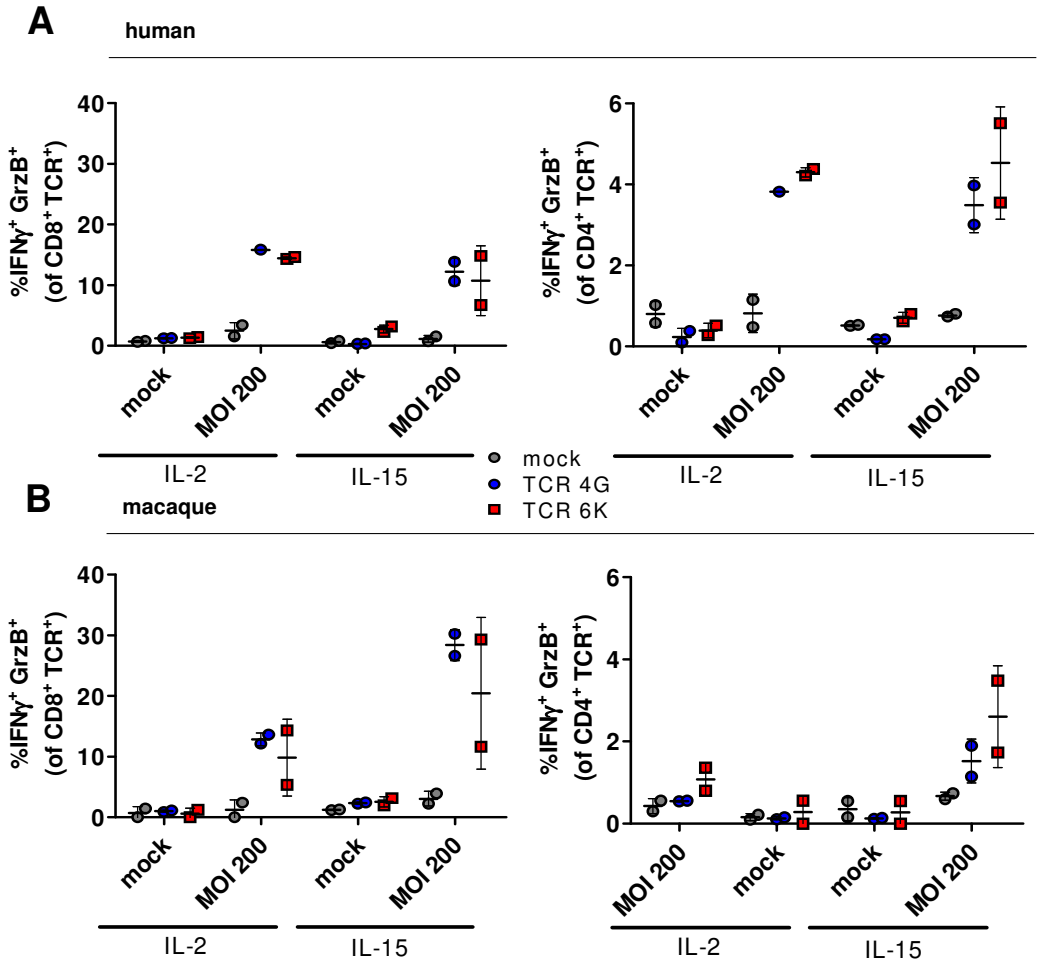

Figure 2.45 Activation of human HBV-specific HLA-A*02 restricted TCRs expressed on macaque T cells towards HBV-infected HepG2-NTCP cells.
Intracellular cytokine staining of **(A)** human and **(B)** macaque CD8$^+$ T cells after 16h co-culture with HBV-infected hepatoma cells HepG2-NTCP (MOI 200) or uninfected HepG2-NTCP (mock) cells. Frequency of CD8$^+$ or CD4$^+$ IFNγ$^+$ GrzB$^+$ T cells. T cells were either stimulated with IL-2 or IL-15 during transduction. Mean and SD is shown.

16h after start of co-incubation, secretion of IFNγ as well as GrzB expression of T cells was analyzed by flow cytometry. Human CD8$^+$ as well as CD4$^+$ T cells, respectively, were activated

to secrete IFNγ and GrzB when co-cultured with HBV-infected hepatoma cells (MOI 200). The frequency of responding cells was much higher in the $CD8^+$ T cell population, with around 15 % for $CD8^+$ and 4 % for $CD4^+$ T cells. Moreover, cytokine release and cytolysis seemed to be independent of pre-stimulation during transduction, as I could not observe a difference between IL-2 or IL-15 stimulation (Figure 2.45 A). TCR^+ T cells were not activated after co-culture with uninfected HepG2-NTCP cells (mock). Mock transduced T cells did not express IFNγ or GrzB (Figure 2.45 A). TCR 4G- and TCR 6K-redirected macaque T cells demonstrated specific activation upon co-culture with HBV-infected HepG2-NTCP cells, but not with uninfected cells. Again, mock T cells did not respond with IFNγ or GrzB secretion (Figure 2.45 B). In contrast to human cells, type of pre-stimulation had a huge effect on activation capacity of TCR^+ macaque T cells. IL-15 pre-stimulation doubled the amount of $IFN\gamma^+$ and $GrzB^+$ T cells for both $CD4^+$ and $CD8^+$ T cells (15 % and 30 % for $CD8^+$ T cells, 2 % and 4 % for $CD4^+$ T cells) (Figure 2.45 B).

Taken together, macaque T cells equipped with TCR 4G or 6K were specifically activated when co-incubated with HBV-infected HepG2-NTCP cells.

2.3.3 Antiviral effect of TCR-equipped macaque T cells on HBV replicating/ Ad-HLA-A*02 transduced primary macaque hepatocytes

As I could demonstrate specific activation of HBV-specific TCRs expressed on macaque T cells, functionality of TCR-redirected macaque T cells towards HBV^+ macaque target cells was investigated. The following experiments were performed in cooperation with M. Festag in the laboratory of B. Burwitz at the Vaccine and Gene Therapy Institute (Portland, OR, USA). To investigate functionality of HLA-A*02 restricted TCRs towards macaque cells, it is essential that HLA-A*02 is expressed on macaque target cells. For this purpose, an adenovirus encoding for HLA-A*02 and hβ2m (Ad-HLA-A*02) was produced (Figure 2.46 A). Its integrity and replication ability were proven by transducing Huh7 cells which naturally do not express HLA-A*02. Flow cytometry analysis of Ad-HLA-A*02 transduced Huh7 cells revealed HLA-A*02 surface expression (Figure 2.46 B). Importantly, HLA-A*02 surface expression could be observed for primary macaque hepatocytes (PMaH) after Ad-HLA-A*02 transduction in a titer dependent manner and reached 16% for an MOI of 200 (Figure 2.46 C).

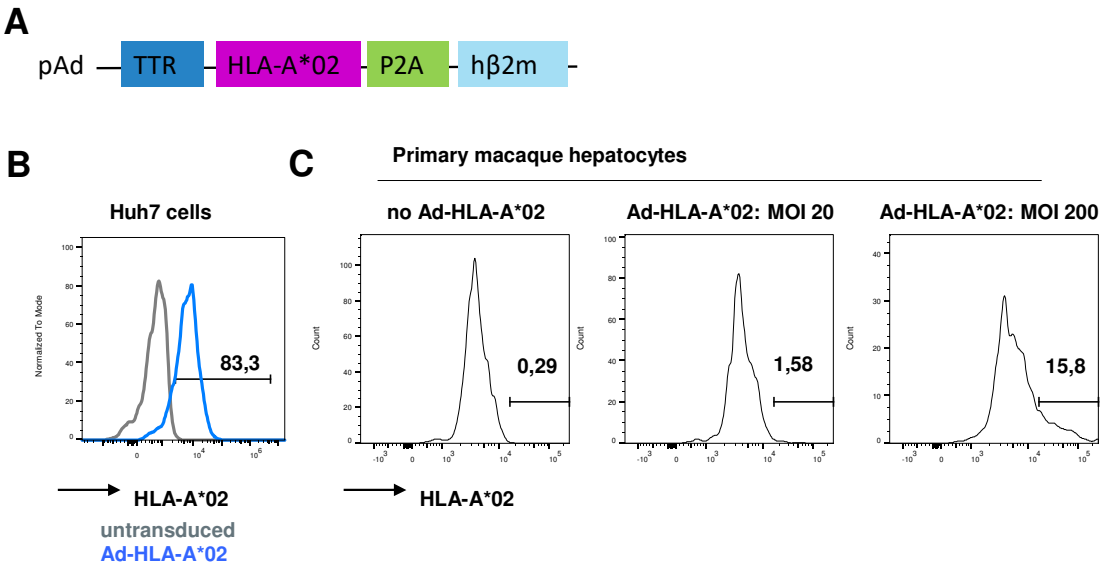

Figure 2.46 HLA-A*02 surface expression on primary macaque hepatocytes.
(A) Schematic representation of Ad-HLA-A*02 construct: HLA-A*02 and hβ2m are expressed under control of the liver-specific TTR promoter. Flow cytometry analyses of verification of HLA-A*02 surface expression after Ad-HLA-A*02 transduction in **(B)** Huh7 cells and **(C)** primary macaque hepatocytes (PMaH) transduced with different MOIs.

As we could provide evidence for HLA-A*02 expression on primary macaque hepatocytes, we next investigated the antiviral potential of HBV-specific macaque T cells towards HBV$^+$ hepatocytes. To this end, PMaHs were co-transduced with Ad-HBV and Ad-HLA-A*02 and co-cultured with macaque T cells equipped with TCR 4G or 6K as well as with mock T cells (Figure 2.47 A). We analyzed HBeAg and HBsAg levels in the supernatant at the end of the co-culture and compared it to day 0. HBV-specific T cells could not diminish marker of HBV persistence after six days of co-culture in Ad-HBV and Ad-HLA-A*02 transduced PMaHs (Figure 2.47 B and C). On the contrary, TCR 6K redirected T cells revealed to have secreted high amounts of IFNγ of 1000 pg/ml when co-incubated with double transduced target cells (Figure 2.47 D). Interestingly, treatment with 6K$^+$ T cells led to a 2-fold reduction of intracellular HBV DNA in HBV$^+$ HLA-A*02$^+$ PMaHs (Figure 2.47 E).

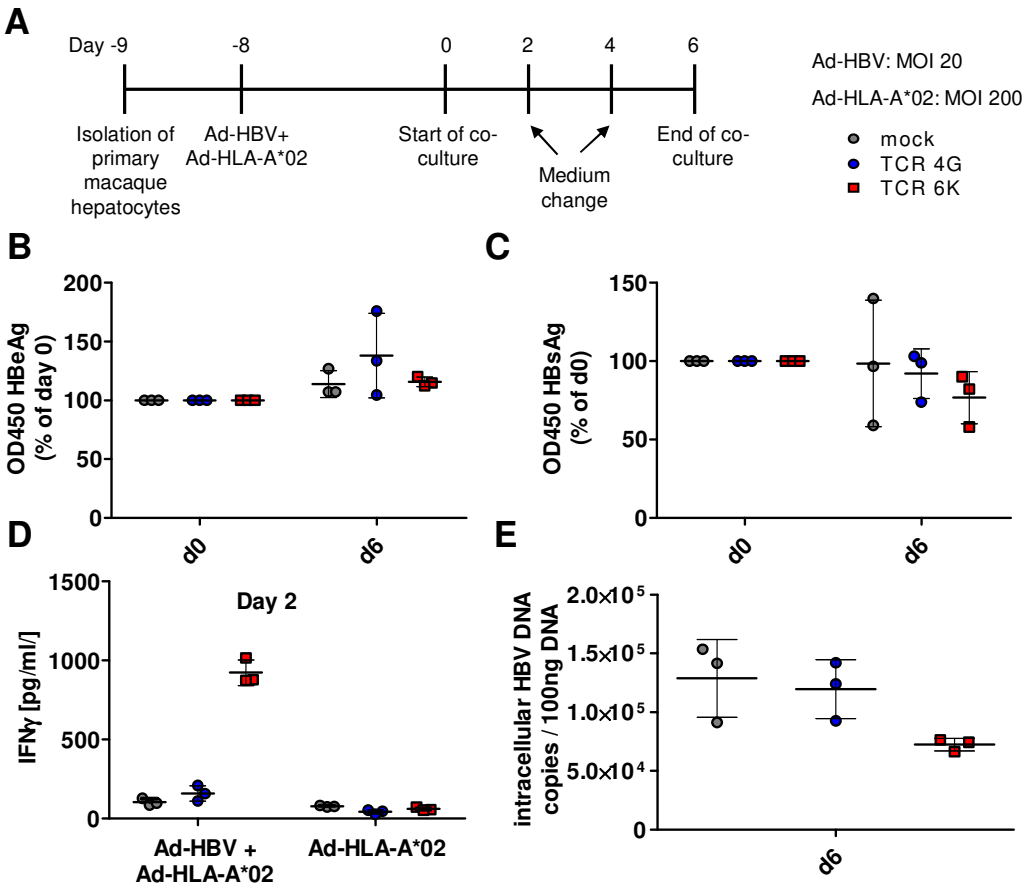

Figure 2.47 Antiviral effect of HBV-specific HLA-A*02 restricted TCR-redirected macaque T cells towards Ad-HBV and Ad-HLA-A*02 transduced primary macaque hepatocytes.
(A) Schematic overview: one day after isolation, primary macaque hepatocytes were co-transduced with Ad-HBV (MOI 20) and Ad-HLA-A*02 (MOI 200). Co-culture with TCR 4G- and TCR 6K-redirected macaque T cells was started eight days later and lasted for six days, whereby medium was exchanged every other day. **(B)** HBeAg and **(C)** HBsAg levels in supernatant of co-cultures plotted as % of day 0. **(D)** Supernatant of day 2 after start of co-culture was analyzed for IFNγ via ELISA. **(E)** Ad-HBV transduced PMaHs were lysed six days after start of co-culture and their intracellular HBV DNA copies per 100ng DNA was analyzed by qPCR. Mean and SD of triplicates are shown.

Furthermore, we implemented a co-culture as described above, but performed a natural HBV infection instead of a vector-mediated HBV genome transfer. Therefore, PMaHs were co-transduced with Ad-HLA-A*02 and an adenovirus encoding for the HBV entry receptor NTCP (Ad-NTCP). Subsequently cells were infected with HBV and used for a co-culture assay (Figure 2.48 A). HBV-specific T cells were able to reduce HBeAg and HBsAg levels at day 6 after start of co-incubation when compared to day 0 as well as to mock T cell treated controls for around 25 % (Figure 2.48 B and C). In addition, 6K-redirected T cells were activated to secrete IFNγ (400 pg/ml) when co-cultured with HLA-A*02$^+$ HBV-infected hepatocytes and did substantially reduce intracellular HBV DNA (2-fold) compared to mock treated cells (Figure 2.48 D and E). Overall, the antiviral affect was more pronounced when TCR 6K was present during co-culture experiments.

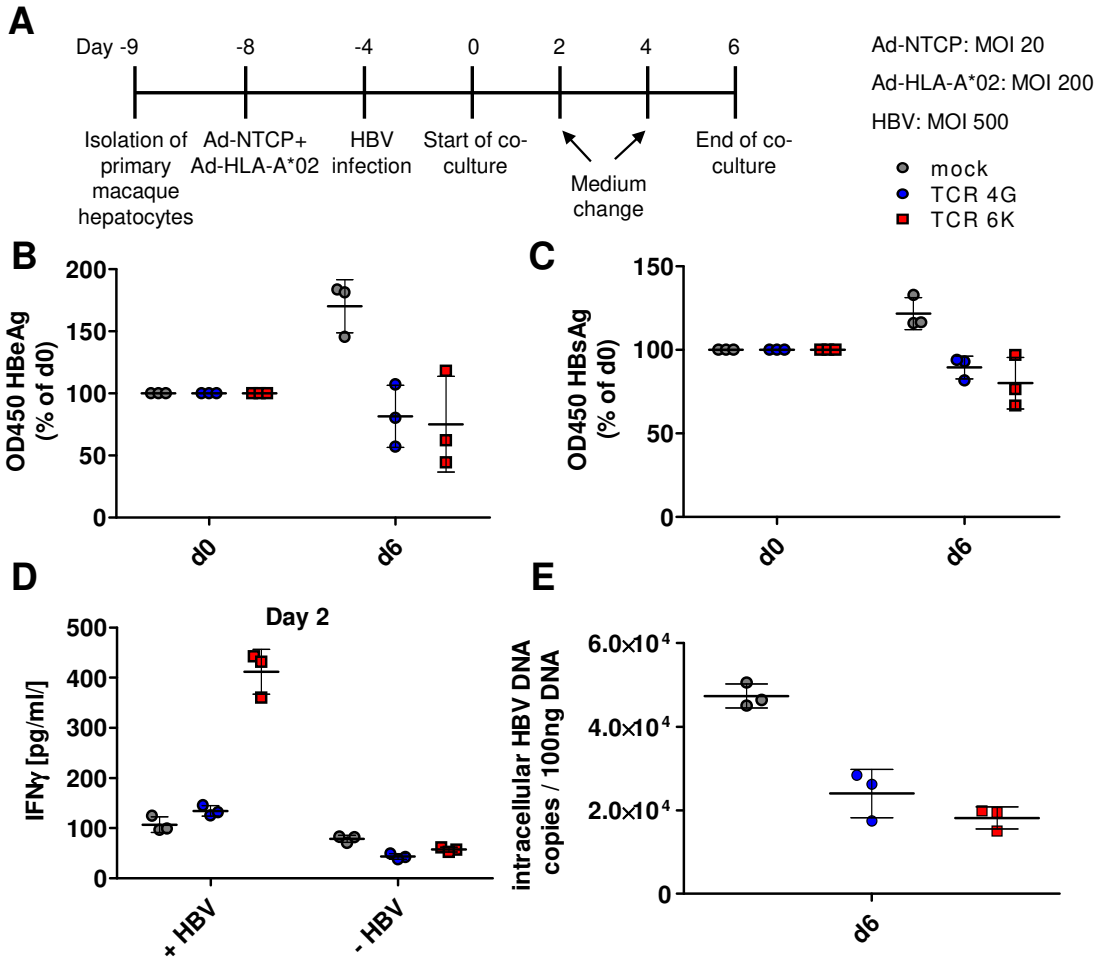

Figure 2.48 Antiviral effect of HBV-specific HLA-A*02 restricted TCR-redirected macaque T cells towards Ad-NTCP + Ad-HLA-A*02 transduced and HBV-infected primary macaque hepatocytes.
(A) Schematic overview: one day after isolation, primary macaque hepatocytes were co-transduced with Ad-NTCP (MOI 20) and Ad-HLA-A*02 (MOI 200). Four days later PMaHs were infected with HBV (MOI 500). Co-culture with TCR 4G- and TCR 6K-redirected macaque T cells was started another four days later and lasted for six days, whereby medium was exchanged every other day. **(B)** HBeAg and **(C)** HBsAg levels in supernatant of co-cultures plotted as % of day 0. **(D)** Supernatant of day two after start of co-culture was analyzed for IFNγ content via ELISA. **(E)** HBV-infected PMaHs were lysed six days after start of co-culture and their intracellular HBV DNA copies per 100ng DNA was analyzed by qPCR. Mean and SD of triplicates are shown.

In conclusion, HBV-specific HLA-A*02 restricted TCR 4G- and 6K- redirected T cells represent a remarkable antiviral effect towards HLA-A*02$^+$ and HBV$^+$ PMaHs *in vitro*.

2.3.4 Functionality of human T cells expressing HBV-specific TCRs on HBV-infected/HLA-A*02 transduced primary pig hepatocytes

As the pig represents another physiologically relevant preclinical animal model, we investigated it's suitability to serve as a preclinical model of HBV infection to test therapeutic approaches. Primary pig hepatocytes equipped with NTCP demonstrated to be permissive for natural HBV infection (Lempp et al., 2017). To determine, if HBV^+ primary pig hepatocytes would serve as an appropriate model for investigation of HBV-specific HLA-A*02 restricted TCRs, a co-culture with human T cells redirected with either TCR 4G or TCR 6K was performed. Therefore, primary pig hepatocytes were transduced with Ad-NTCP or Ad-HLA-A*02 or with an adenovirus encoding for both transgenes (Ad-HLA-A*02-NTCP) and subsequently infected with HBV. Four days later, HBV-specific human T cells were added (Figure 2.49 A). Human T cells engrafted with TCR 4G or 6K displayed only a slight loss in HBeAg levels as compared to mock treated controls when hepatocytes were HBV-infected after Ad-HLA-A*02-NTCP transduction. This effect was not observed if cells were HLA-$A*02^-$ (Figure 2.49 B). Importantly, TCR 4G and TCR 6K redirected T cells were activated to secrete IFNγ (600 pg/ml and 1500 pg/ml, respectively) upon contact with HLA-$A*02^+$ and HBV-infected hepatocytes (Figure 2.49 C).

In summary, human T cells engrafted with HBV-specific TCRs 4G- or 6K did not reveal a pronounced antiviral effect towards HLA-A*02 + NTCP transduced and HBV-infected primary pig hepatocytes in this set-up. Nevertheless, TCR^+ T cells were specifically activated to secrete IFNγ.

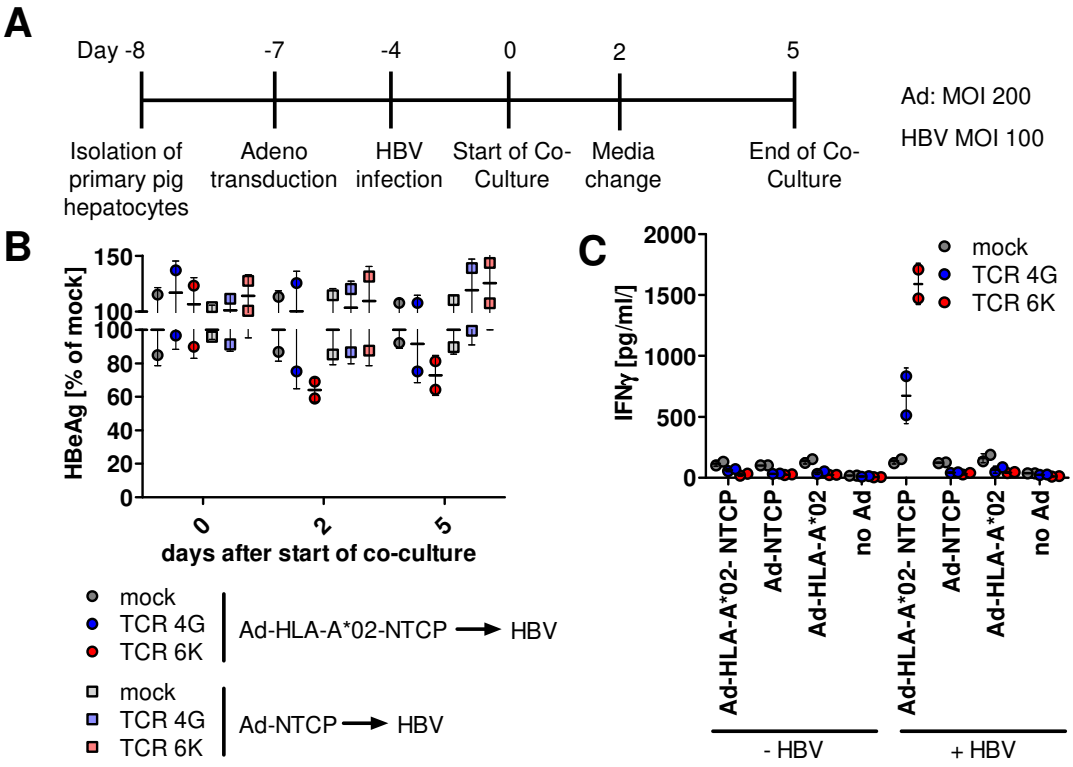

Figure 2.49 Antiviral effect of HBV-specific HLA-A*02 restricted TCR-redirected human T cells towards Ad-NTCP + Ad-HLA-A*02 transduced and HBV-infected primary pig hepatocytes.
A) Schematic overview: one day after isolation, primary macaque hepatocytes were transduced with respective adenoviruses (MOI 200). Three days later PMHs were infected with HBV (MOI 500). Co-culture with TCR 4G- and TCR 6K-redirected macaque T cells was started another four days later and lasted for five days, whereby medium was exchanged after two days. **(B)** HBeAg and levels in supernatant of co-cultures plotted as % of mock. **(D)** Supernatant of day two after start of co-culture was analyzed for IFNγ content via ELISA. Mean and SD are shown.

2.4 Immunotherapy using the GPC3-specific HLA-A*02 restricted TCR P1-1 for treatment of GPC3$^+$ HCC

T-cell therapy is an interesting option to treat HBV-infection, but also HBV-related HCC. Next to viral antigens that might be present in HBV-associated HCC, T cells could also be redirected towards TAAs expressed on HCC. Engrafting T cells with a natural TCR against glypican-3 (GPC3) is a promising approach for treatment of GPC3$^+$ HCC. TCR P1-1 has been cloned to recognize the GPC3-derived peptide GPC_{367} in context of HLA-A*02 (Dargel et al., 2015). T cells equipped with TCR P1-1 have already been evaluated concerning effector functions such as cytokine production and cytotoxicity towards of the GPC3$^+$ HLA-A*02$^+$ hepatoma cell line HepG2 *in vitro* (Dargel et al., 2015). To allow clinical application of TCR P1-1-redirected T cells, their functionality must be shown *in vivo*, as their ability to migrate to the tumor, penetrate the tumor tissue and perform within the tumor environment cannot be demonstrated *in vitro*.

2.4.1 *In vivo* cytotoxicity of P1-1-equipped T cells

As GPC3 is a human protein, I chose an orthotopic xenograft HCC model in order to demonstrate cytotoxic effect of TCR P1-1-redirected T cells *in vivo*. To this end, immunodeficient SCID/Beige mice were intrasplenically transplanted with HepG2 hepatoma cells expressing the *Gaussian* luciferase (HepG2-Gluc) to induce growth of HepG2-cell derived tumors in the liver, followed by adoptive transfer of TCR P1-1-redirected human T cells (Figure 2.50 A). This experiment was performed in cooperation with J. Bockman, F. Thiele, C. Dargel and the group of K. Stemmer (Institute of Diabetes and Obesity, Helmholtz Zentrum München). Out of 20 mice that were intrasplenically injected with HepG2-Gluc cells, bioluminescence signal was only measured in seven of them indicating established HepG2 tumors after nine days. On day 0, tumor-bearing animals were treated with TCR P1-1-engrafted T cells or mock T cells. Tumor growth was efficiently reduced in animals that received TCR P1-1$^+$ T cells when compared to the control group treated with mock T cells (Figure 2.50 B and C). In three of four animals tumor size was decreased, one mouse experienced a relapse after initial response (Figure 2.50 C) (Dargel et al., 2015).

To confirm these results, follow-up experiments using Rag2$^{-/-}\gamma c^{-/-}$ mice were performed. In detail, I generated HepG2 cells expressing the *firefly* luciferase (HepG2-Fluc) as a new cell line for HCC xenografts. First, their suitability as a target cell line was tested *in vitro*. For this purpose, I analyzed the ability of TCR P1-1-redirected T cells to recognize and eliminate HepG2-Fluc cells in a co-culture assay. Significant killing of HepG2-Fluc cells by TCR P1-1$^+$ T cells was observed, whereas co-incubation of mock T cells did not lead to reduced target cell viability (Figure 2.51 A). Target cell killing was accompanied by IFNγ secretion measured

in the supernatant of the co-cultures. The amount of IFNγ increased with increased effector to target cell (E:T) ratios. Moreover, activation of T cells to secrete IFNγ was equally high comparing parental HepG2 cells with HepG2-Fluc cells (Figure 2.51 B). Hence, HepG2-Fluc cells were suitable target cells for TCR P1-1-redirected T cells.

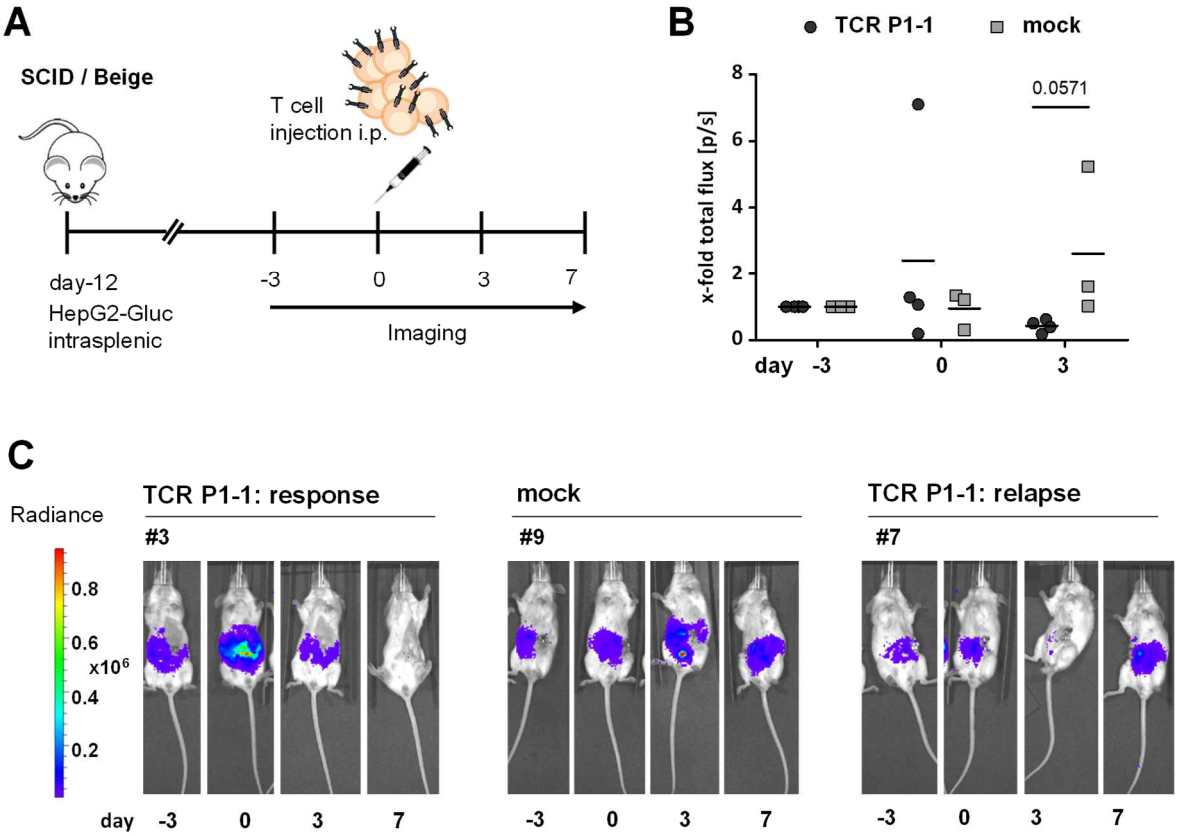

Figure 2.50 Anti-tumor effect of TCR P1-1-redirected human T cells in a murine xenograft HCC model.
(A) Schematic overview: SCID/Beige mice were intrasplenically transplanted with HepG2 cells expressing the *Gaussian* luciferase (HepG2-Gluc). Mice received either 1 x 10^7 human PBMC containing 1 x 10^6 TCR P1-1 grafted T cells or 1 x 10^7 mock PBMC intraperitoneally on day 0. Bioluminescence imaging was performed every three to four days. **(B)** Quantification of bioluminescence. The total flux is depicted in fold change of photons/second for individual mice relative to initial measurement at day -3. Mean is shown. **(C)** *In vivo* bioluminescence imaging of representative mice treated with TCR P1-1-equipped or mock T cells. Images were adjusted to the same pseudo color scale to show relative bioluminescence changes over time. Color scale: minimum 7.14 x 10^3; maximum 0.35 x 10^5 photons. (n=3-4, Mann-Whitney test, number in graph indicates p value)

As described above, only in seven out of 20 mice tumors were established after intrasplenic injection of hepatoma cells. We therefore aimed at optimizing the administration route and compared tumor development after intraperitoneal versus subcutaneous injection of HepG2-Fluc cells. Subcutaneous injection led to comparable tumor sizes throughout all mice and appropriate bioluminescence signals measured 14 days after transplantation. On the contrary, intraperitoneal injection led to tumor formation spread throughout the peritoneum (data not shown) but was not measurable by bioluminescence imaging (Figure 2.51 C). Hence,

subsequent experiments were performed using HepG2-Fluc cells for subcutaneous tumor formation.

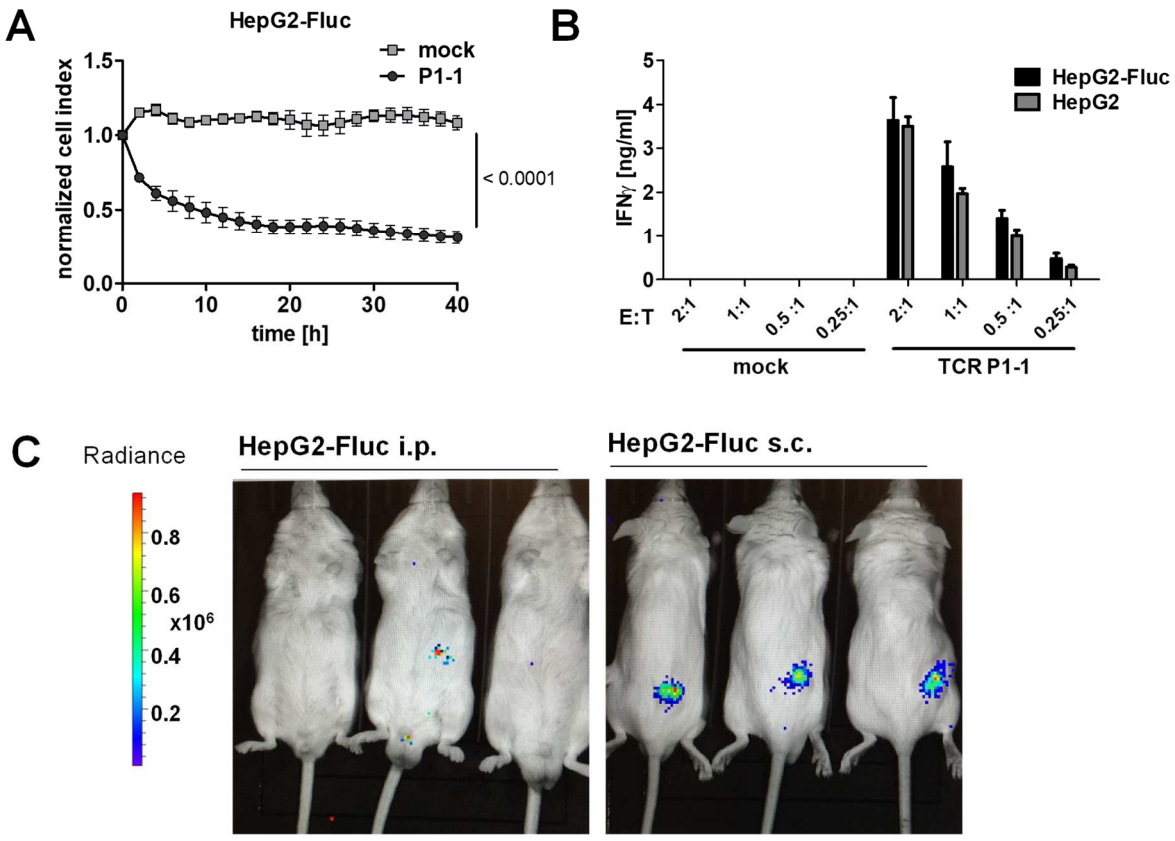

Figure 2.51 Optimization of HCC xenograft model.
Hepatoma cells stably expressing the *firefly* luciferase (HepG2-Fluc) were generated. **(A)** Cytotoxic effect of TCR P1-1-redirected T cells on HepG2-Fluc cells. Viability of target cells was analyzed over time using the xCELLigence system. Mean and SD of triplicates are shown (Mann-Whitney test, number in graph indicates p value). **(B)** Supernatant of co-cultures of TCR P1-1$^+$ T cells with HepG2 or HepG2-Fluc cells using different effector to target cell (E:T) ratios was analyzed for IFNγ secretion via ELISA. Mean and SD of triplicates are shown. **(C)** *In vivo* bioluminescence imaging of Rag2$^{-/-}$γc$^{-/-}$ mice transplanted with HepG2-Fluc cells intraperitoneally or subcutaneously. Images (day 14 after tumor transplantation) were adjusted to the same pseudo color scale. Color scale: minimum 7.14 x 10^3; maximum 0.35 x 10^5 photons. (n=3)

Hence, Rag2$^{-/-}$γc$^{-/-}$ mice were subcutaneously transplanted with HepG2-Fluc cells, followed by sublethal whole-body irradiation seven days thereafter to improve engraftment. 2 x 10^6, 4 x 10^6 CD8$^+$ P1-1$^+$ or mock CD8$^+$ human T cells were adoptively transferred on day 0, as well as on day 7 and 14 (Figure 2.52 A). P1-1-equipped T cells were able to control the tumor initially but subsequently could only decrease the bioluminescence signal indicating tumor growth (Figure 2.52 B). Furthermore, we did not detect significant CD8$^+$ T cell infiltration into the tumor (Figure 2.52 C). This was accompanied by a reduced GPC3 expression in established tumors, indicated by GPC3 mRNA levels and immunohistochemistry (Figure 2.52 D and E).

Consequently, TCR P1-1 engrafted T cells were only able to initially control tumor growth, but then the tumor cells seemed to downregulate the target antigen (Dargel et al., 2015).

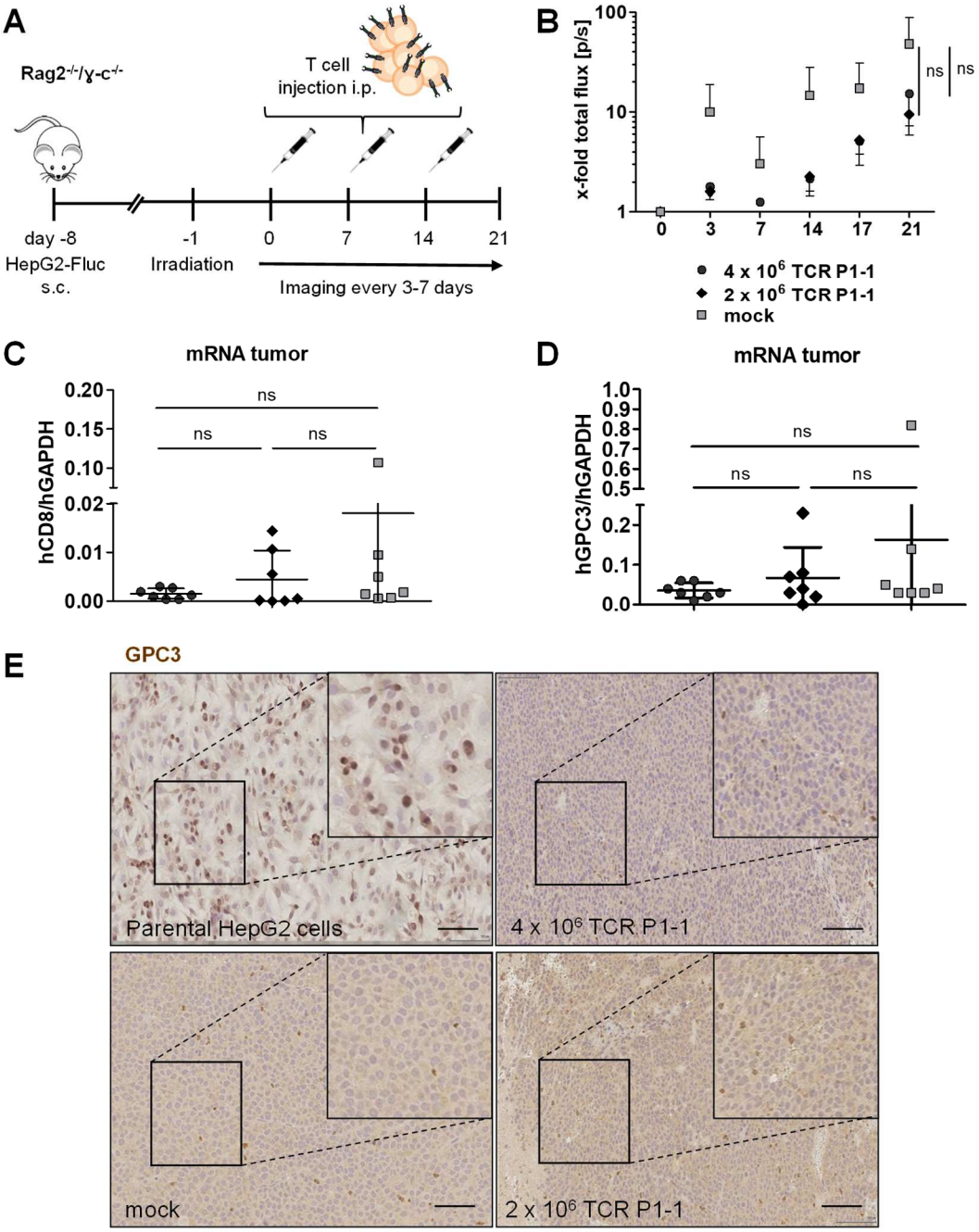

Figure 2.52 Anti-tumor effect of repeated adoptive transfer of TCR P1-1-redirected human T cells in a murine xenograft HCC model.
(A) Schematic overview: Rag2$^{-/-}\gamma c^{-/-}$ mice were transplanted with HepG2-Fluc cells by subcutaneous injection, irradiated after seven days, and received 2 x10^6, 4 x10^6 CD8$^+$ P1-1$^+$ or mock CD8$^+$ human T cells on day 0, 7 and 14 by intraperitoneal injection. Bioluminescence imaging was performed every three to seven days. **(B)** Quantification of bioluminescence. The total flux is depicted in fold change of photons/second for individual mice relative to initial measurement at day 0. **(C)** Intratumoral human CD8 (hCD8) expression relative to hGAPDH. **(D)** Intratumoral human GPC3 (hGPC3) expression relative to hGAPDH. **(E)** Representative immunohistochemical GPC3 stainings of tumor sections as well as the parental cell line HepG2. Scale bars indicate 500 µm. Mean and SD are shown. (n=7, Kruskal-Wallis test and Dunn's Multiple Comparison test, ns = not significant)

2.4.2 Fratricide of TCR P1-1-redirected T cells

2.4.2.1 Cytotoxic effect of TCR P1-1-engrafted T cells on various HLA-A*02$^+$ target cells

As mentioned above, the cytotoxic effect of TCR P1-1-redirected T cells on the GPC3$^+$ HLA-A*02$^+$ target cell line HepG2 has already been demonstrated (Dargel et al., 2015). HepG2-derived tumors revealed reduced GPC3 expression *in vivo* (Figure 2.52 D and E), thus, we aimed to test if other cell lines would serve as suitable target cells for the recognition and elimination of TCR P1-1$^+$ T cells. Therefore, the hepatoma cell lines Huh7 and HepaRG, both expressing GPC3, but harboring a different HLA type, were stably transfected with HLA-A*02 to serve as target cells for TCR P1-1. Furthermore, Hela cells, a cervix carcinoma cell line, that is supposed to be GPC3$^-$ (Khan et al., 2001) was included as a negative control after HLA-A*02 transfection. Expression of HLA-A*02 was verified by flow cytometry analyses (Figure 2.53 A). Notably, all newly established cell lines were effectively eliminated by TCR P1-1-engrafted T cells, including Hela-HLA-A*02 that were supposed to be GPC3$^-$. Conversely, the viability of the parental cell lines not expressing HLA-A*02 was not reduced (Figure 2.53 B). Taken together, TCR P1-1$^+$ T cells killed all HLA-A*02$^+$ target cells investigated, irrespective of their GPC3 status.

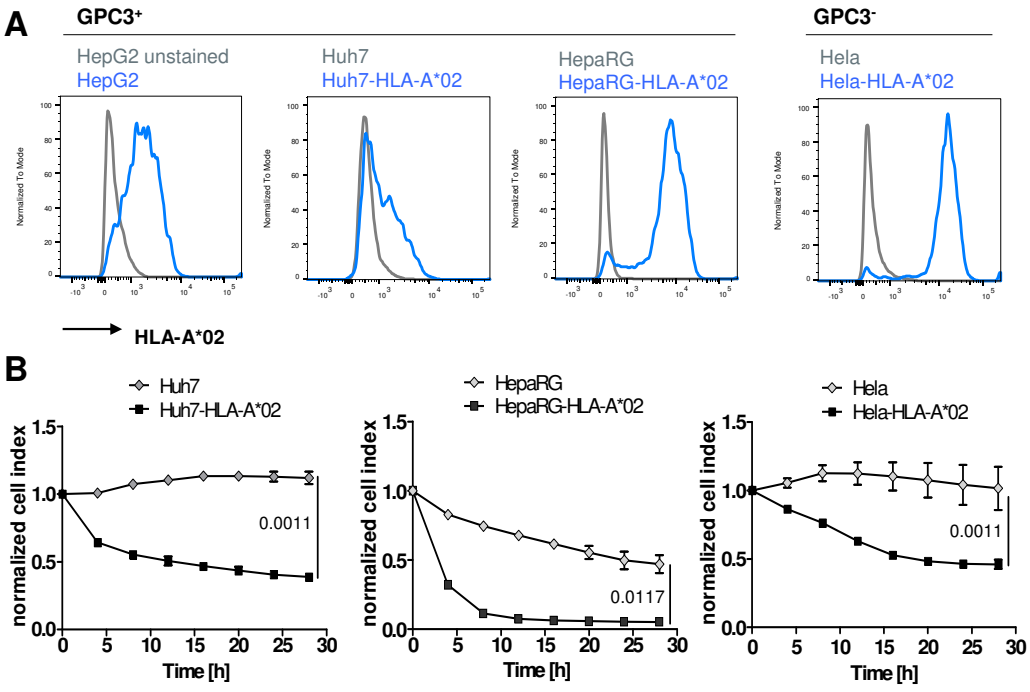

Figure 2.53 Cytotoxic effect of TCR P1-1$^+$ T cells towards different HLA-A*02$^+$ target cell lines. **(A)** HLA-A*02 expression analyzed by flow cytometry. **(B)** Cytotoxic effect of TCR P1-1-redirected T cells towards Huh7-HLA-A*02, HepaRG-HLA-A*02 and Hela-HLA-A*02 cells as well as on their parental HLA-A*02$^-$ cell lines. Viability of target cells was analyzed over time using the xCELLigence system. Mean and SD of triplicates are shown (Mann-Whitney test, numbers in graphs indicate p values).

Hela cells, which are supposed to be GPC3$^-$ (Khan et al., 2001) but HLA-A*02 $^+$ were also eliminated by TCR P1-1$^+$ T cells. Therefore, the possibility of reactivity of TCR P1-1 towards HLA-A*02 presenting a different peptide than GPC_{367} or HLA-A*02 alloreactivity was investigated. For this purpose, I transduced PBMC of different HLA-A*02$^+$ and HLA-A*02$^-$ donors with TCR P1-1, as we would expect fratricide in HLA-A*02$^+$ T cells if an alloreactive TCR was introduced, whereas HLA-A*02$^-$ T cells should not be affected. Four days after transduction the cell number of TCR P1-1-transduced cells was substantially reduced to <10 % compared to mock cells in the group of HLA-A*02$^+$ donors. In comparison, only a minor reduction in cell number was observed if donors were HLA-A*02$^-$ or if a control TCR (TCR D1) was used (Figure 2.54 A). To determine, if the lower expansion of P1-1-transduced HLA-A*02$^+$ T cells was due to alloreactivity, a co-culture of HLA-A*02$^+$ T cells as target cells and P1-1-transduced or mock HLA-A*02$^-$ T cells as effector cells was performed. A flow cytometry analysis for HLA-A*02$^+$ cells 24 h later revealed, that a considerably low amount of 7 % of HLA-A*02$^+$ target cells remained if TCR P1-1$^+$ T cells were present in the co-culture (Figure 2.54 B). Thus one can conclude that TCR P1-1 engrafted T cells eliminated HLA-A*02$^+$ PBMC.

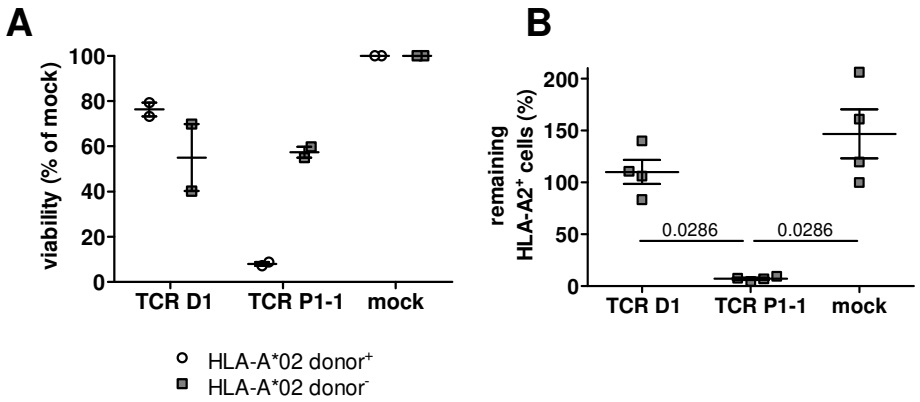

Figure 2.54 Cytotoxic effect of TCR P1-1-equipped T cells on HLA-A*02$^+$ PBMC.
(A) Total number of PBMC four days after retroviral transduction of HLA-A*02$^+$ and HLA-A*02$^-$ donors determined by counting with a Neubauer chamber using trypan blue staining. TCR D1 served as control TCR. Mean and SD are shown. (n=2). **(B)** P1-1 engrafted HLA-A*02$^-$ T cells were co-cultured with HLA-A*02$^+$ PBMC. After 24h of co-incubation, the amount of remaining living HLA-A*02$^+$ cells was measured by flow cytometry. TCR D1 served as control TCR. Mean and SD are shown. (n=4, Mann-Whitney test, numbers in graphs indicate p values)

TCR P1-1-redirected T cells eliminated HLA-A*02^{+} but GPC3^{-} Hela as well as HLA-A*02^{+} PBMC. To exclude GPC3 expression in those cells, GPC3 RNA level was determined by qPCR. Indeed, Hela cells as well as PBMC expressed low levels of GPC3 (Figure 2.55). Thus, it remained unclear whether fratricide of TCR P1-1-redirected T cells is a consequence of low level GPC3 expression or HLA-A*02 alloreactivity.

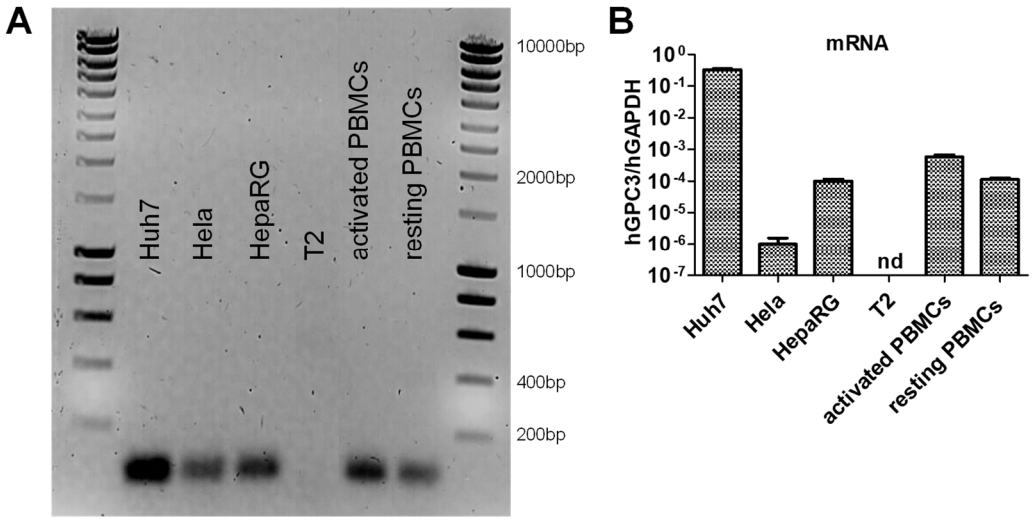

Figure 2.55 hGPC3 expression on RNA level for different cell lines and PBMC.
(A) Agarose gel of the amplicon of the hGPC3 qPCR (product length: 89 bp). **(B)** hGPC3 expression of different cell lines as well as for PBMC relative to hGAPDH determined by qPCR. nd= not detected

2.4.2.2 Cytotoxicity of TCR P1-1 redirected T cells on GPC3 knock-out cell lines

As the fratricide described in section 2.4.2.1 could also be an effect of weak GPC3 expression in T cells, we decided to create a GPC3^{-} but HLA-A*02^{+} Hela cell line using CRISPR/Cas9 technology. Therefore, I first designed guideRNAs (gRNAs) to ensure a target specific cleavage and subsequently induction of frame-shift-mutations at the GPC3 locus (Table 2.1).

gRNA	nucleotide sequence	gRNA target
gRNA1-GPC3	CCCCAAGCTTATTATGACCC	Exon 3
gRNA2-GPC3	TCAGGTCACGTCTTGCTCCT	Exon 3
gRNA3-GPC3	GGTCACGTCTTGCTCCTCGG	Exon 3

Table 2.1 Nucleotide sequence and target regions of three different gRNAs for GPC3.

Subsequently, those gRNAs were used to create Hela-HLA-A*02 GPC3 knock-out lines (procedure explained in detail in Figure 2.56). In total, I received seven single-cell clones, whereof four were transduced with gRNA1-GPC3, one with gRNA3-GPC3 and two with both gRNA1-GPC3 and gRNA3-GPC3 (Figure 2.57 A).

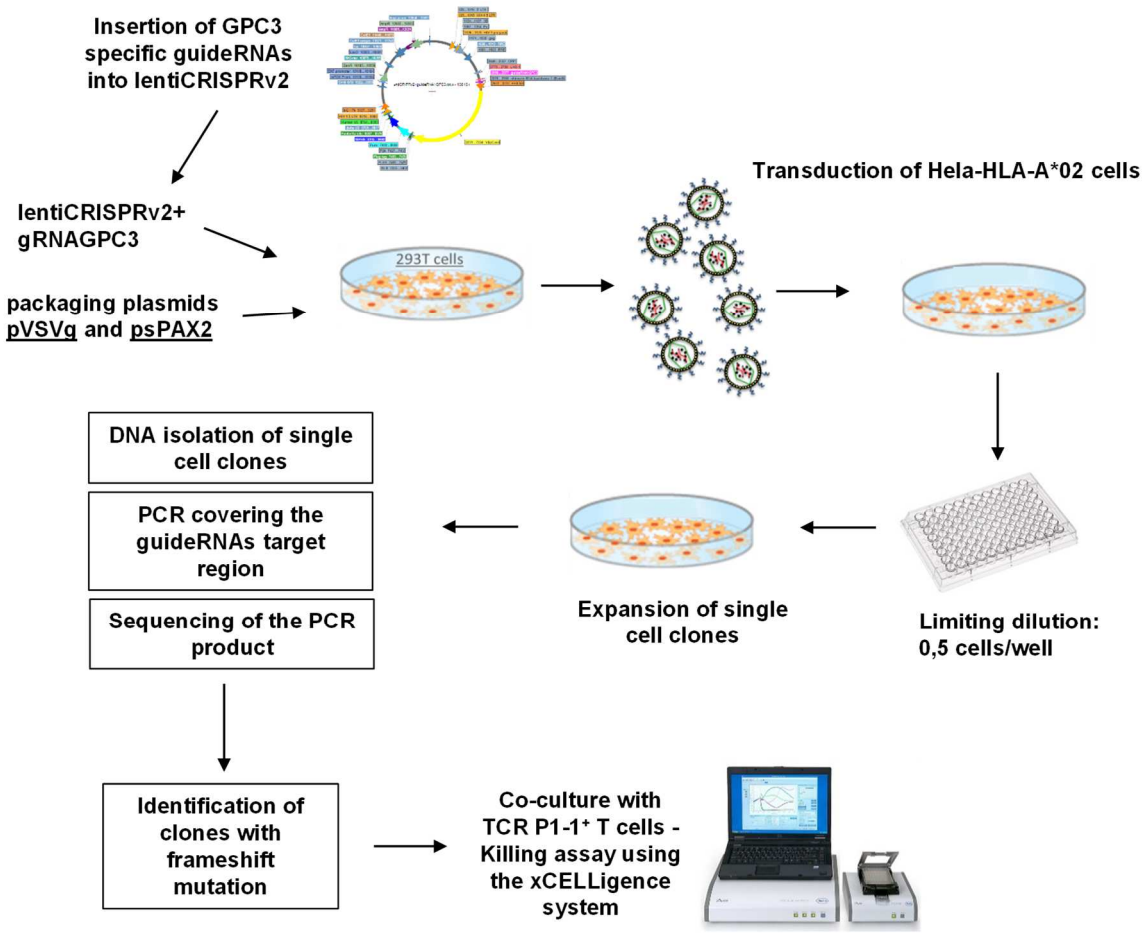

Figure 2.56 Schematic overview of the generation and verification of a Hela-HLA-A*02 GPC3 knock-out line.
gRNAs were cloned into the vector lentiCRISPRv2. A co-transfection of this newly generated plasmids together with the packaging plasmids pVSVg and psPAX2 into 293FT cells allowed production of lentivirus that was used to transduce Hela-HLA-A*02 cells. After a limiting dilution, single cell clones were expanded and analyzed to identify clones with a frameshift mutation within the GPC3 gene. Finally, GPC3 knock-out cell lines were co-cultured with TCR P1-1-redirected T cells using the xCELLigence system.

PCR analysis of the gRNA target region revealed that the PCR product of Hela-HLA-A*02 gRNA1 clone 2 (Hela-HLA-A*02 gRNA1-2) was of unexpected size, indicating a potential deletion after a double strand break (Figure 2.57 A). In addition, all PCR products were sequenced and aligned with the original GPC3 sequence to identify insertion, deletions or frameshift mutations (Figure 2.57 B and C). Two clones, namely Hela-HLA-A*02 gRNA1-2 and

Hela-HLA-A*02 gRNA3-1 presented frameshift mutations and subsequent loss of the peptide $GPC3_{367}$ (Dargel et al., 2015). In contrast, the GPC3 sequence did not change for the clone Hela-HLA-A*02 gRNA1-6.

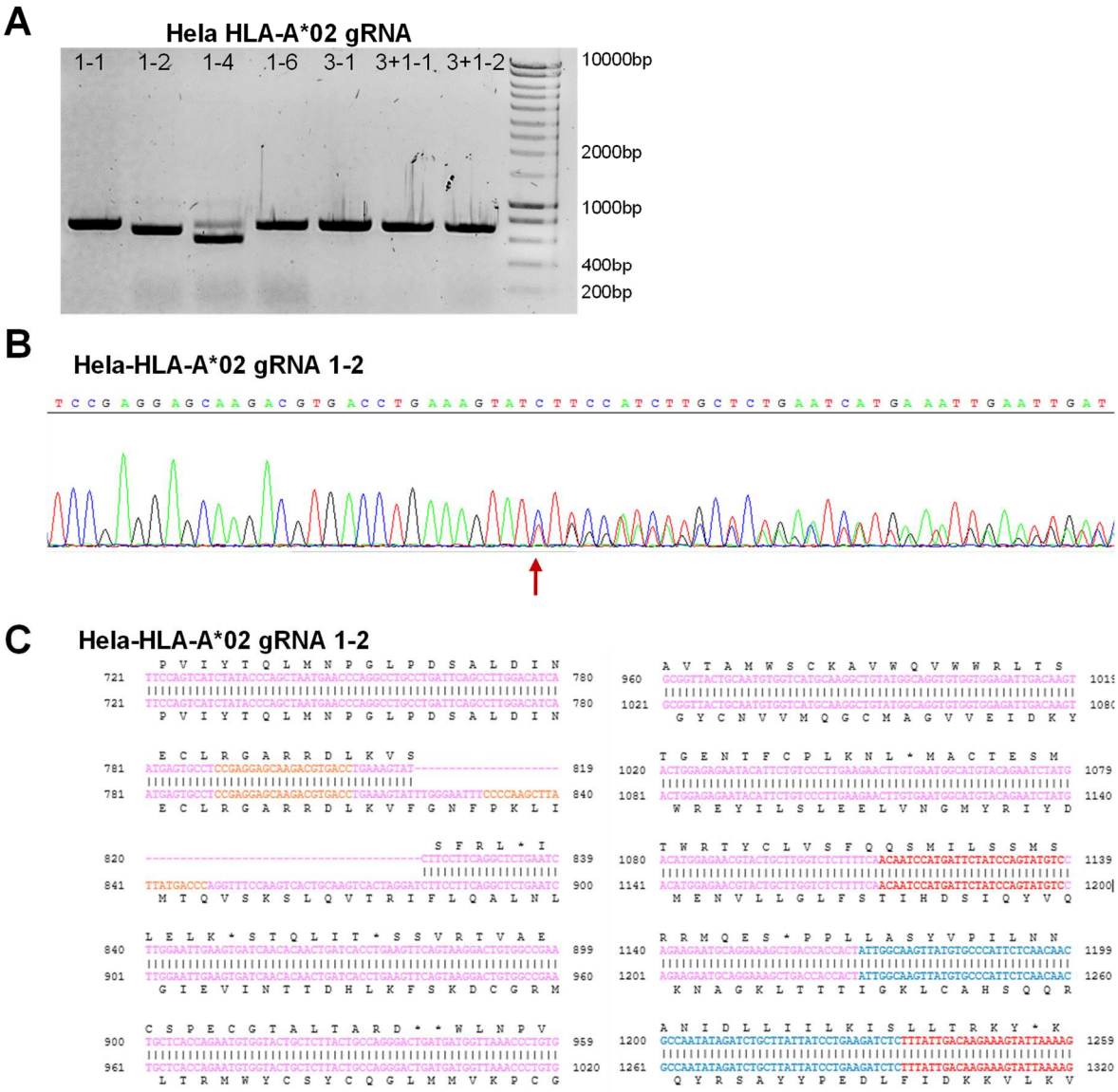

Figure 2.57 Identification of a Hela-HLA-A*02 GPC3 knock-out cell line.
(A) PCR product covering the gRNAs target region for all single cell clones analyzed on an agarose gel. Length of PCR product without insertion or deletion: 695 bp. **(B)** Representative analysis of single cell clone gRNA1-clone 2 (Hela-HLA-A*02 gRNA1-2). Sequencing result for gRNA1-2. Arrow indicates site where double-strand break occurred. **(C)** Alignment of original nucleotide and amino acid sequence with the sequences of clone gRNA1-2. Color code: pink: exon 3, orange: gRNAs, red: peptides $GPC3_{367}$ and $GPC3_{326}$ (Dargel et al., 2015), blue: exon 4.

In order to use the generated Hela-HLA-A*02 GPC3 knock-out cell lines as target cells for TCR P1-1$^+$ T cells in a co-culture assay, their HLA-A*02 surface expression had to be verified. All clones as well as Hela-HLA-A*02 GPC3K3, a clone that overexpresses GPC3, were stably expressing HLA-A*02 (Figure 2.58 A). Finally, the Hela-HLA-A*02 GPC3 knock-out cell lines were used for a killing assay with TCR P1-1$^+$ T cells. All Hela-HLA-A*02 target cell lines -

independent of their GPC3 expression - were eliminated by T cells equipped with TCR P1-1 (Figure 2.58 B). Conversely, the HBV-specific HLA-A*02 restricted TCR 4G did not reduce cell viability in those cell lines. In summary, P1-1^{+} T cells recognized HLA-A*02^{+} target cells independent of GPC3 expression. Therefore weak expression of the peptide GPC3$_{367}$ in HLA-A*02^{+} Hela as well as HLA-A*02^{+} PBMC were not the cause for their elimination by TCR P1-1-redirected T cells, but rather alloreactivity of TCR P1-1.

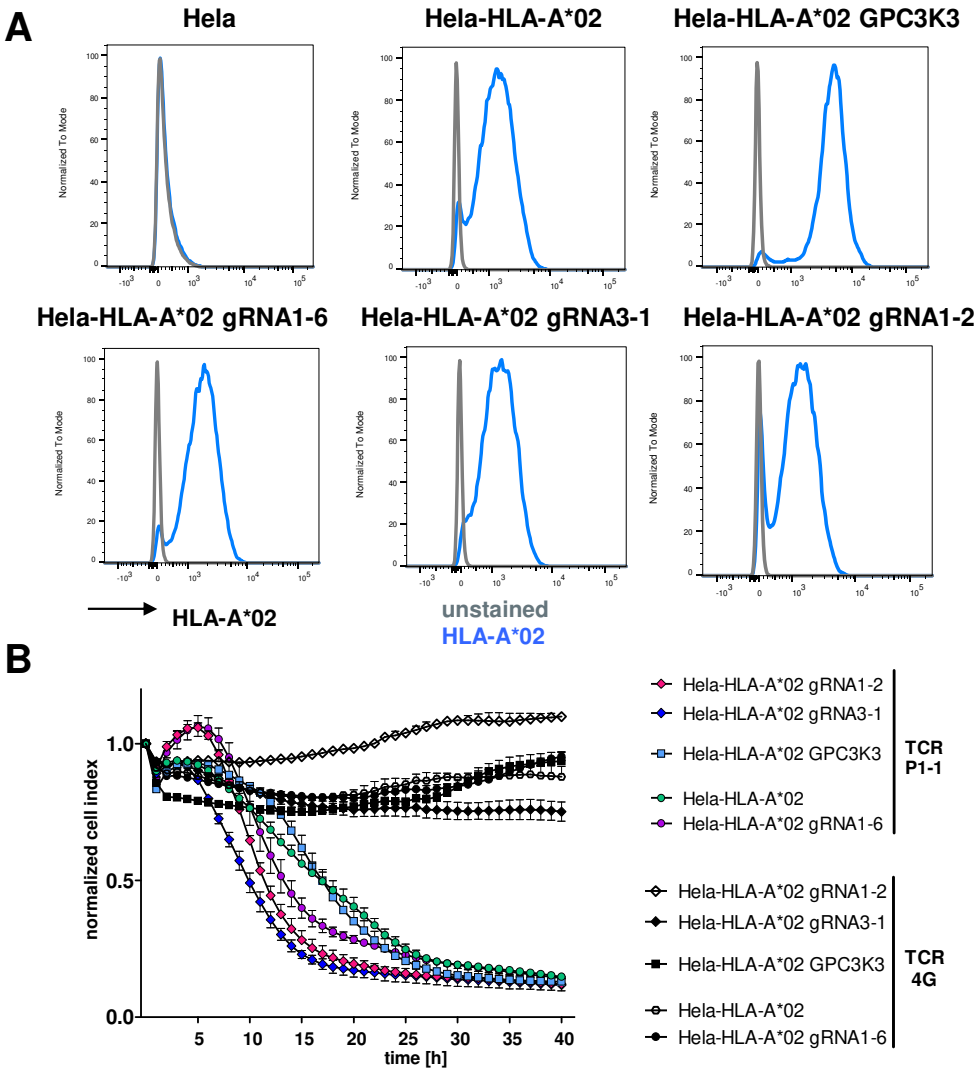

Figure 2.58 Cytotoxic effect of TCR P1-1-redirected T cells on Hela-HLA-A*02 GPC3 knock-out cell lines.
(A) HLA-A*02 expression analyzed by flow cytometry. **(B)** Cytotoxic effect of TCR P1-1-engrafted T cells on Hela-HLA-A*02 GPC3 knock-out cell lines (Hela-HLA-A*02 gRNA1-2 and Hela-HLA-A*02 gRNA3-1), parental cell lines Hela-HLA-A*02, Hela-HLA-A*02 gRNA1-6 and Hela-HLA-A*02 GPC3K3 that overexpresses GPC3. TCR 4G served as control TCR. Viability of target cells was analyzed over time using the xCELLigence system. Mean and SD of triplicates are shown.

2.4.2.3 Cytotoxicity of TCR P1-1 expressing T cells on $GPC3_{367}$-like peptides

To elucidate, if elimination of HLA-A*02$^+$ GPC3 knockout cell lines as well as HLA-A*02$^+$ PBMC was due to cross-reactivity of TCR P1-1 with another peptide presented on HLA-A*02, I finally determined, whether TCR P1-1 would be activated by HLA-A*02 presented peptides that share similarities with $GPC3_{367}$ (Figure 2.59 A). Therefore, a co-culture experiment was set up. T2 cells were loaded with the respective peptides and co-incubated with TCR P1-1-engrafted T cells. Considerably high secretion levels of IFNγ were observed after co-culture with TCR P1-1$^+$ T cells independent of the peptide that was loaded onto T2 cells or even without peptide loading. Mock T cells or HBV-specific T cells were not activated to secrete IFNγ by $GPC3_{367}$ like peptides or unloaded T2 cells (Figure 2.59 B). In conclusion, TCR P1-1-redirected T cells did not show sufficient specificity for peptide $GPC3_{367}$ but demonstrated fratricide due to HLA-A*02 alloreactivity.

A

Peptide	Sequence	Origin (human)
$GPC3_{367}$	TIHDSIQYV	
$GPC3_{367}$ like 2	DIHDSIQPR	brefeldin A-inhibited guanine nucleotide-exchange protein 1
$GPC3_{367}$ like 3	AIHDVIRYV	DEAH (Asp-Glu-Ala-His) box polypeptide 40, isoform CRA_b
$GPC3_{367}$ like 4	TIHDHINYN	leucine-rich repeat-containing protein 4 precursor

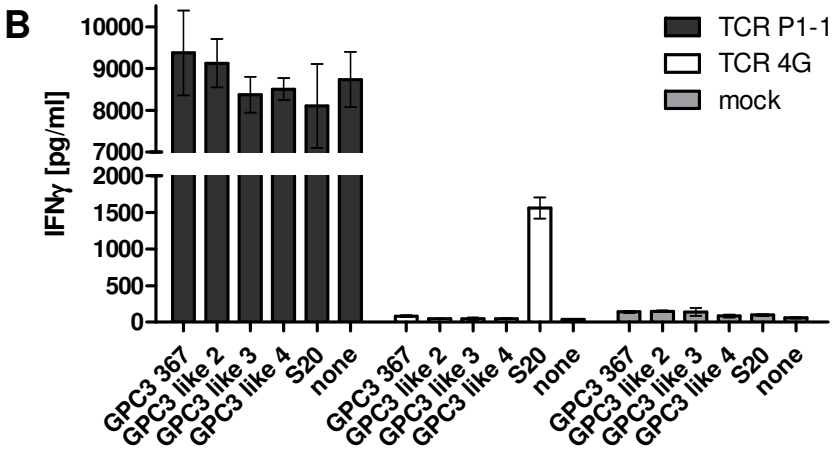

Figure 2.59 Activation of TCR P1-1-redirected T cells by $GPC3_{367}$ -like peptides.
(A) Amino acid sequence of $GPC3_{367}$ and additional three peptides exhibiting three amino acid changes compared to $GPC3_{367}$. **(B)** T2 cells were loaded with 1 µM of the respective peptides and co-cultured with TCR P1-1$^+$, TCR 4G$^+$ or mock T cells. 24 h later the supernatant was analyzed for IFNγ secretion via ELISA. TCR 4G (specific for peptide S20) served as a control TCR. Mean and SD of triplicates are shown.

3 DISCUSSION

Currently, curative treatment options are not available for chronic HBV infections as well as for hepatocellular carcinoma, highlighting the need for new therapies. Immunotherapies like therapeutic vaccination and adoptive T-cell therapy represent promising approaches to treat chronic HBV infections as well as HCC. In this thesis, mouse models for the evaluation of antiviral strategies were explored and new immunotherapeutic approaches against HBV infection and HCC were investigated as discussed in the following sections.

3.1 HBV mouse models: vector-mediated HBV genome transfer

3.1.1 Comparison of HBV genome delivery by adenoviral-, high capacity adenoviral- and adeno-associated viral vector

To investigate the treatment of chronic HBV infection and HBV-related HCC, small animal models are needed. Immunocompetent transgenic mice expressing a 1.3 overlength copy of the HBV genome (HBV1.3) exist, but clearance of the virus cannot be obtained, as the HBV genome is integrated into the mouse genome. To overcome this obstacle, we generated and compared different vectors in order to achieve HBV genome transfer into mouse hepatocytes. For this purpose, we first established an AAV-mediated HBV genome transfer (Dion et al., 2013; Kan et al., 2017; Yang et al., 2014; Ye et al., 2015). Indeed, we could reproduce published results, as AAV-HBV infection in immunocompetent mice led not only to liver-specific HBV replication, but also to HBV persistence and no HBV-specific immune responses were detected (Figure 2.1-Figure 2.3).

Next, we compared AAV-mediated HBV genome transfer to an already established adenovirus (Ad, first generation adenovirus) (Huang et al., 2012; von Freyend et al., 2011) and a newly generated high capacity adenovirus (HCA; gutless adenovirus) mediated HBV genome transfer for their potential to mimic chronic HBV infection. For this purpose, a 1.3 overlength HBV genome containing a translational stop in the X ORF (HBV 1.3 X^-) was chosen, as previous work was done with an Ad-HBV 1.3X^- (Huang et al., 2012; von Freyend et al., 2011). Moreover, the X protein is characterized as an oncogene (Kim et al., 1991). Therefore, working with the HBV genome harboring the intact X protein delivered by an adenoviral or AAV vector demands special safety measures, as HBV-specific antibodies induced by prophylactic vaccination would not neutralize AAV or adenoviral vectors carrying the HBV genome. Due to this reason, working with an X-deficient HBV genome allows broader laboratory applicability. Ad-HBV X^- has been demonstrated to induce a transient high level expression of HBV proteins

if medium to high titer dosages are used for infection, reflecting the situation of an acute, self-limiting infection (von Freyend et al., 2011). In contrast, low dose infection with Ad-HBV X^- induces persistent infection (Huang et al., 2012), however, the number of transduced hepatocytes is also low. Furthermore, Ad-HBV X^- induces a strong vector-mediated immune response which can alter viral replication and the immune response against HBV (Sprinzl et al., 2004). In order to reduce this vector-mediated immune response, the HCA-HBV X^-, lacking all protein-coding adenoviral sequences, was generated.

This study demonstrates, that all above described viral vectors induced a persistent HBV infection in immunocompetent mice (Figure 2.5 - Figure 2.7). In contrast to adenoviral vectors, AAV vector-based HBV genome delivery exhibited slow increase of serum HBeAg and HBsAg levels (Figure 2.5), likely resulting from vector-based characteristics: the ssDNA genome has to be replenished to dsDNA to reach full potential. In contrast, transfer of the HBV genome using both adenoviral vectors directly provides complete templates and the expression maximum is reached earlier (Figure 2.5), though supporting the induction of vector-mediated as well as HBV-specific immune responses (Sprinzl et al., 2004; von Freyend et al., 2011).

Here, we developed a new animal model for HBV persistence using HCA-HBV X^-. In contrast to Ad-HBV X^-, high dose infection with HCA-HBV X^- (2×10^9 pfu) did not lead to liver damage, as ALT levels remained within the physiological range (Figure 2.5). Hence, the cytotoxic immune response caused by Ad-HBV X^- might be diminished. Moreover, a high number of hepatocytes were transduced, resulting in strong expression of HBV proteins characterized by the presence of high serum HBeAg levels. Strikingly, HCA-HBV X^- infected mice demonstrated high levels of serum anti-HBs accompanied by a decrease in serum HBsAg levels (Figure 2.5, Figure 2.6). As they still contained large numbers of HBV DNA in the serum, the reason of decreasing serum HBsAg is likely due to complexation with anti-HBs antibodies. Chronically HBV-infected patients, that are serum HBsAg negative, but HBV DNA positive while anti-HBc and/or anti-HBs antibodies are detected, are suffering from a so-called occult hepatitis B infection (OBI) (Chen et al., 2014). HCA-HBV X^- infected immunocompetent mice therefore mimic the situation of OBI patients, who are still in risk of developing sequelae. Hence, HCA-HBV X^- infection is an appropriate animal model to study therapeutic interventions for OBI patients.

Interestingly, serum HBeAg levels after high dose infection of Ad-HBV X^- did not decrease as fast as observed previously (von Freyend et al., 2011) but rather showed a very slow decline over time. However, HBV replication and the expression level of HBV proteins was greatly reduced when compared to HCA-HBV X^- three months after infection indicated by serum HBeAg and HBcAg staining of hepatocytes (Figure 2.5, Figure 2.7). To determine if this difference was due to an initial difference in hepatocytes transduced or elimination of HBV^+

hepatocytes over time, we assessed the amount of HBV DNA as well as HBc^+ hepatocytes at day 5 after infection, aiming to perform the analysis before onset of immunity. Indeed, transduction levels were comparable at day 5 post infection (Figure 2.7 and data not shown) indicating that HBV^+ hepatocytes were identified and eliminated when the first-generation adenoviral vector was used. Taken together, in high titer doses, HCA-HBV X^- provides an improvement compared to Ad-HBV X^- as HBV persistence was stable over three months. For medium or low titer doses, both adenoviral vectors revealed comparable results mimicking a chronic HBV infection.

AAV-mediated transfer of the HBV genome was reported to result in establishment of cccDNA (Lucifora et al., 2017) which could also be confirmed in our experiment by qPCR. The cccDNA qPCR was performed after digestion of extracted DNA with a T5 exonuclease, which removes linear ssDNA, rcDNA or nicked DNA but spares cccDNA, leading to an increased selectivity for cccDNA as described previously (Xia et al., 2017). In contrast, we did not detect cccDNA after HBV genome delivery with neither adenoviral-based vector. Establishment of cccDNA in AAV-HBV-infected animals therefore might provide the unique opportunity to study drugs targeting cccDNA which highlights an important advantage of using the AAV vector instead of adenoviral vectors. So far it is not known, whether this cccDNA molecule is formed by recombination from AAV-HBV episomes or by recycling of *de novo*-formed cytoplasmic nucleocapsids in AAV-HBV transduced hepatocytes (Lucifora et al., 2017). In HBV-transgenic mice cccDNA cannot be detected (Guidotti et al., 1995), arguing the reason for cccDNA establishment might rather be due to recombination of AAV-HBV episomes. Infection of animals with an AAV-HBV vector that is HBc deficient could help to answer this question, as in this setting recycling of newly-formed nucleocapsids would not be possible. If cccDNA would still be detectable, it would provide further evidence that it is formed because of the characteristics of the AAV forming episomes that allow for recombination. However, the AAV-HBV model might in any case be suitable to study the potential of molecules capable to silence or induce degradation of cccDNA.

The AAV-mediated transfer of the HBV genome will likely be the most applicable model, as it induced persistent viral replication without inducing an immune response. Furthermore, HBV-specific antibodies were absent (anti-HBc- and anti-HBe-antibodies) or appeared only occasionally and at very low levels (anti-HBs antibodies) in AAV-HBV-infected animals in contrast to both adenoviral vectors investigated. Moreover, AAV-HBV-transduced hepatocytes exhibited formation of cccDNA. Importantly, AAV production is not as difficult as especially the production of the HCA. As HCAs are free of all adenoviral coding regions, adenoviral proteins have to be provided by a helper virus. Subsequent contamination of helper virus has to be removed from the preparation which makes the production complex and demands specific in-depth know-how (Kreppel, 2014).

Nevertheless, the HCA might be of great interest for certain scientific questions, for instance to study the therapeutic potential of S-CAR T-cell therapy, HBV-specific bispecific antibodies or therapeutic vaccination strategies in a setting with pre-existing anti-HBs antibodies, which would compete for binding-sites with their target. Moreover, the HCA has the capacity to insert a larger transgene compared to the AAV. Therefore, another transgene can be transferred in addition to the HBV genome. For instance, the HBV genome could be transferred together with HLA-A*02 in one vector to investigate the potential of HLA-A*02-restricted HBV-specific TCRs as discussed below. In the present thesis, the delivery of the two transgenes was performed by co-injection of two AAVs, but transferring both transgenes with one vector would prevent the presence of single-positive cells.

3.1.2 Investigation of HBV genome variants using the adeno-associated viral vector

Beside the comparison of different viral vectors for HBV genome delivery, I generated and compared different HBV genome variants using an AAV for genome delivery. After *in vitro* verification of the vectors replication ability, immunocompetent mice were infected with AAVs encoding for HBV 1.3WT, HBV 1.3X$^-$ as well as HBV 1.3E$^-$.

As HBV replicates through an RNA intermediate, an active viral reverse transcriptase/polymerase enzyme is required for replication. HBV exhibits a mutation rate that is more than 10-fold higher than in other DNA viruses, because its reverse transcriptase lacks a proofreading function (Girones and Miller, 1989). Common mutations are naturally occurring within the pre-core/core region. A dominant mutant is a stop codon mutation at position 1896, which leads to inability to express HBeAg (Lok et al., 1994) and was inserted in the AAV-HBV 1.3E$^-$ investigated in this study. Beside this mutation, mutations at positions 1762 and 1764 result in reduced production of HBeAg and may increase viral replication and host immune responses (Hunt et al., 2000). Preliminary studies demonstrated the pre-core mutation may be associated with severe chronic liver disease and fulminant hepatitis (acute liver failure) (Fagan et al., 1986; Hasegawa et al., 1991), but larger epidemiological studies could not confirm enhanced virulence in patients harboring HBV with the pre-core stop mutation (Lindh et al., 1996). Indeed, in the present work, we did not obtain any evidence that lack of HBeAg as in the pre-core stop codon variant induces a fulminant hepatitis. ALT levels were not increased (Figure 2.9), and histological analysis did not reveal any particular features, like influx of neutrophils (data not shown), which would be expected in a case of acute liver failure (Takai et al., 2005). In contrast, it is likely, that multiple pre-core or core mutations are required to increase viral virulence (Hur et al., 1996). Thus, an AAV encoding for the HBV genome harboring more than the pre-core stop mutation should be generated to have the possibility to preclinically evaluate the consequences of multiple pre-core/core mutations. However,

molecular and immunological conditions might differ from mouse to human and results should therefore be interpreted carefully.

We found reduced serum HBsAg levels as well as HBV DNA copies in serum and liver tissue of animals infected with the AAV encoding for the pre-core stop mutation compared to wildtype HBV, although the same amount of input AAV was used (Figure 2.9, Figure 2.10). The same observation was made in a study, in which viral load was significantly reduced using an HBeAg negative- compared to wildtype-HBV genome in a mouse model. It was possible to revert this effect by blockade of IFNα, indicating HBeAg possibly acts as a natural IFNα antagonist (Verheyen, 2016). In contrast, pre-core mutants have been found to decrease responsiveness to treatment with peg-IFNα (Peeridogaheh et al., 2018), highlighting the need of preclinical models harboring HBV genome mutations to study the effect of therapeutic interventions for the treatment of chronic HBV infection.

Moreover, we analyzed an X-deficient HBV variant in the AAV-HBV mouse model. The absence of the X protein had a huge impact on HBV replication. This was demonstrated by decreased expression of serum HBeAg, HBsAg, HBc expression in hepatocytes as well rcDNA in serum and liver tissue (Figure 2.9, Figure 2.10). Importantly, the amount of cccDNA copies was not different compared to the WT genome (Figure 2.10). The dependency on the X protein to initiate and maintain HBV replication during natural infection has been reported *in vitro* (Lucifora et al., 2011) and it would be desirable to be able to study the functions of the X protein *in vivo*. Interestingly, after AAV-HBV infection, the X protein did not have the same key regulator effects as in a natural occurring infection (Lucifora et al., 2011), as not only HBV DNA but also the AAV genome was greatly reduced three months after infection when compared to the WT. We provide evidence, that this is not an effect of lower AAV dose used for infection, as we find the same amount of AAV as well as rcDNA in the liver on day 3 post infection in all genome variants investigated (Figure 2.10). Moreover, it is very unlikely that the different AAVs would exhibit unequal infectivity, as they all share the same capsid. However, it has been observed, that HBV greatly improves AAV transduction *in vitro* and *in vivo*. The X protein has been found to be responsible for this enhanced susceptibility by promoting delivery of AAVs to the nucleus through phosphatidylinositol 3-kinase (PI3K) (Hosel et al., 2014). Consequently, AAV-1.3WT as well as AAV-1.3E^{-} which harbor an intact X protein might enter the nucleus of transduced hepatocytes more efficiently as any other AAV, for instance the AAV-1.3X^{-}. This would become effective after first AAVs have entered the nucleus and X has been produced. Alternatively, the effect might be a consequence of X on the established cccDNA. The cccDNA molecule can be in a transcriptionally open conformation associated with high levels of active chromatin markers (Tropberger et al., 2015). The X protein attached to the cccDNA minichromosome might have a function in the establishment of an accessible chromatin by regulating the recruitment of chromatin modifying enzymes (Alarcon et al., 2016; Belloni et al.,

2009; Riviere et al., 2015). Therefore, enhanced production of HBV proteins in WT and E^- variants could be an effect of the X protein influencing transcriptional activity, if HBV is transcribed from the cccDNA pool established after AAV-HBV infection. Thus, in future experiments one should try to complement hepatocytes with the X protein once AAV-1.3X^- infection has already been established. This will give insight if initial steps of AAV entry to the nucleus, the effect on cccDNA conformation or both lead to the observed differences in the X-deleted compared to X-expressing HBV variants.

In conclusion the role of the X protein remains obscure in using the AAV as a vector for HBV genome delivery. If it is necessary to use the HBV X^- version due to safety aspects, adenoviral vectors are more suitable for *in vivo* experiments at the current level of knowledge, as the X protein was not demonstrated to have an impact on initiation and maintenance of HBV replication when using adenoviral vectors (data not shown). Moreover, we show that the AAV model of HBV genome delivery enables us to investigate HBV genome variants as for instance the pre-core stop mutation in preclinical models. Next to the course of infection, the effect of therapeutic interventions for the treatment of chronic HBV infection in patients harboring HBV genome variants can be studied.

3.2 Immunotherapeutic approaches against chronic HBV infection/ HBV-associated HCC

In this dissertation, the potential of different immunotherapeutic strategies towards chronic HBV infection and HBV-related HCC was investigated. Previous studies on such therapeutic interventions were either not yet transferred to the *in vivo* setting or performed in HBV-transgenic mice. To be able to demonstrate 'functional cure' of the explored immunotherapeutic approaches, defined by the loss of HBsAg and/or seroconversion to anti-HBs and undetectable HBV DNA in serum (Levrero et al., 2016), the AAV-HBV mouse model inducing persistent HBV infection was used. The results of therapeutic vaccination and adoptive T-cell therapy for treatment of chronic HBV infection are discussed below.

3.2.1 Therapeutic vaccination

Therapeutic vaccination is considered a promising strategy to treat chronically HBV-infected patients although clinical data demonstrated limited effects so far (Kosinska et al., 2017). Most therapeutic vaccination regimes evaluated in clinical trials to date concentrated on inducing a potent T-cell response but did not aim to activate antibody responses. In order to break immune tolerance and give rise to or boost HBV-specific immune responses by therapeutic vaccination, in our opinion, it is crucial to induce both the humoral and the cellular arm of the adaptive immune response. *In vivo* data obtained from HBV-transgenic mice primed with HBV proteins,

followed by an MVA boost vaccination demonstrated promising results as it was able to break tolerance by inducing HBV-specific B- and T-cell responses (Backes et al., 2016). Here, we adapted this vaccination scheme, called TherVacB, and used AAV-HBV-infected mice to be able to achieve viral clearance. Beside the vaccination scheme, important factors that influence efficacy of the therapeutic effect include the co-administration of an appropriate adjuvant as well as the administration route. Cyclic-di-AMP has been reported to serve as a promising vaccine adjuvant by inducing a balanced T_h1/T_h2-response that simultaneously allows to prime virus-specific effector T cells and was therefore chosen for our experiments (Chen et al., 2010b; Parvatiyar et al., 2012). Moreover, we administered recombinant HBV proteins as well as the MVA vector intramuscularly which has been demonstrated to be superior to s.c. or i.p. delivery (Su, Kosinska et al, unpublished data).

3.2.1.1 High viremia limit immunological responsiveness to therapeutic vaccination

We immunized AAV-HBV-infected immunocompetent wildtype mice with c-di-AMP adjuvanted HBV proteins (HBsAg and HBcAg) followed by an MVA boost (encoding for HBsAg and HBcAg). Our results demonstrated that TherVacB-induced immune responses inversely correlated with HBV antigen levels as it was seen previously in HBV-transgenic mice (Backes et al., 2016). Animals infected with low doses of AAV-HBV showed functional B- as well as T-cell responses that successfully combated persistent viral infection, whereas functional HBV-specific $CD8^+$ T cells were absent after high dose infections on day 6 after MVA boost. As expected, HBV-specific T cells were more abundant within the intrahepatic lymphocyte population than in the periphery (Figure 2.12, Figure 2.13). Moreover, HBcAg staining of liver sections revealed profound elimination of HBc^+ hepatocytes after TherVacB treatment in low titer groups (Figure 2.14). Analyses of liver DNA revealed that HBV and AAV DNA was still detected in low titer infected mice that demonstrated ‘functional cure’ (Figure 2.14). Thus, HBV was not eradicated from the liver of those animals 6 days after MVA boost. It has been suggested that high antigen loads lead to T-cell exhaustion. High numbers of antigen-expressing hepatocytes were reported to induce functional exhaustion and subsequent deletion of antigen-specific T cells, therefore causing antigen persistence (Kumar et al., 2017; Ochel et al., 2016). Along this line, in mice harboring high HBV titers, TherVacB-induced T cells might experience functional exhaustion and cannot be detected by *ex vivo* peptide stimulation at day 6 after their induction.

We performed the same experiment in HHDII-HLA-DR1 mice, in which murine MHC genes have been replaced by the human MHC genes HLA-A*02 and HLA-DR1 (Pajot et al., 2004). Therefore, these mice are considered as a powerful preclinical model to evaluate immunotherapeutic strategies. Mice did not reveal seroconversion of neither anti-HBs nor anti-HBe after TherVacB treatment, and importantly, this was independent of viremia (Figure

2.15). Vaccination induced HBcAg- and HBsAg-specific cytotoxic T cells in all groups (Figure 2.16). In contrast to wildtype mice, the frequency of functional HBV-specific T cells did not inversely correlate with serum HBV antigen levels and interestingly, their distribution hardly differed between liver and spleen (Figure 2.16). First, these results indicate that the induction of an HBV-specific humoral immune response in HHDII-HLA-DR1 mice was not sufficient to induce seroconversion, as serum antigen levels did not change. In contrast, in wildtype mice serum antigens were already undetectable after protein prime in the lowest titer group mediated by TherVacB-induced antibody responses. The lack of neutralizing HBV-specific antibodies after therapeutic vaccination in HHDII-HLA-DR1 mice could be an issue of a general compromised B-cell response, a matter of insufficient B-cell priming, or induced antibodies exhibit very low avidity towards their antigen. Vaccination with recombinant HBsAg and HBcAg was reported to induce anti-HBs as well as anti-HBc antibodies but also failed to neutralize HBV antigens in AAV-HBV-infected HHDII-HLA-DR1 mice (Bourgine et al., 2018). Second, the observation that the frequency of HBV-specific cytotoxic T cells was the same in high and low titer mice leads to the conclusion that the induction of HBV-specific T cells upon immunization in the periphery is independent of viremia. As described in section (2.2.3.3) we provided evidence that the HHDII molecule (HLA-A*02) on hepatocytes of HHDII-HLA-DR1 mice is insufficient to present endogenously processed peptides. If AAV-HBV-transduced hepatocytes of those animals lack presentation of the corresponding HBV peptides, the induced HBV-specific $CD8^+$ T cells migrating to the liver do not find their target HLA - peptide complex. Therefore, they do not get functionally exhausted or die of activation induced cell death and their amount stays the same independent of viremia. This theory is supported by other vaccination studies using AAV-HBV-infected HHDII-HLA-DR1 mice. As presented in this thesis, they report that HBV-specific T cells are induced upon immunization, but did not affect serum HBeAg and HBsAg levels as well as intrahepatic HBcAg expression and HBV DNA, again indicating that those T cells do not find their target in the liver (Bourgine et al., 2018; Dion et al., 2013).

To elucidate if HBV-specific T cells were induced in the periphery by immunization but underwent exhaustion in high viremic animals, we analyzed the abundance as well as the functionality of C93-specific $CD8^+$ T cells already three days after MVA boost. Importantly, the number as well as functionality of intrahepatic C93-specific T cells was much lower in high compared to low viremic animals upon TherVacB treatment already on day 3 after MVA boost (Figure 2.18). This leads to the suggestion that HBV-specific T cells do either not proliferate in high viremic animals or have already been depleted as a consequence of exposure to high antigen levels. As results from immunization of HHDII-HLA-DR1 mice described above indeed demonstrate induction of HBV-specific T cells in high viremic mice, the latter is more likely. Moreover, it is known, that circulating HBeAg and HBsAg, secreted as subviral particles, have

no apparent role in viral replication. Therefore, circulating antigens are believed to represent an immune evasive strategy of HBV to prevent its B- and T-cell mediated clearance and therefore allow HBV to establish and maintain chronic infection. They would therefore also limit success of TherVacB-induced immunity in high viremic animals.

Moreover, we analyzed the frequency of lymphocyte subpopulations and hence the microenvironment in the liver as this could also influence HBV-specific effector cells induced by TherVacB. We found that the frequency of T cells, B cells and NKT cells were comparable in low and high viremic animals upon TherVacB treatment. In contrast the abundance of NK cells was significantly enhanced in immunized high titer animals compared to low titer animals. NK cell frequency in the periphery, measured amongst splenocytes, did not differ, indicating a liver-specific rise in NK cell numbers (Figure 2.19). At this point, we do not know if this is only an effect of high titer infection or an effect of vaccination in high viremic animals as we lack a group of animals with high titer infection but without subsequent vaccination. NK cells represent the majority of innate immune cells in the healthy human liver. In chronic HBV infection their frequency is even further increased in the liver and decreased in the blood (Rehermann, 2013), and therefore the amount of infected cells alone could already influence the frequency of NK cells. Studies from LCMV (lymphocytic choriomeningitis virus) infection, in which NK cells do not exert a direct antiviral effect, demonstrated a distinct role in regulating T-cell-dependent viral persistence and immunopathology. Here, NK cells eliminated $CD4^+$ T cells which in turn affected $CD8^+$ T-cell function and exhaustion. Therefore, NK cells prevented fatal pathology at high titer doses, as they enabled T-cell exhaustion and virus persistence. In contrast, in medium doses, NK cells facilitated T-cell mediated pathology, demonstrating NK cells being a regulator of $CD4^+$ T-cell mediated support for virus-specific cytotoxic T cells (Waggoner et al., 2011).

It is possible that NK cells also act as regulators of T-cell responses during chronic HBV infection. For instance, it has been demonstrated that *in vitro* depletion of NK cells from PBMC of HBV-infected patients increases HBV-specific but not CMV-specific $CD8^+$ T-cell responses (Peppa et al., 2013). The proposed mechanism behind this is that HBV-specific T cells upregulate the death receptor TRAIL 2 (Tumor Necrosis Factor Related Apoptosis Inducing Ligand), making them susceptible to NK-cell mediated deletion via TRAIL (Peppa et al., 2013). Therefore, an enhanced frequency of NK cells that dampen the potential tissue damage of vaccination induced HBV-specific T cells in high viremic animals would be reasonable and analyzing expression of TRAIL on NK cells as well as its receptor on T cells in the liver would help to clarify the underlying mechanism. Additionally, selective depletion of NK cells by antibody administration would allow to study their role in tuning T-cell responses during chronic HBV infection. Again, one has to consider existing differences between NK cells found in

humans and in mice, however, the possibility to study fundamental principles of NK cell biology and function has been reported (Sungur and Murphy, 2013).

To elucidate the fate of HBV-specific T cells in high viremic animals, analyses at selected time points after MVA boost should be performed. As an alternative, animals that allow tracking of T cells could be used for AAV-HBV infection and subsequent therapeutic vaccination. An example are the so-called BLITC (bioluminescence imaging of T cells) mice, in which T cells express an NFAT-dependent click-beetle luciferase and a constitutive *Renilla* luciferase, which supports concomitant *in vivo* analysis of migration and activation of T cells (Szyska et al., 2018). Thus, the activation and fate of T cells induced by therapeutic vaccination could be monitored in real time by bioluminescence measurement. However, a different vaccination scheme, as for instance a peptide-based vaccination, has to be applied, as MVA- and HBV-specific T cells could not be distinguished in this setting.

Our results suggest that success of TherVacB in high viremic patients would not be as pronounced as in low viremic patients. This might be the main obstacle that has to be overcome to demonstrate clinical efficacy. To improve efficacy of TherVacB for high viremic HBV carriers, the viral load should be reduced prior to vaccination. This could either be achieved by pretreatment with nucleos(t)ide analogs (Kosinska et al., 2013), RNA interference strategies that reduce overall HBV protein synthesis and secretion (Javanbakht et al., 2018; Michler et al., 2016) or antivirals that block the release of antigen, for instance nucleic acid polymers (Al-Mahtab et al., 2016).

3.2.1.2 Prolonged exposure to HBV negatively influences success of therapeutic vaccination

Beside the level of viremia, the duration of exposure to HBV had great impact on the success of TherVacB. In detail, HBV-specific immunity was significantly reduced in mice that were infected three months prior to vaccination compared to only one-month exposure to HBV. This was illustrated by a lack of seroconversion from HBeAg to anti-HBe, although seroconversion from HBsAg to anti-HBs as well as the induction of anti-HBc antibodies was not different (Figure 2.21). The frequency of HBV-specific T cells, in detail peptide C93-specific T cells, did not differ, but they demonstrated significantly higher expression of the exhaustion marker Tim-3 as well as FasR in animals that were exposed to HBV three months compared to one-month prior TherVacB treatment (Figure 2.22). Those intrahepatic HBc-specific T cells, that were likely prone to apoptosis also revealed lower functionality in an *ex vivo* peptide stimulation assay (Figure 2.22). We did not detect differences in functionality of HBV-specific T cells isolated from the spleen (data not shown). The reduced efficacy of TherVacB-induced immunity after long-term exposure to HBV was also confirmed by a less pronounced reduction of HBc^+ hepatocytes as well as HBV DNA in the liver (Figure 2.23). $CD8^+$ T cells are thought

to be impaired in effector functions, in particular in cytotoxicity and cytokine production, after chronic exposure to their antigens (Wherry, 2011; Wherry et al., 2003). This might hold true for the HBV-specific T cells induced by TherVacB, especially when animals were infected three months before vaccination. The persistence of HBV demands for virus-specific immune tolerance that prevents immune pathology, however, also impedes clearance of the virus. In general, immune tolerance can be a result of antigen-specific deletion of T cells, a lack of expansion, functional adaptation or exhaustion of the immune reaction (Protzer and Knolle, 2016). Functional tolerance demonstrates a possible reason why TherVacB-induced T-cell responses were impaired after long-term exposure to their antigens in our experiment, as tolerance is intended to prevent tissue damage and is dependent on the microenvironment in which the immune response becomes effective. The liver demonstrates unique immune regulatory functions that promote the induction of tolerance (Knolle and Thimme, 2014; Thomson and Knolle, 2010). We did not detect a difference in the amount of HBc-specific T cells induced upon therapeutic vaccination after three or one month of HBV exposure. Still, it is unclear whether the T cells in long-term infected mice become functionally impaired as a result of the liver environment or because of the high levels of secreted viral antigens in the circulation, that possibly skew T-cell functions (Utzschneider et al., 2016). The latter is also reasonable, as protein vaccinations did not reduce serum HBeAg and HBsAg levels as efficient in the group that was infected three months compared to one month to prior start of vaccination, probably a result of insufficient $CD4^+$ T-cell functionality. It is desirable to elucidate if TherVacB-induced HBV-specific T cells in long-term HBV-exposed animals exhibit dysfunctionality per se or if their microenvironment is responsible for it. To this end, one could compare the effect of HBV-specific T cells induced by TherVacB in one month and three months infected mice by adoptively transferring them into HBV^+ immunodeficient recipient mice. If the T cells from the group that was infected three months prior vaccination would still exhibit a less pronounced antiviral effect, T cells per se would lack proper effector functions as a reason of long-term exposure to HBV. This in turn is of utmost importance for any therapeutic vaccination approach aiming to treat chronically HBV-infected patients, as they by definition exhibit long-term exposure to viral antigens. Moreover, dysfunctionality in dendritic cells resulting in impaired activation of T cells have been associated with chronic HBV infection (Op den Brouw et al., 2009; Wang et al., 2001) and could present another possible explanation for the decreased functionality of HBV-specific T cells after long-term exposure to HBV in the here presented study.

3.2.1.3 Therapeutic vaccination does not eradicate intrahepatic HBV DNA

Six days after MVA boost we still detected AAV as well as HBV DNA in low titer AAV-HBV-infected wildtype animals, although they demonstrated ‘functional cure’ as indicated by profound B- and T-cell responses as well as elimination of HBc^+ hepatocytes (section 2.2.1.1).

In order to assess whether TherVacB-induced immunity would be able to eradicate the virus once it would have more time to perform, we conducted analyses ten weeks after MVA boost. Interestingly, one out of six animals experienced a relapse in serum HBeAg five weeks after MVA immunization, that could not be cleared thereafter, although we still detected functional HBV-specific T cells five weeks after relapse in serum HBeAg levels (Figure 2.20). Future experiments should therefore analyze the phenotype of those HBV-specific T cells, unable to control a relapse of HBeAg secretion. The amount of HBV DNA in liver tissue did not differ when comparing analyses six days to ten weeks after MVA boost (Figure 2.20). There is evidence, that HBV cccDNA persists in the liver of patients that resolved an acute HBV infection. Viral infection can be reestablished in the setting of immunosuppression, such as renal transplantation (Chen et al., 2013) or rituximab treatment for lymphoma (Kusumoto et al., 2015; Mozessohn et al., 2015; Seto et al., 2014). This fact leads to the suggestion, that HBV infection might never be cured completely during natural resolution of disease. Thus, complete eradication of HBV and all its replicative intermediates might be an unrealistic aim for therapeutic interventions towards chronic HBV infections (Revill et al., 2016). However, the more realistic goal to achieve 'functional cure', viral control as well as the induction of a strong HBV-specific immune response was reached using TherVacB at least in low viremic animals.

3.2.1.4 HBV-specific immunity in X- and E-negative HBV carriers is successfully induced by therapeutic vaccination

As mentioned in section 3.1.2, pre-core mutations have been found to be associated with a decreased response to treatment with peg-IFNα (Peeridogaheh et al., 2018), emphasizing the need to demonstrate efficacy of therapeutic approaches in mice infected with AAV-HBV harboring HBV genome mutations. To facilitate clinical application of TherVacB, it is of utmost importance to prove that this treatment would also be beneficial for patients harboring for instance the pre-core stop mutation. For this purpose, we immunized immunocompetent wildtype mice with AAVs encoding for either HBV-1.3WT, -1.3E$^-$ or -1.3X$^-$. Importantly, animals of all groups revealed 'functional cure' upon TherVacB treatment (Figure 2.24) suggesting efficacy of our therapeutic vaccination strategy towards HBeAg$^-$ and HBcAg$^-$ chronic carriers. Additionally, functionality of HBsAg- and HBcAg-specific T cells was enhanced in the HBeAg$^-$ group, although their frequency was lower measured by *ex vivo* streptamer staining (Figure 2.25). This again pointed to the fact that high serum antigen levels, here HBeAg, might skew T-cell function (Utzschneider et al., 2016) and its absence might give rise to more potent effector T cells.

3.2.1.5 General remarks and future directions

In all experiments performed we found a tremendous difference in the frequency of HBsAg- and HBcAg-specific CD8$^+$ T cells. This was true for H2-k^b (C93, S190, S208) and HLA-A*02

(C18, S20, S172) restricted peptides in wildtype and HHDII-HLA-DR1 mice, respectively. We only used predicted immune dominant epitopes for *ex vivo* peptide stimulation. However, those responses do not necessarily demonstrate the overall immune response to the whole protein and stimulation with overlapping peptide pools might lead to more sophisticated results. For peptide S208 we did not observe any response in any experiment. This was not expected, as previous results in HBV-transgenic mice demonstrated a high frequency of T cells responding to peptide S208 upon *ex vivo* stimulation of lymphocytes isolated from the spleen or the liver from vaccinated animals (Backes et al., 2016). In their study, S208 responses were even superior to responses towards peptide S190. Striking differences include the mouse model, a higher MVA titer (1 x 10^8 pfu MVA-HBsAg), in contrast to 1 x 10^7 pfu MVA-HBsAg in our experiments, as well as the usage of different adjuvants. It is unclear whether these differences are the reason why our results do not match the results obtained in the study using transgenic mice (Backes et al., 2016). The HBV genome of both, the HBV-transgenic mice as well as the AAV-HBV used in this study are genotype D, serotype ayw. Possible other reasons include an effect of central tolerance to HBV in transgenic mice or a difference in quality of the proteins and the MVAs used for immunization.

In the present thesis all animals were infected with the same AAV-HBV and thus also with the same geno- and serotype (genotype D, serotype ayw). For a better representation of the clinical setting, efficacy of TherVacB should also be verified for other HBV geno-and serotypes. For this purpose, preclinical investigations of TherVacB in immunocompetent mice infected with AAVs encoding for different geno- and serotypes should be implemented in the future.

Beside the combination of therapeutic vaccination with nucleosid(t)e analogues or other antivirals, the combination therapy with checkpoint inhibitors could greatly improve success of therapy (see section 1.3.2.2). This is supported by our finding that long-term exposure to HBV prior to immunization led to functionally impaired HBV-specific T cells which demonstrated enhanced expression of Tim-3 and FasR (Figure 2.22). Although efficacy of a monotherapy targeting PD-L1 only demonstrated minor therapeutic benefit in the woodchuck model (Balsitis et al., 2018), combination of PD-1/ PD-L1 blockade and DNA-based vaccination after antiviral treatment increased functionality of HBV-specific T cells (Liu et al., 2014). This combination therapy resulted in anti-WHs seroconversion and sustained virus control in chronically infected animals (Liu et al., 2014) illustrating the great potential of combination therapies that could also be evaluated in the mouse models developed in this thesis.

3.2.2 Adoptive T-cell therapy

Next to therapeutic vaccination, adoptive transfer of HBV-specific T cells represents another possibility to restore the patient's immune response towards HBV-infected hepatocytes or HBV-related HCC. Here, the patient's own T cells are redirected by genetically introducing a CAR or a TCR that recognize a viral antigen.

3.2.2.1 Chimeric antigen receptor

T cells engrafted with a CAR directed against the HBV envelope protein (S-CAR) have previously been reported to induce a transient antiviral effect in HBV-transgenic mice (Krebs et al., 2013). To determine whether S-CAR-redirected T cells would be able to achieve viral clearance, the AAV-HBV mouse model of persistent infection was applied in the present thesis. One reason why S-CAR-equipped T cells only induced a transient antiviral effect in HBV-transgenic mice was an immune response against the human-derived domains within the S-CAR molecule (Festag, 2018). For this reason, immunodeficient Rag2$^{-/-}$ mice were used in this study and infected with a low or a high dose of AAV-HBV.

Engraftment of S-CAR^{+} T cells was independent of the AAV-HBV titer used for infection and reached tremendous numbers of up to 10^7 per ml blood (Figure 2.26). Moreover, they were able to induce a long lasting antiviral effect measured by a decrease of serum HBeAg and HBsAg accompanied by slight but stable serum ALT elevations, indicating elimination of HBV^{+} hepatocytes (Figure 2.27). Serum HBsAg levels demonstrated a faster drop than HBeAg levels, but might be explained by the fact, that S-CAR-redirected T cells can bind circulating HBsAg and subsequently decrease the amount of free, measurable HBsAg. In contrast, decline of HBeAg levels is a strong indicator for a direct antiviral effect of adoptively transferred T cells, as Rag2$^{-/-}$ mice lack B cells, and therefore masking of serum antigen by neutralizing antibodies can be excluded. Additionally, the antiviral effect of S-CAR-equipped T cells was demonstrated by a reduction of HBc^{+} hepatocytes and HBV DNA from liver tissue (Figure 2.29).

However, adoptive transfer of S-CAR-redirected T cells did also not lead to complete viral clearance, as we still detected viral antigens in the serum as well as HBc^{+} hepatocytes and HBV DNA in the liver of S-CAR treated mice. Concurrently, high numbers of S-CAR^{+} T cells were found in the liver but also the periphery (blood, spleen) and they were activated upon culture on plate-bound HBsAg *ex vivo* (Figure 2.28). Furthermore, we observed that HBV serum antigen levels as well as the number of remaining HBc^{+} hepatocytes were approximately the same after S-CAR^{+} T cells treatment, independent of initial HBV-titers and number of transduced hepatocytes, respectively (Figure 2.27, Figure 2.29). These results lead to the conclusion that there is probably a certain threshold of HBV surface antigen needed to be

translocated to the cell membrane of HBV$^+$ hepatocytes in order to be recognized by S-CAR-redirected T cells. If expression of the S protein is decreasing below this threshold, S-CAR-engrafted T cells may not bind strong enough or do not get activated leading to stagnation of the antiviral effect. This 'threshold effect' has also been observed in *in vitro* experiments with HBV-infected HepG2-NTCP cells (Wisskirchen et al, unpublished data). Either S-protein expression is reduced through cytokine-mediated effect of S-CAR$^+$ T cells or alternatively, HBV$^+$ cells that per se exhibited low-level expression of HBV surface antigen were not recognized. It has been demonstrated that the affinity of the scFv component of a HER2- or EGFR-CAR correlated with its sensitivity, meaning low affinity CARs recognized only high-level expressing target cells, whereas high affinity CARs maintained effector functions also if density of the target protein was diminished (Caruso et al., 2015; Liu et al., 2015). This leads to the suggestion, that the C8 scFv within the S-CAR might have a medium to low affinity towards the HBV surface protein used in these experiments. The HBV genome used in the AAV-HBV in the present experiment as well as the HBV stock for infection of HepG2-NTCP cells is genotype D, serotype ayw. The C8 scFv is responsible for antigen recognition within the S-CAR and was generated by phage display against recombinant HBsAg from serotype adw (Kürschner, 2000). Recent results revealed that C8 as a soluble molecule displays a weaker binding capacity towards serotype ayw than serotype adw (Malo et al, unpublished data). The same was true for S-CAR$^+$ T cells, as they exhibited a stronger activation towards stimulation with recombinant HBsAg from serotype adw in contrast to ayw (Krebs et al., 2013). Therefore, S-CAR$^+$ T cells might demand for higher expression levels of serotype ayw than adw to get activated. To elucidate, if the threshold that is needed to activate S-CAR-redirected T cells is lower when using HBV from serotype adw and subsequently viral clearance is achieved, experiments using an AAV-HBV encoding for serotype adw have to be performed.

Beside the specific activation in culture on plate-bound HBsAg, we also stimulated lymphocytes isolated from liver and spleen unspecifically using anti-CD3 and anti-CD28 antibodies *ex vivo*. Here, S-CAR-redirected T cells had a tendency to respond less well than control SΔ-CAR T cells (Figure 2.28) indicating that they might have been partially exhausted due to prior antigen contact *in vivo* and T-cell exhaustion could be further clarified by phenotypical analyses of the isolated lymphocytes.

3.2.2.2 Natural T-cell receptors

HHDII-HLA-DR1 mice represent a suitable animal model to investigate human HLA-A*02- or HLA-DR1-restricted TCRs *in vivo*, as these mice express human MHC class I (HLA-A*0201) and MHC class II (HLA-DR*0101) molecules and are simultaneously devoid of endogenous murine class I (β_2m and D^b) and class II (IAb) molecules (Pajot et al., 2004). We therefore chose those animals for exploring the antiviral effect of selected human HBV-specific

HLA-A*02-restricted TCRs that have been previously evaluated *in vitro* (Wisskirchen et al., 2017).

However, we did not observe an antiviral effect of TCR-redirected T cells after adoptive transfer into AAV-HBV-infected HHDII-HLA-DR1 mice (Figure 2.30). This was surprising as we detected them in the circulation and also found functional TCR-redirected T cells amongst lymphocytes isolated from liver and spleen after *ex vivo* peptide stimulation (Figure 2.31). Thus, we could recover functional HBV-specific TCR-engrafted T cells, suggesting the reason for the lacking antiviral effect is not T-cell exhaustion or dysfunction. As the cytotoxic effect of $CD8^+$ T cells is dependent on binding their cognate antigen in context of a peptide-MHC complex, we analyzed the expression of the HHDII molecule on the surface of primary hepatocytes from HHDII-HLA-DR1 mice and could hardly detect its expression on the hepatocyte surface (Figure 2.32). In contrast, splenocytes of HHDII-HLA-DR1 mice revealed expression of the HHDII molecule to some extent (Figure 2.32). It has been reported that HLA-A*02 expression varies in between cells isolated from spleen, bone marrow and thymus of HLA-A*02.1 transgenic mice (Le et al., 1989). I also observed differences in HHDII expression on splenocytes isolated from individual mice (Figure 2.32). Thus, one can imagine, that expression of hepatocytes deviates from expression on lymphocytes, although the molecule is inserted into the mouse genome.

The HHDII molecule includes murine domains: α_3 ($H\text{-}2D^b$), transmembrane and cytoplasmic domains, whereas α_1 and α_2 as well as β_2m are from human origin (Figure 2.33). Keeping the murine domains was found to lead to better functionality (Pascolo et al., 1997), which is likely due to the interaction of the murine CD8 co-receptor on the murine T cell with the murine α_3 domain. Additionally, the HHDII molecule is expressed as a monochain, another important difference to the natural HLA-A*02 molecule (Pascolo et al., 1997). Expression of the HHDII molecule was superior when expressed from an AAV than from a transgene (Huang et al., 2014). Consequently, AAVs encoding for either the HHDII molecule, β-globin intron and the HHDII molecule as well as for HLA-A*02 and human β_2-microglobulin under control of a liver-specific promotor were generated.

To assess whether HLA-A*02 or HHDII would be expressed on hepatocytes upon delivery by an AAV vector, HHDII-HLA-DR1$^{WT/HHDII}$ mice were infected followed by isolation of their hepatocytes. Analysis of their HLA-A*02 surface expression revealed, that the anti-HLA-A*02 antibody almost exclusively bound to hepatocytes of mice infected with the AAV-HLA-A*02, but not with AAV-HHDII, AAV-βG-intron-HHDII or uninfected HHDII-HLA-DR1 mice (Figure 2.34). In contrast, Huh7 cells transfected with the HHDII molecule depicted its profound surface expression (Figure 2.34), which provided evidence that the anti-HLA-A*02 antibody used for staining was able to recognize the HHDII molecule. Therefore, the missing staining after

delivering the HHDII molecule by an AAV vector was most likely not due to technical issues of the staining. To further analyze presence of the HHDII molecule on the cell surface, we externally loaded the hepatocytes with HBV peptides. Upon co-culture with these peptide loaded hepatocytes, HBV-specific TCR-redirected T cells secreted tremendous amounts of IFNγ, serving as an indicator for T-cell activation independent of prior AAV transduction. We excluded that peptides were presented by lymphocytes within the co-culture, as TCR-engrafted T cells did not respond with IFNγ secretion upon co-culture with peptide loaded hepatocytes isolated from a wildtype C57Bl/6J mouse (Figure 2.35).

Furthermore, isolated hepatocytes were Ad-HBV-infected and co-cultured with HBV-specific T cells. This experiment should give insight, whether the AAV-encoded expression of HLA-A*02/HHDII leads to presentation of HBV peptides that can be recognized by T cells. Target cell viability, HBeAg in supernatant, remaining amount of rcDNA as well as IFNγ in supernatant was analyzed from the co-cultures. Interestingly, Ad-HBV transduced hepatocytes were only specifically eliminated when mice were infected with the AAV-HHDII, but not in any of the other settings tested (Figure 2.35). The release of IFNγ was increased when HBV-specific TCR-engrafted T cells were co-incubated with AAV-HLA-A*02- and Ad-HBV-co-transduced hepatocytes (Figure 2.35 B). We also observed a reduction of HBeAg in supernatant as well intracellular rcDNA in the co-cultures of AAV-HLA-A*02- and AAV-HHDII-transduced hepatocytes (Figure 2.36). Interestingly, the antiviral effect observed in HBV^+ and $HLA\text{-}A*02^+$ hepatocytes was predominantly cytokine-mediated but not cytotoxic, whereas the cytotoxic effect was the leading cause of the antiviral effect in HBV^+ and HHDII transduced cells (Figure 2.35, Figure 2.36). The major difference in between the different TCR-peptide-MHC complexes is the possible interaction of the murine CD8 co-receptor with its counterpart on the HHDII molecule but not on HLA-A*02. CD8 co-receptor binding has been demonstrated to play a pivotal role in stabilization of the TCR-peptide MHC complex (Artyomov et al., 2010). To elucidate, if the intact CD8 co-receptor binding results mainly in a cytotoxic response whereas lacking CD8 co-receptor binding favors cytokine secretion could be evaluated using a CD8 blocking antibody in co-cultures with HBV^+ and HHDII transduced hepatocytes.

In fact, the HHDII molecule might be expressed in non-transduced HHDII-HLA-DR1 mice as it functions very well once exogenous peptide is provided, even though we were not able to stain it by flow cytometry. The discrepancy between staining with the antibody and recognition by TCRs might be explained by the 10^5-fold enhanced sensitivity of TCRs in comparison to a conventional antibody (Sharma and Kranz, 2016). It is unclear, why the HHDII molecule can be stained by flow cytometry after transfection into Huh7 cells or on splenocytes, but not on hepatocytes isolated from HHDII mice. Hepatocytes were isolated through digestion of liver tissue using the enzyme collagenase, representing a difference in pre-treatment to the other

cell types analyzed. Theoretically this should not affect surface expression of the HHDII molecule, especially because we were able to stain the HLA-A*02 molecule after collagenase treatment. However, immunohistochemical analyses of liver tissue of the respective groups could help to clarify if the HHDII molecule is indeed expressed but cannot be visualized with the method applied. Endogenous proteins might either not be properly processed or presented, as TCR-engrafted T cells were not activated if hepatocytes had to present HBV peptides from endogenously expressed proteins upon Ad-HBV transduction. A defect in peptide presentation is also supported by the fact that therapeutic vaccination using AAV-HBV-infected HHDII-HLA-DR1 mice did not induce any antiviral effect even after proven presence of HBV-specific cytotoxic T cells. This phenomenon was observed in this thesis (Figure 2.15, Figure 2.16, discussed in section 3.2.1) and in other studies (Bourgine et al., 2018; Dion et al., 2013). However, my experiments provide evidence that using an AAV vector for delivery of HLA-A*02 or the HHDII molecule leads to suitable target cells for evaluation of HLA-A*02 restricted TCRs.

AAV-HLA-A*02 was chosen to be used for further experiments. Co-infection of HHDII-HLADR1$^{WT/HHDII}$ mice with AAV-HBV and AAV-HLA-A*02 led to HLA-A*02 expression on subsequently isolated PMHs (Figure 2.37). Additionally, co-incubation of HBV^{+} and HLA-A*02^{+} hepatocytes with HBV-specific HLA-A*02-restricted TCR-redirected T cells confirmed that those double-transduced hepatocytes are suitable target cells (Figure 2.38) rendering AAV-HBV and AAV-HLA-A*02 co-infected HHDII-HLA-DR1$^{WT/HHDII}$ mice appropriate animals to study the *in vivo* efficacy of HBV-specific HLA-A*02-restricted TCRs.

Nevertheless, a mix of T cells redirected with different HBV-specific TCRs (4G, 6K and WL31) adoptively transferred into AAV-HBV and AAV-HLA-A*02 co-infected HHDII-HLA-DR1$^{WT/HHDII}$ mice did not show any antiviral effect, as serum HBeAg and HBsAg levels stayed constant in all groups (Figure 2.39). Strikingly, we observed that transferred mock T cells engrafted better than T cells expressing HBV-specific TCRs (Figure 2.39). We therefore assessed whether recipient mice developed an immune response against the TCR-redirected T cells. Indeed, already on day 7 post T-cell transfer, we found specific antibodies directed against all TCRs investigated, especially pronounced for TCRs 6K and WL31, in serum of recipient mice (in six out of eight mice) (Figure 2.40). We did not analyze serum of later time points, but it is likely, that the amount of antibodies further increased, as this was seen when S-CAR^{+} T cells were transferred into immunocompetent animals (Festag, 2018). Moreover, we provide evidence for a cell-mediated rejection of TCR 6K and WL31 expressing T cells (Figure 2.40). TCR 4G did not induce a T-cell response in recipient mice, which is probably a result of sequence homology to a mouse self-protein. In conclusion, the data suggested that TCR-redirected T cells vanished because the human domains within the TCRs were recognized as foreign in recipient mice leading to their elimination.

To demonstrate efficacy of HBV-specific HLA-A*02 restricted TCRs, subsequent experiments were performed in immunodeficient Rag2$^{-/-}$ γc$^{-/-}$ mice. To this end, animals were either infected with AAV-HBV, AAV-HLA-A*02 or co-infected with both. Adoptively transferred HBV-specific TCR-redirected T cells (mix of 4G, 6K and WL31) but not mock T cells induced a profound antiviral effect only in the group that was infected with both, AAV-HBV and AAV-HLA-A*02, but not in animals whose hepatocytes either expressed HBV proteins or HLA-A*02 (Figure 2.41, Figure 2.42). Interestingly, TCR^{+} T cells seemed to have specifically infiltrated the liver, as their numbers in circulation was greatly decreased in AAV-HBV and AAV-HLA-A*02 co-infected mice when compared to mono-infected animals (Figure 2.41). *Ex vivo* re-stimulation of lymphocytes isolated from liver and spleen with the corresponding peptides rarely activated CD8^{+} T cells to secrete IFNγ when isolated from double-infected mice (Figure 2.42). In contrast, CD8^{+} T cells from mono-infected animals demonstrated IFNγ secretion upon co-incubation with their respective peptides. Therefore, we suggest that T cells that were activated *in vivo* and exhibited an antiviral effect subsequently displayed an exhausted phenotype and did not express cytokines upon *ex vivo* re-stimulation. Interesting, this discrepancy was less pronounced for peptide S172 (TCR WL31) leading to the suggestion that peptide S172 might be less frequently presented and therefore S172-specific T cells get less exhausted. Immunogenicity of peptide S172 was proven, although only 15 % of patients suffering from a chronic HBV infection responded to peptide S172, in contrast to a 30 % response rate to peptide C18 (Desmond et al., 2008). Moreover, S172-specific TCR engineered human T cells were not activated upon co-culture with HBV-infected HepG2 cells, pointing towards a defect in antigen processing or presentation of this peptide in these cells (Wisskirchen et al., 2017). DNA-based immunization as well as peptide immunization only sporadically induced S172-specific T cells in mice (4 out of 16 animals), whereas DNA-based immunization induced S20-specific T cells in all animals (Loirat et al., 2000), suggesting a low immunogenicity of the peptide in mice. Following experiments should elucidate the individual effect of all investigated TCRs and could, next to finding the most promising TCR candidate, help to elucidate whether presentation of S172 is less abundant on mouse hepatocytes.

In addition to CD8^{+} T cells we also analyzed the frequency of CD4^{+} T cells responding to peptide stimulation *ex vivo*. Importantly, we do not see a difference in IFNγ^{+} CD4^{+} T cells upon stimulation with the corresponding peptide between all groups that received TCR-redirected T cells (Figure 2.42). Moreover, we only detected IFNγ^{+} CD4^{+} T cells for peptide S20 and C18, but not for S172. CD4^{+} T cells redirected with an MHC I-restricted TCR are also able to exert cytotoxic effector functions if the respective TCR is of high affinity and subsequently does not depend on CD8 co-receptor binding (Stone and Kranz, 2013). The functionality of TCRs 4G and 6K in human CD4^{+} T cells has previously been demonstrated. In contrast, TCR WL31 seems to depend on CD8 co-receptor binding, as it did not reveal functionality in human CD4^{+}

T cells (Wisskirchen et al., 2017). Thus, it is not surprising, that we did not recover IFNγ$^+$ CD4$^+$ T cells upon S172 peptide stimulation *ex vivo*. CD4$^+$ T cells expressing TCR 4G or 6K seemed to be less exhausted than CD8$^+$ T cells after they potentially exerted antiviral activity in animals that were AAV-HBV and AAV-HLA-A*02 co-infected. Possibly, CD4$^+$ TCR 4G- and 6K-redirected T cells can be activated to secrete IFNγ without CD8 co-receptor binding when plenty of their corresponding peptide-MHC complex is available. This it is for instance the case during the artificial setting created with the *ex vivo* peptide stimulation. Here, the binding avidity might be enough for activation, whereas the *in vivo* setting does not provide enough of the peptide-MHC complex resulting in low avidity.

The presence of a mix of TCR 4G$^+$, 6K$^+$ and WL31$^+$ T cells was able to reduce viral load if immunodeficient Rag2$^{-/-}$ γc$^{-/-}$ mice were co-infected with AAV-HBV and AAV-HLA-A*02 long time after T-cell transfer but did not clear the infection. Viral parameters initially rose in the mock T cell as well as in the TCR$^+$ T cell treated group, however, ALT levels peaked 14 days post infection in the treatment group which was accompanied by a drop in serum HBeAg and HBsAg levels (Figure 2.43). This indicates, that HBV-specific T cells that are present before infection initially need time to be activated and control the infection. In fact, the results obtained from this experiment suggest, that pre-existing T-cell mediated immunity is capable to deal with HBV infection. Clinical relevance of the result is supported by the fact that patients with leukemia and chronic HBV infection were able to clear the infection after bone marrow transplant from donors that exhibited a HBV-specific T-cell response (Ilan et al., 1993; Lau et al., 1997).

HBV-specific T cells, however, were not able to eradicate HBV in AAV-HBV/AAV-HLA-A*02-co-infected Rag2$^{-/-}$ γc$^{-/-}$ mice, although they could be recovered from liver and spleen 60 days post transfer/30 days post infection. As we used different AAVs to deliver the two transgenes, it is very likely that some hepatocytes are transduced with only one of the AAVs. We tried to compensate for that possibility by using an extremly high titer of AAV-HLA-A*02, aiming to reach almost all hepatocytes and simultaneously reduce the probability for HBV$^+$ and HLA-A*02$^-$ hepatocytes that therefore cannot present HBV peptides properly. Hepatocytes, only expressing HBV but not HLA-A*02 are not recognized by our TCR$^+$ T cells, as demonstrated by the AAV-HBV-infected and TCR-redirected T cell treated group (Figure 2.41). Consequently, HBV$^+$ but HLA-A*02$^-$ hepatocytes after AAV-HBV/AAV-HLA-A*02-co-infection are not targeted and continue to express viral proteins despite circulating TCR$^+$ T cells. To overcome this obstacle, a one-vector system has to be used. This needed to be a gutless adenovirus, whose capacity would allow for the delivery of both transgenes, as the packaging limit of AAVs is limited to 5 kilobases (Wu et al., 2010) and just fits the 1.3 overlength HBV

genome. This vector would pave the way to study if our selected HBV-specific TCR-redirected T cells are able to eradicate HBV from the liver of infected animals.

An adoptive transfer of a mix of TCR 4G$^+$ and 6K$^+$ human T cells into HBV-infected uPA-SCID mice, repopulated with HLA-A*02$^+$ hepatocytes, achieved clearance of HBV (Wisskirchen et al, unpublished data). For sure, this human liver/immune system animal model (described in detail in section 1.4.1.1) represents great advantages over the one established here: i) hepatocytes and T cells are both from human origin allowing perfect interaction of the TCR with the peptide/MHC complex, ii) natural peptide processing and presentation on human hepatocytes, and iii) natural HBV infection leading to (real) cccDNA formation. Both animal models, however, have the disadvantage of working with an immunodeficient mouse, making it impossible to study interaction of adoptively transferred T cells with the endogenous immune system. For this purpose, one has to use chimeric mice reconstituted with both, immune cells and hepatocytes of human origin (Bility et al., 2014; Washburn et al., 2011). As both animal models are not available in a bigger scale due to high costs and an enormous effort to generate them, I am convinced that the model established in this thesis will be broadly applied. Future experiments should focus on the evaluation of single TCRs, however, interesting questions could also include transfer of CD8$^+$ TCR$^+$ vs. CD4$^+$ TCR$^+$ T cells, the number of transferred TCR-redirected T cells that is needed to achieve an antiviral effect or the viral load necessary to activate transferred T cells. In addition, it will improve our understanding of functional alterations of the T cells transferred. Importantly, the model established here could be transferred to other adoptive T-cell therapy approaches depending on other MHC-restrictions.

3.2.2.3 Comparison of strategies for T-cell redirection

In the present thesis two strategies to redirect T cells with subsequent adoptive transfer were investigated. Both S-CAR-redirected and TCR-redirected T cells were studied in immunodeficient animals. Moreover, in both experiments the same total amount of CD8$^+$ redirected T cells (1 x 10^6) was used, allowing for a functional comparison of both approaches.

The first drastic difference observed is, that numbers of S-CAR T cells measured in the blood of adoptively transferred animals massively exceeded the TCR$^+$ T cells by three logs (Figure 2.26, Figure 2.41). While TCR-redirected T cell numbers even dropped when compared to the respective controls, S-CAR T cells seemed to undergo a tremendous expansion in the periphery. It has been reported that tonic signaling of CAR$^+$ T cells triggered by antigen-independent clustering of CAR scFv could lead to their activation and subsequently to proliferation (Long et al., 2015). This tonic signaling was demonstrated to be dependent on the scFv and also led to antigen-independent exhaustion of CAR$^+$ T cells. Alternatively, S-CAR T cells could expand due to the presence of the large amount of soluble HBsAg in the circulation of AAV-HBV-infected animals. S-CAR$^+$ T cells did not proliferate in HBV negative

immunodeficient mice (Festag, 2018), thus the expansion is HBV dependent. Using an AAV that is encoding for an HBV genome that is unable to secrete HBsAg due to a mutation could help to answer the question, whether soluble HBsAg triggers S-CAR T-cell expansion in the periphery. To my knowledge, other studies only investigated whether soluble antigen could compete with binding to and killing of the malignant cells, for instance for a CEA-CAR (Hombach et al., 1999; Nolan et al., 1999) or a GPC3-CAR (Gao et al., 2014; Yu et al., 2018), but did not determine the effect of soluble antigen on proliferation and activation of CAR T cells.

Beside their abundance in circulation, we recovered many more S-CAR-engrafted T cells from liver and spleen than TCR-redirected T cells (Figure 2.28 and data not shown), although their antiviral effect was less pronounced. In fact, S-CAR-redirected T cells might be less sensitive than TCR$^+$ T cells, as the physiological TCR affinity range is 10^4 – 10^6 M^{-1}, in contrast to an affinity range of 10^6 – 10^9 M^{-1} for most scFv on CARs (Harris and Kranz, 2016). The lower affinity of a TCR seems to correlate with a higher sensitivity. We observed that the antiviral effect TCR-redirected T cells took place within 14 days post T-cell transfer, as serum HBeAg levels did not decrease remarkably from day 14 onwards. This was accompanied by a drastic but transient ALT peak, illustrating the narrow timeframe of cytotoxic T-cell responses towards HBV$^+$ hepatocytes (Figure 2.41). In contrast, the decrease in serum HBeAg levels was not as distinct until day 14 post S-CAR$^+$ T-cell transfer but continued to decrease slowly, even more pronounced when mice were infected with the lower titer of AAV-HBV (Figure 2.27). Here, ALT levels increased only moderately, but stayed on these elevated levels for the whole experiment. CARs depend on higher surface expression of their ligand to induce T-cell activation, for instance anti-CD20 CAR T cells need as many as 200 molecules per target cell to induce its lysis (Watanabe et al., 2015). In contrast, only one MHC molecule presenting the correct peptide on the target cell has been demonstrated to be sufficient for T-cell activation (Huang et al., 2013). Admittedly, the comparison made for our experiments is biased. First, pretreatment of transferred cells was different, as transduction of TCRs was made in presence of IL-2 for bulk splenocytes, whereas it was performed with IL-12 after CD8$^+$ T cell pre-selection for the S-CAR (for details see section 4.2.9.2) which could lead to differences in their long-term performance. Second, TCR$^+$ T cell-treated animals were provided with T cells of three specificities (peptide S20, S172 and C18) compared to one specificity for S-CAR T cells. Comparing the potential of one S-specific TCR with the S-CAR would be preferable. A recent study demonstrated distinct antiviral effect of a HBsAg-specific CAR in HBV-infected human liver chimeric mice (Kruse et al., 2018). Using HBV-infected human liver chimeric mice would lead to a better comparison of the S-CAR to a S-specific TCR. Here, human T cells would be transferred and both S-CAR and TCR-redirected T cells would harbor human signaling domains while affinities and ligands would stay different. Another study comparing T-cell activities mediated by human TCRs and CARs that used the same recognition domains

allowing a direct comparison demonstrated that CAR-redirected T cells were 10-100-fold less sensitive, even in the absence of the CD8 coreceptor (Harris et al., 2018). Nevertheless, CARs still exhibit the advantage to be suitable for any patient, independent of MHC restriction and avoid the creation of new specificities caused by mispairing of the introduced and the endogenous TCR. A possible approach to combine sensitivity of a classical MHC Ia-restricted TCR with the broad applicability of a CAR might be in using TCRs recognizing their target peptide in context of a nonclassical MHC class Ib molecule that exert limited polymorphism, for instance MHC E. In humans, there are only two known functional HLA-E alleles that differ by a single amino acid and predominantly bind and present MHC class Ia leader sequence-derived peptides for NK cell regulation. Additionally, MHC-E also binds pathogen-derived peptide antigens for presentation to $CD8^+$ T cells and hence, represents an attractive target for immunotherapeutic approaches (Wu et al., 2018). Engineering MHC-E restricted HBV-specific T cells for adoptive transfer would represent a promising approach to treat chronic HBV infection as well as HBV-related HCC if MHC E is expressed on hepatocytes and HBV-derived peptides are presented on it.

3.3 HBV-specific T cells - translation to big animal models

As a final step prior to clinical application, evaluating the safety and efficacy of immunotherapeutic approaches in relevant preclinical animal models, that allow for natural HBV infection, is desirable. Expression of human NTCP has been reported to be the limiting factor in order to support natural HBV infection for the rhesus macaque *in vitro* (Lempp et al., 2017) and *in vivo* (Burwitz et al., 2017) and paved the way to be able to study HBV infection, pathogenesis as well as its therapy in non-human primate models.

In the present thesis, HBV-specific TCR^+ T cells were evaluated towards HBV-infected macaque hepatocytes *in vitro*. As a first step, the equipment of T cells with exogenous TCRs had to be transferred from the human/murine setting to the rhesus macaque. Macaque $CD8^+$ as well as $CD4^+$ T cells were successfully engrafted with the human HBV-specific HLA-A*02 restricted TCRs 4G and 6K in the presence of either IL-2 or IL-15 (Figure 2.44) and resulted in high transduction rates, comparable to human T cells (data not shown). Moreover, we could demonstrate activation of TCR-redirected macaque T cells upon co-culture with HBV-infected HepG2-NTCP cells. In contrast to human cells, the type of stimulation during engraftment seemed to play an important role in activation capacity, as IL-15 pre-stimulated $CD8^+$ and $CD4^+$ TCR^+ T cells demonstrated higher frequencies of $IFN\gamma^+$ and $GrzB^+$ cells upon co-incubation with HBV^+ target cells (Figure 2.45).

As described for the murine setting, HLA-A*02-expression and associated presentation of target peptides is essential to investigate the potential of our HLA-A*02-restricted HBV-specific

TCRs. Due to pre-existing immunity, macaques can hardly be infected using AAV vectors (Burwitz et al., 2017). Using an adenovirus to deliver human HLA-A*02 and human β_2m into primary macaque hepatocytes resulted in HLA-A*02 surface expression *in vitro* (Figure 2.46). Future experiments should try to further enhance HLA-A*02 expression by using a higher titer of Ad-HLA-A*02. Ad-HLA-A*02/Ad-HBV-co-transduced or Ad-HLA-A*02/Ad-NTCP-co-transduced and HBV-infected hepatocytes were proven to serve as appropriate target cells to study the antiviral effect of TCR-redirected macaque T cells. TCR 4G or 6K engrafted T cells were specifically activated to secrete IFNγ when co-cultured with HBV^+ and HLA-$A*02^+$ PMaHs and displayed a profound antiviral effect (Figure 2.47, Figure 2.48). TCR-redirected T cells did not eliminate HBV completely, but as in the case of murine hepatocyte transduction, co-transduction with both adenoviral vectors is essential to allow for T-cell effector function. HBV^+ but HLA-$A*02^-$ target cells cannot be recognized by the T cells and continue replicating HBV. Here, an adenovirus encoding for both NTCP and HLA-A*02 should be used, rendering only HLA-$A*02^+$ cells susceptible for HBV infection. Subsequent co-culture experiments could reveal if TCR 4G- or 6K-equipped T cells are able to clear viral infection. Moreover, their potential, safety and efficacy should be evaluated in an HBV-infected rhesus macaque *in vivo* as a last step prior clinical use. Other T-cell therapy approaches using a ROR1-CAR (Berger et al., 2015) or an anti-CD27-CAR (Kunkele et al., 2017) successfully took advantage of the macaque model to address safety issues before first clinical trials.

Beside PMaHs, pig hepatocytes allowed establishment of HBV infection when expressing human NTCP, whereas hepatocytes of mouse, rat and dog were not susceptible to natural HBV infection despite expression of human NTCP (Lempp et al., 2017). Pigs also serve as important animal models for viral infections like for instance hepatitis E virus (Wang and Wang, 2016) or ebolavirus (Shurtleff and Bavari, 2015). Here, we were aiming to initially evaluate if HBV-infected Ad-HLA-A*02-transduced pig hepatocytes and therefore the animal itself would serve as an appropriate animal model to study our adoptive T-cell therapy approach. For this purpose, we co-cultured human TCR-redirected T cells with HLA-$A*02^+$ and HBV^+ pig hepatocytes. Indeed, human T cells expressing TCR 4G or 6K were activated to secrete $IFN\gamma^+$ when co-cultured with Ad-NTCP/Ad-HLA-A*02 co-transduced pig hepatoyctes, but not when transduced with either one, prior to HBV infection. However, they did not reveal a considerable antiviral effect (Figure 2.49) which might be a result of a mismatch of receptors/molecules of human T cells and pig hepatocytes. Still, we have proven to be able to render pig hepatocytes a suitable target to study TCR-redirected HBV-specific T cells. As a next step, the well-established protocol for equipment of T cells with the respective TCRs should be transferred to the pig setting, allowing for a co-culture of pig hepatocytes with TCR-engrafted pig T cells. Furthermore, the vector encoding for both NTCP and HLA-A*02 was demonstrated to be functional and can be used for further experiments, for instance with macaque hepatocytes.

Here, we provide evidence that HLA-A*02 is functional in macaque and pig cells, allowing the evaluation of human HLA-A*02-restricted TCRs in the macaque and pig setting. I believe, that this approach might also be applicable for other MHC restrictions paving the way for safety and efficacy studies of human TCRs in physiologically relevant preclinical animal models.

3.4 GPC3-specific HLA-A*02 restricted TCR P1-1 for immunotherapy of HCC

HCC is characterized by expression of tumor-associated antigens (TAA), for instance GPC3 and AFP. Next to viral antigens expressed in HBV-associated HCC, targeting those TAAs might represent a promising approach to treat HCC. Raising T-cell responses against these antigens that are either only differentially expressed on tumor versus healthy cells or are expressed during embryogenesis is very difficult. Using an allogenic stimulation approach, the GPC3-specific TCR P1-1 has been identified. Since TCR P1-1 engrafted T cells revealed distinct effector functions towards the $GPC3^+$ HCC cell line HepG2 (Dargel et al., 2015), their anti-tumor functionality was analyzed in a xenograft model *in vivo* in the present study. In a first experiment luciferase expressing HepG2 cells were injected intrasplenically, and a subsequent adoptive transfer of $P1\text{-}1^+$ T cells demonstrated a potent antitumor effect, as bioluminescence signals in most mice was decreased or eliminated (Dargel et al., 2015). In a subsequent experiment with established subcutaneous tumors, TCR P1-1-equipped T cells were only able to slow down tumor growth. Importantly, varying number and repeated adoptive transfer of P1-1-redirected T cells did not have an impact on the anti-tumor effect. Additionally, established tumors displayed a reduced GPC3 expression in comparison to cultured HepG2 cells as well as a lack of $CD8^+$ T cell infiltration (Dargel et al., 2015). These results might lead to the suggestion that GPC3 expression is the limiting factor for recognition and elimination of tumor cells by TCR P1-1-redirected T cells. If GPC3 is not expressed in tumor cells, peptide GPC_{367} will not be presented on HLA-A*02, and P1-1 equipped T cells will not be able to identify them.

In fact, this is a scenario that very likely also happens in patients, as expression of TAAs, here GPC3, often exhibits a mosaic pattern with expression levels reaching from 1 % to 100 % in HCC tissue (Capurro et al., 2003). A subsequent GPC3-specific treatment will allow for selection of $GPC3^-$ cells. This was observed in a phase II clinical trial using a GPC3 peptide vaccine as adjuvant therapy for advanced HCC. Although vaccination induced sufficient numbers of GPC3-specific cytotoxic T cells, two patients experienced a relapse. Indeed, recurrent tumors were $GPC3^-$ (Sawada et al., 2016).

This obstacle could be overcome by combination therapies. Beside GPC3, HCC has been demonstrated to express several TAAs including AFP (Butterfield et al., 2001), NY-ESO1 (Gehring et al., 2009), hERT (Mizukoshi et al., 2006), as well as MAGE-1 and MAGE-3 (Zerbini

et al., 2004). Therefore, engineered T cells directed against GPC3 could be administered in combination with T cells recognizing one of the above mentioned TAAs expressed in HCC. This may be even in accordance with the patients individual TAA profile. Importantly, T cells redirected against the TAAs NY-ESO-1 (Robbins et al., 2015) and MAGE-A3 (Lu et al., 2017) are already under clinical investigation. Beside TAAs, HCCs also express so-called neoantigens as a product of mutated genes. Those neoantigens represent ideal targets for immune cells, as they are not exposed to the immune system before the emergence of cancer cells and T cells specific for neoantigens are not deleted during maturation. For HCC, telomerase reverse transcriptase is an example of a commonly expressed neoantigen (Nishida and Kudo, 2017).

As chronic HBV infection is causing about 60 % and 23 % of HCC cases in developing countries and developed countries, respectively, T cells specifically recognizing viral proteins, like TCR-engineered (Gehring et al., 2011; Kah et al., 2017; Koh et al., 2018; Wisskirchen et al., 2017) or CAR-redirected (Bohne et al., 2008; Krebs et al., 2013; Kruse et al., 2018) T cells could be used in combination with TAA-specific T-cell therapy. Furthermore, a study combined two complementary CARs in one T cell directed against GPC3 and asialoglycoprotein receptor 1 (ASGR1), a liver tissue-specific protein, and was aiming to thereby enhance on-target and decrease off-tumor effect. However, next to enhanced specificity, those CAR T cells have been proven to exhibit significantly higher antitumor activity than single-targeted CAR-T cells in preclinical HCC xenograft models (Chen et al., 2017) revealing an advantage of combining two specificities.

Moreover, adoptive T-cell therapy could be combined with checkpoint inhibitors. Checkpoint inhibition is a promising approach to treat HCC patients, as T cells from HCC patients display an exhausted phenotype (Gehring et al., 2009; Song et al., 2016) and might help to overcome the inhibitory effects of the liver environment. A CTLA-4 as well as a PD-1 antibody have already been investigated in phase I clinical trials for HCC patients, resulted in accumulation of intratumoral $CD8^+$ T cells and demonstrated durable objective response rates of 20 %, respectively (Duffy et al., 2017; El-Khoueiry et al., 2017) and their anti-tumor effect might be increased in combination with T-cell therapy.

As HepG2 cells revealed very low GPC3 expression in established tumors *in vivo*, another appropriate target cell line had to be identified. Therefore, suitability of the $GPC3^+$ hepatoma cell lines Huh7 and HepaRG, engineered to stably express HLA-A*02, was analyzed. As a negative control the supposedly $GPC3^-$ cervix carcinoma cell line Hela (Khan et al., 2001), which was also HLA-A*02 transduced, was included. Interestingly, P1-1^+ T cells eliminated Huh7-HLA-A*02 and HepaRG-HLA-A*02 cells (Dargel et al., 2015), but also Hela-HLA-A*02 cells (Figure 2.53). To exclude the possibility of alloreactivity of the TCR P1-1-redirected

T cells, a series of experiments was performed. First, T cells of different HLA-A*02^{+} and HLA-A*02^{-} donors were engrafted with the TCR P1-1. HLA-A*02^{+} T cells equipped with the TCR P1-1 showed elimination of HLA-A*02^{+} T cells (Figure 2.54). As both Hela cells and PBMC showed low GPC3 expression on RNA level (Figure 2.55), the activation and subsequent cytotoxic potential of TCR P1-1^{+} T cells could also be a consequence of this weak GPC3 expression and associated presentation on HLA-A*02.

This phenomenon has been observed in a study using an HLA-A*02 restricted TCR-redirected against the apoptosis inhibitor protein survivin which is overexpressed in many tumors. Survivin-redirected T cells exhibited an HLA-A*02–restricted fratricide that occurred due to low-level survivin expression in lymphocytes (Leisegang et al., 2010). In order to determine if GPC3 expression was the reason for fratricide of TCR P1-1^{+} T cells, HLA-A*02^{+} Hela GPC3 knockout cell lines were established (Figure 2.56, Figure 2.57). As the GPC3 knockout cell lines were eliminated like the parental cell line or even a cell line overexpressing GPC3 (Figure 2.58), TCR P1-1 mediated killing was not dependent on GPC3 expression, that would result in presentation of peptide GPC3$_{367}$ on HLA-A*02. In contrast, TCR P1-1 could exhibit cross-reactivity with similar peptides presented on HLA-A*02.

A fatal case of TCR cross-reactivity was reported for MAGE-A3 redirected T cells. Here, preclinical investigation demonstrated specificity of this TCR, but during initial clinical testing the first two treated patients developed cardiogenic shock and died within a few days. Indeed, the investigated TCR displayed cross-reactivity towards a peptide derived from the muscle protein titin, most likely causing the *in vivo* toxicity. Importantly, the amino acid sequence between MAGE-A3 and off-target peptide differed in 4 positions of the 9mer (Cameron et al., 2013; Linette et al., 2013). To get an idea, if elimination of GPC3 knockout cell lines was due to cross-reactivity of TCR P1-1, I finally assessed the activation of TCR P1-1-redirected T cells upon contact with T2 cells loaded with peptides that differed to GPC3$_{367}$ in 3 amino acids on different positions (Table 2.1). GPC3$_{367}$ specificity in context of HLA-A*02 had been demonstrated for TCR P1-1 engrafted T cells for instance by co-incubation with peptide loaded T2 cells (Dargel et al., 2015). The *in vitro* results reported in Dargel et al. (2015) could not be repeated. In my hands, TCR P1-1^{+} T cells demonstrated high secretion of IFNγ, independent of the loaded peptide or even if no peptide was loaded on T2 cells (Figure 2.59). This result illustrates, that TCR P1-1-engrafted T cells did not specifically recognize peptide GPC3$_{367}$ in context of HLA-A*02, but rather displayed alloreactivity.

Since this TCR was found by an allorestricted approach (Dargel et al., 2015), finding alloreactive TCRs is not unexpected. TAA-specific T cells, reacting towards a self-antigen, are deleted by negative selection in the thymus during T-cell development (Murphy and Weaver, 2016). To identify a TAA-specific TCR, this MHC restricted central tolerance has to be

overcome. This is possible by a so-called allorestricted approach. Therefore, T cells are stimulated by a foreign MHC molecule presenting the self-antigen, thereby taking advantage of approximately 1-10 % of the natural T-cell repertoire that is thought to be reactive to another MHC haplotype (Fischer Lindahl and Wilson, 1977). TCR P1-1 was identified using dendritic cells from an HLA-A*02^{-} donor, that were co-transfected with GPC3 and HLA-A*02 RNA, to stimulate and expand allorestricted antigen-specific T cells (Wilde et al., 2012). The corresponding autologous T cells of the HLA-A*02^{-} donor were not subjected to negative selection by HLA-A*02 and can give rise not only to HLA-A*02^{-} alloreactive T cells but also to peptide-specific T cells that recognize GPC3-derived peptides presented by HLA-A*02.

A common approach to analyze peptide-specificity of HLA-A*02 restricted TCRs is the co-culture with peptide loaded T2 cells. As T2 cells, a lymphoblast cell line (Salter et al., 1985), are deficient in a peptide transporter involved in antigen processing (TAP), they fail to correctly translocate endogenous (processed) peptides to the site of MHC loading in the endoplasmic reticulum/ Golgi apparatus (Hosken and Bevan, 1990). Nevertheless. they very well display MHC class I molecules associated with exogenously administered peptides. TCR P1-1-redirected T cells responded with high IFNγ secretion upon co-culture with T2 cells, even if no peptide was loaded (Figure 2.59). Therefore, those T cells might also react upon contact with HLA-A*02 loaded with a limited set of endogenous peptides of T2 cells as demonstrated by Wei and Cresswell (1992). Alternatively, they could respond to ‘empty’ HLA-A*02 molecules as it has been reported that the transported HLA-A*02 molecules may weakly interact with an unknown retaining factor in the ER and consequently are able to assemble despite the deficiency of peptides (Hosken and Bevan, 1990). In conclusion, TCR P1-1 recognized HLA-A*02 independent of the presented peptide and therefore represents an HLA-A*02 alloreactive TCR that is not suited for further clinical development.

With the *in vitro* data obtained in the present study, the reason of the limited efficacy of TCR P1-1 redirected T cells *in vivo* might rather be downregulation of HLA-A*02 than loss of GPC3 expression. Therefore, HLA-A*02 expression should be visualized by immunohistochemical analyses of tumor sections. Nevertheless, adoptive T-cell therapy is a promising approach for the treatment of HCC. GPC3 peptide vaccination, GPC3 specific chimeric antigen receptors as well as a GPC3 bispecific antibody have revealed profound antitumor activity, demonstrating the high potential of immunotherapies for HCC (for details see 1.3). Importantly, therapies based on antibody-binding (chimeric antigen receptors and bispecific antibodies) might represent a safer approach as the TCR-based methods (natural TCRs and vaccination), as they may be already activated by the low-level GPC3 expression we detected in several tissues (Figure 2.55), representing sites for off-target toxicity.

Next to the allorestricted approach used to identify TCR P1-1 (Dargel et al., 2015), central tolerance to TAA can be circumvented by the usage of transgenic mice with human MHC and TCR genes. Immunization of these mice with TAA results in induction of T cell responses (Obenaus et al., 2015) representing an alternative with lower likelihood to generate MHC alloreactive TCRs.

3.5 Conclusion

Treatment options for chronic HBV infection as well as HBV-associated hepatocellular carcinoma remain limited. A lot of effort is invested in the development of immunotherapeutic strategies targeting these malignancies. The present thesis provides evidence, that therapeutic vaccination as well as adoptive T-cell therapy using T cells redirected with either a chimeric antigen receptor or natural TCRs exhibit great potential towards cure of chronic HBV infection and HBV-related HCC. New mouse models for chronic HBV infection as well as HCC have been generated and evaluated and might represent powerful tools to also study other therapeutic interventions. Moreover, first steps in translating the TCR-approach towards functionally relevant preclinical animal models have been made.

4 MATERIAL AND METHODS

4.1 Materials

4.1.1 Devices

Product	Supplier
Aperio AT2 slide scanner	Leica Biosystems
Applied Biosystems® 7500 Real time PCR system	Thermo Fisher Scientific
Architect™ platform	Abbott Laboratories
BEP III platform	Siemens Healthcare
Centrifuge 5920R	Eppendorf
CTL-ImmunoSpot® S6 Ultra-V Analyzer	Cellular Technology Limited (CTL) Europe
CytoFLEX S	Beckman Coulter
ELISA-Reader infinite F200	Tecan
Flow cytometer FACS Canto II™	BD Biosciences
Freezing device	Nalgene / biocision Coolcell
Fusion Fx7	Peqlab
Gel chambers (agarose gel electrophoresis)	Peqlab
High capacity centrifuge 4K15	Sigma
Incubator Heracell 150	Heraeus Holding GmbH
IVIS Series Preclinical In Vivo Imaging System	Perkin Elmer
Leica Bond MAX system	Leica Biosystems
LightCycler® 480 II	Roche Diagnostics
MACS separator MultiStand	Miltenyi Biotech
NanoDrop One	Thermo Fisher Scientific
Nanophotometer OD600	IMPLEN GmbH
Neubauer improved hemocytometer	Brand
NucleoCounter NC-250	Chemometec
Optima L-90K Ultracentrifuge	Beckman Coulter
Pipette ‘Accu-jet pro’	Brand
Pipettes	Eppendorf
Reflotron® Reflovet Plus	Roche Diagnostics
SCN 400 slide scanner	Leica Biosystems
Shaker and incubator for bacteria	INFORS AG; Heraeus Holding GmbH
Sterile hood HERA safe	Thermo Fisher Scientific

T professional Trio Thermocycler	Analytik jena
Table-top centrifuge 5417R	Eppendorf
Thermo Mixer F1.5	Eppendorf
Tissue Lyser LT	Qiagen
Ultracentrifuge SW 50 Ti Rotor	Beckman Coulter
Ultracentrifuge SW 55 Ti Rotor	Beckman Coulter
xCELLigence® RTCA SP	ACEA Biosciences

4.1.2 Consumables

Product	**Supplier**
96 well white microtiter plates	Greiner Bio
96-well plates for qPCR, FrameStar 480/96	4titude
Butterfly cannula	Sarstedt
Cell culture flasks, dishes, plates	TPP
Cell factory easyfill 10-trays	Cell Factory
Cell strainer 70 µm, 100µm	Falcon
Centrifugation Tubes (13 x 51 mm)	Beckman Coulter
Cryo vials	Greiner Bio One
Cuvettes	Implen
ELISA 96-well plates Nunc MaxiSorb	Thermo Fisher Scientific
E-Plate 96	ACEA Biosciences
FACS 96-well V-bottom plates	Roth
Falcon tubes 15ml/50ml	Greiner Bio One
Filcons, sterile, 30 µm	SLG
Filter tips	Greiner Bio One
MACS separation columns (MS, LS)	Miltenyi Biotech
Microvette 1,1 ml Z-Gel	Sarstedt
Microvette 500 LH-Gel	Sarstedt
Needles	Braun
Non-tissue culture treated plates (6-well, 24-well)	Falcon
PCR tubes	Thermo Fisher Scientific
Pipette tips 10µl – 1ml	Biozym / Greiner Bio One / Gilson
Pipettes (disposable) 2, 5, 10, 25, 50ml	Greiner Bio One
Reaction tubes 1.5ml, 2ml	Greiner Bio One, Eppendorf
Reagent reservoirs, sterile	Corning

Reflotron ALT (GPT) stripes	Roche Diagnostics
Sterile filters 0.45µm and 0.2µm	Sarstedt
Surgical Disposable Scalpels	Braun
Syringes	Braun

4.1.3 Chemicals and reagents

Product	**Supplier**
2-Phenoxyethanol	Roth
TMB, stabilized chromogen	Invitrogen
Acetic acid	Roth
Agarose	PeqLab
Ammonium chloride (NH_4Cl)	Roth
Ampicillin	Roth
Antibiotics/Antimicotics, 100x	Thermo Fisher Scientific
Biocoll separating solution (density 1.077 g/ml)	Biochrom
Blasticidin S HCl 50 mg	Invitrogen
Bovine serum albumin (BSA)	Roth
Brefeldin A (BFA)	Sigma
Cyclic-di-AMP	Invivogen
Coelenterazine	PJK
Collagen R	Serva
CountBright Absolute Counting Beads	Thermo Fisher Scientific
Dimethyl sulfoxide (DMSO)	Sigma
D-Luciferin	Perkin Elmer
DMEM/F12	Gibco
DNA Smart ladder 1kb / 100bp	Eurogentec
Dulbecco's Modified Eagle's Medium (DMEM)	Gibco
EDTA	Roth
EDTA di-sodium salt (Na_2EDTA)	Roth
Ethanol	Roth
Ethidium monoazide (EMA)	Sigma
Fetal calf serum (FCS)	Gibco
Fixable viability dye eF780	eBioscience
Geneticin Selective Antibiotic (G418 Sulfate)	Gibco
Gentamicin	Life Technologies or Ratiopharm

Glucose	Roth
Glycerol	Roth
Hank's Balanced Salt Solution (HBSS)	Gibco
Heparin-Natrium 25000	Ratiopharm
Hepes 1 M	Gibco
Human serum	Own production (AG Protzer)
Hydrochloric acid (HCl)	Roth
Hydrocortisone	Pfizer
Hygromycin B Gold	Invivogen
IL-12 (murine)	Provided by Edgar Schmitt, Mainz
IL-15 (recombinant human)	Peprotech
IL-2 Proleukin	Novartis
Inosine	Serva
Insulin	Sanofi-Aventis
Iodixanol (Optiprep density gradient medium)	Progen Biotech
Isoflurane	Henry Schein
Isopropanol	Roth
Kanamycin	Roth
L-Glutamine, 200 mM	Gibco
Lipofectamin 2000	Invitrogen
Magnesium chloride ($MgCl_2$)	Sigma
Non-essential amino acids (NEAA), 100x	Gibco
OptiMEM	Gibco
Paraformaldehyde (PFA), 4 %	ChemCruz
PEG6000	Merck
Penicillin Streptomycin, 10,000 U/ml (100x)	Gibco
Percoll density gradient media	GE Healthcare, München, Germany
Phenol Red solution (0,5% in DPBS)	Sigma-Aldrich
Phosphate-buffered saline (PBS) 10x	Gibco
Polyethylenimine (PEI)	Polysciences
Potassic chlorid (KCl)	Roth
Potassic hydrogenic carbonat ($KHCO_3$)	Roth
Propidiumiodide (PI)	Roth
Protamine sulfate	LEO Pharma
Puromycin	Invivogen
RetroNectin 1µg/µl	Takara
RNA*later* RNA Stabilization Reagent	Qiagen

Roti®-Safe GelStain	Roth
RPMI 1640	Gibco
RPMI 1640 Dutch modified	Gibco
SOC medium	Sigma-Aldrich
Sodium hydroxide (NaOH)	Roth
Sodium pyruvate, 100mM	Gibco
Solution 18	Chemometec
Staphylococcal enterotoxin B (S4881)	Sigma-Aldrich
Tris	Roth
Triton X 100	Roth
Trypan blue	Gibco
Trypsin-EDTA	Gibco
Tryptone	Roth
Tween 20	Roth
Versene	Gibco
Williams Medium E	Gibco
Yeast extract	Roth
β-Mercaptoethanol, 50 mM	Gibco

4.1.4 Buffers and solutions

Buffer	**Ingredients**
50x TAE buffer	Tris 2M Acetic acid 2M EDTA pH 8.0 50mM in H_2O
AAV lysis buffer	50mM Tris 150mM NaCl 5mM $MgCl_2$ x 6 x H_2O in H_2O
ACK lysis buffer	NH_4Cl 150 mM $KHCO_3$ 10 mM Na_2EDTA 0.1 mM pH 7.2 – 7.4 in H_2O
ELISA assay diluent	BSA 1 % in PBS
FACS buffer	BSA 0.1 % in PBS

MACS buffer	BSA 0.5 % EDTA 2 mM pH 7.2 in PBS
PBS- MK	1mM $MgCl_2$ (MG:g/mol) 2,5mM KCl (MG:g/mol) in 1x PBS
PBS-MKN	PBS-MK + 1M NaCl (MG: 58,44 g/mol)
PBS-Tween	0.05 % Tween-20 in PBS

4.1.5 Kits

Product	**Supplier**
AAVpro® Titration Kit	Takara
ARCHITECT anti-HBeAg Reagent Kit	Abbott
ARCHITECT anti-HBsAg Reagent Kit	Abbott
ARCHITECT HBeAg Reagent Kit	Abbott
ARCHITECT HBsAg Reagent Kit	Abbott
CD8a (Ly2) MicroBeads, mouse	Miltenyi Biotech
Cell Proliferation Kit II (XTT)	Roche
CellTrace™ Violet Cell Proliferation Kit	Thermo Fisher Scientific
Cytofix/Cytoperm™ (+ Perm/Wash™ Buffer)	Becton Dickinson
Enzygnost HBe monoclonal kit	Siemens Healthcare Diagnostics
Enzygnost® Anti-HBc monoclonal test	Siemens Healthcare Diagnostics
Firefly Luciferase Assay System	Promega
GeneJET Plasmid Miniprep Kit	Thermo Fisher Scientific
HBeAg BioAssay ELISA Kit	US Biological lifeSci
HBsAg BioAssay ELISA Kit	US Biological lifeSci
Human IFN-γ uncoated ELISA	Invitrogen
LightCycler 480 SYBR green master mix	Roche
Monkey IFN-γ ELISA development kit (HRP)	Mabtech
Mouse IFN-γ uncoated ELISA	Invitrogen
NucleoSpin Tissue DNA and RNA	Macherey-Nagel
Phusion® Hot Start Flex Kit	New England Biolabs
Plasmid *Plus*Midi Kit	Qiagen
PureLink HiPure Plasmid Gigaprep Kit	Invitrogen

QIAamp MinElute Virus Spin Kit	Qiagen
QIAquick Gel Extraction Kit	Qiagen
SuperScript III Kit First-Strand Synthesis	Invitrogen
T-Track basic mouse IFNγ	Lophius Biosciences
ViraPower™ Lentiviral Expression Systems	Invitrogen

4.1.6 Enzymes

Product	**Supplier**
Benzonase	Sigma-Aldrich
Collagenase IV	Sigma-Aldrich
FastAP	Thermo Fisher Scientific
FastDigest restriction enzymes (+FastDigest Green Buffer (10x))	Thermo Fisher Scientific
Phusion Hot Start Flex 2x Master Mix	New England Biolabs
T4 DNA Ligase (+T4 ligase buffer)	Thermo Fisher Scientific
T5 exonuclease (+NEB buffer)	New England Biolabs

4.1.7 Primer

Primers were purchased from Microsynth AG.

Primer name	**Sequence**	**Application**
AAV ITR fw	AACCCGCCATGCTACTTATCTACGT	qPCR, AAV DNA
HBV X rev	CACACAGTCTTTGAAGTAGGCC	qPCR, AAV DNA
Adeno_fw	TTTTCGCGCGGTTTTAGGCG	qPCR, Adeno DNA
Adeno_rev	GTAAACGGTCAAAGTCCCCG	qPCR, Adeno DNA
cccDNA 2251+	AGCTGAGGCGGTATCTA	qPCR, cccDNA
cccDNA 92-	GCCTATTGATT GGAAAGTATGT	qPCR, cccDNA
HBV 1745	GGAGGGATACATAGAGGTTCCTTGA	qPCR, HBV DNA
HBV 1844	GTTGCCCGTTTGTCCTCTAATTC	qPCR, HBV DNA
HBV S fw	GCCTCATCTTCTTGTTGGTTC	qPCR, HBV DNA
HBV S rev	GAAAGCCCTACGAACCACTGAAC	qPCR, HBV DNA

HBV1464_fw	GGACCCCTTCTCGTGTTACA	qPCR, HBV DNA
HBV1464_fw	GGACCCCTTCTCGTGTTACA	qPCR, HBV DNA
HBV1529_probe	FAM-CTAGACTCGTGGTGGAC TTCTCTCAATTTTCT-TAMRA	qPCR, HBV DNA
HBV1599_rev	ACTGCGAATTTTGGCCAAGA	qPCR, HBV DNA
HBV1599_rev	ACTGCGAATTTTGGCCAAGA	qPCR, HBV DNA
PrP fw	TGCTGGGAAGTGCCATGAG	qPCR, normalization
PrP rev	CGGTGCATGTTTTCACGATAGTA	qPCR, normalization
hCD8 fw	GAGACAGTGGAGCTGAAGTGC	qPCR, hCD8 mRNA
hCD8 rev	GCCGAGCAGAAATAGTAGCC	qPCR, hCD8 mRNA
hGAPDH fw	CTGACTTCAACAGCGACACC	qPCR, mRNA reference
hGAPDH rev	GTGGTCCAGGGGTCTTACTC	qPCR, mRNA reference
hGPC3 fw	TGATGAAGATGAGTGCATTGG	qPCR, hGPC3 mRNA
hGPC3 rev	GATCATAGGCCAGTTCTGCAA	qPCR, hGPC3 mRNA

4.1.8 Plasmids

Plasmid	**Transgene product(s)**	**Source**
lentiCRISPRv2_gRNA1-GPC3	gRNA1-GPC3_Cas9	J. Festag
lentiCRISPRv2_gRNA2-GPC3	gRNA2-GPC3_Cas9	J. Festag
lentiCRISPRv2_gRNA3-GPC3	gRNA3-GPC3_Cas9	J. Festag
pAAV-HBV 1.2 E^-	HBV 1.2 E^-	J. Festag
pAAV-HBV 1.2 WT	HBV 1.2 WT	M.L. Michel
pAAV-HBV 1.2 X^-	HBV 1.2 X^-	J. Festag
pAAV-HBV 1.3 E^-	HBV 1.3 E	J. Festag
pAAV-HBV 1.3 WT	HBV 1.3 WT	J. Festag
pAAV-HBV 1.3 X^-	HBV 1.3 X^-	J. Festag
pAAV-HHDII	TTR_HHDII	J. Festag
pAAV-HLA-A*02	TTR_HLA-A*02_P2A_β2m	J. Festag
pAAV-βG-intron-HHDII	TTR_β–G-intron-HHDII	J. Festag
pcDNA3.1(-) GPC3	GPC3	C. Dargel
pcDNA3.1(Hygro)-HLA-A*02	HLA-A*02	M. Sprinzl
pLenti6_v5_CMV_Fluc	CMV_firefly luciferase	J. Festag
pMP71_decoy(FcΔ)+EGFRt	SΔ-CAR (human FcΔ IgG1 - NGFR) - T2A - EGFRt	M. Festag

pMP71_S-CAR(FcΔ)+EGFRt	S-CAR (human FcΔ IgG1 - human CD28 - CD3) - T2A - EGFRt	M. Festag
pMP71_TCR-4G	codon optimized TCR 4G	K. Metzger/ K. Wisskirchen
pMP71_TCR-6K	codon optimized TCR 6K	K. Metzger/ K. Wisskirchen
pMP71_TCR-WL31	codon optimized TCR WL31	K. Metzger/ K. Wisskirchen
pXR8	AAV packaging proteins (Rep, Cap)	H. Büning
pXX6	adenoviral helper proteins (E2A, E4 and V4)	H. Büning

4.1.9 Peptides and Proteins

All peptides were purchased from JPT Peptide Technologies.

Peptide	**Specificity**	**Amino acid sequence**	**Presented on**
B8R	MVA	TSYKFESV	H-2 k^b
C93	HBcAg	MGLKFRQL	H-2 k^b
OVA	ovalbumin	SIINFEKL	H-2 k^b
S190	HBsAg (adw)	VWLSAIWM	H-2 k^b
S208	HBsAg (adw)	IVSPFIPL	H-2 k^b
C18	HBcAg	FLPSDFFPSV	HLA-A*02
$GPC3_{367}$	GPC3	TIHDSIQYV	HLA-A*02
$GPC3_{367}$ like 2	see Figure 2.59	DIHDSIQPR	HLA-A*02
$GPC3_{367}$ like 3	see Figure 2.59	AIHDVIRYV	HLA-A*02
$GPC3_{367}$ like 4	see Figure 2.59	TIHDHINYN	HLA-A*02
S172	HBsAg	WLSLLVPFV	HLA-A*02
S20	HBsAg	FLLTRILTI	HLA-A*02

Peptide pool	**Specificity**	
HBV core pool	HBcAg	genotype D, covering the region between aa 70-157
HBV S pool	HBsAg	genotype D, covering the region between aa 145-226

Protein	application	Supplier
HBcAg, genotype D	Immunization	APP Latvijas Biomedicīnas (Riga, Latvia)
HBsAg, genotype D (adw)	immunization	Biovac (South Africa)
HBsAg (ayw)	Cell-culture	Roche

4.1.10 Cell lines and bacterial strains

Cell line	Description	Source
HEK 293	Human embryonic kidney cell line; transformed with fragments of adenovirus type 5 DNA	AG Protzer
HEK 293T	HEK 293 cells expressing a mutant version of the SV40 large T antigen	AG Protzer
HEK 293FT	Fast growing variant of HEK 293 T cell line	AG Protzer
Hela	Cervical cancer cell line	AG Protzer
Hela-HLA-A*02	Hela cells expressing HLA-A*02	generated by C. Dargel
HepaRG	Human hepatoma derived cell line; can be efficiently differentiated into hepatocyte-like cells, susceptible to infection with HBV	AG Protzer
HepaRG-HLA-A*02	HepaRG cells expressing HLA-A*02	generated by C. Dargel
HepG2	Human hepatoblastoma derived cell line	AG Protzer
HepG2-Fluc	HepG2 cells expressing the firefly luciferase	generated by J. Festag
HepG2-Gluc	HepG2 cells expressing the Gaussian luciferase	generated by C. Dargel
HepG2-NTCP	HepG2 cells expressing NTCP, enabling HBV infection	generated by D. Stadler
Huh7	Human hepatoma cell line	AG Protzer
Huh7-HLA-A*02	Huh7 cells expressing HLA-A*02	generated by J. Festag
PlatE	Retroviral packaging cell line to transduce murine cells	AG Protzer

RD114	Retroviral packaging cell line to transduce human cells	AG Protzer
T2	a lymphoblast cell line; deficient in a peptide transporter involved in antigen processing (TAP)	AG Protzer
E. coli *STBL3*	Chemical competent *Escherichia coli* cells	Invitrogen
E. coli *TOP10*	Chemical competent *Escherichia coli* cells	Invitrogen

4.1.11 Media

Medium	**Ingredients**	
Collagenase medium	DMEM/F12	500 ml
	Gentamicin, 50 mg/ml	0.5 ml
	Collagenase IV	25 mg
Digestion medium	Williams Medium E	500 ml
	Pen/Strep, 10,000 U/ml	5.5 ml
	L-Glutamine, 200 mM	5.5 ml
	Sodium pyruvate, 100 mM	30 ml
	HEPES	11.5 ml
	Insulin, 40 IU/ml	0.328 ml
	Glucose, 50 mg/ml	6 ml
	$CaCl_2$, 1M	1.8 ml
DMEM full medium	DMEM	500 ml
	FCS	50 ml
	Pen/Strep, 10,000 U/ml	5.5 ml
	L-Glutamine, 200 mM	5.5 ml
	NEAA, 100x	5.5 ml
	Sodium pyruvate, 100 mM	5.5 ml
Freezing medium	FCS	90 %
	DMSO	10 %

HepG2 Diff medium	DMEM	500 ml
	FSC	5 ml
	Pen/Strep, 10,000 U/ml	5.5 ml
	L-Glutamine, 200 mM	5.5 ml
	NEAA, 100x	5.5 ml
	Sodium pyruvate, 100mM	5.5 ml
	DMSO	10.5 ml
Human T-cell medium (hTCM)	RPMI 1640	500 ml
	FCS	50 ml
	Pen/Strep, 10,000 U/ml	5.5 ml
	L-Glutamine, 200 mM	5.5 ml
	NEAA, 100x	5.5 ml
	Sodium pyruvate, 100 mM	5.5 ml
	HEPES	5.5 ml
	Gentamicin	208 µl
LB medium pH 7.0 (in 1 l H_2O)	Tryptone	10 g
	Yeast extract	5 g
	NaCl	10 g
Maintenance medium	DMEM	500 ml
	FCS	50 ml
	Pen/Strep, 10,000 U/ml	5.5 ml
	L-Glutamine, 200 mM	5.5 ml
	HEPES	11.5 ml
	Insulin, 40 IU/ml	2.865 ml
	Glucose, 50 mg/ml	6 ml
	Gentamicin, 50mg/ml	0.55 ml
	Hydrocortisone, 4.42 mg/ml	0.549 ml
	Inosine, 2.5 mg/ml	2.8 ml
Murine T-cell medium (mTCM)	RPMI Dutch modified	500 ml
	FCS	50 ml
	Pen/Strep, 10,000 U/ml	5.5 ml
	L-Glutamine, 200 mM	5.5 ml
	NEAA, 100x	5.5 ml
	Sodium pyruvate, 100 mM	5.5 ml
	β-Mercaptoethanol	550 µl

PMaH medium	DMEM/F12	500 ml
	bovine growth serum	55 ml
	HEPES buffer, 1 M	11.5 ml
	Glucose, 50 mg/ml	6 ml
	L-glutamine, 200 mM	5.5 ml
	antibiotic/antimycotic, 100x	5.5 ml
	Gentamicin, 50mg/ml	1 ml
Preperfusion medium	HBSS	500 ml
	Pen/Strep, 10,000 U/ml	5.5 ml
	L-Glutamine, 200 mM	5.5 ml
	Sodium pyruvate, 100 mM	28 ml
	HEPES	11.5 ml
	Insulin, 40 IU/ml	0.328 ml
	Glucose, 50 mg/ml	6 ml
	EGTA, 100mM	2.8 ml
R15 medium	RPMI 1640	500 ml
	FCS	75 ml
	Pen/Strep	5.5 ml
	L-Glutamine, 200mM	5.5 ml
RPMI full medium	RPMI 1640	500 ml
	FCS	50 ml
	Pen/Strep, 10,000 U/ml	5.5 ml
	L-Glutamine, 200 mM	5.5 ml
	NEAA, 100x	5.5 ml
	Sodium pyruvate, 100 mM	5.5 ml
Transfection medium	DMEM	500 ml
	FCS	50 ml
	L-Glutamine, 200 mM	5.5 ml
	NEAA, 100x	5.5 ml
	Sodium pyruvate, 100 mM	5.5 ml
Wash medium	RPMI 1640	500 ml
	Pen/Strep, 10,000 U/ml	5.5 ml

4.1.12 Mouse strains

Mouse strain	Description	Source
C57Bl/6J	Wildtype C57Bl/6J	Charles River or JANVIER LABS
C57Bl/6J-CD45.1	C57Bl/6J, expressing congenic marker CD45.1	In house breeding
HHDII-HLA-DR1	C57Bl/6J, express human MHC class I (HLA-A*0201) and MHC class II (HLA-DR*0101), are devoid of endogenous murine class I (β_2m and D^b) and class II (IAb) molecules	In house breeding
HHDII-HLA-DR1-CD45.1/2	HHDII-HLA-DR1, expressing congenic marker CD45.1/2	In house breeding
$Rag2^{-/-}$	C57Bl/6J, homozygous deficiency in Rag2 locus; no B- and T-cell development	Dirk Wohlleber, Institute of Molecular Immunology, TUM
$Rag2^{-/-}$ $\gamma c^{-/-}$	C57Bl/6J, homozygous deficiency in Rag2 and IL-2Rγ locus; no B-, T- and NK-cell development	Günther Richter, CCRC, TUM or in house breeding
SCID/Beige (CB17.Cg-*Prkdc*^{scid}*Lyst*$^{bg-J}$/Crl)	C.B-17 SCID/SCID breed with C57BL/6J bg/bg mice: severe combined immunodeficiency; no B- and T-cell development, defective NK cells	Charles River

4.1.13 Viral vectors

All adeno-associated viral vectors (AAVs) in this study are AAVs serotype 2 packed with an AAV serotype 8 capsid resulting in liver-specificity. All adenoviral vectors (Ad) were of serotype 5 (Ad 5) backbone with deletions of E1A/E1B and E3.

Vector name	Abbreviation	Source
AAV-HBV 1.2 WT	AAV-HBV	Plateforme de Thérapie Génique in Nantes, France (INSERM U1089) or produced by J. Festag

AAV-HBV 1.3 WT	-	generated by J. Festag
AAV-HBV 1.3 X^-	-	generated by J. Festag
AAV-HBV 1.3 E^-	-	generated by J. Festag
AAV-HLA-A*02_P2A_β2m	AAV-HLA-A*02	generated by J. Festag
AAV-HHDII	-	generated by J. Festag
AAV-βG-intron-HHDII	-	generated by J. Festag
AAV-empty	-	provided by T. Michler
Ad-HBV 1.3 X^-	Ad-HBV	provided by by A. Malo
Ad-HLA-A*02_P2A_ β2m	Ad-HLA-A*02	provided by J. Wettengel
Ad-HLA-A*02-β2m-hNTCP-tdTomato	Ad-HLA-A*02-NTCP	provided by J. Wettengel
Ad-hNTCP	-	provided by J. Wettengel
Ad-GOva	-	provided by M. Mück-Häusl
HCA- HBV 1.3 X^-	HCA-HBV	provided by M. Mück-Häusl
MVA-HBsAg	-	provided by A. Kosinska, J. Su
MVA-HBcAg	-	provided by A. Kosinska, J. Su

4.1.14 Antibodies

Antibodies used for flow cytometry:

Antibody	**Dilution**	**Article number**	**Supplier**
Cetuximab-Biotin	1:100	7862371012	Merck Serono
Granzyme B-PE	1:100	GRB04	Invitrogen
hCD4-APC	1:200	17-0048-42	eBioscience
hCD8-Pb	1:50	PB984	Dako
hIFN-γ-FITC	1:50	554700	BD Biosciences
hIgG-FITC	1:200	SLBG4031	Sigma
hTNF-α-Pb	1:50	48-7349-42	eBioscience
mCasp-3-BV650	1:150	564096	BD Biosciences
mCD16/CD32 (Fc block)	1:100	553142	BD Biosciences
mCD19-PerCp-Cy5.5	1:200	561113	BD Biosciences

mCD3-FITC	1:100	100203	Biolegend
mCD45.1-APC-eF780	1:200	47-0453-82	eBioscience
mCD45.1-BV660	1:200	563754	BD Biosciences
mCD45.2-PE	1:200	12-0454-83	eBioscience
mCD49b APC	1:400	103515	Biolegend
mCD4-APC	1:100	17-0041-83	eBioscience
mCD4-PE-Cy7	1:200	25-0042-82	eBioscience
mCD4-V500	1:200	560782	BD Biosciences
mCD8a-Pb	1:100	558106	BD Biosciences
mCTLA-4-PerCP-Cy5.5	1:200	106316	Biolegend
mFas-FITC	1:100	152606	Biolegend
mIFN-γ-FITC	1:300	554411	BD Biosciences
mIgG-PE	1:200	12-4010-82	eBioscience
mNK1.1-PE-Cy7	1:100	25-5941-82	eBioscience
mPD-1-FITC	1:100	11-9981-85	eBioscience
mTim-3-APC	1:100	134006	Biolegend
mTNF-α-PE-Cy7	1:200	557644	BD Biosciences
Strep Tactin-PE	1:50	6-5000-001	IBA
Strep Tactin-APC	1:50	6-5010-001	IBA
Streptavidin-PE	1:250	12-4317-87	eBioscience
TCR-Vβ 13.1	1:10	IM1554	Beckman Coulter
TCR-Vβ 14	1:10	IM2047	Beckman Coulter
TCR-Vβ 20	1:10	IM1562	Beckman Coulter
TCR-Vβ 5.1	1:10	IM1552	Beckman Coulter

Antibodies used for stimulation of T cells:

Antibody	**Article number**	**Supplier**
hCD28	16-0289-85	eBioscience
hCD3	16-0037-85	eBioscience
hCD3	560770	BD Biosciences
hCD49b	16-0499-85	eBioscience
mCD28	-	AG Feederle, HMGU
mCD3	-	AG Feederle, HMGU
monkey-CD28	3608-1-50	Mabtech
monkey-CD3	3610-1-50	Mabtech

4.1.15 Multimers

Streptamers are a subgroup of multimers, consisting of MHC I-peptide complexes and were kindly provided by Dirk Busch (Technical University of Munich, Germany).

Streptamers used for flow cytometry:

Streptamer
C_{93}: MGLKFRQL
MVA_{B8R}: TSYKFESV
OVA_{S8L}: SIINFEKL
S_{190}: VWLSAIWM
$GPC3_{367}$: TIHDSIQYV

4.1.16 Software

Software	**Supplier**
Aperio Image Scope	Leica Biosystems
CytExpert	Beckman Coulter
FACS Diva™	Becton Dickinson
Flow Jo 10.4	BD Biosciences
Graph Pad Prism 5.01	Graph Pad Software Inc
i-control™ software	Tecan
LightCycler 480 Software 1.5.1.62	Roche
Living Image® software	Perkin Elmer
RTCA Software 2.0	ACEA Biosciences
Serial Cloner 2.6.1	Serial Basics
Windows 7/8/10, MS Office	Windows

4.2 Methods

4.2.1 Molecular biological methods

4.2.1.1 Polymerase chain reaction (PCR)

PCRs for molecular cloning of plasmids described in section 4.1.8 were implemented using the Phusion Hot Start Flex 2x Master Mix according to manufacturer's instructions. In brief, 2.5 µl of each 10 µM primer and 1 – 10 ng plasmid DNA were added to 25 µl 2x master mix. H_2O was added to a total reaction volume of 50 µl. Amplification of gene of interest was performed using the following PCR program:

	Temperature [°C]	**Time [sec]**	**Cycles**
Denaturation	98	30	1
Denaturation	98	10	30
Annealing	55-65 (depending on primers)	30	
Elongation	72	30 per 1kb	
Elongation	72	600	1
Cooling	4	∞	1

To fuse two DNA fragments by PCR, equimolar fragments (total of about 150 ng) with ~ 30 bp overlap were run without primers with a PCR program (see above) for 15 cycles. After adding primers, additional 15 cycles were conducted. Annealing temperature differed between the two PCR runs.

4.2.1.2 Restriction enzyme digestion

To obtain fragments for molecular cloning, restriction enzymes were used to digest plasmids and PCR products. Moreover, control digests were performed to analyze plasmid DNA after its isolation. Plasmid DNA or PCR products were added to 2 µl FastDigest Green Buffer (10x) and up to 1 µl of the appropriate FastDigest restriction enzyme not exceeding 10 % (v/v) of total volume. H_20 was added to a total reaction volume of 20 µl with subsequent incubation at 37°C for 30 – 60 min. If restriction digests were implemented to obtain a plasmid backbone for a following ligation, 1 µl FastAP for dephosphorylation of 5' and 3' ends was added in order to prevent self-ligation without an insert. Inactivation of enzymes was performed according to manufacturer's instructions.

4.2.1.3 DNA gel electrophoresis and gel extraction

PCR products and plasmid DNA were analyzed on a 1 % agarose gel prepared with TAE buffer (1x) and 10 µl SYBR safe DNA gel stain per 100 ml total volume. For estimating size of DNA fragments, a DNA ladder was run together with the samples at 80 – 150 mV until desired separation of fragments had been reached. DNA Fragments needed for further molecular cloning steps were cut out from the agarose gel using a scalpel. Subsequently, DNA was extracted using the QIAquick Gel Extraction Kit according to manufacturer's instructions.

4.2.1.4 Ligation

For ligation, a total of 100 ng of DNA fragments were ligated in a molar ratio of 3:1 (insert : backbone) with 2 µl T4 ligase buffer and 1 µl T4 ligase. H_20 was added to a total reaction volume of 20 µl with subsequent incubation at RT for 30 min.

4.2.1.5 Culture of E. coli

E. coli *STBL3* or E. coli *TOP10* were thawed on ice and 5 µl of the ligation reaction was added to 50 µl bacteria. After an incubation on ice for 20 min, the heat shock was performed for 45-90 sec at 42°C. Bacteria were chilled on ice for 2 – 3 min before 500 µl SOC medium was added and bacteria shook for one hour at 225 rpm. Next, bacteria were spun down at 500g for 5 min, resuspended in 100 µl of SOC medium and spread on antibiotic-resistance LB plates. Finally, bacteria were incubated overnight at 37°C.

4.2.1.6 Isolation of Plasmid DNA

E. coli *STBL3* or E. coli *TOP10* transformed with the respective plasmids were amplified in overnight cultures in LB medium supplemented with 100 µg/ml ampicillin or 50 µg/ml kanamycin (depending on the resistance gene on the plasmid) at 37°C, 185 rpm. Bacteria cultures were harvested by centrifugation (3400g, 10 min, 4°C) after they had grown until a maximal absorbance (OD_{600}) of 1.5. Plasmid DNA was isolated using the GeneJET Plasmid Miniprep Kit (for small cultures of 1 – 3 ml), the Plasmid *Plus*Midi Kit (for large cultures (20 – 50 ml) or the PureLink HiPure Plasmid Gigaprep Kit (for huge cultures of 500 ml) according to manufacturer's instructions.

4.2.1.7 Sequencing

For sequencing samples were diluted to a concentration of 30 – 100 ng/µl and 20 µl sample as well as 20 µl primer (10 µM) were sent to the external provider GATC Biotech (Konstanz, Germany). Sequencing results were downloaded for subsequent analysis using Serial Cloner 2.6.1.

4.2.1.8 DNA isolation

4.2.1.8.1 Isolation of DNA from cell culture and animal tissue

Cellular DNA from cell cultures was extracted using the Nucleo Spin Tissue Kit according to manufacturer's instructions for cultured cells. For DNA extraction from mouse tissue, samples were frozen in 180 µl T1 Buffer of the Nucleo Spin Tissue Kit and DNA was isolated according to the manufacturer's instructions after thawing.

4.2.1.8.2 Isolation of DNA from mouse serum

25 µl of serum was used for DNA extraction using the QIAamp MinElute Virus Spin Kit according to manufacturer's instructions and finally eluted into 50 µl H_2O.

4.2.1.9 RNA isolation

Fresh tumor tissue was stabilized in RNA*later* reagent and stored at -80°C until further processing. At time of isolation, samples were thawed and mechanically disrupted using a Tissue Lyser LT according to manufacturer's instructions. Next, RNA of pre-treated tumor tissue or cultured cells was isolated using the Nucleo Spin RNA Kit according to manufacturer's instructions.

4.2.1.10 Determination of DNA or RNA concentration

Plasmid and genomic DNA as well as RNA concentrations were determined on a NanoDrop One using the appropriate buffer solution as blank.

4.2.1.11 cDNA synthesis

RNA was reversely transcribed into cDNA using the SuperScript III Kit according to manufacturer's instructions. Obtained cDNA was diluted 1:4 in H_2O for further analysis.

4.2.1.12 quantitative PCR

Quantitative PCR (qPCR) for HBV DNA in mouse serum was performed on an Applied Biosystems® 7500 Real time PCR system using primers HBV1464_fw, HBV1599_rev and the HBV-specific taqman probe HBV1529_probe with incorporated 5´ reporter dye 6-Carboxyfluorescein (FAM) and 3´ quencher Tetramethylrhodamine (TAMRA) serum (lower limit of quantification [LLOQ]: 1.705 copies / µl serum). The test was performed by J. Seebach from the diagnostics department. Cycling conditions were: 2 min 50°C, 10 min 95°C followed by 45 x (15 s 95°C, 1 min 60°C).

Quantitative PCR was performed to determine total intracellular HBV DNA (primers: HBV S fw, HBV S rev), rcDNA (primers: HBV 1745, HBV 1844), cccDNA (primers: cccDNA 92-, cccDNA 2251+), AAV DNA (primers: AAV ITR fw, HBV X rev), adenovirus DNA (primers:

Adeno-fw, Adeno-rev) and PrP (primers: PrP fw, PrP rev) on a LightCycler 480 Real-time PCR system. Data was either analyzed quantitively using an external plasmid standard or by advanced relative quantification considering primer efficiency and normalization to the single copy prion protein (Prp) gene. Importantly, analysis of cccDNA qPCR was performed by prior digestion of extracted DNA with a T5 exonuclease, which removes linear DNA, rcDNA or nicked DNA but spares cccDNA, increasing the selectivity for cccDNA as described previously (Xia et al., 2017). Therefore, 8.5 µl extracted DNA (concentration of 12,5 ng/µl) were mixed with 1 µl NEB buffer 4 and 0.5 µl T5 exonuclease, incubated at 37 °C for 30 minutes with subsequent heat inactivation at 99 °C for 5 minutes. Next, the sample was diluted 1:4 in water.

Moreover, qPCR was used for relative quantification of hCD8 (primers: hCD8 fw, hCD8 rev), hGPC3 (primers: hGPC3 fw, hGPC3 rev) and hGAPDH (primers: hGAPDH fw, hGAPDH rev) from cDNA from tumor tissue or cultured cells. A relative quantification of hCD8 and hGPC3 levels was achieved by normalization to the housekeeping gene GAPDH measured in the same sample.

Per reaction, 5 µl LightCycler 480 SYBR green master mix were mixed with 0.5 µl of each primer (stock concentration = 20 µM) and 4 µl sample (≤50 ng total DNA).

Total intracellular HBV DNA, rcDNA, AAV DNA, adenovirus DNA, PrP, hCD8, hGPC3 and hGAPDH were measured with following qPCR program:

	T [°C]	t [sec]	Ramp [°C/sec]	Acquisition mode	Cycles
Denaturation	95	300	4.4		1
Amplification	95	15	4.4	single	45
	60	10	2.2		
	72	25	4.4		
Melting	95	10	4.4	continuous: 5/°C	1
	65	60	2.2		
	95		0.11		
Cooling	40	1	2.2		1

The qPCR program for cccDNA was the following:

	T [°C]	t [sec]	Ramp [°C/sec]	Acquisition mode	Cycles
Denaturation	95	600	4.4		1
Amplification	95	15	4.4	single	50
	60	5	2.2		

	72	45	4.4		
	88	2	4.4		
	95	1	4.4		
Melting	65	15	2.2	continuous: 5/°C	1
	95		0.11		
Cooling	40	30	2.2		1

4.2.2 General cell culture methods

All primary cells and cell lines were cultured under sterile conditions and only handled under a clean hood with laminar air flow. Cells were incubated at 37°C, 5% CO_2 and 95% humidity.

4.2.2.1 Maintenance of cell lines

Adherent cell lines were cultured in DMEM full medium. Depending on confluency, cells were passaged 1:5 to 1:10 every three to four days. HEK 293, HEK 293T, HEK 293 FT, PlatE and RD114 cells were harvested by vigorous resuspension, all HepG2-, Hela-, HepaRG- and Huh7-derived cell lines were treated with trypsin and versene in a 1:1 ratio (5 – 10 min, 37°C) to obtain a single-cell suspension. Culture flasks or plates for HepG2-derived cells were collagenized (collagen R, 1:10 in H_2O, 30 min, 37°C) and washed twice with PBS before seeding cells.

T2 cells, a suspension cell line was kept in RPMI full medium and passaged in a ratio of 1:10 every three to four days.

4.2.2.2 Counting of cells

After harvesting, cells were resuspended thoroughly to obtain a single-cell suspension. Counting was performed manually by diluting 10 µl of the cell suspension with 10 µl trypan blue to stain dead cells and counted on a Neubauer improved hemocytometer under a light microscope. Automated counting was performed on a NucleoCounter NC-250. Here, cells were prepared by adding 1 µl of Solution 18 to 20 µl of cell suspension.

4.2.2.3 Transfection of cells

Cells were seeded in 6-well plates to obtain a confluency of 60 – 80 % at day of transfection. Four µg plasmid DNA was diluted in OptiMEM to a total volume of 250 µl. Ten µl Lipofectamine 2000 was added to 240 µl OptiMEM in a separate tube. After incubation for 5 min at RT, the DNA mix was added to the Lipofectamine 2000 mix, carefully resuspended and incubated for 20 min at RT. In the meantime, medium of cells was exchanged to 1 ml transfection medium.

The DNA/Lipofectamine mix was added dropwise to the cells and incubated for four to six hours. Thereafter, medium was replaced with 2 ml fresh culture medium.

4.2.2.4 Freezing/Thawing of cells

For freezing, cells were centrifuged at 450g for 5 minutes and pelleted cells were resuspended in 1 ml freezing medium per cryo vial. Subsequently, cryo vials were transferred into a freezing device and stored immediately at -80 °C for slow temperature decline. After at least one day, cryo vials were transferred to a box at -80 °C or in liquid nitrogen. In order to thaw cells, 1 ml prewarmed medium was added to frozen cells and slowly transferred forth and back until the solution was thawed. Next, cell suspension was transferred into a new tube containing 15 ml prewarmed medium. Cells were centrifuged (450g, 5 min, RT) and seeded in an appropriate cell culture flask with the respective culture medium.

4.2.3 Generation of *Firefly*-Luciferase expressing HepG2 cells

The newly generated plasmid pLenti6_v5_CMV_Fluc encoding for the *Firefly* luciferase under the CMV promotor was linearized by digestion with FastDigest restriction enzyme Acc I. Next, HepG2 cells were transfected with the linearized plasmid by standard lipofectamine transfection. As the plasmid also encoded for a blasticidine resistance, transfected cells were selected for antibiotic resistance by addition of 5 µg/ml blasticidine to the culture medium beginning two days after transfection. Cells were expanded, and luciferase activity from HepG2-Fluc cells was measured from cell lysates of 5 x 10^4 cells using the Firefly Luciferase Assay System according to manufacturer's instructions but only using 50 % of luciferase assay reagent. Bioluminescence was measured on the Tecan Infinite F200 reader. The background was normalized by measuring untransfected HepG2 cells.

4.2.4 Generation of HLA-A*02 expressing Huh7 cells

The plasmid pcDNA3.1(Hygro)-HLA-A*02 was linearized by digestion with FastDigest restriction enzyme Spe I. Subsequently, Huh7 cells were transfected with the linearized plasmid by standard lipofectamine transfection. Transfected cells could be selected by adding 600 µg/ml hygromycin B to the cell culture medium, as the plasmid additionally encoded a hygromycin B resistance. Resistant cells were expanded and HLA-A*02 surface expression was verified by flow cytometry (see section 4.2.16.1).

4.2.5 Generation of GPC3 overexpressing Hela-HLA-*02 cells

The plasmid pcDNA3.1(-) GPC3 was used to generate Hela-HLA-A*02 cells overexpressing GPC3. For this purpose, Hela-HLA-A*02 cells were transfected by standard lipofectamine

transfection and transfected cells were selected by addition of 2 mg/ml geneticin (encoded on pcDNA3.1(-) GPC3). After performing a limiting dilution (0.5 cells/96 well), single cell clones grew out and their GPC3 expression was analyzed by qPCR.

4.2.6 Generation of CRISPR/Cas9 GPC3 knock-out Hela-HLA-A*02 cell lines

First, GPC3 specific guideRNAs (gRNAs) were designed to ensure a target specific cleavage and subsequently induction of frame-shift-mutations at the GPC3 locus. Therefore, the online platforms https://www.dna20.com/eCommerce/cas9/input and http://crispr.mit.edu/ were used. Three gRNAs (see Table 2.1) were designed to be inserted into the vector lentiCRISPRv2 (Sanjana et al., 2014; Shalem et al., 2014) with all of them targeting Exon 3 within the GPC3 locus. Lentivirus encoding for gRNAs and Cas9 were produced in HEK 293 FT cells using the ViraPower Lentiviral Expression Systems Kit according to manufacturer's instruction. In short, a co-transfection of the vectors encoding gRNA and Cas9 together with the packaging plasmids pVSVg and psPAX2 allowed production of lentivirus that was subsequently used to transduce Hela-HLA-A*02 cells. Transduced cells were selected by addition of 1 µg/ml puromycin (encoded on lentiCRISPRv2). In order to achieve a single cell clone, a limiting dilution was performed (0.5 cells/96 well). Single cell clones were expanded and analyzed to identify clones with a frameshift mutation within the GPC3 gene. The amplicon of a PCR of the gRNAs target region was sequenced in order to identify insertions, deletions or frameshift mutations.

4.2.7 Infection with HBV

The HBV virus stock used for infection of HepG2-NTCP and primary hepatocytes was kindly provided by J. Wettengel. HepG2-NTCP cells were infected after 10 to 14 days of differentiation using HepG2 Diff medium. Primary hepatocytes were infected at indicated time points. Cells were infected with indicated MOIs in the presence of 5 % PEG in either HepG2 Diff medium or PMaH medium overnight. Fourteen to 16 hours after infection, cells were washed three times with PBS before HepG2 Diff and PMaH medium, respectively, was added.

4.2.8 Isolation of primary immune cells

4.2.8.1 Isolation of murine and rhesus macaque splenocytes

To isolate splenocytes of mice, spleens were collected and crushed through 100 µm cell strainers using a plunger of a 5 ml syringe. Remaining cells on the cell strainer were removed by cold wash medium. Cells were pelleted (450g, 5 min, 4°C) and erythrocytes were lysed in2 ml ACK lysis buffer for 2 min at RT. After reaction was stopped by addition of 30 ml wash medium, cells were pelleted (450g, 5 min, 4°C) and resuspended in a suitable volume of

murine T-cell medium (mTCM). For rhesus macaque cells, a piece of the spleen was used to isolate splenocytes. Procedure was performed as described for murine splenocytes. Finally, splenocytes were resuspended in a suitable volume of R15 medium.

4.2.8.2 Isolation of murine liver-associated lymphocytes

To prepare liver-associated lymphocytes (LALs), livers were perfused with PBS in order to remove non-liver-associated lymphocytes before crushing through 100 µm cell strainers using a plunger of a 5 ml syringe. The cell strainer was repeatedly cleaned with cold wash medium followed by additional mashing. Cells were sedimented (450g, 5 min, 4°C), cell pellets were resuspended in 12 ml collagenase-medium (wash medium + 10 mg collagenase type IV) and digested for 20 minutes at 37°C with repeated shaking. After an additional washing step cells were resuspended in 4 ml PBS-buffered 40 % Percoll, carefully layered onto 4 ml PBS-buffered 80 % Percoll in a 15 ml falcon tube and centrifuged at 1200g for 20 min at room temperature without breaks. Lymphocytes located in between Percoll layers were collected, transferred in a new tube, washed and cultivated in mTCM.

4.2.8.3 Isolation of murine PBMC

Ten µl of heparinized whole blood collected in Microvette 500 LH-Gel tubes was transferred to a V-bottom plate and 250 µl of ACK lysis buffer was added to lyse the erythrocytes. After an incubation of 5 min at RT, cells were centrifuged at 450g for 2 min at 4°C and washed once with PBS and once with FACS buffer. Thereafter, staining for flow cytometry analyses was started.

4.2.8.4 Isolation of human and rhesus macaque PBMC

Human PBMC were isolated out of whole blood from healthy donors. Fresh blood was mixed with heparin to avoid coagulation and diluted 1:1 in wash medium. 25 ml of diluted blood was carefully overlayered onto 15 ml Biocoll separating solution and centrifuged at 960g for 20 min without breaks. The lymphocyte ring was collected, transferred into a new 50 ml tube and washed twice with wash medium (350g, 10 min). Finally, cells were resuspended in an appropriate volume of human T-cell medium (hTCM).

Isolation of macaque PBMC was performed by M. Festag. Macaque peripheral citrate blood was obtained from the “Deutsches Primatenzentrum” in Göttingen, Germany and PBMC were isolated as described for human PBMC.

4.2.9 Retroviral transduction of T cells

4.2.9.1 Production of retroviral supernatants

Retroviral supernatants enabling transgenic expression of TCR- or CAR-constructs were either obtained from transiently transfected or stably transduced producer cell lines PlatE or RD114. Retrovirus produced from PlatE cells enables transduction of murine T cells, whereas retrovirus produced from RD114 cells is capable of transducing human T cells. For transient production, producer cell lines were transfected with pMP71 plasmids encoding for TCR- or CAR-constructs by standard lipofectamine transfection. Two and three days later, the supernatant comprising the retroviruses was collected and filtered through a 0.45 μm filter. At day 2 fresh medium was added and collected 24 hours later. Retroviral supernatant from transiently transfected PlatE or RD114 cells was used to transduce PlatE and RD114 cells, respectively, on two subsequent days in order to generate stably transduced producer cell lines. Here, surface expression of the transgene was used to identify transduced cells that were then sorted by FACS. Stably producing packaging cell lines were supplied with fresh media when they reached ~70 % confluency and supernatant was collected 24 hours later. Supernatant containing retrovirus was filtered through a 0.45 μm filter and was stored at -80°C when not needed directly.

4.2.9.2 Transduction of mouse splenocytes

4.2.9.2.1 Transduction with IL-2 stimulation

Retroviral transduction with IL-2 stimulation was performed for all experiments using natural TCRs. Freshly isolated splenocytes (see section 4.2.8.1) were counted, adjusted to 6×10^6 cells/ml mTCM and supplemented with IL-2 (300 U/ml), anti-CD3 (2 μg/ml) and anti-CD28 (0.1 μg/ml) antibodies (day 1). Cells were incubated overnight at 37°C. The following day (day 2), non-tissue culture-treated 6- or 24-well plates were coated with RetroNectin (20 μg/ml in PBS, 1 ml or 250 μl/well, 2 hours, RT). RetroNectin was removed and stored at 4°C for re-use on the following day. After wells were blocked with 2 % BSA in PBS (30 min, 37°C), they were washed twice with PBS and 5 ml or 1 ml retroviral supernatant was added per well. Next, plates containing retroviral supernatant were centrifuged (2000g, 2 hours, 32°C). Meanwhile, splenocytes were counted, washed and adjusted to 1×10^6 cells/ml in fresh mTCM supplemented with IL-2 (300 U/ml). Viral supernatant was removed from the RetroNectin coated plates and 5 ml or 1 ml of cell suspension containing activated splenocytes were applied. After an additional centrifugation step (1000g, 10 min, 32°C), cells were incubated at 37°C. The next day (day 3), a second round of transduction was performed with minor changes: splenocytes were transferred well-by-well and their medium was not refreshed. On day 4, transduction rate was determined by flow cytometry. Cells were

collected, washed and adjusted to 1.25 x 10^5 cells/ml mTCM supplemented with IL-15 (10ng/ml) for expansion. Cells were readjusted to the mentioned conditions every 3 – 4 days until functional assessment or freezing. Alternatively, cells were immediately used for adoptive transfer experiments.

4.2.9.2.2 Transduction with IL-12 stimulation

IL-12 stimulation during transduction was used for the S-CAR adoptive transfer experiment. Tissue culture-treated 12-well plates were coated with anti-CD3 and anti-CD28 antibodies (each 10 µg/ml in PBS, 460 µl/well, 2 hours, 37°C) and were washed twice with PBS thereafter. Freshly isolated splenocytes (see section 4.2.8.1) were enriched for $CD8^+$ T cells by magnetic activated cell sorting (MACS) using CD8a (Ly2) MicroBeads. $CD8^+$ T cells were isolated according to manufacturer's instructions. Thereafter, $CD8^+$ T cells were adjusted to 5 x 10^5 cells/ml mTCM supplemented with IL-12 (5 ng/ml) and 3 ml/well were seeded in antibody-coated 12-well plates (day 1). Cells were incubated overnight at 37°C. The following day (day 2), 2 ml of supernatant of T cells was carefully removed and kept at 37°C. T cells were resuspended in the remaining 1 ml and transferred to a new 12-well plate. Next, 1 ml retroviral supernatant supplemented with protamine sulfate (4 µg/ml) was applied to the T cells. Therefore, final concentration of protamine sulfate during spinoculation (850g, 2 hours, 32°C) was 2 µg/ml. After centrifugation, 1 ml supernatant was removed, 2 ml of the stored supernatant was supplemented with 2 µg/ml protamine sulfate and added to the cells. The next day (day 3), a second round of transduction was performed with minor changes: cells were not transferred to a new plate and supernatant was not removed after spinoculation, leading to a final volume of 4 ml per well. On day 4, cells were harvested, the transduction frequency was determined by flow cytometry and prepared for adoptive transfer.

4.2.9.3 Transduction of human PBMC

For activation of human PBMC, non-tissue culture 6- or 24-well plates were coated with anti-CD3 (5 µg/ml) and anti-CD28 (0.05 µg/ml) antibodies diluted in PBS (250 µl/well, 2 hours, 37°C). Thereafter, wells were blocked with 2 % BSA in PBS (30 min, 37°C) and subsequently washed twice with PBS. Freshly isolated or thawed human PMBC were counted, adjusted to 0.66 x 10^6 cells/ml hTCM supplemented with IL-2 (300 U/ml) and 7 ml or 1.5 ml of the cell suspension was seeded per well (day 1). After incubation for 48 hours at 37°C, two rounds of transduction were performed as described for mouse cells with IL-2 stimulation (see section 4.2.9.2.1) on two consecutive days (day 3 and 4). On day 5, transduction rate was determined by flow cytometry. Cells were collected, washed and adjusted to 1.25 x 10^5 cells/ml hTCM supplemented with IL-2 (180 U/ml) for expansion. Cells were readjusted to the mentioned conditions every 3 – 4 days until functional assessment, freezing or adoptive transfer experiments.

4.2.9.4 Transduction of rhesus macaque PBMC and splenocytes

4.2.9.4.1 Plate-bound antibodies and human IL-2 or IL-15

Transduction was performed as described for human PBMC (see 4.2.9.3) with minor changes. For coating of non-tissue culture plates, a different anti-CD3 antibody was used (1 µg/ml, BD). Medium was either supplemented with IL-2 (300 U/ml) or IL-15 (10 ng/ml). After harvesting, cells were adjusted to 2.5 x 10^5 cells/ml hTCM supplemented with either IL-2 (180 U/ml) or IL-15 (10 ng/ml) for expansion.

4.2.9.4.2 Soluble antibodies and staphylococcal enterotoxin b

Up to 5 x 10^6 PBMC or splenocytes were stimulated in 1 ml R15 medium supplemented with IL-2 (100 U/ml), Staphylococcal enterotoxin b (SEB) (2 µg/ml), anti-monkeyCD3 (0.3 µg/ml), anti-monkeyCD28 (1.5 µg/ml) and anti-hCD49d (1.5 µg/ml) antibodies at 37°C over night (day 1). The next day (day 2), cells were collected and washed three times with 5 ml RPMI full medium. Finally, cells were resuspended in 1 ml R15 medium supplemented with IL-2 (100 U/ml) and incubated at 37°C over night. On the following day (day 3) cells were counted and transduction was performed as described for human PBMC (see 4.2.9.3) in presence of IL-2 (180 U/ml). Macaque PBMC and splenocytes were only transduced once and harvested and expanded the next day (day 4) as described for human PBMC (see 4.2.9.3).

4.2.10 Isolation of primary hepatocytes

4.2.10.1 Isolation of primary murine hepatocytes

Collagenase IV was added to digestion medium (30 mg ad 100 ml medium/mouse), filtered through a 45 µm filter and prewarmed at 37°C for 30-60 min in order to allow collagenase to dissolve. Approximately 30 min before starting isolation of primary murine hepatocytes (PMHs), mice were i.p. injected with 200 µl heparin (1000 IU/ml) to ensure anticoagulation. Mice were sacrifice with CO_2 and opened to access the internal organs. The cannula was inserted into the portal vein, perfusion was started with preperfusion medium and once cannulation was confirmed to be successful, the inferior vena cava was cut. After the liver was perfused with 60 ml preperfusion medium, 80 ml of digestion medium supplemented with collagenase was used for perfusion of the liver. Next, liver was excised without injuring the gallbladder. Using scalpels and forceps, cells were gently removed from the liver capsule and filtered through a 70 µM filter to remove cell clumps and obtain a single-cell suspension. Cells were washed three times with maintenance medium (50g, 2 min, 4°C), counted, adjusted to 2.5 x 10^5 cells/ml maintenance medium and seeded on collagen-coated 12-well plates (1 ml/well). After four hours, when cells were attached, cells were washed with PBS and

cultured with maintenance medium overnight. The next day, medium was exchanged to maintenance medium supplemented with 1.8 % DMSO.

4.2.10.2 Isolation of primary macaque and pig hepatocytes

For isolation of primary macaque hepatocytes (PMaHs) an intact liver lobe was first perfused with 250 ml HBSS followed by perfusion with 100 ml collagenase medium. Additional 150 ml collagenase medium was used for repeated re-circulation through the liver lobe at 42°C for 1 hour. Next, the liver lobe was physically broken up using scalpels and forceps. The thereby generated cell suspension was first filtered through a tea filter and subsequently through a 70 µM filter to remove cell clumps and obtain a single-cell suspension. Cells were washed with PMaH medium three times with distinct centrifugation steps in between (1.: 100g, 3min, 2.: 70g, 3 min, 3.: 50g, 3 min, all 4°C) resulting in enrichment of hepatocytes. Finally, freshly isolated PMaHs were adjusted to 2.5 x 10^5 cells/ml PMaH medium and seeded on collagen-coated 12-well plates (1 ml/well). Four hours later, cells were carefully washed three times with HBSS and cultured with PMaH medium overnight. The next day, medium was exchanged to PMaH medium supplemented with 1.8 % DMSO.

Primary pig hepatocytes were isolated by S. Jeske and J. Wettengel as described for macaque hepatocytes.

4.2.11 Co-cultures experiments

For the determination of their functional activity, T cells were co-incubated with different target cells and viability of target cells as well as activation of T cell was assessed.

4.2.11.1 Real-time viability: xCELLigence

The xCELLigence system was used to determine cell viability of target cells in co-culture experiments. Here, adherent target cells were seeded on specially designed microtiter plates (E-plate 96 culture plates), which contain interdigitated gold microelectrodes to noninvasively monitor cell viability, measured as electrical impedance. The electrical impedance is displayed as cell index (CI) values. For co-cultures with Huh7-derived cells 7.5 x 10^4 target cells, for co-cultures with HepG2-, Hela-, and HepaRG-derived cell lines 5 x 10^5 target cells were seeded per well three days prior co-incubation with T cells to achieve approximately 90 % confluency of target cells at start of co-culture. Redirected T cells were used at day 4 post-transduction or later and were deprived from IL-2 one day prior start of co-culture. At day of start of co-culture, 100 µl medium was removed from the cells and T cells were added in 100 µl hTCM medium. All experiments in this thesis were performed with an effector to target ratio (E:T) of 0.5 : 1 unless otherwise stated. Cell viability is illustrated as cell index normalized to the start of co-culture.

4.2.11.2 XTT assay

End-point viability of target cells in co-cultures with PMHs was determined using a Cell Proliferation Kit II (XTT) according to manufacturer's instructions with minor modifications. This assay is based on the cleavage of the yellow tetrazolium salt XTT to form an orange formazan dye by metabolic active cells. Per 12-well 200 µl XTT labeling reagent and 4 µl of electron coupling reagent were mixed to obtain the XTT labeling mixture. Supernatant of cells was removed and washed with PBS. 800 µl fresh medium was applied followed by 200 µl XTT labeling mixture. After cells were incubated at 37°C for 14 hours substrate conversion was determined by measurement of OD_{450} subtracted by OD_{650} on an ELISA-Reader infinite F200.

4.2.11.3 Co-cultures with soluble target cells

4.2.11.3.1 Co-culture of redirected T cells with peptide loaded T2 cells

Activation of redirected T cells towards HLA-A*02 presented peptides was determined in co-cultures with peptide loaded T2 cells. T2 cells lack the ability to present endogenous peptides but very well display HLA-A*02 molecules associated with exogenously administered peptides. T2 cells were adjusted to 1 x 10^6 cells/200 µl hTCM and respective peptides were added (1 µM). After incubation at 37°C for 2 hours, cells were washed three times and 1 x 10^5 peptide loaded T2 cells were used for co-incubation with respective effector cells. In order to assess activation of modified T cells, supernatants were harvested at indicated time points to analyze IFNγ content by ELISA (see section 4.2.14.1).

4.2.11.3.2 Determination of T-cell immune response in immunocompetent mice

In order to analyze if recipient mice of TCR-redirected T cells developed a T-cell mediated immune response towards TCR-expressing cells a co-culture experiment was performed. Here, 1 x 10^6 freshly isolated splenocytes (see section 4.2.8.1) from mice, that had received TCR^+ or mock T cells, were co-incubated with 1 x 10^5 freshly transduced TCR^+ or mock $CD8^+$ T cells at 37°C. One hour after start of co-culture, Brefeldin A (1 µg/ml) was added and the co-culture continued for 16 hours at 37°C until an ICS (see section 4.2.16.3) was performed on the following day.

Alternatively, elimination of freshly transduced TCR^+ or mock $CD8^+$ T cells was assessed by a killing experiment. Therefore, target cells (freshly transduced TCR^+ or mock $CD8^+$ T cells) were stained with Cell Trace Violet using the CellTrace Violet Cell Proliferation Kit according to manufacturer's instructions. Next, 2 x 10^6 freshly isolated splenocytes (see section 4.2.8.1) from mice, that had received TCR^+ or mock T cells, were co-incubated with 2 x 10^4 freshly transduced TCR^+ or mock $CD8^+$ T cells at 37°C. Three days later, the remaining TCR^+ target cells were determined by flow cytometry.

4.2.12 Adeno-associated viral vector production

Adeno-associated virus (AAV) serotype 2 packed with an AAV serotype 8 capsid were produced in HEK 293T cells by triple transfection. HEK 293T were grown on 15 cm^2 dishes (in total 18) and were harvested when they reached a confluency of ~80 %. Cells were diluted in two bottles DMEM full media and poured into a cell factory. The next day, cells were transfected with pXX6 (Xiao et al., 1998), a vector plasmid (pAAV-HBV 1.2WT, pAAV-HBV 1.3WT, pAAV-HBV 1.3X-, pAAV-HBV 1.3E-, pAAV-HLA-A*02, pAAV-HHDII, pAAV-βG-intron-HHDII) and the AAV helper plasmid pXR8 (Gao et al., 2004) in a ratio of 4:1:1 using 1 mg/mL polyethylenimine (PEI). In detail, 442.5 µg of pXR8, 442.5 µg of the vector plasmid and 1720.8 µg of pXX6 were diluted in 45 ml of transfection medium. Moreover, 4 ml of PEI was added to 45 ml of transfection medium. The DNA mix was added to the PEI mix, carefully resuspended and incubated for 15 min at RT. Next, transfection mix was added to 1l of transfection medium and used to replace the medium of the cell factory. After six hours, medium was replaced by DMEM full medium. 72 hours after transfection, cells were harvested, pelleted (1000g, 15 min, 8°C), washed with PBS and resuspended in 7.4 ml AAV lysis buffer. Next, cell lysate was exposed to three freezing-thawing cycles (-80°C – 37°C) and finally treated with 50 U/ml benzonase for 30' at 37°C. Vector stocks were purified by an iodixanol gradient: 60% iodixanol was diluted to 15, 25, and 40 % in PBS-MK. NaCl was added to the 15% phase at 1 M final concentration (PBS-MKN). A 1,25 µl and 2,5 µl volume of 0.5 % phenol red was added per milliliter to the 60 and 25 % iodixanol solutions, respectively, to facilitate easier distinguishing of the phase boundaries within the gradient. 600 µl of 60 % were overlayered by 600 µl of 40 %, followed by 25 % and 15 % of iodixanol solutions and finally overlayered by the processed cell layer (in total 6 tubes). After centrifugation in a SW50Ti or SW55Ti rotor for 2 hours at 50,000 rpm at 4°C, AAVs were collected from the fractions obtained from the 40 % phase. Viral DNA was isolated by incubating 5 µl virus stock with 5 µl TE Buffer (from the Plasmid Gigaprep Kit) and 10 µl NaOH (2M) for 30 min at 56°C and adding 480 µl HCl (40mM) thereafter. Viral genome titers were determined by qPCR using the AAVpro® Titration Kit following manufacturer's instructions. AAV stocks were stored at -80°C.

4.2.13 Mice experiments

Animal experiments were conducted in accordance to the German regulations of the Society for Laboratory Animal Science (GV-SOLAS) and the European Health Law of the Federation of Laboratory Animal Science Associations (FELASA). Experiments were approved by the local Animal Care and Use Committee of Upper Bavaria. Animals were kept in a pathogen-free (SPF) facility and experiments were performed during the light phase of the day. All mice

were kept in the animal facilities of the Helmholtz Zentrum Munich or of the Institute of Virology/ Microbiology, TUM.

4.2.13.1 Injections

For luciferase expressing HepG2 transplantation experiments, either 5 x 10^5 HepG2 cells expressing the Gaussian luciferase (HepG2-Gluc) were injected into the splenic pulp of SCID/Beige mice or 3 x 10^6 HepG2 expressing the firefly luciferase (HepG2-Fluc) were injected intraperitoneally (i.p.) or subcutaneously (s.c.) into Rag2$^{-/-}$ γc$^{-/-}$ mice. When tumors were established after 12 or 8 days respectively, mice were injected i.p. with 1 x, 2 x or 4 x 10^6 P1-1$^+$ or mock human T cells in 200 µl PBS as indicated.

All viral vectors expressing HBV or HLA-A*02-β2m/HHDII were injected intravenously (i.v.) in 200 µl PBS into the tail vein of the mice.

For adoptive transfer experiments T cells were modified as described in section 4.2.9. Expression of the CAR/TCR was determined by flow cytometry before T cells were injected i.p. in 200 µl PBS. The number of transferred T cells is given in the respective experiments.

For protein vaccinations, mice were immunized intramuscularly (i.m.) with 10 µg HBsAg and 10 µg HBcAg in 60 µl (30 µl per leg) using 10 µg ci-di-AMP as adjuvant. 1 x 10^7 pfu MVA-HBsAg and 1 x 10^7 pfu MVA-HBcAg were injected i.m. in 60 µl PBS (30 µl per leg).

4.2.13.2 Bioluminescence imaging

Animals, that were injected with luciferase expressing hepatoma cells were monitored every 3-4 days by bioluminescence imaging using the IVIS Imaging System. For this purpose, mice were i.p. injected with 4 mg/kg coelenterazine (for HepG2-Gluc) or 15 mg/ml D-Luciferin (for HepG2-Fluc) and anesthetized using 2% isoflurane before *in vivo* imaging. For quantification, regions of interest (ROI) were selected and quantified as photons/second using Living Image® software.

4.2.13.3 Bleeding

Mice were bled from the cheek at different time points after vector transduction, immunization or T-cell transfer. Blood was either collected in Microvette 500 LH-Gel tubes if analyses of whole blood and serum was necessary or in Microvette 1,1 ml Z-Gel tubes if only serum components were of interest.

4.2.13.4 Serum analyses

Whole blood collected in Microvette 1,1 ml Z-Gel tubes was centrifuged at 10.000g for 5 min at RT. The serum (located above the gel matrix) was collected and transferred into a new reaction tube for further analyses. Serum alanine aminotransferase (ALT) activity was

measured in a 1:4 dilution in phosphate buffered saline (PBS) using the Reflotron® GPT/ALT test. Serum HBsAg, HBeAg, anti-HBs and anti-HBe antibody levels were quantified on an Architect™ platform using the quantitative HBsAg test (Ref.: 6C36-44; Cutoff: 0.25 IU/ml), the HBeAg Reagent Kit (Ref.: 6C32-27) with HBeAg Quantitative Calibrators (Ref.: 7P24-01; Cutoff: 0.20 PEIU/ml), the anti-HBs test (Ref.: 7C18-27; Cutoff: 12.5 mIU/ml) and the anti-HBe test (Ref.: 6C34-25, competitive test with S/CO > 1 being negative, 1:25 dilution in PBS). Anti-HBc antibody levels were determined using the Enzygnost® Anti-HBc monoclonal test on the BEP III platform.

4.2.13.5 Dissection and processing of organs

On the day of final analysis, mice were sacrificed with CO_2 and opened to access the internal organs. Blood was drawn with a 23 G syringe from the vena cava and collected in either a Microvette 500 LH-Gel tube or a Microvette 1,1 ml Z-Gel tube. In order to remove non-liver-associated lymphocytes, the liver was perfused with PBS through the portal vain until the complete liver was well-perfused indicated by blanching. The gallbladder was removed before excising the liver. Moreover, the spleen was removed and both organs were stored in wash medium on ice until further processing. Tissue from indicated organs or tumors were used for the extraction of DNA, RNA or for histological analysis and were therefore cut into cubic pieces of ~5 mm edge length with a clean scalpel. Tissue for DNA analysis was frozen in T1 buffer (Nucleo Spin Tissue Kit), tissue for RNA isolation was frozen in RNA*later* reagent. For histological analysis, tissue was fixed in 4% paraformaldehyde (PFA) for 24 hours and transferred in a PBS container until paraffin embedding. Livers were weight before and after pieces were removed for other analyzes to determine which proportion of the organ was used for LAL isolation. LALs and splenocytes were isolated as described in section 4.2.8.

4.2.13.6 *Ex vivo* peptide stimulation

For *ex vivo* peptide stimulation up to 4 x 10^6 freshly isolated splenocytes or LALs were plated into a U-bottom 96-well plate and stimulated with indicated peptides in a final concentration of 1 µg/ml. After one hour at 37°C, Brefeldin A (BFA) was added (1 mg/ml) leading to a total volume of 270 µl. Stimulation was continued for 16 hours at 37°C until an ICS (see section 4.2.16.3) was performed on the following day.

4.2.13.7 Immunohistochemistry

Tissue pieces were fixed in 4% paraformaldehyde (PFA) for 24 hours and stored in PBS until paraffin-embedding. Liver sections (2 µm) were stained with hematoxylin/eosin (HE), anti-GPC3 or anti-HBcAg. Immunohistochemistry was performed by the group of M. Heikenwälder or the Comparative experimental Pathology (CeP) supervised by K. Steiger. Immunohisto-chemistry was performed using a Leica Bond MAX system and tissue slides were scanned

using a SCN 400 slide scanner or an Aperio AT2 slide scanner. For quantification, tissue slides were analyzed using the algorithm “positive count v9” in Aperio Image Scope.

4.2.14 Enzyme-linked immunosorbent assay (ELISA)

4.2.14.1 IFNγ ELISA

To determine the concentration of IFNγ in supernatant of co-culture experiments, commercial available ELISA kits were used. Experiments were performed on MaxiSorb ELISA 96-well plates following manufacturer’s instructions. TMB substrate conversion was determined by measurement of OD_{450} subtracted by OD_{560} on an ELISA-Reader infinite F200.

4.2.14.2 HBV parameters

For *in vitro* experiments, success of infection and viremia, respectively, were determined by measurement of HBeAg levels in the supernatant of infected cells using Enzygnost HBe monoclonal kit on the BEP III platform. Alternatively, HBeAg BioAssay ELISA Kit and HBsAg BioAssay ELISA Kit were performed according to manufacturer’s instructions.

4.2.15 Enzyme-linked immuno spot assay

To identify and enumerate cytokine-producing cells at a single cell level, an enzyme-linked immuno spot assay (ELISPOT) was performed. For this purpose, splenocytes were thawed, resuspended in mTCM and rested overnight at 37°C. The following day, 1 x 10^5 splenocytes were incubated with either 1 µg/ml of indicated peptides or PMA/Ionomycin (400 ng/µl / 1 µg/ml) for 24 hours at 37°C. The assay was performed using the T-Track basic mouse IFNγ kit according to manufacturer’s instructions. Measurement of plates were performed on a CTL-ImmunoSpot® S6 Ultra-V Analyzer.

4.2.16 Flow cytometry

4.2.16.1 Surface staining

For surface staining, up to 1 x 10^6 cells were transferred to a V-bottom 96-well plate and washed twice with FACS buffer before the first staining step (450g, 2 min, 4°C). Subsequently cells were stained in a volume of 50 µl/well with respective antibodies diluted in FACS buffer. After incubation for 30 min on ice and in the dark, cells were washed three times with FACS buffer, finally resuspended in 100 – 200 µl FACS buffer and analyzed on a FACS Canto II or CytoFLEX S flow cytometer. Data analysis was performed using FlowJo.

In order to exclude dead cells from the analysis, dead cells were stained with i) propidium iodide (1 mg/ml) which was added to the cell suspension directly before measurement without

subsequent washing, ii) fixable viability dye eF780 added to the surface staining or iii) fixable EMA (1 µg/ml) 20 min in bright light before the addition of fluorochrome labelled antibodies.

If surface expression of the S-CAR (SΔ-CAR) and EGFRt were analyzed, three sequential staining steps were implemented. First, the S-CAR (SΔ-CAR) was stained with an anti-hIgG antibody. Next, EGFRt was stained with a biotin-labelled cetuximab. Finally, bound cetuximab was visualized with a fluorochrome-labelled Streptavidin together with the regular surface staining. In between serial staining steps, two washing steps with FACS buffer were performed.

4.2.16.2 Multimer staining

MHC I streptamers were used to stain for HBV-specific TCRs. Streptamers are a subgroup of multimers, consisting of MHC I-peptide complexes non-covalently attached to fluorescently labelled Strep-Tactin. Thereby, TCRs of certain specificities can be stained and detected by the fluorescent signal. Per sample, 0.4 µg multimer was labelled with 0.4 µg Strep-Tactin in 30 µl FACS buffer and incubated for 20 min on ice in the dark before adding to the cells. Thereafter, cell surface antibodies diluted in 20 µl FACS buffer were added and incubated for another 30 min on ice following the protocol for standard surface staining.

4.2.16.3 Intracellular cytokine staining

For intracellular cytokine staining (ICS), cells had to be permeabilized. Dead cells had to be stained before permeabilization using either EMA or fixable viability dye eF780. Cells were exposed to regular surface staining (see section 4.2.16.1) followed by two washing steps. Next, cells were permeabilized by resuspension in 100µl Cytofix/Cytoperm and incubated for 20 min on ice and in the dark. Subsequently, cells were washed two times with Perm/Wash buffer (650g, 3 min, 4°C), before intracellular staining was performed. Intracellular staining was performed according to surface staining, but antibodies were diluted in Perm/Wash buffer. After three final washing steps with Perm/Wash Buffer, cells were resuspended in 100 – 200 µl Perm/Wash and analyzed on a FACS Canto II or CytoFLEX S flow cytometer.

4.2.16.4 Determination of absolute cell count by flow cytometry

To be able to determine the absolute number of for instance transferred cells after adoptive transfer, 10 µl CountBright™ Absolute Counting Beads were added to the cell suspension directly before measurement on the flow cytometer. The absolute input cell count was calculated with the following formula:

$$\text{input cells} = \text{measured cells} \times \frac{\text{input beads}}{\text{measured beads}}$$

The valule obtained was extrapolated to the concentration in blood or to the whole organ considering the proportion of the organ that was used to isolate splenocytes or LALs.

4.2.17 Statistical analysis

Data are presented as (individual values in addition to) mean values with standard deviation (SD) or standard error of mean (SEM). Statistical significance was calculated as stated in individual figures using Prism 5.01 software.

FIGURES

REFERENCES

Abou-Alfa, G. K., Puig, O., Daniele, B., Kudo, M., Merle, P., Park, J. W., Ross, P., Peron, J. M., Ebert, O., Chan, S.*, et al.* (2016). Randomized phase II placebo controlled study of codrituzumab in previously treated patients with advanced hepatocellular carcinoma. Journal of hepatology *65*, 289-295.

Abou-Alfa, G. K., Yen, C. J., Hsu, C. H., O'Donoghue, J., Beylergil, V., Ruan, S., Pandit-Taskar, N., Gansukh, B., Lyashchenko, S. K., Ma, J.*, et al.* (2017). Phase Ib study of codrituzumab in combination with sorafenib in patients with non-curable advanced hepatocellular carcinoma (HCC). Cancer chemotherapy and pharmacology *79*, 421-429.

Al-Mahtab, M., Bazinet, M., and Vaillant, A. (2016). Safety and Efficacy of Nucleic Acid Polymers in Monotherapy and Combined with Immunotherapy in Treatment-Naive Bangladeshi Patients with HBeAg+ Chronic Hepatitis B Infection. PloS one *11*, e0156667.

Alarcon, V., Hernandez, S., Rubio, L., Alvarez, F., Flores, Y., Varas-Godoy, M., De Ferrari, G. V., Kann, M., Villanueva, R. A., and Loyola, A. (2016). The enzymes LSD1 and Set1A cooperate with the viral protein HBx to establish an active hepatitis B viral chromatin state. Scientific reports *6*, 25901.

Artyomov, M. N., Lis, M., Devadas, S., Davis, M. M., and Chakraborty, A. K. (2010). CD4 and CD8 binding to MHC molecules primarily acts to enhance Lck delivery. Proceedings of the National Academy of Sciences of the United States of America *107*, 16916-16921.

Azuma, H., Paulk, N., Ranade, A., Dorrell, C., Al-Dhalimy, M., Ellis, E., Strom, S., Kay, M. A., Finegold, M., and Grompe, M. (2007). Robust expansion of human hepatocytes in Fah-/-/Rag2-/-/Il2rg-/- mice. Nature biotechnology *25*, 903-910.

Backes, S., Jäger, C., Dembek, C. J., Kosinska, A. D., Bauer, T., Stephan, A.-S., Dišlers, A., Mutwiri, G., Busch, D. H., Babiuk, L. A.*, et al.* (2016). Protein-prime/modified vaccinia virus Ankara vector-boost vaccination overcomes tolerance in high-antigenemic HBV-transgenic mice. Vaccine *34*, 923-932.

Baeuerle, P. A., and Reinhardt, C. (2009). Bispecific T-cell engaging antibodies for cancer therapy. Cancer research *69*, 4941-4944.

Balar, A. V., Galsky, M. D., Rosenberg, J. E., Powles, T., Petrylak, D. P., Bellmunt, J., Loriot, Y., Necchi, A., Hoffman-Censits, J., Perez-Gracia, J. L.*, et al.* (2017). Atezolizumab as first-line treatment in cisplatin-ineligible patients with locally advanced and metastatic urothelial carcinoma: a single-arm, multicentre, phase 2 trial. Lancet (London, England) *389*, 67-76.

Balsitis, S., Gali, V., Mason, P. J., Chaniewski, S., Levine, S. M., Wichroski, M. J., Feulner, M., Song, Y., Granaldi, K., Loy, J. K.*, et al.* (2018). Safety and efficacy of anti-PD-L1 therapy in the woodchuck model of HBV infection. PloS one *13*, e0190058.

Belloni, L., Pollicino, T., De Nicola, F., Guerrieri, F., Raffa, G., Fanciulli, M., Raimondo, G., and Levrero, M. (2009). Nuclear HBx binds the HBV minichromosome and modifies the epigenetic

regulation of cccDNA function. Proceedings of the National Academy of Sciences of the United States of America *106*, 19975-19979.

Bengsch, B., Martin, B., and Thimme, R. (2014). Restoration of HBV-specific CD8+ T cell function by PD-1 blockade in inactive carrier patients is linked to T cell differentiation. Journal of hepatology *61*, 1212-1219.

Berger, C., Sommermeyer, D., Hudecek, M., Berger, M., Balakrishnan, A., Paszkiewicz, P. J., Kosasih, P. L., Rader, C., and Riddell, S. R. (2015). Safety of targeting ROR1 in primates with chimeric antigen receptor-modified T cells. Cancer immunology research *3*, 206-216.

Berger, C., Turtle, C. J., Jensen, M. C., and Riddell, S. R. (2009). Adoptive transfer of virus-specific and tumor-specific T cell immunity. Current opinion in immunology *21*, 224-232.

Bi, Y., Jiang, H., Wang, P., Song, B., Wang, H., Kong, X., and Li, Z. (2017). Treatment of hepatocellular carcinoma with a GPC3-targeted bispecific T cell engager. Oncotarget *8*, 52866-52876.

Bility, M. T., Cheng, L., Zhang, Z., Luan, Y., Li, F., Chi, L., Zhang, L., Tu, Z., Gao, Y., Fu, Y., *et al.* (2014). Hepatitis B virus infection and immunopathogenesis in a humanized mouse model: induction of human-specific liver fibrosis and M2-like macrophages. PLoS pathogens *10*, e1004032.

Bissig, K. D., Wieland, S. F., Tran, P., Isogawa, M., Le, T. T., Chisari, F. V., and Verma, I. M. (2010). Human liver chimeric mice provide a model for hepatitis B and C virus infection and treatment. The Journal of clinical investigation *120*, 924-930.

Bohne, F., Chmielewski, M., Ebert, G., Wiegmann, K., Kürschner, T., Schulze, A., Urban, S., Krönke, M., Abken, H., and Protzer, U. (2008). T Cells Redirected Against Hepatitis B Virus Surface Proteins Eliminate Infected Hepatocytes. Gastroenterology *134*, 239-247.

Boni, C., Fisicaro, P., Valdatta, C., Amadei, B., Di Vincenzo, P., Giuberti, T., Laccabue, D., Zerbini, A., Cavalli, A., Missale, G., *et al.* (2007). Characterization of hepatitis B virus (HBV)-specific T-cell dysfunction in chronic HBV infection. Journal of virology *81*, 4215-4225.

Bouchard, M. J., and Schneider, R. J. (2004). The enigmatic X gene of hepatitis B virus. Journal of virology *78*, 12725-12734.

Bourgine, M., Crabe, S., Lobaina, Y., Guillen, G., Aguilar, J. C., and Michel, M. L. (2018). Nasal route favors the induction of CD4(+) T cell responses in the liver of HBV-carrier mice immunized with a recombinant hepatitis B surface- and core-based therapeutic vaccine. Antiviral research *153*, 23-32.

Brahmer, J., Reckamp, K. L., Baas, P., Crino, L., Eberhardt, W. E., Poddubskaya, E., Antonia, S., Pluzanski, A., Vokes, E. E., Holgado, E., *et al.* (2015). Nivolumab versus Docetaxel in Advanced Squamous-Cell Non-Small-Cell Lung Cancer. The New England journal of medicine *373*, 123-135.

Bruix, J., Qin, S., Merle, P., Granito, A., Huang, Y. H., Bodoky, G., Pracht, M., Yokosuka, O., Rosmorduc, O., Breder, V., *et al.* (2017). Regorafenib for patients with hepatocellular

carcinoma who progressed on sorafenib treatment (RESORCE): a randomised, double-blind, placebo-controlled, phase 3 trial. Lancet (London, England) *389*, 56-66.

Bruix, J., Reig, M., and Sherman, M. (2016). Evidence-Based Diagnosis, Staging, and Treatment of Patients With Hepatocellular Carcinoma. Gastroenterology *150*, 835-853.

Burdette, D. L., Monroe, K. M., Sotelo-Troha, K., Iwig, J. S., Eckert, B., Hyodo, M., Hayakawa, Y., and Vance, R. E. (2011). STING is a direct innate immune sensor of cyclic di-GMP. Nature *478*, 515-518.

Burwitz, B. J., Wettengel, J. M., Mück-Häusl, M. A., Ringelhan, M., Ko, C., Festag, M. M., Hammond, K. B., Northrup, M., Bimber, B. N., Jacob, T.*, et al.* (2017). Hepatocytic expression of human sodium-taurocholate cotransporting polypeptide enables hepatitis B virus infection of macaques. Nature Communications *8*, 2146.

Butterfield, L. H., Meng, W. S., Koh, A., Vollmer, C. M., Ribas, A., Dissette, V. B., Faull, K., Glaspy, J. A., McBride, W. H., and Economou, J. S. (2001). T cell responses to HLA-A*0201-restricted peptides derived from human alpha fetoprotein. Journal of immunology (Baltimore, Md : 1950) *166*, 5300-5308.

Byam, J., Renz, J., and Millis, J. M. (2013). Liver transplantation for hepatocellular carcinoma. Hepatobiliary surgery and nutrition *2*, 22-30.

Cameron, B. J., Gerry, A. B., Dukes, J., Harper, J. V., Kannan, V., Bianchi, F. C., Grand, F., Brewer, J. E., Gupta, M., Plesa, G.*, et al.* (2013). Identification of a Titin-derived HLA-A1-presented peptide as a cross-reactive target for engineered MAGE A3-directed T cells. Science translational medicine *5*, 197ra103.

Capurro, M., Wanless, I. R., Sherman, M., Deboer, G., Shi, W., Miyoshi, E., and Filmus, J. (2003). Glypican-3: a novel serum and histochemical marker for hepatocellular carcinoma. Gastroenterology *125*, 89-97.

Caruso, H. G., Hurton, L. V., Najjar, A., Rushworth, D., Ang, S., Olivares, S., Mi, T., Switzer, K., Singh, H., Huls, H.*, et al.* (2015). Tuning Sensitivity of CAR to EGFR Density Limits Recognition of Normal Tissue While Maintaining Potent Antitumor Activity. Cancer research *75*, 3505-3518.

Cavenaugh, J. S., Awi, D., Mendy, M., Hill, A. V., Whittle, H., and McConkey, S. J. (2011). Partially randomized, non-blinded trial of DNA and MVA therapeutic vaccines based on hepatitis B virus surface protein for chronic HBV infection. PloS one *6*, e14626.

Chandran, S. S., Somerville, R. P. T., Yang, J. C., Sherry, R. M., Klebanoff, C. A., Goff, S. L., Wunderlich, J. R., Danforth, D. N., Zlott, D., Paria, B. C.*, et al.* (2017). Treatment of metastatic uveal melanoma with adoptive transfer of tumour-infiltrating lymphocytes: a single-centre, two-stage, single-arm, phase 2 study. The Lancet Oncology *18*, 792-802.

Chen, C., Li, K., Jiang, H., Song, F., Gao, H., Pan, X., Shi, B., Bi, Y., Wang, H., Wang, H., and Li, Z. (2017). Development of T cells carrying two complementary chimeric antigen receptors against glypican-3 and asialoglycoprotein receptor 1 for the treatment of hepatocellular carcinoma. Cancer Immunology, Immunotherapy *66*, 475-489.

Chen, G. D., Gu, J. L., Qiu, J., and Chen, L. Z. (2013). Outcomes and risk factors for hepatitis B virus (HBV) reactivation after kidney transplantation in occult HBV carriers. Transplant Infectious Disease *15*, 300-305.

Chen, J. D., Yang, H. I., Iloeje, U. H., You, S. L., Lu, S. N., Wang, L. Y., Su, J., Sun, C. A., Liaw, Y. F., and Chen, C. J. (2010a). Carriers of inactive hepatitis B virus are still at risk for hepatocellular carcinoma and liver-related death. Gastroenterology *138*, 1747-1754.

Chen, L., Zhao, H., Yang, X., Gao, J. Y., and Cheng, J. (2014). HBsAg-negative hepatitis B virus infection and hepatocellular carcinoma. Discovery medicine *18*, 189-193.

Chen, M. T., Billaud, J. N., Sallberg, M., Guidotti, L. G., Chisari, F. V., Jones, J., Hughes, J., and Milich, D. R. (2004). A function of the hepatitis B virus precore protein is to regulate the immune response to the core antigen. Proceedings of the National Academy of Sciences of the United States of America *101*, 14913-14918.

Chen, W., Kuolee, R., and Yan, H. (2010b). The potential of 3',5'-cyclic diguanylic acid (c-di-GMP) as an effective vaccine adjuvant. Vaccine *28*, 3080-3085.

Cheng, A. L., Kang, Y. K., Chen, Z., Tsao, C. J., Qin, S., Kim, J. S., Luo, R., Feng, J., Ye, S., Yang, T. S.*, et al.* (2009). Efficacy and safety of sorafenib in patients in the Asia-Pacific region with advanced hepatocellular carcinoma: a phase III randomised, double-blind, placebo-controlled trial. The Lancet Oncology *10*, 25-34.

Chiba, S., Baghdadi, M., Akiba, H., Yoshiyama, H., Kinoshita, I., Dosaka-Akita, H., Fujioka, Y., Ohba, Y., Gorman, J. V., Colgan, J. D.*, et al.* (2012). Tumor-infiltrating DCs suppress nucleic acid-mediated innate immune responses through interactions between the receptor TIM-3 and the alarmin HMGB1. Nature immunology *13*, 832-842.

Chisari, F. V., Isogawa, M., and Wieland, S. F. (2010). Pathogenesis of hepatitis B virus infection. Pathologie-biologie *58*, 258-266.

Cornberg, M., Protzer, U., Petersen, J., Wedemeyer, H., Berg, T., Jilg, W., Erhardt, A., Wirth, S., Sarrazin, C., Dollinger, M. M.*, et al.* (2011). [Prophylaxis, diagnosis and therapy of hepatitis B virus infection - the German guideline]. Zeitschrift fur Gastroenterologie *49*, 871-930.

Dandri, M., Burda, M. R., Torok, E., Pollok, J. M., Iwanska, A., Sommer, G., Rogiers, X., Rogler, C. E., Gupta, S., Will, H.*, et al.* (2001). Repopulation of mouse liver with human hepatocytes and in vivo infection with hepatitis B virus. Hepatology (Baltimore, Md) *33*, 981-988.

Dane, D. S., Cameron, C. H., and Briggs, M. (1970). Virus-like particles in serum of patients with Australia-antigen-associated hepatitis. Lancet (London, England) *1*, 695-698.

Dargan, A., Wong, S. Y., Coben, R., Conn, M., Dimarino, A. J., and Hann, H. W. (2017). Persistent risk for hepatocellular carcinoma after more than a decade of successful hepatitis B virus suppression. Minerva gastroenterologica e dietologica *63*, 74-76.

Dargel, C., Bassani-Sternberg, M., Hasreiter, J., Zani, F., Bockmann, J.-H., Thiele, F., Bohne, F., Wisskirchen, K., Wilde, S., Sprinzl, M. F.*, et al.* (2015). T Cells Engineered to Express a T-Cell Receptor Specific for Glypican-3 to Recognize and Kill Hepatoma Cells In Vitro and in Mice. Gastroenterology *149*, 1042-1052.

Davila, M. L., Riviere, I., Wang, X., Bartido, S., Park, J., Curran, K., Chung, S. S., Stefanski, J., Borquez-Ojeda, O., Olszewska, M.*, et al.* (2014). Efficacy and toxicity management of 19-28z CAR T cell therapy in B cell acute lymphoblastic leukemia. Science translational medicine *6*, 224ra225.

Desmond, C. P., Bartholomeusz, A., Gaudieri, S., Revill, P. A., and Lewin, S. R. (2008). A systematic review of T-cell epitopes in hepatitis B virus: identification, genotypic variation and relevance to antiviral therapeutics. Antiviral therapy *13*, 161-175.

Dion, S., Bourgine, M., Godon, O., Levillayer, F., and Michel, M.-L. (2013). Adeno-Associated Virus-Mediated Gene Transfer Leads to Persistent Hepatitis B Virus Replication in Mice Expressing HLA-A2 and HLA-DR1 Molecules. Journal of virology *87*, 5554-5563.

Duffy, A. G., Ulahannan, S. V., Makorova-Rusher, O., Rahma, O., Wedemeyer, H., Pratt, D., Davis, J. L., Hughes, M. S., Heller, T., ElGindi, M.*, et al.* (2017). Tremelimumab in combination with ablation in patients with advanced hepatocellular carcinoma. Journal of hepatology *66*, 545-551.

Eke, A. C., Eleje, G. U., Eke, U. A., Xia, Y., and Liu, J. (2017). Hepatitis B immunoglobulin during pregnancy for prevention of mother-to-child transmission of hepatitis B virus. The Cochrane database of systematic reviews *2*, Cd008545.

El-Khoueiry, A. B., Sangro, B., Yau, T., Crocenzi, T. S., Kudo, M., Hsu, C., Kim, T. Y., Choo, S. P., Trojan, J., Welling, T. H. R.*, et al.* (2017). Nivolumab in patients with advanced hepatocellular carcinoma (CheckMate 040): an open-label, non-comparative, phase 1/2 dose escalation and expansion trial. Lancet (London, England) *389*, 2492-2502.

El-Serag, H. B. (2011). Hepatocellular carcinoma. The New England journal of medicine *365*, 1118-1127.

El-Serag, H. B., Tran, T., and Everhart, J. E. (2004). Diabetes increases the risk of chronic liver disease and hepatocellular carcinoma. Gastroenterology *126*, 460-468.

Fagan, E., Davison, F., Smith, P., and Williams, R. (1986). FULMINANT HEPATITIS B IN SUCCESSIVE FEMALE SEXUAL PARTNERS OF TWO ANTI-HBe-POSITIVE MALES. The Lancet *328*, 538-540.

Ferrari, C., Penna, A., Bertoletti, A., Valli, A., Antoni, A. D., Giuberti, T., Cavalli, A., Petit, M. A., and Fiaccadori, F. (1990). Cellular immune response to hepatitis B virus-encoded antigens in acute and chronic hepatitis B virus infection. Journal of immunology (Baltimore, Md : 1950) *145*, 3442-3449.

Festag, M. M. (2018). Approaches to improve outcome of hepatitis B virus-specific chimeric antigen receptor T cell therapy. Dissertation.

Fischer Lindahl, K., and Wilson, D. (1977). Histocompatibility antigen-activated cytotoxic T lymphocytes. II. Estimates of the frequency and specificity of precursors, Vol 145).

Fontaine, H., Kahi, S., Chazallon, C., Bourgine, M., Varaut, A., Buffet, C., Godon, O., Meritet, J. F., Saidi, Y., Michel, M. L.*, et al.* (2015). Anti-HBV DNA vaccination does not prevent relapse

after discontinuation of analogues in the treatment of chronic hepatitis B: a randomised trial--ANRS HB02 VAC-ADN. Gut *64*, 139-147.

Forner, A., Llovet, J. M., and Bruix, J. (2012). Hepatocellular carcinoma. Lancet (London, England) *379*, 1245-1255.

Gaiser, M. R., Bongiorno, M., and Brownell, I. (2018). PD-L1 inhibition with avelumab for metastatic Merkel cell carcinoma. Expert review of clinical pharmacology *11*, 345-359.

Ganem, D. (1991). Assembly of hepadnaviral virions and subviral particles. Current topics in microbiology and immunology *168*, 61-83.

Ganem, D., and Prince, A. M. (2004). Hepatitis B virus infection--natural history and clinical consequences. The New England journal of medicine *350*, 1118-1129.

Gao, G., Vandenberghe, L. H., Alvira, M. R., Lu, Y., Calcedo, R., Zhou, X., and Wilson, J. M. (2004). Clades of Adeno-associated viruses are widely disseminated in human tissues. Journal of virology *78*, 6381-6388.

Gao, H., Li, K., Tu, H., Pan, X., Jiang, H., Shi, B., Kong, J., Wang, H., Yang, S., Gu, J., and Li, Z. (2014). Development of T Cells Redirected to Glypican-3 for the Treatment of Hepatocellular Carcinoma. Clinical Cancer Research *20*, 6418.

Gehring, A. J., Ho, Z. Z., Tan, A. T., Aung, M. O., Lee, K. H., Tan, K. C., Lim, S. G., and Bertoletti, A. (2009). Profile of tumor antigen-specific CD8 T cells in patients with hepatitis B virus-related hepatocellular carcinoma. Gastroenterology *137*, 682-690.

Gehring, A. J., Xue, S. A., Ho, Z. Z., Teoh, D., Ruedl, C., Chia, A., Koh, S., Lim, S. G., Maini, M. K., Stauss, H., and Bertoletti, A. (2011). Engineering virus-specific T cells that target HBV infected hepatocytes and hepatocellular carcinoma cell lines. Journal of hepatology *55*, 103-110.

Ghouri, Y. A., Mian, I., and Rowe, J. H. (2017). Review of hepatocellular carcinoma: Epidemiology, etiology, and carcinogenesis. Journal of Carcinogenesis *16*, 1.

Girones, R., and Miller, R. H. (1989). Mutation rate of the hepadnavirus genome. Virology *170*, 595-597.

Godon, O., Fontaine, H., Kahi, S., Meritet, J. F., Scott-Algara, D., Pol, S., Michel, M. L., and Bourgine, M. (2014). Immunological and antiviral responses after therapeutic DNA immunization in chronic hepatitis B patients efficiently treated by analogues. Molecular therapy : the journal of the American Society of Gene Therapy *22*, 675-684.

Goebeler, M. E., Knop, S., Viardot, A., Kufer, P., Topp, M. S., Einsele, H., Noppeney, R., Hess, G., Kallert, S., Mackensen, A.*, et al.* (2016). Bispecific T-Cell Engager (BiTE) Antibody Construct Blinatumomab for the Treatment of Patients With Relapsed/Refractory Non-Hodgkin Lymphoma: Final Results From a Phase I Study. Journal of clinical oncology : official journal of the American Society of Clinical Oncology *34*, 1104-1111.

Gross, G., Waks, T., and Eshhar, Z. (1989). Expression of immunoglobulin-T-cell receptor chimeric molecules as functional receptors with antibody-type specificity. Proceedings of the National Academy of Sciences of the United States of America *86*, 10024-10028.

Guedan, S., Posey, A. D., Jr., Shaw, C., Wing, A., Da, T., Patel, P. R., McGettigan, S. E., Casado-Medrano, V., Kawalekar, O. U., Uribe-Herranz, M.*, et al.* (2018). Enhancing CAR T cell persistence through ICOS and 4-1BB costimulation. JCI insight *3*.

Guidotti, L. G., and Chisari, F. V. (2006). Immunobiology and pathogenesis of viral hepatitis. Annual review of pathology *1*, 23-61.

Guidotti, L. G., Matzke, B., Schaller, H., and Chisari, F. V. (1995). High-level hepatitis B virus replication in transgenic mice. Journal of virology *69*, 6158-6169.

Guidotti, L. G., Rochford, R., Chung, J., Shapiro, M., Purcell, R., and Chisari, F. V. (1999). Viral clearance without destruction of infected cells during acute HBV infection. Science (New York, NY) *284*, 825-829.

Harris, D. T., Hager, M. V., Smith, S. N., Cai, Q., Stone, J. D., Kruger, P., Lever, M., Dushek, O., Schmitt, T. M., Greenberg, P. D., and Kranz, D. M. (2018). Comparison of T Cell Activities Mediated by Human TCRs and CARs That Use the Same Recognition Domains. Journal of immunology (Baltimore, Md : 1950) *200*, 1088-1100.

Harris, D. T., and Kranz, D. M. (2016). Adoptive T Cell Therapies: A Comparison of T Cell Receptors and Chimeric Antigen Receptors. Trends in pharmacological sciences *37*, 220-230.

Hartmann, J., Schüßler-Lenz, M., Bondanza, A., and Buchholz, C. J. (2017). Clinical development of CAR T cells—challenges and opportunities in translating innovative treatment concepts. EMBO Molecular Medicine *9*, 1183-1197.

Hasegawa, K., Huang, J., Wands, J. R., Obata, H., and Liang, T. J. (1991). Association of hepatitis B viral precore mutations with fulminant hepatitis B in Japan. Virology *185*, 460-463.

Hasegawa, M., Kawai, K., Mitsui, T., Taniguchi, K., Monnai, M., Wakui, M., Ito, M., Suematsu, M., Peltz, G., Nakamura, M., and Suemizu, H. (2011). The reconstituted 'humanized liver' in TK-NOG mice is mature and functional. Biochemical and biophysical research communications *405*, 405-410.

Hasreiter, J. (2014). Evaluation of bispecific antibodies for therapeutic applications in chronic hepatitis B. Master's Thesis.

Heiss, M. M., Murawa, P., Koralewski, P., Kutarska, E., Kolesnik, O. O., Ivanchenko, V. V., Dudnichenko, A. S., Aleknaviciene, B., Razbadauskas, A., Gore, M.*, et al.* (2010). The trifunctional antibody catumaxomab for the treatment of malignant ascites due to epithelial cancer: Results of a prospective randomized phase II/III trial. International Journal of Cancer Journal International du Cancer *127*, 2209-2221.

Hiroishi, K., Eguchi, J., Baba, T., Shimazaki, T., Ishii, S., Hiraide, A., Sakaki, M., Doi, H., Uozumi, S., Omori, R.*, et al.* (2010). Strong CD8(+) T-cell responses against tumor-associated antigens prolong the recurrence-free interval after tumor treatment in patients with hepatocellular carcinoma. Journal of gastroenterology *45*, 451-458.

Hodi, F. S., O'Day, S. J., McDermott, D. F., Weber, R. W., Sosman, J. A., Haanen, J. B., Gonzalez, R., Robert, C., Schadendorf, D., Hassel, J. C.*, et al.* (2010). Improved survival with ipilimumab in patients with metastatic melanoma. The New England journal of medicine *363*, 711-723.

Hombach, A., Koch, D., Sircar, R., Heuser, C., Diehl, V., Kruis, W., Pohl, C., and Abken, H. (1999). A chimeric receptor that selectively targets membrane-bound carcinoembryonic antigen (mCEA) in the presence of soluble CEA. Gene therapy *6*, 300-304.

Hooks, M. A., Wade, C. S., and Millikan, W. J., Jr. (1991). Muromonab CD-3: a review of its pharmacology, pharmacokinetics, and clinical use in transplantation. Pharmacotherapy *11*, 26-37.

Hosel, M., Lucifora, J., Michler, T., Holz, G., Gruffaz, M., Stahnke, S., Zoulim, F., Durantel, D., Heikenwalder, M., Nierhoff, D.*, et al.* (2014). Hepatitis B virus infection enhances susceptibility toward adeno-associated viral vector transduction in vitro and in vivo. Hepatology (Baltimore, Md) *59*, 2110-2120.

Hosken, N. A., and Bevan, M. J. (1990). Defective presentation of endogenous antigen by a cell line expressing class I molecules. Science (New York, NY) *248*, 367-370.

Hu, J., and Liu, K. (2017). Complete and Incomplete Hepatitis B Virus Particles: Formation, Function, and Application. Viruses *9*.

Huang, J., Brameshuber, M., Zeng, X., Xie, J., Li, Q. J., Chien, Y. H., Valitutti, S., and Davis, M. M. (2013). A single peptide-major histocompatibility complex ligand triggers digital cytokine secretion in CD4(+) T cells. Immunity *39*, 846-857.

Huang, J., Li, X., Coelho-dos-Reis, J. G. A., Wilson, J. M., and Tsuji, M. (2014). An AAV Vector-Mediated Gene Delivery Approach Facilitates Reconstitution of Functional Human CD8(+) T Cells in Mice. PloS one *9*, e88205.

Huang, L. R., Gäbel, Y. A., Graf, S., Arzberger, S., Kurts, C., Heikenwalder, M., Knolle, P. A., and Protzer, U. (2012). Transfer of HBV Genomes Using Low Doses of Adenovirus Vectors Leads to Persistent Infection in Immune Competent Mice. Gastroenterology *142*, 1447-1450.e1443.

Huang, L. R., Wu, H. L., Chen, P. J., and Chen, D. S. (2006). An immunocompetent mouse model for the tolerance of human chronic hepatitis B virus infection. Proceedings of the National Academy of Sciences of the United States of America *103*, 17862-17867.

Huang, Y. H., Zhu, C., Kondo, Y., Anderson, A. C., Gandhi, A., Russell, A., Dougan, S. K., Petersen, B. S., Melum, E., Pertel, T.*, et al.* (2015). CEACAM1 regulates TIM-3-mediated tolerance and exhaustion. Nature *517*, 386-390.

Hunt, C. M., McGill, J. M., Allen, M. I., and Condreay, L. D. (2000). Clinical relevance of hepatitis B viral mutations. Hepatology (Baltimore, Md) *31*, 1037-1044.

Hur, G. M., Lee, Y. I., Suh, D. J., Lee, J. H., and Lee, Y. I. (1996). Gradual accumulation of mutations in precore core region of HBV in patients with chronic active hepatitis: implications

of clustering changes in a small region of the HBV core region. Journal of medical virology *48*, 38-46.

Ikeda, M., Ohkawa, S., Okusaka, T., Mitsunaga, S., Kobayashi, S., Morizane, C., Suzuki, I., Yamamoto, S., and Furuse, J. (2014). Japanese phase I study of GC33, a humanized antibody against glypican-3 for advanced hepatocellular carcinoma. Cancer science *105*, 455-462.

Ilan, Y., Nagler, A., Adler, R., Naparstek, E., Or, R., Slavin, S., Brautbar, C., and Shouval, D. (1993). Adoptive transfer of immunity to hepatitis B virus after T cell-depleted allogeneic bone marrow transplantation. Hepatology (Baltimore, Md) *18*, 246-252.

Ishiguro, T., Sano, Y., Komatsu, S. I., Kamata-Sakurai, M., Kaneko, A., Kinoshita, Y., Shiraiwa, H., Azuma, Y., Tsunenari, T., Kayukawa, Y.*, et al.* (2017). An anti-glypican 3/CD3 bispecific T cell-redirecting antibody for treatment of solid tumors. Science translational medicine *9*.

Ishiguro, T., Sugimoto, M., Kinoshita, Y., Miyazaki, Y., Nakano, K., Tsunoda, H., Sugo, I., Ohizumi, I., Aburatani, H., Hamakubo, T.*, et al.* (2008). Anti-glypican 3 antibody as a potential antitumor agent for human liver cancer. Cancer research *68*, 9832-9838.

Javanbakht, H., Mueller, H., Walther, J., Zhou, X., Lopez, A., Pattupara, T., Blaising, J., Pedersen, L., Albaek, N., Jackerott, M.*, et al.* (2018). Liver-Targeted Anti-HBV Single-Stranded Oligonucleotides with Locked Nucleic Acid Potently Reduce HBV Gene Expression In Vivo. Molecular therapy Nucleic acids *11*, 441-454.

Jemal, A., Bray, F., Center, M. M., Ferlay, J., Ward, E., and Forman, D. (2011). Global cancer statistics. CA: a cancer journal for clinicians *61*, 69-90.

Jiang, S. S., Tang, Y., Zhang, Y. J., Weng, D. S., Zhou, Z. G., Pan, K., Pan, Q. Z., Wang, Q. J., Liu, Q., He, J.*, et al.* (2015). A phase I clinical trial utilizing autologous tumor-infiltrating lymphocytes in patients with primary hepatocellular carcinoma. Oncotarget *6*, 41339-41349.

Jiang, Z., Jiang, X., Chen, S., Lai, Y., Wei, X., Li, B., Lin, S., Wang, S., Wu, Q., Liang, Q.*, et al.* (2016). Anti-GPC3-CAR T Cells Suppress the Growth of Tumor Cells in Patient-Derived Xenografts of Hepatocellular Carcinoma. Frontiers in Immunology *7*, 690.

Jin, H. T., Anderson, A. C., Tan, W. G., West, E. E., Ha, S. J., Araki, K., Freeman, G. J., Kuchroo, V. K., and Ahmed, R. (2010). Cooperation of Tim-3 and PD-1 in CD8 T-cell exhaustion during chronic viral infection. Proceedings of the National Academy of Sciences of the United States of America *107*, 14733-14738.

Johnson, L. A., Morgan, R. A., Dudley, M. E., Cassard, L., Yang, J. C., Hughes, M. S., Kammula, U. S., Royal, R. E., Sherry, R. M., Wunderlich, J. R.*, et al.* (2009). Gene therapy with human and mouse T-cell receptors mediates cancer regression and targets normal tissues expressing cognate antigen. Blood *114*, 535-546.

Joshua, A. M., Monzon, J. G., Mihalcioiu, C., Hogg, D., Smylie, M., and Cheng, T. (2015). A phase 2 study of tremelimumab in patients with advanced uveal melanoma. Melanoma research *25*, 342-347.

Julander, J. G., Colonno, R. J., Sidwell, R. W., and Morrey, J. D. (2003). Characterization of antiviral activity of entecavir in transgenic mice expressing hepatitis B virus. Antiviral research *59*, 155-161.

Kageyama, S., Ikeda, H., Miyahara, Y., Imai, N., Ishihara, M., Saito, K., Sugino, S., Ueda, S., Ishikawa, T., Kokura, S.*, et al.* (2015). Adoptive Transfer of MAGE-A4 T-cell Receptor Gene-Transduced Lymphocytes in Patients with Recurrent Esophageal Cancer. Clinical cancer research : an official journal of the American Association for Cancer Research *21*, 2268-2277.

Kah, J., Koh, S., Volz, T., Ceccarello, E., Allweiss, L., Lutgehetmann, M., Bertoletti, A., and Dandri, M. (2017). Lymphocytes transiently expressing virus-specific T cell receptors reduce hepatitis B virus infection. The Journal of clinical investigation *127*, 3177-3188.

Kan, F., Ye, L., Yan, T., Cao, J., Zheng, J., and Li, W. (2017). Proteomic and transcriptomic studies of HBV-associated liver fibrosis of an AAV-HBV-infected mouse model. BMC Genomics *18*, 641.

Khan, S., Blackburn, M., Mao, D. L., Huber, R., Schlessinger, D., and Fant, M. (2001). Glypican-3 (GPC3) expression in human placenta: localization to the differentiated syncytiotrophoblast. Histology and histopathology *16*, 71-78.

Kim, C. M., Koike, K., Saito, I., Miyamura, T., and Jay, G. (1991). HBx gene of hepatitis B virus induces liver cancer in transgenic mice. Nature *351*, 317-320.

Knolle, P. A., and Thimme, R. (2014). Hepatic immune regulation and its involvement in viral hepatitis infection. Gastroenterology *146*, 1193-1207.

Koh, S., Kah, J., Tham, C. Y. L., Yang, N., Ceccarello, E., Chia, A., Chen, M., Khakpoor, A., Pavesi, A., Tan, A. T.*, et al.* (2018). Non-lytic Lymphocytes Engineered to Express Virus-specific T-cell Receptors Limit HBV Infection by Activating APOBEC3. Gastroenterology.

Koh, S., Shimasaki, N., Suwanarusk, R., Ho, Z. Z., Chia, A., Banu, N., Howland, S. W., Ong, A. S., Gehring, A. J., Stauss, H.*, et al.* (2013). A practical approach to immunotherapy of hepatocellular carcinoma using T cells redirected against hepatitis B virus. Molecular therapy Nucleic acids *2*, e114.

Komori, H., Nakatsura, T., Senju, S., Yoshitake, Y., Motomura, Y., Ikuta, Y., Fukuma, D., Yokomine, K., Harao, M., Beppu, T.*, et al.* (2006). Identification of HLA-A2- or HLA-A24-restricted CTL epitopes possibly useful for glypican-3-specific immunotherapy of hepatocellular carcinoma. Clinical cancer research : an official journal of the American Association for Cancer Research *12*, 2689-2697.

Kontermann, R. E., and Brinkmann, U. (2015). Bispecific antibodies. Drug Discovery Today *20*, 838-847.

Kosinska, A. D., Bauer, T., and Protzer, U. (2017). Therapeutic vaccination for chronic hepatitis B. Current opinion in virology *23*, 75-81.

Kosinska, A. D., Zhang, E., Johrden, L., Liu, J., Seiz, P. L., Zhang, X., Ma, Z., Kemper, T., Fiedler, M., Glebe, D.*, et al.* (2013). Combination of DNA Prime – Adenovirus Boost

Immunization with Entecavir Elicits Sustained Control of Chronic Hepatitis B in the Woodchuck Model. PLoS pathogens *9*, e1003391.

Kosinska, A. D., Zhang, E., Lu, M., and Roggendorf, M. (2010). Therapeutic Vaccination in Chronic Hepatitis B: Preclinical Studies in the Woodchuck. Hepatitis Research and Treatment *2010*, 817580.

Kramvis, A. (2014). Genotypes and genetic variability of hepatitis B virus. Intervirology *57*, 141-150.

Krebs, K., Böttinger, N., Huang, L. R., Chmielewski, M., Arzberger, S., Gasteiger, G., Jäger, C., Schmitt, E., Bohne, F., Aichler, M.*, et al.* (2013). T Cells Expressing a Chimeric Antigen Receptor That Binds Hepatitis B Virus Envelope Proteins Control Virus Replication in Mice. Gastroenterology *145*, 456-465.

Kreppel, F. (2014). Production of high-capacity adenovirus vectors. Methods in molecular biology (Clifton, NJ) *1089*, 211-229.

Krummel, M. F., and Allison, J. P. (1995). CD28 and CTLA-4 have opposing effects on the response of T cells to stimulation. The Journal of experimental medicine *182*, 459-465.

Kruse, R. L., Shum, T., Legras, X., Barzi, M., Pankowicz, F. P., Gottschalk, S., and Bissig, K. D. (2017). In Situ Liver Expression of HBsAg/CD3-Bispecific Antibodies for HBV Immunotherapy. Molecular therapy Methods & clinical development *7*, 32-41.

Kruse, R. L., Shum, T., Tashiro, H., Barzi, M., Yi, Z., Whitten-Bauer, C., Legras, X., Bissig-Choisat, B., Garaigorta, U., Gottschalk, S., and Bissig, K. D. (2018). HBsAg-redirected T cells exhibit antiviral activity in HBV-infected human liver chimeric mice. Cytotherapy *20*, 697-705.

Kudo, M., Finn, R. S., Qin, S., Han, K. H., Ikeda, K., Piscaglia, F., Baron, A., Park, J. W., Han, G., Jassem, J.*, et al.* (2018). Lenvatinib versus sorafenib in first-line treatment of patients with unresectable hepatocellular carcinoma: a randomised phase 3 non-inferiority trial. Lancet (London, England) *391*, 1163-1173.

Kumar, S. R. P., Hoffman, B. E., Terhorst, C., de Jong, Y. P., and Herzog, R. W. (2017). The Balance between CD8(+) T Cell-Mediated Clearance of AAV-Encoded Antigen in the Liver and Tolerance Is Dependent on the Vector Dose. Molecular therapy : the journal of the American Society of Gene Therapy *25*, 880-891.

Kunkele, A., Taraseviciute, A., Finn, L. S., Johnson, A. J., Berger, C., Finney, O., Chang, C. A., Rolczynski, L. S., Brown, C., Mgebroff, S.*, et al.* (2017). Preclinical Assessment of CD171-Directed CAR T-cell Adoptive Therapy for Childhood Neuroblastoma: CE7 Epitope Target Safety and Product Manufacturing Feasibility. Clinical cancer research : an official journal of the American Association for Cancer Research *23*, 466-477.

Kürschner, T. (2000). Konstruktion und Screening von Antikörperbibliotheken gegen Oberflächenantigene. Dissertation.

Kusumoto, S., Tanaka, Y., Suzuki, R., Watanabe, T., Nakata, M., Takasaki, H., Fukushima, N., Fukushima, T., Moriuchi, Y., Itoh, K.*, et al.* (2015). Monitoring of Hepatitis B Virus (HBV) DNA and Risk of HBV Reactivation in B-Cell Lymphoma: A Prospective Observational Study.

Clinical infectious diseases : an official publication of the Infectious Diseases Society of America *61*, 719-729.

Larkin, J., Hodi, F. S., and Wolchok, J. D. (2015). Combined Nivolumab and Ipilimumab or Monotherapy in Untreated Melanoma. The New England journal of medicine *373*, 1270-1271.

Lau, G. K., Lok, A. S., Liang, R. H., Lai, C. L., Chiu, E. K., Lau, Y. L., and Lam, S. K. (1997). Clearance of hepatitis B surface antigen after bone marrow transplantation: role of adoptive immunity transfer. Hepatology (Baltimore, Md) *25*, 1497-1501.

Le, A. X., Bernhard, E. J., Holterman, M. J., Strub, S., Parham, P., Lacy, E., and Engelhard, V. H. (1989). Cytotoxic T cell responses in HLA-A2.1 transgenic mice. Recognition of HLA alloantigens and utilization of HLA-A2.1 as a restriction element. Journal of immunology (Baltimore, Md : 1950) *142*, 1366-1371.

Lee, J. H., Lee, Y., Lee, M., Heo, M. K., Song, J. S., Kim, K. H., Lee, H., Yi, N. J., Lee, K. W., Suh, K. S.*, et al.* (2015). A phase I/IIa study of adjuvant immunotherapy with tumour antigen-pulsed dendritic cells in patients with hepatocellular carcinoma. British journal of cancer *113*, 1666-1676.

Leisegang, M., Wilde, S., Spranger, S., Milosevic, S., Frankenberger, B., Uckert, W., and Schendel, D. J. (2010). MHC-restricted fratricide of human lymphocytes expressing survivin-specific transgenic T cell receptors. The Journal of clinical investigation *120*, 3869-3877.

Lempp, F. A., Wiedtke, E., Qu, B., Roques, P., Chemin, I., Vondran, F. W. R., Le Grand, R., Grimm, D., and Urban, S. (2017). Sodium taurocholate cotransporting polypeptide is the limiting host factor of hepatitis B virus infection in macaque and pig hepatocytes. Hepatology (Baltimore, Md) *66*, 703-716.

Levrero, M., Testoni, B., and Zoulim, F. (2016). HBV cure: why, how, when? Current opinion in virology *18*, 135-143.

Li, G., Zhu, Y., Shao, D., Chang, H., Zhang, X., Zhou, D., Gao, Y., Lan, K., and Deng, Q. (2018). Recombinant covalently closed circular DNA of hepatitis B virus induces long-term viral persistence with chronic hepatitis in a mouse model. Hepatology (Baltimore, Md) *67*, 56-70.

Li, H., Wu, K., Tao, K., Chen, L., Zheng, Q., Lu, X., Liu, J., Shi, L., Liu, C., Wang, G., and Zou, W. (2012). Tim-3/galectin-9 signaling pathway mediates T-cell dysfunction and predicts poor prognosis in patients with hepatitis B virus-associated hepatocellular carcinoma. Hepatology (Baltimore, Md) *56*, 1342-1351.

Li, K., Pan, X., Bi, Y., Xu, W., Chen, C., Gao, H., Shi, B., Jiang, H., Yang, S., Jiang, L., and Li, Z. (2016a). Adoptive immunotherapy using T lymphocytes redirected to glypican-3 for the treatment of lung squamous cell carcinoma. Oncotarget *7*, 2496-2507.

Li, W., Guo, L., Rathi, P., Marinova, E., Gao, X., Wu, M.-F., Liu, H., Dotti, G., Gottschalk, S., Metelitsa, L. S., and Heczey, A. (2016b). Redirecting T Cells to Glypican-3 with 4-1BB Zeta Chimeric Antigen Receptors Results in Th1 Polarization and Potent Antitumor Activity. Human Gene Therapy *28*, 437-448.

Lindh, M., Horal, P., Dhillon, A. P., Furuta, Y., and Norkrans, G. (1996). Hepatitis B virus carriers without precore mutations in hepatitis B e antigen-negative stage show more severe liver damage. Hepatology (Baltimore, Md) *24*, 494-501.

Linette, G. P., Stadtmauer, E. A., Maus, M. V., Rapoport, A. P., Levine, B. L., Emery, L., Litzky, L., Bagg, A., Carreno, B. M., Cimino, P. J.*, et al.* (2013). Cardiovascular toxicity and titin cross-reactivity of affinity-enhanced T cells in myeloma and melanoma. Blood *122*, 863-871.

Liu, J., Zhang, E., Ma, Z., Wu, W., Kosinska, A., Zhang, X., Moller, I., Seiz, P., Glebe, D., Wang, B.*, et al.* (2014). Enhancing virus-specific immunity in vivo by combining therapeutic vaccination and PD-L1 blockade in chronic hepadnaviral infection. PLoS pathogens *10*, e1003856.

Liu, X., Jiang, S., Fang, C., Yang, S., Olalere, D., Pequignot, E. C., Cogdill, A. P., Li, N., Ramones, M., Granda, B.*, et al.* (2015). Affinity-Tuned ErbB2 or EGFR Chimeric Antigen Receptor T Cells Exhibit an Increased Therapeutic Index against Tumors in Mice. Cancer research *75*, 3596-3607.

Llovet, J. M., and Bruix, J. (2008). Novel advancements in the management of hepatocellular carcinoma in 2008. Journal of hepatology *48*, S20-S37.

Llovet, J. M., Ricci, S., Mazzaferro, V., Hilgard, P., Gane, E., Blanc, J. F., de Oliveira, A. C., Santoro, A., Raoul, J. L., Forner, A.*, et al.* (2008). Sorafenib in advanced hepatocellular carcinoma. The New England journal of medicine *359*, 378-390.

Loirat, D., Lemonnier, F. A., and Michel, M. L. (2000). Multiepitopic HLA-A*0201-restricted immune response against hepatitis B surface antigen after DNA-based immunization. Journal of immunology (Baltimore, Md : 1950) *165*, 4748-4755.

Lok, A. S., Akarca, U., and Greene, S. (1994). Mutations in the pre-core region of hepatitis B virus serve to enhance the stability of the secondary structure of the pre-genome encapsidation signal. Proceedings of the National Academy of Sciences of the United States of America *91*, 4077-4081.

Lok, A. S., Pan, C. Q., Han, S. H., Trinh, H. N., Fessel, W. J., Rodell, T., Massetto, B., Lin, L., Gaggar, A., Subramanian, G. M.*, et al.* (2016). Randomized phase II study of GS-4774 as a therapeutic vaccine in virally suppressed patients with chronic hepatitis B. Journal of hepatology *65*, 509-516.

Long, A. H., Haso, W. M., Shern, J. F., Wanhainen, K. M., Murgai, M., Ingaramo, M., Smith, J. P., Walker, A. J., Kohler, M. E., Venkateshwara, V. R.*, et al.* (2015). 4-1BB costimulation ameliorates T cell exhaustion induced by tonic signaling of chimeric antigen receptors. Nature medicine *21*, 581-590.

Lu, Y. C., Parker, L. L., Lu, T., Zheng, Z., Toomey, M. A., White, D. E., Yao, X., Li, Y. F., Robbins, P. F., Feldman, S. A.*, et al.* (2017). Treatment of Patients With Metastatic Cancer Using a Major Histocompatibility Complex Class II-Restricted T-Cell Receptor Targeting the Cancer Germline Antigen MAGE-A3. Journal of clinical oncology : official journal of the American Society of Clinical Oncology *35*, 3322-3329.

Lucifora, J., Arzberger, S., Durantel, D., Belloni, L., Strubin, M., Levrero, M., Zoulim, F., Hantz, O., and Protzer, U. (2011). Hepatitis B virus X protein is essential to initiate and maintain virus replication after infection. Journal of hepatology *55*, 996-1003.

Lucifora, J., Salvetti, A., Marniquet, X., Mailly, L., Testoni, B., Fusil, F., Inchauspe, A., Michelet, M., Michel, M. L., Levrero, M.*, et al.* (2017). Detection of the hepatitis B virus (HBV) covalently-closed-circular DNA (cccDNA) in mice transduced with a recombinant AAV-HBV vector. Antiviral research *145*, 14-19.

Maini, M. K., Boni, C., Ogg, G. S., King, A. S., Reignat, S., Lee, C. K., Larrubia, J. R., Webster, G. J., McMichael, A. J., Ferrari, C.*, et al.* (1999). Direct ex vivo analysis of hepatitis B virus-specific CD8(+) T cells associated with the control of infection. Gastroenterology *117*, 1386-1396.

Maio, M., Scherpereel, A., Calabro, L., Aerts, J., Cedres Perez, S., Bearz, A., Nackaerts, K., Fennell, D. A., Kowalski, D., Tsao, A. S.*, et al.* (2017). Tremelimumab as second-line or third-line treatment in relapsed malignant mesothelioma (DETERMINE): a multicentre, international, randomised, double-blind, placebo-controlled phase 2b trial. The Lancet Oncology *18*, 1261-1273.

Mancini-Bourgine, M., Fontaine, H., Scott-Algara, D., Pol, S., Brechot, C., and Michel, M. L. (2004). Induction or expansion of T-cell responses by a hepatitis B DNA vaccine administered to chronic HBV carriers. Hepatology (Baltimore, Md) *40*, 874-882.

Mason, W. S. (2015). Animal Models and the Molecular Biology of Hepadnavirus Infection. Cold Spring Harbor perspectives in medicine *5*, a021352.

Maude, S. L., Frey, N., Shaw, P. A., Aplenc, R., Barrett, D. M., Bunin, N. J., Chew, A., Gonzalez, V. E., Zheng, Z., Lacey, S. F.*, et al.* (2014). Chimeric antigen receptor T cells for sustained remissions in leukemia. The New England journal of medicine *371*, 1507-1517.

Maude, S. L., Laetsch, T. W., Buechner, J., Rives, S., Boyer, M., Bittencourt, H., Bader, P., Verneris, M. R., Stefanski, H. E., Myers, G. D.*, et al.* (2018). Tisagenlecleucel in Children and Young Adults with B-Cell Lymphoblastic Leukemia. The New England journal of medicine *378*, 439-448.

Michler, T., Grosse, S., Mockenhaupt, S., Roder, N., Stuckler, F., Knapp, B., Ko, C., Heikenwalder, M., Protzer, U., and Grimm, D. (2016). Blocking sense-strand activity improves potency, safety and specificity of anti-hepatitis B virus short hairpin RNA. EMBO Mol Med *8*, 1082-1098.

Milich, D., and Liang, T. J. (2003). Exploring the biological basis of hepatitis B e antigen in hepatitis B virus infection. Hepatology (Baltimore, Md) *38*, 1075-1086.

Mingozzi, F., Liu, Y. L., Dobrzynski, E., Kaufhold, A., Liu, J. H., Wang, Y., Arruda, V. R., High, K. A., and Herzog, R. W. (2003). Induction of immune tolerance to coagulation factor IX antigen by in vivo hepatic gene transfer. The Journal of clinical investigation *111*, 1347-1356.

Mizukoshi, E., Nakamoto, Y., Marukawa, Y., Arai, K., Yamashita, T., Tsuji, H., Kuzushima, K., Takiguchi, M., and Kaneko, S. (2006). Cytotoxic T cell responses to human telomerase reverse

transcriptase in patients with hepatocellular carcinoma. Hepatology (Baltimore, Md) *43*, 1284-1294.

Mozessohn, L., Chan, K. K., Feld, J. J., and Hicks, L. K. (2015). Hepatitis B reactivation in HBsAg-negative/HBcAb-positive patients receiving rituximab for lymphoma: a meta-analysis. Journal of viral hepatitis *22*, 842-849.

Murphy, K., and Weaver, C. (2016). Janeway's immunobiology. Garland Science Publishing.

Nakagawa, H., Mizukoshi, E., Kobayashi, E., Tamai, T., Hamana, H., Ozawa, T., Kishi, H., Kitahara, M., Yamashita, T., Arai, K.*, et al.* (2017). Association Between High-Avidity T-Cell Receptors, Induced by alpha-Fetoprotein-Derived Peptides, and Anti-Tumor Effects in Patients With Hepatocellular Carcinoma. Gastroenterology *152*, 1395-1406.e1310.

Nakano, K., Orita, T., Nezu, J., Yoshino, T., Ohizumi, I., Sugimoto, M., Furugaki, K., Kinoshita, Y., Ishiguro, T., Hamakubo, T.*, et al.* (2009). Anti-glypican 3 antibodies cause ADCC against human hepatocellular carcinoma cells. Biochemical and biophysical research communications *378*, 279-284.

Nakayama, M., Akiba, H., Takeda, K., Kojima, Y., Hashiguchi, M., Azuma, M., Yagita, H., and Okumura, K. (2009). Tim-3 mediates phagocytosis of apoptotic cells and cross-presentation. Blood *113*, 3821-3830.

Nassal, M. (2015). HBV cccDNA: viral persistence reservoir and key obstacle for a cure of chronic hepatitis B. Gut *64*, 1972-1984.

Neelapu, S. S., Locke, F. L., Bartlett, N. L., Lekakis, L. J., Miklos, D. B., Jacobson, C. A., Braunschweig, I., Oluwole, O. O., Siddiqi, T., Lin, Y.*, et al.* (2017). Axicabtagene Ciloleucel CAR T-Cell Therapy in Refractory Large B-Cell Lymphoma. The New England journal of medicine *377*, 2531-2544.

Ngiow, S. F., von Scheidt, B., Akiba, H., Yagita, H., Teng, M. W., and Smyth, M. J. (2011). Anti-TIM3 antibody promotes T cell IFN-gamma-mediated antitumor immunity and suppresses established tumors. Cancer research *71*, 3540-3551.

Nishida, N., and Kudo, M. (2017). Immunological Microenvironment of Hepatocellular Carcinoma and Its Clinical Implication. Oncology *92 Suppl 1*, 40-49.

Nolan, K. F., Yun, C. O., Akamatsu, Y., Murphy, J. C., Leung, S. O., Beecham, E. J., and Junghans, R. P. (1999). Bypassing immunization: optimized design of "designer T cells" against carcinoembryonic antigen (CEA)-expressing tumors, and lack of suppression by soluble CEA. Clinical cancer research : an official journal of the American Association for Cancer Research *5*, 3928-3941.

Obenaus, M., Leitao, C., Leisegang, M., Chen, X., Gavvovidis, I., van der Bruggen, P., Uckert, W., Schendel, D. J., and Blankenstein, T. (2015). Identification of human T-cell receptors with optimal affinity to cancer antigens using antigen-negative humanized mice. Nature biotechnology *33*, 402-407.

Ochel, A., Cebula, M., Riehn, M., Hillebrand, U., Lipps, C., Schirmbeck, R., Hauser, H., and Wirth, D. (2016). Effective intrahepatic CD8+ T-cell immune responses are induced by low but not high numbers of antigen-expressing hepatocytes. Cell Mol Immunol *13*, 805-815.

Op den Brouw, M. L., Binda, R. S., van Roosmalen, M. H., Protzer, U., Janssen, H. L., van der Molen, R. G., and Woltman, A. M. (2009). Hepatitis B virus surface antigen impairs myeloid dendritic cell function: a possible immune escape mechanism of hepatitis B virus. Immunology *126*, 280-289.

Pajot, A., Michel, M. L., Fazilleau, N., Pancre, V., Auriault, C., Ojcius, D. M., Lemonnier, F. A., and Lone, Y. C. (2004). A mouse model of human adaptive immune functions: HLA-A2.1-/HLA-DR1-transgenic H-2 class I-/class II-knockout mice. European journal of immunology *34*, 3060-3069.

Palmiter, R. D., Sandgren, E. P., Avarbock, M. R., Allen, D. D., and Brinster, R. L. (1991). Heterologous introns can enhance expression of transgenes in mice. Proceedings of the National Academy of Sciences of the United States of America *88*, 478-482.

Pancholi, P., Lee, D. H., Liu, Q., Tackney, C., Taylor, P., Perkus, M., Andrus, L., Brotman, B., and Prince, A. M. (2001). DNA prime/canarypox boost-based immunotherapy of chronic hepatitis B virus infection in a chimpanzee. Hepatology (Baltimore, Md) *33*, 448-454.

Parkin, D. M. (2006). The global health burden of infection-associated cancers in the year 2002. International journal of cancer *118*, 3030-3044.

Parry, R. V., Chemnitz, J. M., Frauwirth, K. A., Lanfranco, A. R., Braunstein, I., Kobayashi, S. V., Linsley, P. S., Thompson, C. B., and Riley, J. L. (2005). CTLA-4 and PD-1 receptors inhibit T-cell activation by distinct mechanisms. Molecular and cellular biology *25*, 9543-9553.

Parvatiyar, K., Zhang, Z., Teles, R. M., Ouyang, S., Jiang, Y., Iyer, S. S., Zaver, S. A., Schenk, M., Zeng, S., Zhong, W.*, et al.* (2012). The helicase DDX41 recognizes the bacterial secondary messengers cyclic di-GMP and cyclic di-AMP to activate a type I interferon immune response. Nature immunology *13*, 1155-1161.

Pascolo, S., Bervas, N., Ure, J. M., Smith, A. G., Lemonnier, F. A., and Perarnau, B. (1997). HLA-A2.1-restricted education and cytolytic activity of CD8(+) T lymphocytes from beta2 microglobulin (beta2m) HLA-A2.1 monochain transgenic H-2Db beta2m double knockout mice. The Journal of experimental medicine *185*, 2043-2051.

Peeridogaheh, H., Meshkat, Z., Habibzadeh, S., Arzanlou, M., Shahi, J. M., Rostami, S., Gerayli, S., and Teimourpour, R. (2018). Current concepts on immunopathogenesis of hepatitis B virus infection. Virus research *245*, 29-43.

Peng, G., Li, S., Wu, W., Sun, Z., Chen, Y., and Chen, Z. (2008). Circulating CD4(+) CD25(+) regulatory T cells correlate with chronic hepatitis B infection. Immunology *123*, 57-65.

Peppa, D., Gill, U. S., Reynolds, G., Easom, N. J. W., Pallett, L. J., Schurich, A., Micco, L., Nebbia, G., Singh, H. D., Adams, D. H.*, et al.* (2013). Up-regulation of a death receptor renders antiviral T cells susceptible to NK cell–mediated deletion. The Journal of experimental medicine *210*, 99.

Peters, S., Gettinger, S., Johnson, M. L., Janne, P. A., Garassino, M. C., Christoph, D., Toh, C. K., Rizvi, N. A., Chaft, J. E., Carcereny Costa, E.*, et al.* (2017). Phase II Trial of Atezolizumab As First-Line or Subsequent Therapy for Patients With Programmed Death-Ligand 1-Selected Advanced Non-Small-Cell Lung Cancer (BIRCH). Journal of clinical oncology : official journal of the American Society of Clinical Oncology *35*, 2781-2789.

Pol, S., Nalpas, B., Driss, F., Michel, M. L., Tiollais, P., Denis, J., and Brecho, C. (2001). Efficacy and limitations of a specific immunotherapy in chronic hepatitis B. Journal of hepatology *34*, 917-921.

Protzer, U., and Knolle, P. (2016). "To Be or Not to Be": Immune Tolerance in Chronic Hepatitis B. Gastroenterology *151*, 805-806.

Qasim, W., Brunetto, M., Gehring, A. J., Xue, S. A., Schurich, A., Khakpoor, A., Zhan, H., Ciccorossi, P., Gilmour, K., Cavallone, D.*, et al.* (2015). Immunotherapy of HCC metastases with autologous T cell receptor redirected T cells, targeting HBsAg in a liver transplant patient. Journal of hepatology *62*, 486-491.

Quitt, O. (2013). Generation and functional analysis of bispecific antibodies for immunotherapy of chronic hepatitis B virus infection. Master's Thesis.

Raziorrouh, B., Schraut, W., Gerlach, T., Nowack, D., Gruner, N. H., Ulsenheimer, A., Zachoval, R., Wachtler, M., Spannagl, M., Haas, J.*, et al.* (2010). The immunoregulatory role of CD244 in chronic hepatitis B infection and its inhibitory potential on virus-specific CD8+ T-cell function. Hepatology (Baltimore, Md) *52*, 1934-1947.

Rehermann, B. (2013). Pathogenesis of chronic viral hepatitis: differential roles of T cells and NK cells. Nature medicine *19*, 859-868.

Revill, P., Testoni, B., Locarnini, S., and Zoulim, F. (2016). Global strategies are required to cure and eliminate HBV infection. Nature reviews Gastroenterology & hepatology *13*, 239-248.

Riviere, L., Gerossier, L., Ducroux, A., Dion, S., Deng, Q., Michel, M. L., Buendia, M. A., Hantz, O., and Neuveut, C. (2015). HBx relieves chromatin-mediated transcriptional repression of hepatitis B viral cccDNA involving SETDB1 histone methyltransferase. Journal of hepatology *63*, 1093-1102.

Robbins, P. F., Kassim, S. H., Tran, T. L., Crystal, J. S., Morgan, R. A., Feldman, S. A., Yang, J. C., Dudley, M. E., Wunderlich, J. R., Sherry, R. M.*, et al.* (2015). A pilot trial using lymphocytes genetically engineered with an NY-ESO-1-reactive T-cell receptor: long-term follow-up and correlates with response. Clinical cancer research : an official journal of the American Association for Cancer Research *21*, 1019-1027.

Robert, C., Schachter, J., Long, G. V., Arance, A., Grob, J. J., Mortier, L., Daud, A., Carlino, M. S., McNeil, C., Lotem, M.*, et al.* (2015). Pembrolizumab versus Ipilimumab in Advanced Melanoma. The New England journal of medicine *372*, 2521-2532.

Rosenberg, S. A., Yang, J. C., Sherry, R. M., Kammula, U. S., Hughes, M. S., Phan, G. Q., Citrin, D. E., Restifo, N. P., Robbins, P. F., Wunderlich, J. R.*, et al.* (2011). Durable complete responses in heavily pretreated patients with metastatic melanoma using T-cell transfer

immunotherapy. Clinical cancer research : an official journal of the American Association for Cancer Research *17*, 4550-4557.

Royal, R. E., Levy, C., Turner, K., Mathur, A., Hughes, M., Kammula, U. S., Sherry, R. M., Topalian, S. L., Yang, J. C., Lowy, I., and Rosenberg, S. A. (2010). Phase 2 trial of single agent Ipilimumab (anti-CTLA-4) for locally advanced or metastatic pancreatic adenocarcinoma. Journal of immunotherapy (Hagerstown, Md : 1997) *33*, 828-833.

Sabatos-Peyton, C. A., Nevin, J., Brock, A., Venable, J. D., Tan, D. J., Kassam, N., Xu, F., Taraszka, J., Wesemann, L., Pertel, T.*, et al.* (2018). Blockade of Tim-3 binding to phosphatidylserine and CEACAM1 is a shared feature of anti-Tim-3 antibodies that have functional efficacy. Oncoimmunology *7*, e1385690.

Sakuishi, K., Apetoh, L., Sullivan, J. M., Blazar, B. R., Kuchroo, V. K., and Anderson, A. C. (2010). Targeting Tim-3 and PD-1 pathways to reverse T cell exhaustion and restore anti-tumor immunity. The Journal of experimental medicine *207*, 2187-2194.

Salter, R. D., Howell, D. N., and Cresswell, P. (1985). Genes regulating HLA class I antigen expression in T-B lymphoblast hybrids. Immunogenetics *21*, 235-246.

Sanjana, N. E., Shalem, O., and Zhang, F. (2014). Improved vectors and genome-wide libraries for CRISPR screening. Nature methods *11*, 783-784.

Sartorius, K., Sartorius, B., Aldous, C., Govender, P. S., and Madiba, T. E. (2015). Global and country underestimation of hepatocellular carcinoma (HCC) in 2012 and its implications. Cancer epidemiology *39*, 284-290.

Sawada, Y., Yoshikawa, T., Nobuoka, D., Shirakawa, H., Kuronuma, T., Motomura, Y., Mizuno, S., Ishii, H., Nakachi, K., Konishi, M.*, et al.* (2012). Phase I trial of a glypican-3-derived peptide vaccine for advanced hepatocellular carcinoma: immunologic evidence and potential for improving overall survival. Clinical cancer research : an official journal of the American Association for Cancer Research *18*, 3686-3696.

Sawada, Y., Yoshikawa, T., Ofuji, K., Yoshimura, M., Tsuchiya, N., Takahashi, M., Nobuoka, D., Gotohda, N., Takahashi, S., Kato, Y.*, et al.* (2016). Phase II study of the GPC3-derived peptide vaccine as an adjuvant therapy for hepatocellular carcinoma patients. Oncoimmunology *5*, e1129483.

Schurich, A., Khanna, P., Lopes, A. R., Han, K. J., Peppa, D., Micco, L., Nebbia, G., Kennedy, P. T., Geretti, A. M., Dusheiko, G., and Maini, M. K. (2011). Role of the coinhibitory receptor cytotoxic T lymphocyte antigen-4 on apoptosis-Prone CD8 T cells in persistent hepatitis B virus infection. Hepatology (Baltimore, Md) *53*, 1494-1503.

Seeger, C., and Mason, W. S. (2015). Molecular biology of hepatitis B virus infection. Virology *479-480*, 672-686.

Seto, W. K., Chan, T. S., Hwang, Y. Y., Wong, D. K., Fung, J., Liu, K. S., Gill, H., Lam, Y. F., Lie, A. K., Lai, C. L.*, et al.* (2014). Hepatitis B reactivation in patients with previous hepatitis B virus exposure undergoing rituximab-containing chemotherapy for lymphoma: a prospective study. Journal of clinical oncology : official journal of the American Society of Clinical Oncology *32*, 3736-3743.

Shalem, O., Sanjana, N. E., Hartenian, E., Shi, X., Scott, D. A., Mikkelson, T., Heckl, D., Ebert, B. L., Root, D. E., Doench, J. G., and Zhang, F. (2014). Genome-scale CRISPR-Cas9 knockout screening in human cells. Science (New York, NY) *343*, 84-87.

Sharma, P., and Kranz, D. M. (2016). Recent advances in T-cell engineering for use in immunotherapy. F1000Research *5*, F1000 Faculty Rev-2344.

Shurtleff, A. C., and Bavari, S. (2015). Animal models for ebolavirus countermeasures discovery: what defines a useful model? Expert opinion on drug discovery *10*, 685-702.

Song, B., Zhen, S., and Meng, F. (2016). T cell inflammation profile after surgical resection may predict tumor recurrence in HBV-related hepatocellular carcinoma. International immunopharmacology *41*, 35-41.

Sprinzl, M., Dumortier, J., and Protzer, U. (2004). Construction of recombinant adenoviruses that produce infectious hepatitis B virus. Methods in molecular medicine *96*, 209-218.

Stone, J. D., and Kranz, D. M. (2013). Role of T cell receptor affinity in the efficacy and specificity of adoptive T cell therapies. Front Immunol *4*, 244.

Sungur, C. M., and Murphy, W. J. (2013). Utilization of mouse models to decipher natural killer cell biology and potential clinical applications. Hematology American Society of Hematology Education Program *2013*, 227-233.

Szyska, M., Herda, S., Althoff, S., Heimann, A., Russ, J., D'Abundo, D., Dang, T. M., Durieux, I., Dorken, B., Blankenstein, T., and Na, I. K. (2018). A Transgenic Dual-Luciferase Reporter Mouse for Longitudinal and Functional Monitoring of T Cells In Vivo. Cancer immunology research *6*, 110-120.

Takai, H., Kato, A., Kinoshita, Y., Ishiguro, T., Takai, Y., Ohtani, Y., Sugimoto, M., and Suzuki, M. (2009). Histopathological analyses of the antitumor activity of anti-glypican-3 antibody (GC33) in human liver cancer xenograft models: The contribution of macrophages. Cancer biology & therapy *8*, 930-938.

Takai, S., Kimura, K., Nagaki, M., Satake, S., Kakimi, K., and Moriwaki, H. (2005). Blockade of neutrophil elastase attenuates severe liver injury in hepatitis B transgenic mice. Journal of virology *79*, 15142-15150.

Tan, W., Meng, Y., Li, H., Chen, Y., Han, S., Zeng, J., Huang, A., Li, B., Zhang, Y., and Guo, Y. (2013). A bispecific antibody against two different epitopes on hepatitis B surface antigen has potent hepatitis B virus neutralizing activity. mAbs *5*, 946-955.

Thakur, A., and Lum, L. G. (2016). “NextGen” Biologics: Bispecific Antibodies and Emerging Clinical Results. Expert Opinion on Biological Therapy *16*, 675-688.

Thimme, R., Wieland, S., Steiger, C., Ghrayeb, J., Reimann, K. A., Purcell, R. H., and Chisari, F. V. (2003). CD8(+) T cells mediate viral clearance and disease pathogenesis during acute hepatitis B virus infection. Journal of virology *77*, 68-76.

Thomson, A. W., and Knolle, P. A. (2010). Antigen-presenting cell function in the tolerogenic liver environment. Nature reviews Immunology *10*, 753-766.

Topp, M. S., Gokbuget, N., Stein, A. S., Zugmaier, G., O'Brien, S., Bargou, R. C., Dombret, H., Fielding, A. K., Heffner, L., Larson, R. A.*, et al.* (2015). Safety and activity of blinatumomab for adult patients with relapsed or refractory B-precursor acute lymphoblastic leukaemia: a multicentre, single-arm, phase 2 study. The Lancet Oncology *16*, 57-66.

Topp, M. S., Gokbuget, N., Zugmaier, G., Degenhard, E., Goebeler, M. E., Klinger, M., Neumann, S. A., Horst, H. A., Raff, T., Viardot, A.*, et al.* (2012). Long-term follow-up of hematologic relapse-free survival in a phase 2 study of blinatumomab in patients with MRD in B-lineage ALL. Blood *120*, 5185-5187.

Topp, M. S., Gokbuget, N., Zugmaier, G., Klappers, P., Stelljes, M., Neumann, S., Viardot, A., Marks, R., Diedrich, H., Faul, C.*, et al.* (2014). Phase II trial of the anti-CD19 bispecific T cell-engager blinatumomab shows hematologic and molecular remissions in patients with relapsed or refractory B-precursor acute lymphoblastic leukemia. Journal of clinical oncology : official journal of the American Society of Clinical Oncology *32*, 4134-4140.

Topp, M. S., Kufer, P., Gokbuget, N., Goebeler, M., Klinger, M., Neumann, S., Horst, H. A., Raff, T., Viardot, A., Schmid, M.*, et al.* (2011). Targeted therapy with the T-cell-engaging antibody blinatumomab of chemotherapy-refractory minimal residual disease in B-lineage acute lymphoblastic leukemia patients results in high response rate and prolonged leukemia-free survival. Journal of clinical oncology : official journal of the American Society of Clinical Oncology *29*, 2493-2498.

Tropberger, P., Mercier, A., Robinson, M., Zhong, W., Ganem, D. E., and Holdorf, M. (2015). Mapping of histone modifications in episomal HBV cccDNA uncovers an unusual chromatin organization amenable to epigenetic manipulation. Proceedings of the National Academy of Sciences of the United States of America *112*, E5715-5724.

Tsuchiya, N., Yoshikawa, T., Fujinami, N., Saito, K., Mizuno, S., Sawada, Y., Endo, I., and Nakatsura, T. (2017). Immunological efficacy of glypican-3 peptide vaccine in patients with advanced hepatocellular carcinoma. Oncoimmunology *6*, e1346764.

Tsuge, M., Hiraga, N., Takaishi, H., Noguchi, C., Oga, H., Imamura, M., Takahashi, S., Iwao, E., Fujimoto, Y., Ochi, H.*, et al.* (2005). Infection of human hepatocyte chimeric mouse with genetically engineered hepatitis B virus. Hepatology (Baltimore, Md) *42*, 1046-1054.

Unitt, E., Marshall, A., Gelson, W., Rushbrook, S. M., Davies, S., Vowler, S. L., Morris, L. S., Coleman, N., and Alexander, G. J. (2006). Tumour lymphocytic infiltrate and recurrence of hepatocellular carcinoma following liver transplantation. Journal of hepatology *45*, 246-253.

Utzschneider, D. T., Alfei, F., Roelli, P., Barras, D., Chennupati, V., Darbre, S., Delorenzi, M., Pinschewer, D. D., and Zehn, D. (2016). High antigen levels induce an exhausted phenotype in a chronic infection without impairing T cell expansion and survival. The Journal of experimental medicine *213*, 1819-1834.

Vandepapeliere, P., Lau, G. K., Leroux-Roels, G., Horsmans, Y., Gane, E., Tawandee, T., Merican, M. I., Win, K. M., Trepo, C., Cooksley, G.*, et al.* (2007). Therapeutic vaccination of chronic hepatitis B patients with virus suppression by antiviral therapy: a randomized,

controlled study of co-administration of HBsAg/AS02 candidate vaccine and lamivudine. Vaccine *25*, 8585-8597.

Venkatakrishnan, B., and Zlotnick, A. (2016). The Structural Biology of Hepatitis B Virus: Form and Function. Annual review of virology *3*, 429-451.

Verheyen, J. (2016). Neues vom Liver Meeting 2016 - Hepatitis B (Abstract 600). HepNet Journal *Ausgabe 2, 10. Jahrgang*.

von Freyend, M. J., Untergasser, A., Arzberger, S., Oberwinkler, H., Drebber, U., Schirmacher, P., and Protzer, U. (2011). Sequential control of hepatitis B virus in a mouse model of acute, self-resolving hepatitis B. Journal of viral hepatitis *18*, 216-226.

Waggoner, S. N., Cornberg, M., Selin, L. K., and Welsh, R. M. (2011). Natural killer cells act as rheostats modulating antiviral T cells. Nature *481*, 394-398.

Walunas, T. L., Lenschow, D. J., Bakker, C. Y., Linsley, P. S., Freeman, G. J., Green, J. M., Thompson, C. B., and Bluestone, J. A. (1994). CTLA-4 can function as a negative regulator of T cell activation. Immunity *1*, 405-413.

Wang, F. S., Xing, L. H., Liu, M. X., Zhu, C. L., Liu, H. G., Wang, H. F., and Lei, Z. Y. (2001). Dysfunction of peripheral blood dendritic cells from patients with chronic hepatitis B virus infection. World journal of gastroenterology *7*, 537-541.

Wang, L., Cao, M., Wei, Q. L., Zhao, Z. H., Xiang, Q., Wang, H. J., Zhang, H. T., and Lai, G. Q. (2017). A new model mimicking persistent HBV e antigen-negative infection using covalently closed circular DNA in immunocompetent mice. PloS one *12*, e0175992.

Wang, L., and Wang, L. (2016). Animal Models for Hepatitis E Virus. Advances in experimental medicine and biology *948*, 161-173.

Wang, L., Zhao, C., Peng, Q., Shi, J., and Gu, G. (2014a). Expression levels of CD28, CTLA-4, PD-1 and Tim-3 as novel indicators of T-cell immune function in patients with chronic hepatitis B virus infection. Biomedical reports *2*, 270-274.

Wang, L., Zou, Z. Q., Liu, C. X., and Liu, X. Z. (2014b). Immunotherapeutic interventions in chronic hepatitis B virus infection: a review. Journal of immunological methods *407*, 1-8.

Wang, Q., Schwarzenberger, P., Yang, F., Zhang, J., Su, J., Yang, C., Cao, J., Ou, C., Liang, L., Shi, J.*, et al.* (2012). Experimental chronic hepatitis B infection of neonatal tree shrews (Tupaia belangeri chinensis): A model to study molecular causes for susceptibility and disease progression to chronic hepatitis in humans. Virology Journal *9*, 170.

Washburn, M. L., Bility, M. T., Zhang, L., Kovalev, G. I., Buntzman, A., Frelinger, J. A., Barry, W., Ploss, A., Rice, C. M., and Su, L. (2011). A humanized mouse model to study hepatitis C virus infection, immune response, and liver disease. Gastroenterology *140*, 1334-1344.

Watanabe, K., Terakura, S., Martens, A. C., van Meerten, T., Uchiyama, S., Imai, M., Sakemura, R., Goto, T., Hanajiri, R., Imahashi, N.*, et al.* (2015). Target antigen density governs

the efficacy of anti-CD20-CD28-CD3 zeta chimeric antigen receptor-modified effector CD8+ T cells. Journal of immunology (Baltimore, Md : 1950) *194*, 911-920.

Weber, J. S., Kahler, K. C., and Hauschild, A. (2012). Management of immune-related adverse events and kinetics of response with ipilimumab. Journal of clinical oncology : official journal of the American Society of Clinical Oncology *30*, 2691-2697.

Weber, O., Schlemmer, K. H., Hartmann, E., Hagelschuer, I., Paessens, A., Graef, E., Deres, K., Goldmann, S., Niewoehner, U., Stoltefuss, J.*, et al.* (2002). Inhibition of human hepatitis B virus (HBV) by a novel non-nucleosidic compound in a transgenic mouse model. Antiviral research *54*, 69-78.

Wei, M. L., and Cresswell, P. (1992). HLA-A2 molecules in an antigen-processing mutant cell contain signal sequence-derived peptides. Nature *356*, 443-446.

Wherry, E. J. (2011). T cell exhaustion. Nature immunology *12*, 492.

Wherry, E. J., Blattman, J. N., Murali-Krishna, K., van der Most, R., and Ahmed, R. (2003). Viral persistence alters CD8 T-cell immunodominance and tissue distribution and results in distinct stages of functional impairment. Journal of virology *77*, 4911-4927.

WHO (2017). Hepatitis B, Fact sheet. http://wwwwhoint/mediacentre/factsheets/fs204/en/ *updated July 2017, accessed 02.05.2018*.

Wieland, S. F. (2015). The chimpanzee model for hepatitis B virus infection. Cold Spring Harbor perspectives in medicine *5*.

Wilde, S., Geiger, C., Milosevic, S., Mosetter, B., Eichenlaub, S., and Schendel, D. J. (2012). Generation of allo-restricted peptide-specific T cells using RNA-pulsed dendritic cells: A three phase experimental procedure. Oncoimmunology *1*, 129-140.

Wisskirchen, K., Metzger, K., Schreiber, S., Asen, T., Weigand, L., Dargel, C., Witter, K., Kieback, E., Sprinzl, M. F., Uckert, W.*, et al.* (2017). Isolation and functional characterization of hepatitis B virus-specific T-cell receptors as new tools for experimental and clinical use. PloS one *12*, e0182936.

Wu, H. L., Wiseman, R. W., Hughes, C. M., Webb, G. M., Abdulhaqq, S. A., Bimber, B. N., Hammond, K. B., Reed, J. S., Gao, L., Burwitz, B. J.*, et al.* (2018). The Role of MHC-E in T Cell Immunity Is Conserved among Humans, Rhesus Macaques, and Cynomolgus Macaques. Journal of immunology (Baltimore, Md : 1950) *200*, 49-60.

Wu, W., Shi, Y., Li, S., Zhang, Y., Liu, Y., Wu, Y., and Chen, Z. (2012). Blockade of Tim-3 signaling restores the virus-specific CD8(+) T-cell response in patients with chronic hepatitis B. European journal of immunology *42*, 1180-1191.

Wu, Z., Yang, H., and Colosi, P. (2010). Effect of Genome Size on AAV Vector Packaging. Molecular Therapy *18*, 80-86.

Xia, Y., Stadler, D., Ko, C., and Protzer, U. (2017). Analyses of HBV cccDNA Quantification and Modification. Methods in molecular biology (Clifton, NJ) *1540*, 59-72.

Xia, Y., Stadler, D., Lucifora, J., Reisinger, F., Webb, D., Hosel, M., Michler, T., Wisskirchen, K., Cheng, X., Zhang, K., *et al.* (2016). Interferon-gamma and Tumor Necrosis Factor-alpha Produced by T Cells Reduce the HBV Persistence Form, cccDNA, Without Cytolysis. Gastroenterology *150*, 194-205.

Xiao, X., Li, J., and Samulski, R. J. (1998). Production of high-titer recombinant adeno-associated virus vectors in the absence of helper adenovirus. Journal of virology *72*, 2224-2232.

Xu, D. Z., Wang, X. Y., Shen, X. L., Gong, G. Z., Ren, H., Guo, L. M., Sun, A. M., Xu, M., Li, L. J., Guo, X. H., *et al.* (2013). Results of a phase III clinical trial with an HBsAg-HBIG immunogenic complex therapeutic vaccine for chronic hepatitis B patients: experiences and findings. Journal of hepatology *59*, 450-456.

Yan, H., Zhong, G., Xu, G., He, W., Jing, Z., Gao, Z., Huang, Y., Qi, Y., Peng, B., Wang, H., *et al.* (2012). Sodium taurocholate cotransporting polypeptide is a functional receptor for human hepatitis B and D virus. eLife *1*, e00049.

Yang, C., Ruan, P., Ou, C., Su, J., Cao, J., Luo, C., Tang, Y., Wang, Q., Qin, H., Sun, W., and Li, Y. (2015). Chronic hepatitis B virus infection and occurrence of hepatocellular carcinoma in tree shrews (Tupaia belangeri chinensis). Virol J *12*, 26.

Yang, D., Liu, L., Zhu, D., Peng, H., Su, L., Fu, Y.-X., and Zhang, L. (2014). A mouse model for HBV immunotolerance and immunotherapy. Cellular & molecular immunology *11*, 71-78.

Yang, J. C., Hughes, M., Kammula, U., Royal, R., Sherry, R. M., Topalian, S. L., Suri, K. B., Levy, C., Allen, T., Mavroukakis, S., *et al.* (2007). Ipilimumab (anti-CTLA4 antibody) causes regression of metastatic renal cell cancer associated with enteritis and hypophysitis. Journal of immunotherapy (Hagerstown, Md : 1997) *30*, 825-830.

Ye, L., Yu, H., Li, C., Hirsch, M. L., Zhang, L., Samulski, R. J., Li, W., and Liu, Z. (2015). Adeno-Associated Virus Vector Mediated Delivery of the HBV Genome Induces Chronic Hepatitis B Virus Infection and Liver Fibrosis in Mice. PloS one *10*, e0130052.

Yoo, J., Hann, H. W., Coben, R., Conn, M., and DiMarino, A. J. (2018). Update Treatment for HBV Infection and Persistent Risk for Hepatocellular Carcinoma: Prospect for an HBV Cure. Diseases (Basel, Switzerland) *6*.

Yoshikawa, T., Nakatsugawa, M., Suzuki, S., Shirakawa, H., Nobuoka, D., Sakemura, N., Motomura, Y., Tanaka, Y., Hayashi, S., and Nakatsura, T. (2011). HLA-A2-restricted glypican-3 peptide-specific CTL clones induced by peptide vaccine show high avidity and antigen-specific killing activity against tumor cells. Cancer science *102*, 918-925.

Yu, M., Luo, H., Fan, M., Wu, X., Shi, B., Di, S., Liu, Y., Pan, Z., Jiang, H., and Li, Z. (2018). Development of GPC3-Specific Chimeric Antigen Receptor-Engineered Natural Killer Cells for the Treatment of Hepatocellular Carcinoma. Molecular Therapy *26*, 366-378.

Zaghloul, R. A., El-Shishtawy, M. M., El Galil, K. H., Ebrahim, M. A., Metwaly, A. A., and Al-Gayyar, M. M. (2015). Evaluation of antiglypican-3 therapy as a promising target for amelioration of hepatic tissue damage in hepatocellular carcinoma. European journal of pharmacology *746*, 353-362.

Zerbini, A., Pilli, M., Soliani, P., Ziegler, S., Pelosi, G., Orlandini, A., Cavallo, C., Uggeri, J., Scandroglio, R., Crafa, P.*, et al.* (2004). Ex vivo characterization of tumor-derived melanoma antigen encoding gene-specific CD8+cells in patients with hepatocellular carcinoma. Journal of hepatology *40*, 102-109.

Zhang, T. Y., Yuan, Q., Zhao, J. H., Zhang, Y. L., Yuan, L. Z., Lan, Y., Lo, Y. C., Sun, C. P., Wu, C. R., Zhang, J. F.*, et al.* (2016). Prolonged suppression of HBV in mice by a novel antibody that targets a unique epitope on hepatitis B surface antigen. Gut *65*, 658-671.

Zhou, G., Sprengers, D., Boor, P. P. C., Doukas, M., Schutz, H., Mancham, S., Pedroza-Gonzalez, A., Polak, W. G., de Jonge, J., Gaspersz, M.*, et al.* (2017). Antibodies Against Immune Checkpoint Molecules Restore Functions of Tumor-Infiltrating T Cells in Hepatocellular Carcinomas. Gastroenterology *153*, 1107-1119.e1110.

Zhu, A. X., Gold, P. J., El-Khoueiry, A. B., Abrams, T. A., Morikawa, H., Ohishi, N., Ohtomo, T., and Philip, P. A. (2013). First-in-man phase I study of GC33, a novel recombinant humanized antibody against glypican-3, in patients with advanced hepatocellular carcinoma. Clinical cancer research : an official journal of the American Association for Cancer Research *19*, 920-928.

Zhu, C., Anderson, A. C., Schubart, A., Xiong, H., Imitola, J., Khoury, S. J., Zheng, X. X., Strom, T. B., and Kuchroo, V. K. (2005). The Tim-3 ligand galectin-9 negatively regulates T helper type 1 immunity. Nature immunology *6*, 1245-1252.

ACKNOWLEDGMENTS

First of all, I would like to thank Prof. Ulrike Protzer for giving me the opportunity to do my Ph.D. thesis in her lab on these very exiting immunotherapy projects. You provided support and advices when necessary and always found time for urgent matters and questions.

I am grateful to Prof. Percy Knolle, my second supervisor, you provided valuable input during my thesis committee meetings. Additionally, I want to thank Dr. Felix Bohne and Dr. Karin Wisskirchen as members of my thesis committee. Felix, I would not have started this thesis without you, thank you very much!

Thank you so much, Karin! You supported my progress substantially as my supervisor, during weekly meetings, but also when you were on maternity leave you were always available for urgent questions and discussions. Moreover, I am especially thankful for your proofreading of this thesis.

Moreover, I am deeply thankful to Theresa Asen, you are an indispensable person in this lab. You did not only provide great help with mouse and other experiments, you always had time for organizational matters and supported me in every possible way. Special thanks go to our T-cell therapy subgroup members Sophia Schreiber, Antje Malo and Alexandre Klopp. You gave great input during weekly meetings and created a wonderful working atmosphere in the „small lab".

I want to thank Dr. Anna Kosinska, Dr. Martin Mück-Häusl, Dr. Chunkyu Ko, Jochen Wettengel and Dr. Christina Dargel for the implementation of joint projects, help with experiments and fruitful discussions.

Furthermore, I thank all other lab members, including former members, naming especially Oliver Quitt, Lisa Wolff, Wen-Min Chou, Dr. Daniela Stadler, Sebastian Altstetter, Philipp Hagen, Romina Bester, Samuel Jeske, Anindita Chakraborty, Andreas Oswald, Stoyan Velkov, Jinpeng Su, Florian Wilsch, Christoph Blossey, Martin Kächele, Julia Sacherl, Dr. Katrin Singethan, Suliman Afridi, Dr. Jan-Hendrik Bockman, Kathrin Kappes, Natalie Röder, Hortenzia Jacobi, Dr. Thomas Michler, Lili Zhao, Dr. Maarten van de Klundert and Dr. Stefanie Prosser for your direct or indirect help and support to complete this work as well as the great working atmosphere.

Thank you, Dr. Frank Thiele, Doris Pelz and Daniela Rizzi, for your support regarding mouse experiment approvals and other office work.

Furthermore, I would like to thank all members of the virology diagnostics department as well as the members of the animal facilities. Thank you Raza and Marinka for making our lab life so easy.

I am deeply thankful to Prof. Benjamin Burwitz and Prof. Jonah Sacha for inviting me to work in their labs for two months. I also want to thank the members of the Sacha and the Burwitz lab for help and support of experiments, but also for the warm welcome in the team.

An important thank you goes to my parents Alfons and Brigitte, my sister Katharina and my brother Johannes. You supported me throughout my entire life and encouraged me when needed. Thank you so much!

Importantly, I would like to thank Marvin Festag, my favorite person and soulmate. You supported me in every possible way, not only scientifically but also mentally. You helped me to stand up again when I was on the ground. I would not have made it without you. Thank you for being in my life!

PUBLICATIONS

C. Dargel, M. Bassani-Sternberg, **J. Hasreiter**, F. Zani, J.H. Bockmann, F. Thiele, F. Bohne, K. Wisskirchen, S. Wilde, M. F. Sprinzl, D. J. Schendel, A. M. Krackhardt, W. Uckert, D. Wohlleber, M. Schiemann, K. Stemmer, M. Heikenwälder, D. H. Busch, G. Richter, M. Mann, and U. Protzer (2015). T cells Engineered to Express a T-Cell Receptor Specific for Glypican-3 to Recognize and Kill Hepatoma Cells In Vitro and in Mice. *Gastroenterology*, 149(4), pp 1042-1052.

C. Ko, A, Chakraborty, WM. Chou, **J. Hasreiter**, J. M. Wettengel, D. Stadler, R. Bester, T. Asen, K. Zhang, K. Wisskirchen, J.A. McKeating, WS. Ryu and U. Protzer (2018). Hepatitis B virus (HBV) capsid recycling and de novo secondary infect ion events maintain stable cccDNA levels. *J Hepatol*, 69(6), pp 1231-1241.

MM. Festag, **J. Festag**, SP. Fräßle, T. Asen, J. Sacherl, S. Schreiber, MA. Mück-Häusl, DH. Busch, K. Wisskirchen and U. Protzer (2019). Evaluation of a Fully Human, Hepatitis B Virus-Specific Chimeric Antigen Receptor in an Immunocompetent Mouse Model. *Mol Ther*, 27(5), pp 947-959.

AD. Kosinska, A. Moeed, N. Kallin, **J. Festag**, J. Su, K. Steiger, ML. Michel, U. Protzer and PA. Knolle (2019). Synergy of a therapeutic heterologous prime-boost hepatitis B vaccination with CpG-application improve control of a persistent HBV infection (2019). Sci Rep, 9(1), p 10808.

J. Festag et al. Impact of HBx, HBe and vector type on *in vivo* studies for chronic hepatitis B virus infections. *Prepared manuscript.*

J. Festag et al. Vector-mediated delivery of human MHCI enables investigation of TCR-redirected HBV-specific T cells in mice and macaque models. *Manuscript in preparation.*